Study of macromolecular and structural modifications occurring during the building of the tension wood cell wall: a contribution to the understanding of the maturation stress generation in trees

Shan-Shan Chang

Collège Doctoral du Languedoc-Roussillon

THÈSE

Pour obtenir le grade de

Docteur

Délivré par **UNIVERSITE MONTPELLIER 2**

SCIENCES ET TECHNIQUES DU LANGUEDOC

Préparée au sein de l'école doctorale

Information, Structures et Systèmes

Et de l'unité de recherche ***UMR5508 (LMGC)***

Spécialité: ***Mécanique et Génie Civil***

Présentée par **Shan Shan CHANG**

Study of macromolecular and structural modifications occurring during the building of the tension wood cell wall: a contribution to the understanding of the maturation stress generation in trees

Etude des modifications macromoléculaires et structurales ayant lieu pendant la construction de la paroi cellulaire du bois de tension: une contribution à la compréhension de l'origine des contraintes de maturation chez les arbres

Soutenue le 28/01/2014 devant le jury composé de

Gilles PILATE, DR, INRA, Orléans, France	Rapporteur
Hiroyuki YAMAMOTO, Professeur, Université de Nagoya, Japon	Rapporteur
Bruno CLAIR, CR, CNRS, Montpellier, France	Directeur de thèse
Françoise QUIGNARD, DR, CNRS, Montpellier, France	Codirecteur de thèse
Eric BADEL, CR, INRA, Clermont-Ferrand, France	Examinateur
Fabien CHERBLANC, Professeur, Université Montpellier II, France	Examinateur
Tancrède ALMERAS, CR, CNRS, Montpellier, France	Invité

LMGC cnrs UNIVERSITÉ MONTPELLIER 2 ICG Montpellier Institut Charles Gerhardt MACS la Région Languedoc Roussillon

Acknowledgement

Completing my second PhD degree in France is probably one of the most challenging activities in my life. The PhD thesis is the result of the challenging journey, upon which many local and global people have contributed and given their support. Foremost, I would like to thank my advisors Dr. Bruno Clair and Dr. Françoise Quignard for providing me with the opportunity to complete my PhD thesis. Bruno always made time to discuss my work and resulting issues. His endless passion and strict attitude towards research will influence me all the life. I also want to thank Magali, his wife, for her enthusiastic welcome during our first arriving in Montpellier. Deep thanks also go to my thesis advisor, Dr. Françoise Quignard, for her warm encouragement and thoughtful guidance.

I would also like to thank Dr. Gilles Pilate, Prof. Hiroyuki Yamamoto, Dr. Eric Badel, and Prof. Fabien Cherblanc for serving as my thesis committee members.

To all my colleagues from MAB (Equipe Mécanique de l'Arbre et du Bois) at LMGC – many thanks for their kindness and all their help. I would like to make special mention of Prof. Joseph Gril for his encouragements and his selfless help in student's exchange and cooperation, and Dr. Tancrède Alméras for his help in data processing and insightful comments.

I would also like to thank Prof. Lennart Salmén for being a friendly host and allowing me to perform research work in his laboratory at Stockholm Sweden and for being available at all times for discussions. Thanks also go to the colleagues at Innventia AB for providing an enjoyable place to work in.

I would like to thanks the laboratory of ICG (Institut Charles Gerhardt Montpellier), where I preformed most of my experiment there, especially those colleagues for their selfless help with all types of typical problems during the experiments.

Also I thank my colleagues in Central South University of Forestry and Technology (CSUFT, Changsha, China), for their support, understanding, and encouragement throughout this thesis work.

I am forever indebted to my family, especially my parents, my sisters and my husband Jinbo for their love, support, understanding, endless patience and encouragement when it was most required.

The work reported in this thesis would not have been possible without the financial support of the Scientific Council of Montpellier University, for which I am grateful. Part of this work was supported by COST Action FP0802 through the Short Term Scientific Mission (STSM). Part of work was performed in the framework of the project "StressInTrees" funded by the French National Research Agency (ANR-12-BS09-0004). I wish to express my sincere gratitude to all of these.

Abbreviations and symbols

AGPs	Arabinogalactan proteins
BET	Brunauer, Emmett and Teller
CCD	Charge coupled device
DP	Degree of polymerization
E_1	Energy of adsorption in the first layer
E_L	Energy of adsorption in the succeeding layers
FTIR	Fourier transform infrared
G, GL, G-layer	Gelatinous layer
I	Intensity absorbance
IUPAC	International union of pure and applied chemistry
L, R, T	Longitudinal, radial, tangential directions
MCT	Mercury cadmium telluride
MFA	Microfibril angle
ML	Middle lamella
OL	Other layers in cell wall except G-layer
OW	Opposite wood
P, PCW	Primary cell wall
S	Secondary cell wall
S_1	Secondary cell wall layer, first layer
S_2	Secondary cell wall layer, middle layer
S_3	Secondary cell wall layer, third layer
SEM	Scanning electron microscopy
TW	Tension wood
XET	Xyloglucan-endotransglycosylase
XTH	Xyloglucan transglucosylase /hydrolase

Titre: Etude des modifications macromoléculaires et structurales ayant lieu pendant la construction de la paroi cellulaire du bois de tension: une contribution à la compréhension de l'origine des contraintes de maturation chez les arbres

RESUME

Les arbres sont des organismes de grande longévité qui se développent dans un environnement variable. Au cours de leur formation, ils génèrent une tension appelée contrainte de maturation pour remplir des fonctions biomécaniques essentielles. Chez les angiospermes, les arbres adaptent leur état mécanique par la production de bois de tension avec de fortes contraintes de traction sur la face supérieure de la tige penchée. Malgré les recherches considérables dans ce domaine durant de nombreuses années, les connaissances actuelles sur le mécanisme de la génération active de contrainte dans le bois de tension sont encore incomplètes et doivent être améliorées.

La première partie de cette étude était de faire progresser la compréhension de la composition et de l'organisation des polymères de la paroi cellulaire secondaire, ainsi que leur orientation au cours de la maturation de la paroi cellulaire du bois de tension. Les mesures effectuées sur la microscopie FTIR ont indiqué qu'avant même la formation de la couche G, il existait une structure d'hydrates de carbone ordonnée à un angle plus parallèle à l'axe de la fibre dans le bois de tension. Ces résultats étaient clairement différents du comportement du bois opposé. Dans le bois de tension, la lignine était plus fortement orientée dans la couche S_2 que dans le bois opposé. Avec la formation de la couche S_2 dans le bois opposé et de la couche G dans le bois de tension, les signaux d'orientation des hydrates de carbone amorphes tels que les hémicelluloses et les pectines sont différents entre le bois de tension et le bois qui lui est opposé. Pour les bois de tension, l'orientation de ces bandes est la même tout au long du processus de maturation de la paroi cellulaire, ce qui reflète probablement un dépôt continu de xyloglucane ou de xylane, avec une orientation différente de celle de la paroi S_2 pendant tout le processus.

La seconde partie de ce travail était d'améliorer les connaissances actuelles sur le comportement de la matrice par l'étude de la mésoporosité et de son évolution lors de la construction et de la maturation de la paroi cellulaire du bois de tension. Les résultats sur deux types de bois de tension suggèrent que la mésoporosité peut toujours être détectée près de la zone de cambium autant pour le bois de tension que pour le bois opposé. La forte porosité diminue progressivement avec la lignification dans la paroi cellulaire en développement, avec une exception pour le bois de tension à couche G. La porosité de type bouteille d'encre et l'augmentation de la taille médiane des pores sont observées dans les deux types de bois de tension, indiquant que les espèces de bois de tension avec et sans couches G peuvent partager le même mécanisme de génération de contrainte de traction.

Cette étude contribue à une meilleure compréhension de la génération de contraintes de maturation dans les arbres et peut servir de base pour l'amélioration de la modélisation du comportement de la matrice au cours de la maturation de la paroi cellulaire.

MOTS-CLES: Bois de tension, Contrainte de maturation, Maturation cellulaire, Couche gélatineuse, Peuplier, Simarouba, Microscopie à transformée de Fourier infra-rouge (FTIR), Mésoporosité, Sonication

Title: Study of macromolecular and structural modifications occurring during the building of the tension wood cell wall: a contribution to the understanding of the maturation stress generation in trees

ABSTRACT

Trees are long-living organisms which develop in a variable environment. During their formation, they generate a tensile mechanical stress called maturation stress to fulfil essential biomechanical functions. In angiosperm species, trees adapt the mechanical state by producing tension wood with high tensile stresses on the upper side of the leaning stem. Despite considerable research in this field during a number of years, the current knowledge on the mechanism of the active stress generation in tension wood is still incomplete and needs improvement.

The first part of this study was to advance the understanding on the composition and organisation of polymers within the secondary cell wall, as well as its orientation during the maturation of tension wood cell wall. Measurements performed on FTIR microscopy indicated that already before G-layer formation, a more ordered structure of carbohydrates at an angle more parallel to the fibre axis exists in tension wood. This was clearly different to the behaviour of opposite wood. In tension wood, the lignin was more highly oriented in the S_2 layer than in opposite wood. With the formation of the S_2 layer in opposite wood and the G-layer in tension wood, the orientation signals from the amorphous carbohydrates like hemicelluloses and pectins were different between opposite wood and tension wood. For tension wood, the orientation for these bands remains the same all along the cell wall maturation process, probably reflecting a continued deposition of xyloglucan or xylan, with an orientation different to that in the S_2 wall, throughout the whole process.

The second part of this study was to improve the current knowledge on the matrix behaviour by studying the mesoporosity and its evolution during the building and maturation of tension wood cell wall. Results on two kinds of tension wood suggested that mesoporosity can always be detected near cambium zone for both tension and opposite wood. The high porosity decreased gradually with the lignification in the developing cell wall, with an exception in tension wood with G-layer. The typical ink-bottle pore and the increase of median pore size are observed in both kinds of tension wood, indicating non-G-layer species may share the same mechanism of tensile stress generation as in tension wood with G-layer.

This study aims to contribute an increased understanding on the maturation stress generation in trees and may allow to improve the modelling of matrix behaviour during cell wall maturation.

KEYWORDS: Tension wood, Maturation stress, Cell wall maturation, Gelatinous layer, Poplar, Simarouba, Fourier transform infrared (FTIR) microscopy, Mesoporosity, Sonication

Laboratoires où a été préparée la thèse:

Laboratoire de Mécanique et Génie Civil (LMGC), CNRS UMR 5508, Université Montpellier II, pl. E. Bataillon, 34095 Montpellier Cedex 5, France.

Institut Charles Gerhardt Montpellier, UMR 5253 CNRS-UM2-ENSCM-UM1, 8 rue de l'Ecole Normale, 34296 Montpellier Cedex 5, France.

Table of contents

Introduction

Trees generate mechanical stresses to control their orientation by bending their stems or branches to respond to environmental variation (Timell 1986). In some cases, in reaction to asymmetric load, angiosperm trees differentiate tension wood on one side of the trunk with high growth stresses to stabilize themselves (Archer 1986; Wardrop 1964; Fisher and Stevenson 1981). The generation of this stress occurs during the maturation of the cell wall, and is then called maturation stress. This maturation stress appears in wood fibres during the formation of their secondary wall, but the underlying mechanical mechanisms are not fully understood.

Tension wood has specific anatomical, chemical and mechanical features. In most temperate species, the most significant feature in tension wood is a gelatinous layer (G-layer) that forms in the secondary wall of wood fibres (Onaka 1949). The G-layer is mainly constituted of cellulose microfibrils oriented nearly parallel to the fibre axis (Norberg and Meier 1966). Although there is some controversy regarding the origin of the tensile maturation stresses, when it is present, the G-layer is recognised as playing the essential role in the stress generation in tension wood. However, the exact mechanism behind tensile stress generation is still a matter of debate (Goswami et al. 2008; Clair et al. 2011; Mellerowicz and Gorshkova 2012). Different hypotheses (Okuyama et al. 1994; Bamber 2001; Yamamoto 2004; Nishikubo et al. 2007; Mellerowicz et al. 2008; Bowling and Vaughn 2008) have been proposed and discussed to explain this mechanism towards elucidating G-layer functions, but some of them are conflicting. Recently, Alméras et al. (2012) proposed a mechanism where the stress would be transferred to the cellulose microfibrils by the swelling of the matrix in an interconnected network of cellulose microfibrils. The hypothesis assumes that the microfibrils in G-layer are not just parallel to each other but are locally bounded in the transverse direction by matrix polysaccharides. Then the swelling or shrinkage of the matrix substance result to axial tension in the cell. This behaviour should be triggered by molecular changes during maturation and associated with structural modifications occurring during the building of the tension wood cell wall.

G-layer has a structure similar to gels with a large amount of water-filled mesopores (Clair et al. 2008; Chang et al. 2009b, 2011, 2012). Gels are known to be able to exhibit high shrinkage or swelling in response to physicochemical changes, like ion concentration change. Therefore, physicochemical changes by pectin-like substances in the G-layer matrix could make the G-layer matrix swell or shrink and then be the driving force of the maturation stress generation in tension wood. These strains are suspected to modify the mesoporous texture of the G-layer during maturation.

However, it has been shown that two thirds of tropical species do not produce typical G-layer wood in their tension wood (Onaka 1949; Fisher and Stevenson 1981; Clair et al. 2006b). In

these species, the mechanism of maturation stress generation is even more enigmatic as the tension wood cell wall appears lignified similar to normal wood.

This work aims at studying the macromolecular and structural modifications during the building of the tension wood cell wall and to better understand the maturation stress generation in trees.

(a) The first objective was to determine the orientations of the polymers in the cell wall of tension wood fibres and its ultrastructural organisation during maturation of poplar tension wood, in order to better understand how the deposition and organisation of the cell wall polymers relate to tension wood formation by comparing their behaviour to that of opposite wood during wood maturation. The primary technique utilised was imaging Fournier transform infrared (FTIR) microscopy.

FTIR microscopy is a technique suitable for monitoring the development and compositional changes in the cell walls and thus obtaining a clearer picture of cell wall development. Combined with polarised radiation, information on the orientation of specific groups and of the polymer chains containing these groups in the wood structure can be obtained at a µm scale (Olsson et al. 2011).

(b) The second objective was to record the mesoporosity change in developing G-layer and non-G-layer tension wood cell walls, in order to check the assumption of cell wall matrix swelling during maturation stress generation. The primary technique adopted was nitrogen adsorption-desorption volumetry on CO_2 supercritical dried samples. Nitrogen adsorption-desorption method is a powerful tool for studying the pore size and surface area of dried materials with cavities from 2 to 50 nm (Gregg and Sing 1982; Rouquerol et al. 1999). To elucidate the mechanisms associated to tension stress generation, this technique was applied to evaluate the structural change both in poplar, which produce typical G-layer and in simarouba, where G-layer is not visible.

This second objective let us need several methodological developments that are described in the manuscript. First, for a better maintain of texture of tension wood, specific studies have been done to adapt the protocol of dehydration needed for N_2 volumetry measurement to the specificity of tension wood. Since G-layer is recognised as the source of tensile stress in tension wood, a special interest is given to the G-layer itself. As most techniques integrate the whole cell wall, the separation of G-layer by ultrasonication is more and more often used to obtain the isolated G-layers for specific analysis. However, recent study showed that the ultrasonic treatment change the nanostructure of bacterial cellulose when subjected to ultrasonic processing (Tischer et al. 2010). This led us to examine the effect of ultrasound on the morphology and structure of G-layer and to revisit the ultrasonic treatment on G-layer isolation.

1. State of the art

1.1 Wood formation

Wood, also called secondary xylem, is generated seasonally at the periphery of the trunk by the vascular cambium (Déjardin et al. 2010). Wood formation is a highly regulated process. It starts in the vascular cambium by cell division, and follows the cell expansion and cell wall thickening, and then finish with programmed cell death (for review see Fromm 2013). Cells can divide or toward the xylem side or toward the phloem. The cells which are formed on the xylem side differentiate into the secondary xylem, and the cells which are formed on the phloem side differentiate into the secondary phloem. The differentiation process may continue throughout the whole growing season, and the number of xylem cells formed exceeds the number of phloem cells (Pallardy 2008). Wood is therefore formed in a larger quantity than secondary phloem in the stem. The accumulation of these secondary tissues, especially the secondary xylem (wood), causes the stem to slowly increase in diameter.

1.1.1 The vascular cambium

The vascular cambium is a lateral secondary meristem that derives from the procambium, which in turn originates from the apical meristem (Larson 1994). According to Wilson et al. (1966), the term cambium concerns only one layer of juvenile cells, called initials, and the term cambial zone regroups all the cells that are able to divide, including initial cells plus phloem and xylem mother cells. On the stem cross-section, the cambial zone is characterized by a few layers with thin cell walls and small radial diameters (Timel 1980; Antonova and Stasove 1997), as shown in Fig. 1.1. There are two types of initials: elongated fusiform (spindle-shaped) initials and isodiametric ray initials. The former gives rise to the axial cells of the xylem and phloem, like vessel, fibre, tracheid, and axial parenchyma cells, whereas the latter is the origin of the radially oriented ray cells (Mellerowicz et al. 2001; Chaffey et al. 2002).

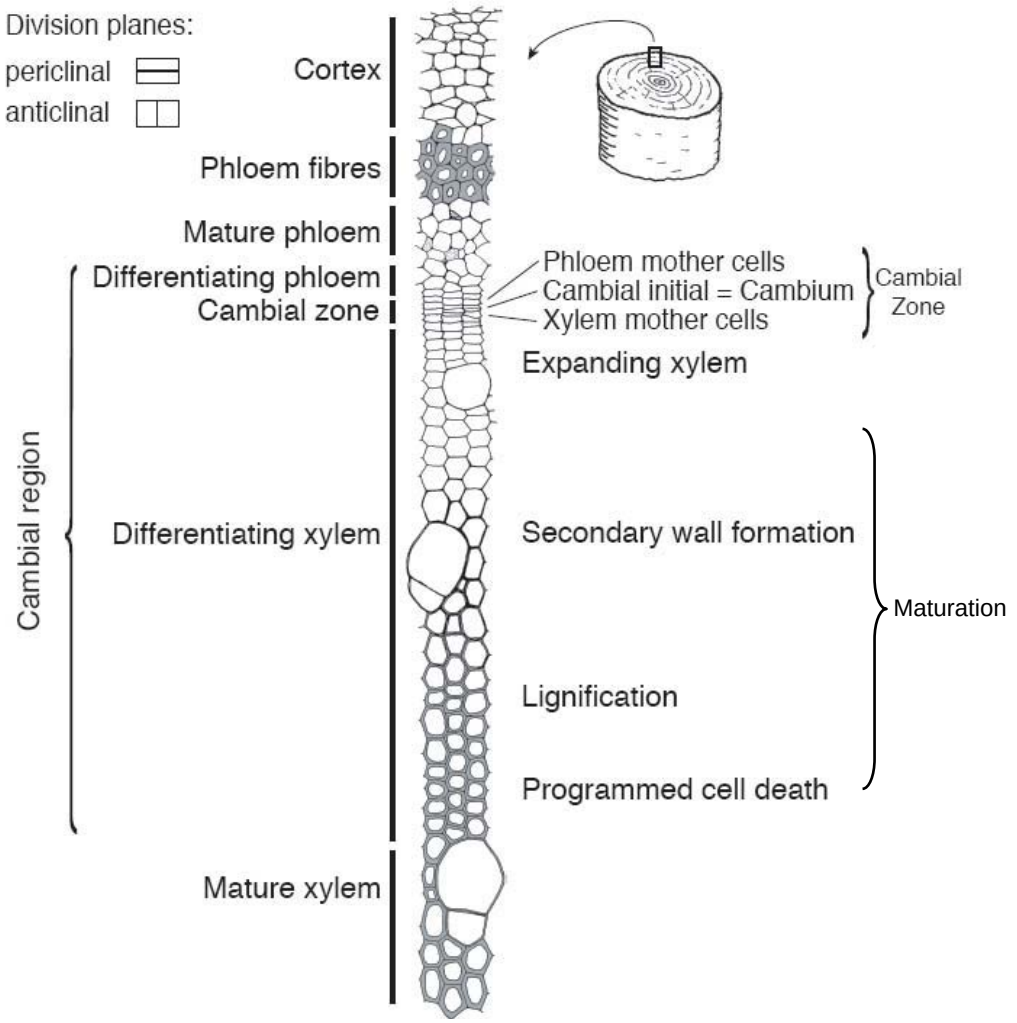

Figure 1.1 Terminology of wood-forming tissues (from Schrader 2003)

The cambium initials produce the daughter cells by the periclinal (tangential plane) divisions, as shown schematically in Figure 1.2. The cambium initials divide to produce two new cells: one remains in the cambium and continues to function as an initial cell, while another becomes phloem or xylem mother cell. The newly formed phloem or xylem mother cells may either mature directly or divide one or more times before they become mature cells (Navi and Sandberg 2012). Initials retain this potential to differentiate throughout the growing season, with one cell always remaining a cambial initial. Since, in most species, xylem mother cells divide more than phloem mother cells, then much more xylem than phloem is produced (Formm 2013). Anticlinal (radial plane) divisions of the fusiform initials also occasionally occur to compensate the need of increased cambium circumference. New ray initials are formed by subsequent anticlinal divisions of fusiform initials (Plomion et al. 2001).

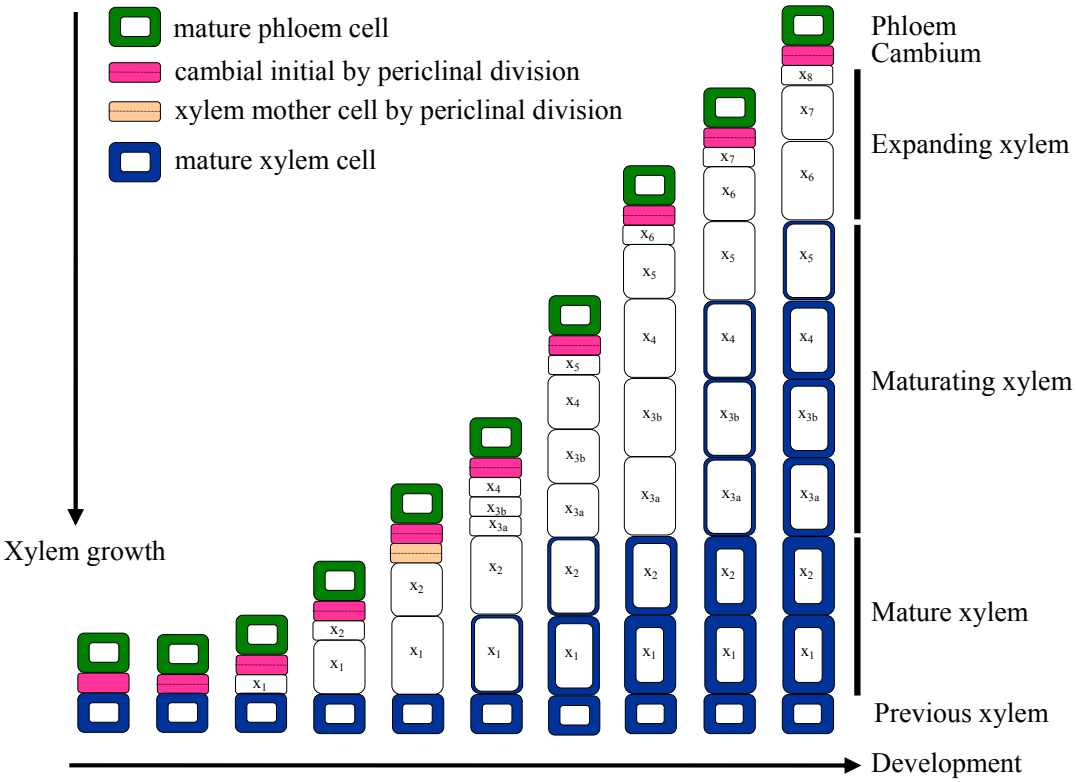

Figure 1.2 A schematic of xylem cell development by periclinal division of the cambial initials

1.1.2 The differentiation or maturation of xylem cells

The differentiation of young xylem cells can be subdivided into four successive stages based on anatomical and cytological cues (Plomion et al. 2001; Déjardin et al. 2010) (Fig. 1.1): (i) cell expansion (cell elongation and radial enlargement) to its final sizes, (ii) secondary cell wall deposition, (iii) lignification and (iv) programmed cell death. At the beginning of their differentiation, the young xylem cells lengthen and widen their size. In this stage, they only have an ultra-thin primary wall, which is composed of cellulose, pectic polysaccharides, xyloglucans and lesser amounts of arabinoxylans and proteins (Cosgrove and Jarvis 2012).

When the cell reaches its final dimensions, the cellular protoplasm is deposited on the inner surface of the cell wall prior to the development of the secondary cell wall (Navi and Sandberg 2012). As a result, the secondary cell wall gradually thickens to form a multilayer (S_1, S_2 and S_3) covering the primary wall. Each of these layers is composed of a network of cellulose microfibril bundles, oriented at a fixed angle, and embedded in an amorphous matrix of hemicelluloses with lignin deposited lastly of the wood polymers. Lignification starts before all layers of the secondary cell wall are deposited (Donaldson 2001; Yoshinaga et al. 2012) and first deposits from the cell corners, to the compound middle lamella and thereafter to the primary and secondary walls. Lignification makes the cells become both rigid and impermeable. When lignification stage is completed, the cells undergo programmed cell death, except for the parenchyma cells which remain alive and functional for several years (Déjardin et al. 2010). In our study, the term maturation will be used to define the period starting at the end of the cell expansion up to the cell death. It should be noted that the development stages

of a cell, including birth, thickening, maturation and lignification, occur almost simultaneously, in a couple of weeks (Navi and Sandberg 2012).

1.1.3 The ultrastructure of the wood cell walls

The basic unit of wood structure is the cell. The most important wood cells for mechanical purpose are longitudinal tracheids in softwoods and libriform fibres in hardwoods. Both of them are often referred as fibres. Apart from fibres, there is an abundance of ray cells in softwoods, performing storage function, while vessel and ray cells in hardwoods, performing conducting and storage function, respectively. The fibre cell wall is a composite of several layers (Fig. 1.3B) that are fabricated at different periods during cell differentiation. These layers are clearly visible under electron microscope (Fig. 1.3A). The cell is surrounded by a middle lamella (ML), which is developed after cell division, and acts as a gluing connecting the neighbour cells. The middle lamella has varying thickness, especially at the cell corners, from 0.5 to 1.5 µm. The main substances in the middle lamella are pectins at the early stage of growth, and lignin at the later stage of growth (Plomion et al. 2001). The cell wall attached to the middle lamella is the primary cell wall (PCW), which is highly deformable and thin, approximately 0.1 µm thick. The primary cell wall consists of tangled cellulose in which hemicelluloses, pectin, protein and then lignin settled later.

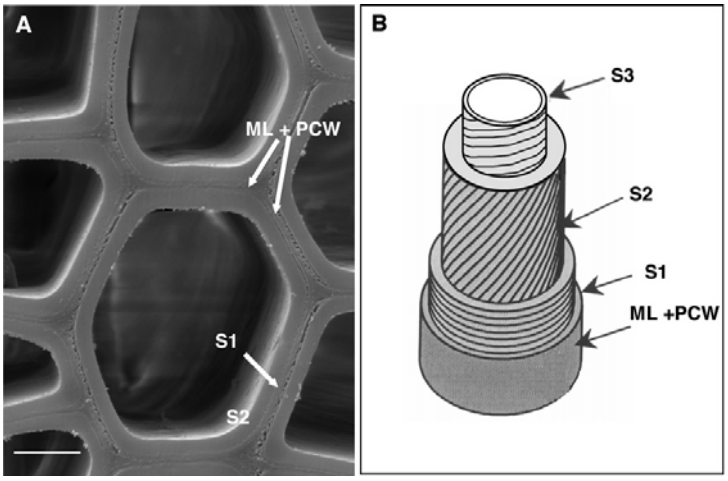

Figure 1.3 Structure of fibre cell wall. Scanning electron microscopy (A) and schematic illustration (B) showing the different cell wall layers. ML: middle lamella; PCW: primary cell wall; S_1, S_2, S_3: different layers of secondary cell wall. The scale bar is 5 µm. (A from Déjardin et al. 2010, B from Sassus 1998)

Inside the primary cell wall is the secondary cell wall, which is the most important layer for the cell, in term of mechanical properties. The secondary cell wall is divided into three sub-layers, the thin outer layer S_1 (0.15-0.35 µm), the thick middle layer S_2 (1-10 µm), and the thin inner layer S_3 (0.5-1.1 µm) (Plomion et al. 2001). Each of these layers is composed of a network of cellulose microfibril bundles, oriented at a fixed angle, and embedded in an amorphous matrix of hemicelluloses (mainly xylans and glucomannans) and lignin. A small quantity of pectins and proteins are also present in each layer (Déjardin et al. 2010). The cell wall characteristics, i.e. the deposition and the chemical composition, can be modified during cell maturation by external mechanical stress such as wind or stem lean, as in the case of

gelatinous fibre formation in tension wood of angiosperms (see the next section on tension wood).

The secondary cell wall contains a large proportion of cellulose in the form of microfibrils. The angle between the microfibrils and the long axis of the fibre refers to microfibril angle (MFA), which has a major effect on the wood properties, in particular stiffness and mechanical strength (Barnett and Bonham 2004). The thin S_1 layer has a large microfibril angle between 60˚ to 80˚. The middle S_2 layer is the thickest one, and microfibril angle of the S_2 layer is the most widely used parameter in wood technology. As microfibril angle increases, the stiffness and tensile stress decrease (Burgert 2006). The microfibril in this layer is 5˚ to 30˚, and can be even lower (close to 0˚) or higher depending on the external mechanical stress (see the next section on tension wood). The inner S3 layer is oriented almost perpendicular to the longitudinal axis of the fibre, with the angle between 60˚ to 90˚ (Plomion et al. 2001).

1.1.4 Major constituents of the cell wall

The principal constituents in wood fibres are cellulose, hemicelluloses, and lignin. Pectin, protein, extractives and some inorganic compounds are also present, but only as minor compounds. A fibre is built up by a number of different cell wall layers, such as primary cell wall and secondary cell wall. The distribution of the chemical components of wood is not uniform within the various layers of the cell (Fig. 1.4). Lignin is present in the compound middle lamella as the most abundant polymer, but because compound middle lamella is thin, the largest quantity is present in the secondary cell wall.

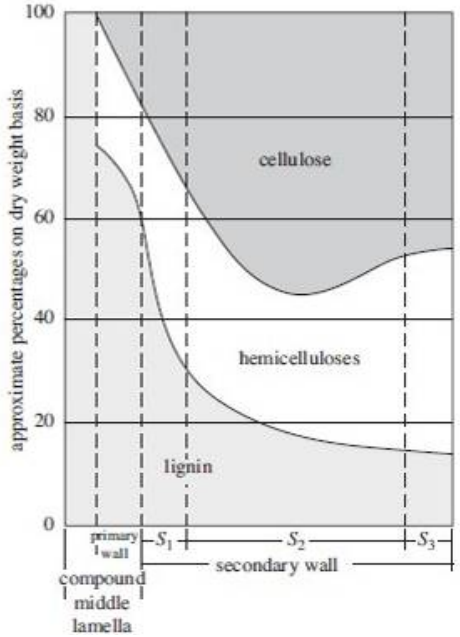

Figure 1.4 Distribution in percentages of cellulose, lignin and hemicelluloses within the cell-wall layers (from Panshin et al. 1964)

- **Cellulose**

The primary component of the wood cell walls is cellulose, which accounts for about 40-50% of the dry weight of wood. Cellulose is a linear polymer built up of D-glucose linked together by β-(1-4)-glycosidic bonds (Fig. 1.5) with a degree of polymerization (DP, i.e. number of

glucose residues in a chain) about 10,000 in native wood (Goring and Timell 1962). Repeating unit in a cellulose chain is the cellobiose which is built of two β-D-glucose units.

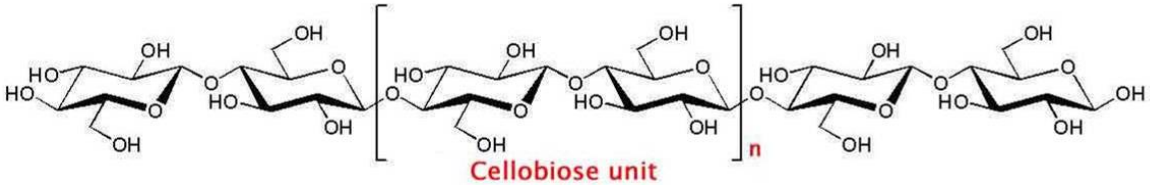

Figure 1.5 Partial structure of cellulose and the cellobiose unit

Since the polymer is linear, cellulose has a strong tendency to form inter- and intra-molecular hydrogen bonds by the hydroxyl groups (Fig. 1.6), which lead to the formation of microfibrils with crystalline and non-crystalline areas (Klemn et al. 2005). In wood cell wall, the basic morphological unit of cellulose is the elementary microfibril, about 3.5 nm in diameter and indefinite length (Wardrop and Dadswell 1957). The bundle aggregations of the microfibrils are referred to as microfibril aggregates. This structure of the cellulose is responsible for the longitudinal tensile stiffness of wood fibres.

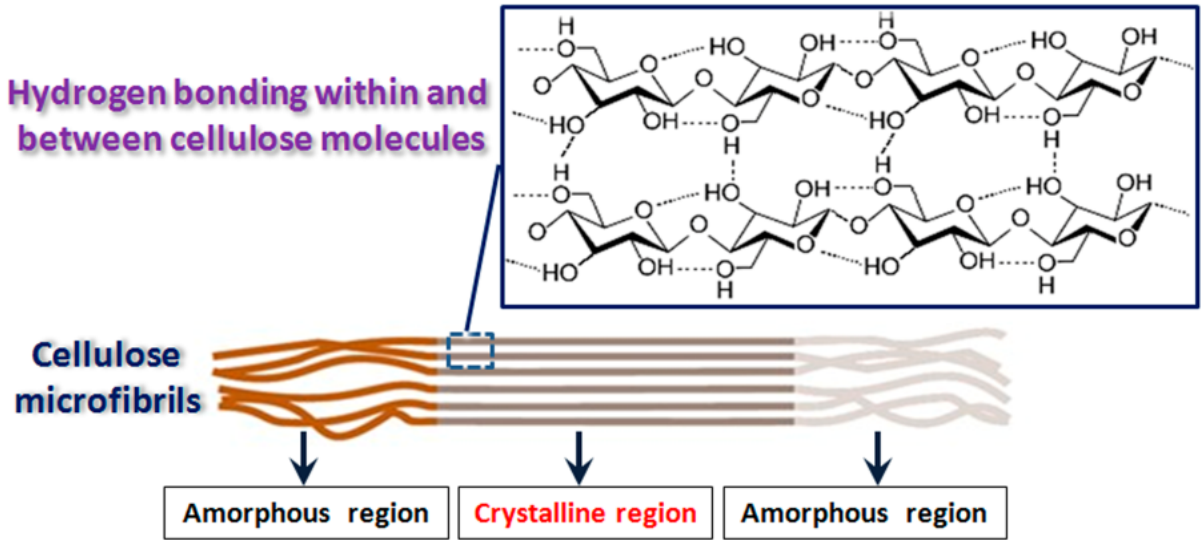

Figure 1.6 Scheme of inter- and intra-molecular hydrogen bonds of cellulose as well as the amorphous and crystalline regions of cellulose microfibrils (from Zhou and Wu 2012)

- **Hemicellulose**

Unlike cellulose, hemicelluloses are heteropolysaccharides, with lower DP (only 100-200) in wood. Hemicelluloses play a supporting role in the fibre wall and account for about 20-30% of the dry weight of wood. Hemicelluloses are a large group of branched heteropolymers, composed of several different monomers, such as arabinose, galactose, glucose, mannose and xylose (Rowell et al. 2005). One or several types of monomers usually build up the backbone of the hemicellulose with short branches containing different types of sugars. The branches make the hemicelluloses can not self-aggregate, and they are amorphous without the tendency to form crystalline region as cellulose. However, hemicelluloses form hydrogen bonds with cellulose and serve as binders in the cell walls providing flexibility.

The main hemicellulose in hardwood is xylan, which makes up about 30% of the dry weight of wood (Rowell et al. 2005). Xylans of the hardwood trees generally possess a principal homopolymeric chain of xylose units which are linked by β-(1-4)-glycosidic bonds. The principal chain comprises the groups 4-O-methylglucuronic acids with an α-(1-2)-glycosidic linkage at the xylose unit (Fig. 1.7). Many hydroxyl groups at C-2 and C-3 of the xylose unit are substituted with O-acetyl groups. The average degree of polymerization of the principal chain, which varies between 100 and 200, depends on the species and the mode of isolation.

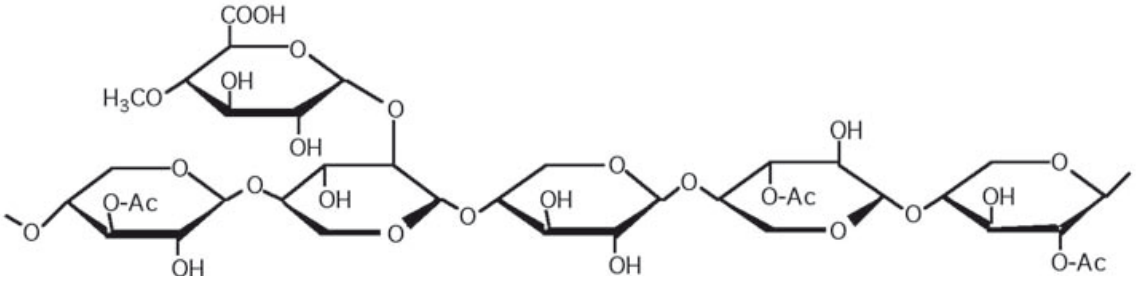

Figure 1.7 Partial chemical structure of O-acetyl-4-O-methylglucuronoxylan of hardwood (from Navi and Sandberg 2012)

In softwoods, galactoglucomannan is the principal hemicellulose (approximately 20 to 25%), with a linear or slightly branched chain with β-(1-4)-linkages (Rowell et al. 2005). Glucose and mannose make up the backbone polymer with branches containing galactose, see Fig. 1.8. On an average of 3-4 sugar units acetyl groups substitute the C-2 and C-3 of glucose and mannose units. The backbone substitution and degree of branching can vary considerably between hemicelluloses of the same category in hardwood and softwood (Sjöström 1981). Fengel and Wegener (1984) show that certain parts of the glucomannans are bonded to lignin. These connections are known as lignin-polysaccharides or lignin-carbohydrates complexes.

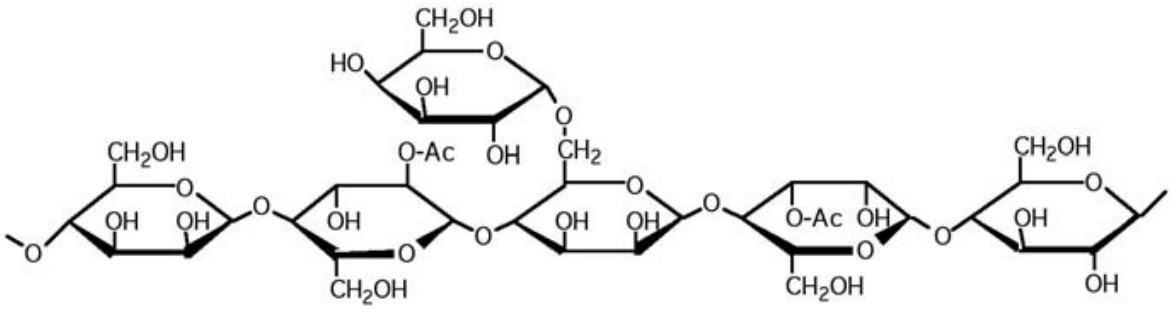

Figure 1.8 Partial chemical structure of O-acetyl-galactoglucomannan of softwood (from Navi and Sandberg 2012)

- **Lignin**

After cellulose, lignin is the second most abundant organic substance in plants and it accounts for 20% to 30% of the dry weight of wood. Lignin is a large family of aromatic branched polymers, built up of phenylpropane units in a three-dimensional structure (Sjöström 1981). The three-dimensional polymer is less hydrophilic than carbohydrates and is made up of C-O-C and C-C linkages. The molecular structure of lignin is not precisely known, however, the precursors of lignin, i.e. coniferyl alcohol, sinapyl alcohol and p-coumaryl alcohol (Fig. 1.9) are well-known thanks to studies with ^{14}C (Navi and Sandberg 2012).

Figure 1.9 Chemical structures of lignin precursors

Lignins from softwoods are mainly a polymerization product of coniferyl alcohol and are called guaiacyl lignin, while hardwood lignins are mainly a copolymer of coniferyl and sinapyl alcohols, called syringyl-guaiacyl lignin (Alder 1977). However, the chemical structure of lignin varies widely within different wood species, tissues, as well as different layers of the cell wall. Lignin is associated with the hemicelluloses. Several investigations have suggested that there are covalent bonds between hemicellulose and lignin, while there is no evidence that lignin is associated with cellulose (Eriksson et al. 1980; Obst 1982). Lignin acts in the cell walls providing fibre a good mechanical resistance (Navi and Sandberg 2012) as well as providing the hydrophobic surface of the fibre needed for the transport of water (Plomion et al. 2001).

1.1.5 Wood formation variation by cambium region activity

In seasonal climates, the cambial activity is largely dependent on temperature/ or photoperiod (Uggla et al. 2001). The greatest variation is typically found within an annual ring. The cambial cell starts the active growth at the beginning of spring, continues in summer, declines in the late summer or autumn, and stops in winter as dormant. The wood produced in the spring is called earlywood and that in the late summer or autumn is called latewood. The annual rings can often be easily distinguished in species with sharp structure and color contrast between latewood formed in one year and earlywood formed in the following year (Navi and Sandberg 2012), such as in the ring-porous hardwoods ash and oak, and in softwoods.

In temperate softwoods, earlywood is generally characterized by a lower density and thin-walled tracheids or fibers with large radial diameter, whereas latewood has high density and thicker cell walls with small tracheids/fibers radial diameter, see Fig. 1.10a. In ring-porous hardwoods, large vessels formed early in the season, while the thick-walled, strength-giving fibers are usually most abundant in the latewood (Fig. 1.10b). However, in many temperate species, differentiation of earlywood and latewood is slight and the annual growth rings are even difficult to recognize.

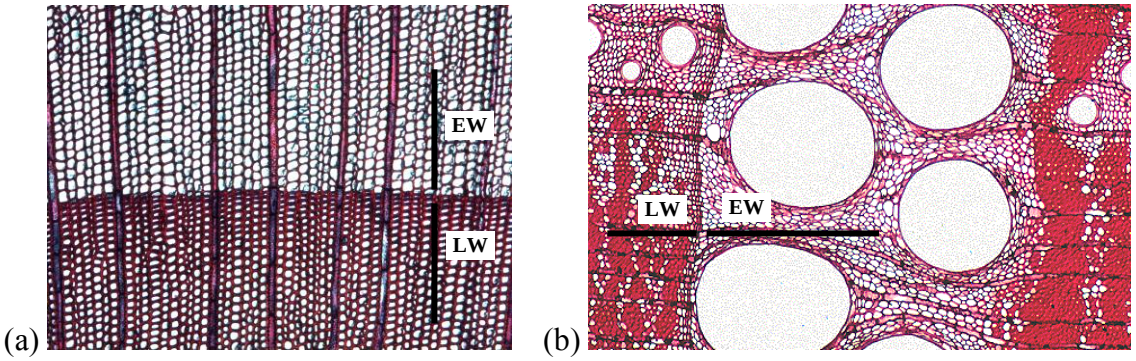

Figure 1.10 Cross section views of (a) a soft wood species (spruce) and (b) a ring-porous hardwood species (red oak) showing differences in earlywood (EW) and latewood (LW)

The cambial activity can also be influenced by the local conditions, i.e. unidirectional winds, snow, slope, or asymmetric crown shape (Plomion et al. 2001). When a tree grows on the slope or is tilted after an accident, the load around the periphery of the stem will be unbalanced. The cambium then starts to increase the cambial activity on one side of the stem and to produce modified wood to compensate the uneven load. This results in the eccentric cambial growth and the formation of reaction wood (Fig. 1.11). Softwood and hardwood adopt different strategies for the formation of reaction wood: in softwood, reaction will be produced by compression stress on the lower side of the tilted stem and is called compression wood, whereas in hardwood reaction is produced by tensile stress on the upper side denoted as tension wood. The developments of reaction wood aims to reorient the leaning stem or branch towards a more favorable position (Timell 1986).

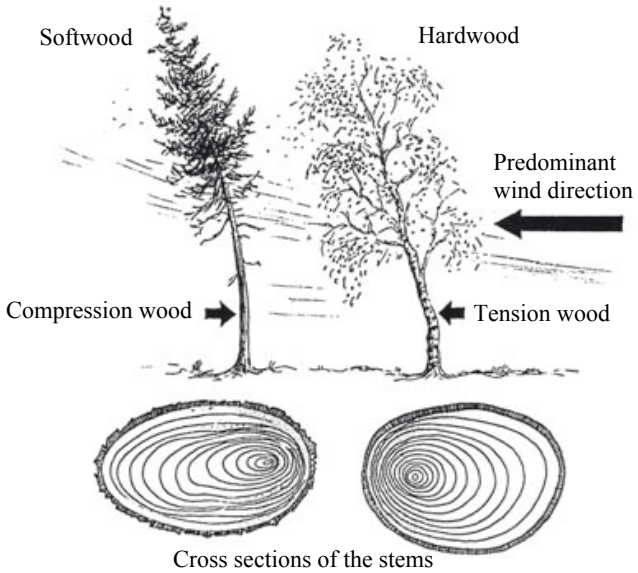

Figure 1.11 Formation of reaction wood in softwoods and hardwoods as a result of a predominant wind direction over a long time (from Navi and Sandberg 2012)

1.2 Tension wood

Reaction wood is often associated with stem eccentricity caused by stimulated cambial growth. Both tension wood and compression wood allow strongly heterogeneous growth stress repartitions at the periphery of stems, generating the bending moments required for

their shape control. Herein we will focus on tension wood. Tension wood differs from normal wood formed in the absence of stimulus, and from opposite wood located on the lower side of the leaning stem, in a number of biochemically, anatomical and mechanical characteristics (Pilate et al. 2004b). The introduction of tension wood will be presented from macro level, micro level and molecular level.

1.2.1 Macro level

The division and differentiation of the cambial initials is controlled differently between the upper and lower side of the trunk. The cell divisions are more activated on tension wood side (upper side) than opposite wood side (lower side). At the macroscopic level, this often leads to an eccentricity on the transverse section of stem, where tension wood side is often wider than the opposite side (Dadswell and Wardrop 1949). But it is also possible that tension wood is formed on the lower side of the trunk for a negative gravitropism (Onaka 1949) and the eccentricity is less obvious in some trees (Panshin and de Zeeuw 1980). In some cases, woolly zone or shiny appearance (Badia et al. 2005) on the machined surface of the log is also common, only for tension wood with a gelatinous layer.

The marked macro features of tension wood is the high longitudinal drying shrinkage compared to normal wood (Onaka 1949; Grzeskowiak et al. 1996; Clair et al. 2003; Yamamoto et al. 2005), which is paradoxical with the low microfibril angle in the cell wall (Chaffey 2000). Mechanically, higher longitudinal maturation stresses are present in tension wood than in normal wood (Fournier et al. 1994). Thus a high proportion of tension wood in a trunk is considered to be a major problem for industrial applications (Panshin and de Zeeuw 1980), as it increases the longitudinal, radial, and tangential shrinkage during the drying process.

1.2.2 Micro level

At the microscopic level, tension wood exhibits important changes in anatomy, chemistry and fibre wall structure in comparison with normal wood. Tension wood has fewer vessels (Jourez et al. 2001; Ruelle et al. 2006) and more fibres (Felten and Sundberg 2013) than normal wood. The fibres, which are the load-bearing cell type in the wood, are responsible for exerting the tensile stress in tension wood (Felten and Sundberg 2013). The most remarkable feature observed in tension wood fibres is the development of a peculiar layer, the so-called gelatinous layer (G-layer) on the lumen side of the fibre (Onaka 1949). However tension wood with high tensile stress but without typical G-layer is also common, which accounts for two third of tree species (Onaka 1949; Fisher and Stevenson 1981; Clair et al. 2006b).

- **Tension wood with G-layer**

The G-layer may be present in tension wood fibres in an additional layer on the lumen side (Fig. 1.12b), or may replace the S_3 layer (Fig. 1.12c) and even part or the entire S_2 layer of the secondary wall (Fig. 1.12d) (Wardrop and Dadswell 1955; Araki et al. 1983). Furthermore the G-layer can vary in its thickness from thin layer to thick layer or even fill the whole lumen of

the fibre (Coutand et al. 2004; Chang et al. 2009b). Due to the particular morphology, on sliding microtome sections, G-layer can be easily identified by its swollen appearance and the detachment from the adjacent layer. This artefact (Clair et al. 2005b) once hampered the understanding of the active role of the G-layer in tension wood properties. However, this detachment is useful as it allows G-layer to be isolated from transverse sections for chemical analysis (Norberg and Meier 1966; Nishikubo et al. 2007; Kaku et al. 2009; Olsson et al. 2011).

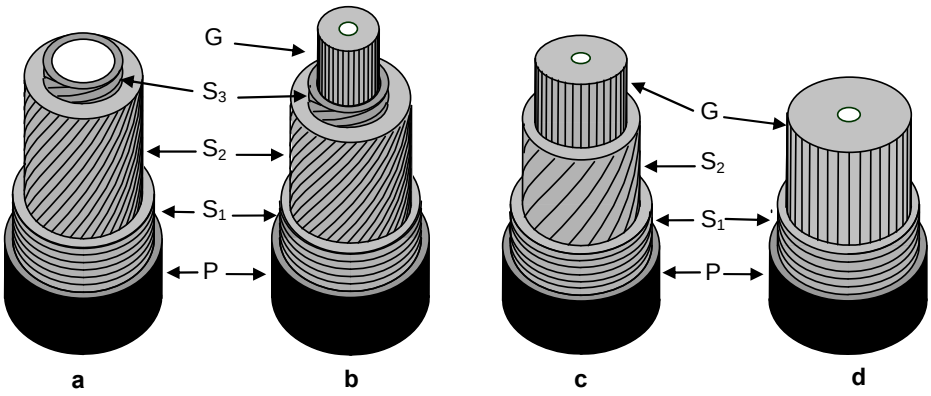

Figure 1.12 A schematic illustration showing the different cell wall layers of normal (a) and tension wood (b, c, d). (a): a normal wood fibre structure with $P+S_1+S_2+S_3$; (b): a G-fibre structure with $P+S_1+S_2+S_3+G$; (c): a G-fibre structure with $P+S_1+S_2+G$; (d): a G-fibre structure with $P+S_1+G$. P: primary cell wall; S_1, S_2, S_3: layers of the secondary wall; G: gelatinous layer in tension wood fibres (modified by Fang 2007)

The G-layer consists mainly of highly crystalline cellulose with microfibrils oriented nearly parallel to the fibre axis (Norberg and Meier 1966). Analyses from the last 10 years indicate that the G-layers in Populus also contain some non-cellulosic polysaccharides like xyloglucans (Nishikubo et al. 2007), pectins (Bowling and Vaughn 2008) and arabinogalactan proteins (AGPs) (Lafarguette et al. 2004; Andersson-Gunneras et al. 2006), which differ strongly from those in the adjacent secondary (S) layers that mainly contain xylans and glucomannans (Bowling and Vaughn 2008; Kim and Daniel 2012). More recently, Kim and Daniel (2012) also found xylan in the G-layer itself. However, the question of the composition is still matter of debate as recent work of F. Guedes proved the absence of xyloglucan (personal communication with F. Guedes and G. Pilate). The presence of lignin in the G-layer has been highly debated (Pilate et al. 2004a), since its presence in the G-layer (Yoshida et al. 2002a), in the lumen side of G-layer (Joseleau et al. 2004) or in the S-layer side of G-layer (Prodhan et al. 1995) has been reported. But all are in very low abundance, which may suggest the minor role of lignin for tension wood function (Felten and Sundberg 2013).

- **Tension wood without G-layer**

Even though the presence of G-layer is often used as an indicator of tension wood, a number of tree species form tension woods without the peculiar G-layer (Onaka 1949; Fisher and Stevenson 1981; Yoshizawa et al. 2000; Yoshida et al. 2002b; Clair et al. 2006b). Although in these species, the trees are able to keep efficiency to produce tensile stress as G-layer species. When G-layer is absente in tension wood, in many cases, the S_2 layer of fibres show the

difference with the corresponding opposite wood fibres and exhibit some similar features as the G-layers, such as a lower microfibril angle, an increased cellulose to lignin ratio, or a higher crystal size (Yoshizawa et al. 2000; Yoshida et al. 2002b; Ruelle et al. 2006, 2007). The low microfibril angle and increased cellulose amount in the S_2 layer of tension wood without G-layer strongly suggest that these are common features of tension wood.

1.2.3 Molecular level

The study of the structure and morphology of G-layer is even more important at molecular level because the well-oriented G-layer cellulose is responsible for generating tensile stress in the wood tissue (Clair et al. 2011). The gelatinous-looking structure of the G-layer inspired researchers to search for its gel-like properties. A high water-filled mesopore (pore size between 2 to 50 nm) of tension wood has been measured using nitrogen adsorption in chestnut (*Castanea sativa* Mill.) tension wood (Clair et al. 2008), poplar tension wood (Chang et al. 2011, 2012) and several tropical species (Chang et al. 2009b). However, a large variation exists in mesopore volume, peak pore size and pore shape depending on the proportion of G-layer and species. The mesopore of tension wood comes from cavities that would be between microfibrils of the G-layer as the high mesoporosity in G-layer tension wood is not shared by the non-G-layer species, where the mesopore volume is very low as in normal wood (Chang et al. 2009b).

The cellulose crystallite dimension is larger in tension wood than in normal wood, which has been observed in tension woods with G-layers (Washusen and Evans 2001; Muller et al. 2006) and without G-layers (Ruelle et al. 2007).

1.3 Micromechanical approach of maturation stresses

1.3.1 The origin of maturation stress

The term *stress* refers here to a force that presses or pulls on the wood (Kubler 1987). Growth stresses have been defined as "*the forces that develop in the wood of growing plants*" (Post 1977), which include support stress, resulting from the increasing weight of the tree, and maturation stress, appearing in wood fibres during its formation. Wood cells are produced in the cambium at the periphery of the stem. The young cambial cells experience cell elongation, secondary cell wall deposition, and lignification to become mature cells. Therefore the cell walls have the capacity to be stressed and exert forces only after they have acquired sufficient stiffness (Ohsako 1978). Therefore, the maturation stress appears in wood cells only during formation of their secondary cell wall. The maturation stress provides the trees with an essential adaptation to various terrestrial environments: achieving adaptive reorientations of the stems, or maintain at a constant angle during growth (Fournier et al. 1994; Alméras and Fournier 2009). At the microscopic level, the maturation stresses are generated during the cell wall maturation, as shown in Figure 1.13. During cells formation, the maturing wood cells tend to contract longitudinally and to expand laterally; but the contraction is impeded by the neighbour older wood cells, which are relatively stiff. Therefore the older cells stretch the

new cells, so that the longitudinal tensile stresses are induced. Concomitantly the lateral expansion of the new cells is restrained by the neighbour old cells, which leads to tangential compression stress in these new cells.

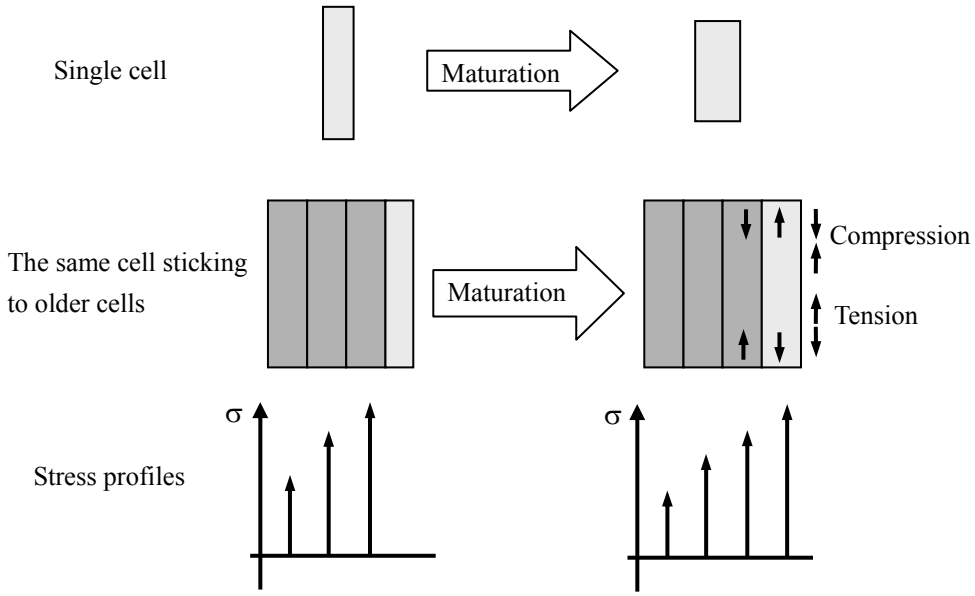

Figure 1.13 Principle of maturation stresses generation (from Clair 2001)

However, the trigger for cell tending to shrink, that is the mechanism of maturation stress generation is still unknown. In the widely accepted lignin swelling hypothesis (Boyd 1985), the stresses appears because the deposition of lignin in the cell wall matrix causes the lateral expansion of the wall. Such lateral expansion of the cell wall causes a tendency of contraction in longitudinal direction, while this tendency is impeded by the rigid neighbour cells. Consequently, tensile stress is generated. This mechanism is largely related to the angle of cellulose microfibrils, which control the anisotropy of strains of the fibre wall. It has been proposed as the primary cause of growth stress generation in normal and compression wood (Boyd 1950). However, this mechanism fails to explain the large tensile stress in tension wood, where the microfibrils are nearly parallel to the fibre axis (Norberg and Meier 1966). Bamber (1987, 2001) disputed the above lignin swelling hypothesis and proposed the cellulose tension hypothesis. In this theory, tensile stress originated from the contraction of cellulose microfibrils and lignin just played the role of connection and did not contribute to stress production. To explain the relation between microfibril angle and released maturation strains by the analytical model, unified hypothesis was necessary (Okuyama et al. 1994; Yamamoto 1998; Alméras et al. 2005). However, the triggers for cellulose tension and lignin swelling are still unknown and no direct evidence yet prove these hypotheses.

1.3.2 Growth stress in tension wood

In tension wood, longitudinal tensile stress far exceeds that of normal wood (Boyd 1950; Okuyama et al. 1994). Although there is some controversy regarding the origin of the tensile maturation stresses, when it is present, the G-layer is recognised as playing the essential role in the mechanism of stress generation in tension wood. First evidence comes from the

relationship between amount of G-layer and the stress level; the higher the amount of G-layers, the higher the tensile stress (Yamamoto et al. 2005; Clair et al. 2003; Fang et al. 2008). Second evidence, at the cell wall level, is the high contracting strain of G-layer when creating a free surface in a tension wood sample (Clair and Thibaut 2001; Clair et al. 2005a), proving that G-layer is not only the trigger but is also the support of the tensile stress. Finally, the observation of the cellulose lattice spacing changes in the fibre direction using synchrotron X-ray diffraction during stress release (Clair et al. 2006a) and following maturation process (Clair et al. 2011) revealed that tensile stress is directly supported by cellulose microfibrils and that the stress is generated synchronously with the synthesis of the G-layer in poplar tension wood. Thus the support of tensile stress generation in G-layer tension wood has been locked at the location of cellulose microfibrils (Clair et al. 2006a, 2011).

Since much research has been devoted to understand the function of G-layer in tensile stress generation, no literature is available for non-G-layer species, in which G-layer are not present but exhibiting high tensile stress. Some common structural aspect e.g. low MFA, increased cellulose and low lignin, are shared by both G-layer and non-G-layer tension wood species, thus the mechanism of tensile stresses could be speculated to be similar in both. Then it is questionable on the advantage/disadvantage of G-layer in the tensile stress generation in tension wood. More experimental evidences are needed to advance the further understanding of the tensile stress generation in tension wood, especially in tension wood without G-layers.

1.3.3 Mechanical modelling about growth stress generation

Although the mechanism of tension wood generation in G-fibres remains unknown, recent progress has greatly improved the knowledge towards elucidating the G-fibre functions. New hypotheses have been proposed and discussed to explain why and how an axial stress appears in tension wood fibres during their formation. The hypotheses are mainly divided into two categories: due to the swelling (or pressure) of the G-layer (Goswami et al. 2008), or due to the tension in microfibrils of G-layer (Okuyama et al. 1994; Yamamoto 2004; Nishikubo et al. 2007; Mellerowicz et al. 2008; Bowling and Vaughn 2008).

The G-layer swelling hypothesis proposed by Goswami et al. (2008) postulates that during cell maturation the stresses developed from the radial swelling of the G-layer are transfered to the adjacent S-layers, where the large MFA allows even a small lateral expansion into large longitudinal shrinkage. The proposed mechanism is based on the observation of the residual strains on the tissues after removing G-layer. But the postulated outward pressure exerted by the G-layer is not consistent with the G-layer behaviour during drying (Fang et al. 2007). As G-layer shrink outwardly because of the absence of reinforcement by a S_3 layer, G-layer in reverse is expected to swell inwardly because of the absence of S_3. Then G would not push on the G-layer as proposed by Goswami et al. (2008).

The microfibrils tension hypothesis seems more consistent with the recent observation of the cellulose microfibrils under tension during the maturation of G-layer in tension wood (Clair et al. 2011). However, it still remains to address the mechanism of maturation stress: what

generates this tension inside G-layer microfibrils? Yamamoto (2004) simulated the multilayered wood fibre by developing the G-fibre model and considered that the tensile stress emerged from the contraction of amorphous zones within the cellulose microfibrils (Okuyama et al. 1994; Yamamoto 2004). Except microfibrils itself, the matrix polysaccharides could also participate in tension generation by entrapment (Nishikubo et al. 2007; Mellerowicz et al. 2008). Xyloglucans or any other compact polysaccharide might play such a role (Gorshkova et al. 2010). But the chemical composition is still a matter of debate as xyloglucan was recently proved to be absent (personal communication with F. Guedes and G. Pilate, INRA France). The hypothesis of swelling reactions of pectin-like substances (Bowling and Vaughn 2008) seems more reasonable since the nanoporous structure of G-layer has been evidenced by nitrogen adsorption isotherms recently (Clair et al. 2008; Chang et al. 2009b).

However, the exact mechanism behind tensile stress generation in the cellulose microfibrils of tension wood fibres is still a matter of debate (Goswami et al. 2008; Clair et al. 2011; Mellerowicz and Gorshkova 2012). The hypothesis discussed above agrees that the G-layer is the primary source of tensile stress in tension wood, but different mechanisms proposed to elucidate its actions: either radial pressure or longitudinal tension.

Alméras et al. (2012) proposed a mechanism (Fig. 1.14) where the microfibrils in G-layer are not just parallel to each other but are partly transversaly-bonded. The stress would be transferred to the cellulose microfibrils by the swelling of the matrix in an interconnected network of cellulose microfibrils.

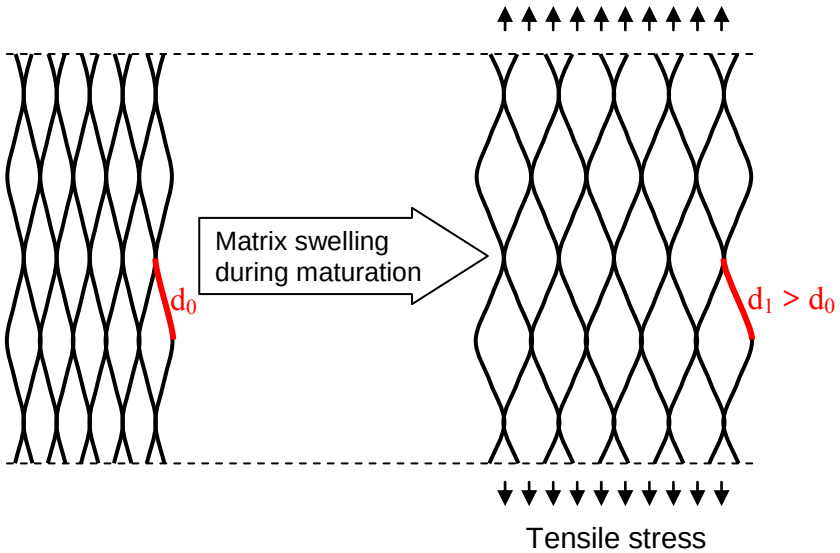

Figure 1.14 Hypotheses regarding the mechanism of tensile stress generation in cellulose microfibrils (from Clair 2013 after Alméras et al. 2012, unpublished)

This mechanism is based on the swelling properties of gels. Indeed, G-layer has a structure similar to gels with a large amount of water-filled mesopores (Clair et al. 2008; Chang et al. 2009b). Gels are known to be able to exhibit high shrinkage or swelling in response to physicochemical changes, like moisture level or ion concentration change. In angiosperm, similar cellulose-based hydrogels have been identified in the pit membranes of vessels and it

has been proposed that the microstructure change depends on the change of cation concentration (van Ieperen 2007). Therefore, physicochemical changes by pectin-like substances in the G-layer matrix could make swell or shrink the G-layer matrix and then be the driving force of the growth stress generation in tension wood. Based on this hypothesis, the strains induced from the tensile stress change should be associated with changes in the mesoporosity of the G-layer as well as macromolecular modifications, which are the main content of this study.

1.4 Conclusion

After reviewing the related work in literature, the origin of maturation stress in tension wood is still subject to discussion. In recent years, the study of tension wood attracted increasing interest since it has interesting mechanical properties, being capable of generating high tensional stress. Understanding the mechanism of maturation stress is essential to the understanding of plant organ movement (Moulia and Fournier 2009), and also provides the possibility for novel biomimetic developments in material science (Mellerowicz and Gorshkova 2012). To explore the origin of maturation stress generation is difficult since the generation process is dynamic in the living plant, and the studies are performed on the residual state of the maturation process. Whereas, the information reflected from the maturation process can always be traced by following the different growth stages, in this study, we will focus on the ultrastructure and chemical composition changes during tension wood maturation and try to advance the discussion on the origin of maturation stresses generation.

2. The basic principles of FTIR and N_2 sorption

As FTIR and nitrogen adsorption are the main tools used in this study, a general description of the basic principles is proposed in this chapter.

2.1. FTIR method

Infrared (IR) spectroscopy is certainly one of the most important analytical techniques available for the characterization of the chemical and physical nature of polymeric materials (Stuart 2004). One of the great advantages is that virtually any sample in virtually any state may be studied. Since the 1940s, infrared spectrometers have been commercially available (Stuart 2004). At that time, the instruments relied on prisms to act as dispersive elements, until the mid 1950s, diffraction gratings had been introduced into dispersive machines, which is the appearance of Fournier-transform spectrometers. This type of instrument exploits the well established mathematical process of Fourier-transformation and has greatly improved the quality of infrared spectra as well as minimized the time required to obtain data.

Infrared spectroscopy is a technique based on the principle that molecules absorb specific frequencies that are characteristic of their structure. The infrared spectrum of a sample is recorded by passing a beam of infrared light through the sample. When the frequency of the IR is the same as the vibration frequency of a bond, absorption occurs. By comparing the change of IR spectrum before and after adsorption, information about the molecules composing the material can be obtained. This is the basis of molecular absorption spectroscopy.

2.1.1. Basic theory of infrared spectroscopy

Infrared radiation is electromagnetic radiation that includes all the wavelengths between the visible and microwave regions of the electromagnetic spectrum. The IR region is usually subdivided into three regions: near-, mid- and far-IR, named for their relation to the visible spectrum. The ranges of the IR spectrum are summed up in Table 2.1.

Table 2.1 Infrared spectral ranges (from Settle 1997)

Infrared region	Wavelength range (μm)	Wavenumber range (cm^{-1})
Near-IR	0.78 - 2.5 μm	13,000 - 4,000
Mid-IR	2.5 - 50 μm	4,000 - 200
Far-IR	50 - 1,000 μm	200 - 10

This study focuses on the most frequently used in mid IR region, between 4000 and 700 cm^{-1}. The higher energy near-IR can excite overtone or harmonic vibrations. The mid-IR may be used to study the fundamental vibrations of most molecules. The far-IR has low energy and may be used for rotational spectroscopy. At temperature above absolute zero, all the atoms in molecules are in continuous vibration with respect to each other. Each atom has three degree

of freedom. For molecules with N atoms in them, linear molecules have 3N-5 degree of freedom, whereas nonlinear molecules have 3N-6 degrees of freedom. Simple diatomic molecules have only one bond and only one vibrational band. Polyatomic molecules can vibrate in different ways. The major types of molecular vibrations are stretching and bending. The various types of vibrations are illustrated in Fig. 2.1. Infrared radiation is absorbed and the associated energy is converted into these types of motions. Stretching vibrations are categorized as symmetric or asymmetric and bending vibrations are characterized as rocking, scissoring, wagging, or twisting.

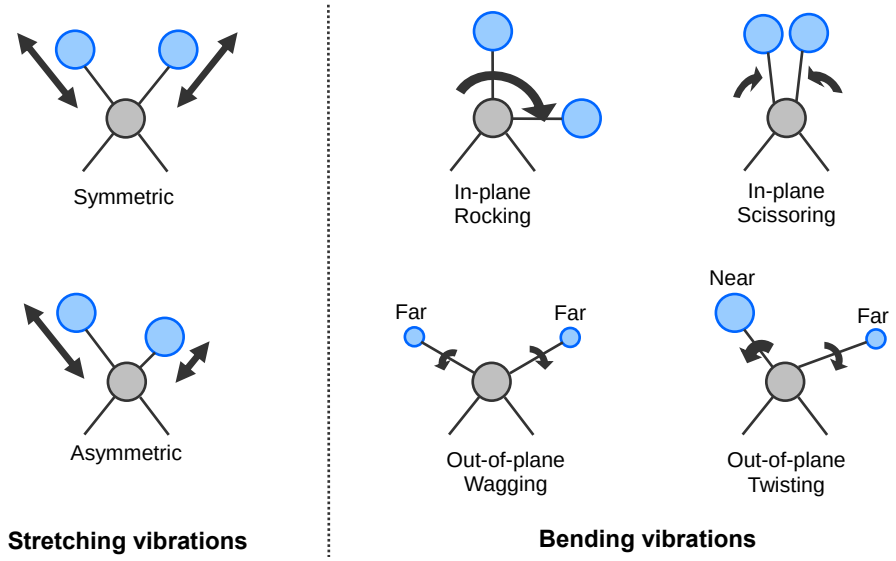

Figure 2.1 Different types of molecular vibration with arrows demonstrating the particular motions (modified from Settle 1997)

Each of a molecule's modes of vibration occurs at a specific frequency and will consequently absorb electromagnetic radiation of this frequency. These unique frequency absorptions result in a characteristic spectral profile for a given molecule or molecular compound.

2.1.2. Instrument of infrared spectroscopy

In simple terms, the infrared spectra are obtained by detecting changes in transmittance (or absorption) intensity as a function of frequency. Most instruments measure IR radiation using dispersive spectrometers or Fourier transform spectrometers. Both spectrometers use similar components, but the method in which spectral data is captured is inherently different. In a typical dispersive IR spectrometer, radiation from a broad-band source passes through the sample and is dispersed by a monochromator into component frequencies (Fig. 2.2). Then the beams fall on the detector, which generates an electrical signal and results in a recorder response. Fourier transform spectrometers have recently replaced dispersive instruments for most applications due to their superior speed and sensitivity. In an FTIR spectrometer, the monochromator is replaced by an interferometer (Fig. 2.2), which divides radiant beams into two paths and recombines them to generate interference signals to the sample before reaching a detector.

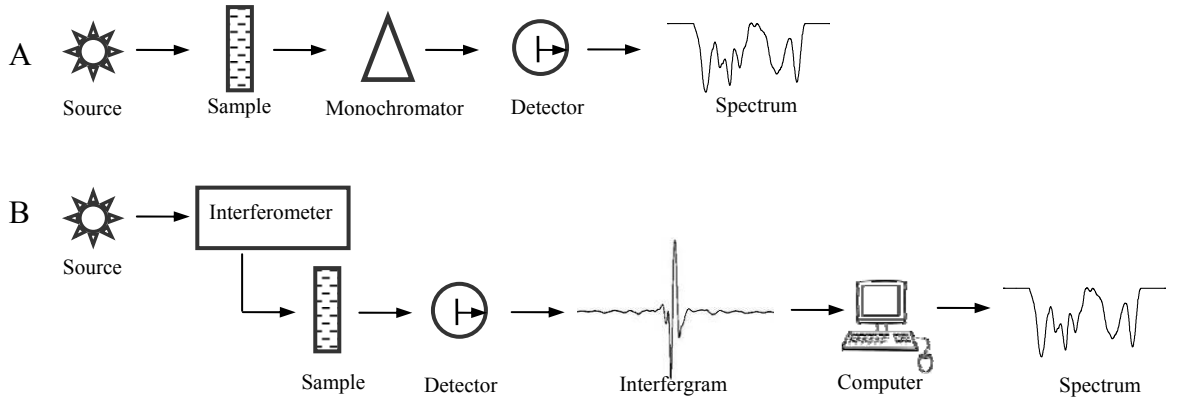

Figure 2.2 Comparison of basic components of dispersive IR spectrometer and FTIR spectrometer

The most commonly used interferometer is a Michelson interferometer. It consists of three active components: a moving mirror, a fixed mirror, and a beam splitter (Fig. 2.3). By the beam splitter, infrared radiation containing all wavelengths splits into two equal beams. One beam is transmitted towards the moving mirror and the remaining half is reflected to the fixed mirror. After the divided beams are reflected from the two mirrors, they are recombined at the beam splitter. Due to changes in the relative position of the moving mirror to the fixed mirror, an interference pattern is generated. The resulting beam then passes through the sample and is eventually focused on the detector.

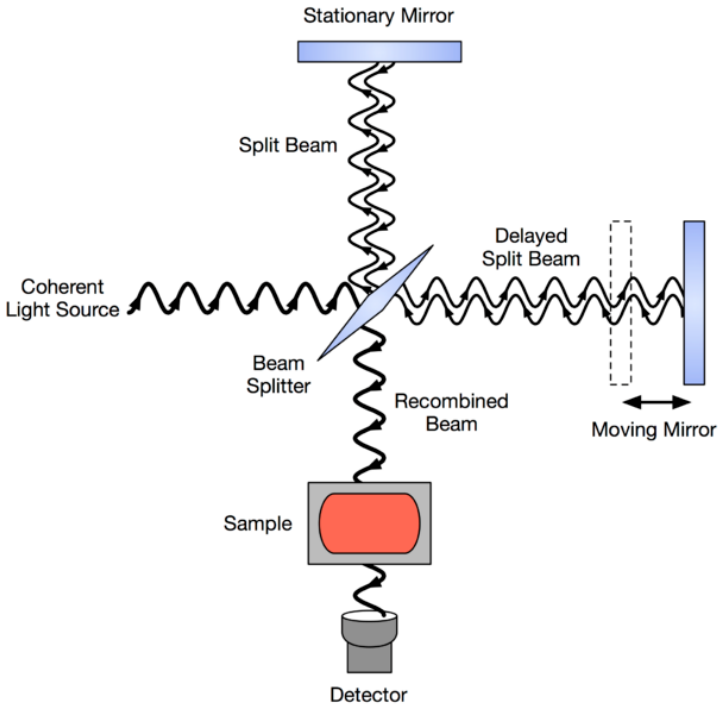

Figure 2.3 Schematic diagram of the Michelson interferometer (from Wikipedia)

An interferogram is obtained by varying the displacement of the movable mirror, which can be explained qualitatively from Fig. 2.4. When the mirrors are equidistant from the beam splitter, the two halves of the recombined beam will be totally in-phase, the power will be a maximum and constructive interference occurs. When the moving mirror travels in either direction by the distance λ/4 (one-quarter wavelength), the optical path is changed by λ/2. The

two beams are 180° out of phase with each other and thus a destructive interference occurs. Further motion will bring the two beams again in phase with each other and result in another constructive interference. This difference is termed as the displacement of the movable mirror or the retardation x. The plot of the output power from the detector versus x is called an interferogram. The interferogram is then converted into the FTIR spectra by applying the mathematical method of *Fourier-transformation*:

$$S(v) = 2\int_{-\infty}^{\infty} I(x)\cos(2\pi vx)dx$$

where S(v) is the intensity at wavenumber v, $I(x)$ is the radiation intensity dependent on the retardation x.

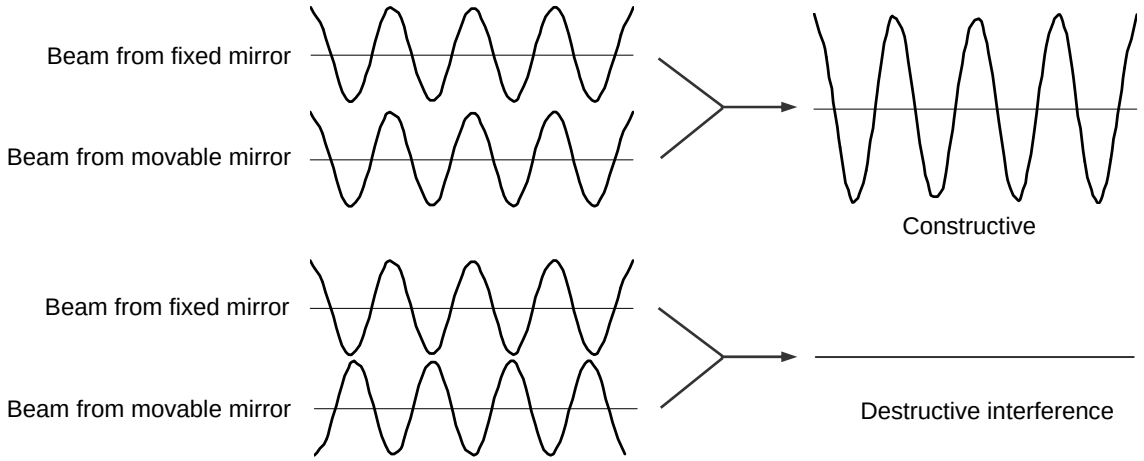

Figure 2.4 Constructive and destructive interference

2.1.3. FTIR microspectroscopy technique

It is possible to combine an infrared spectrometer with a microscope facility in order to study very small samples and provide a continuous view of the sample during data collection (Katon 1996). Figure 2.5 illustrates the layout of a typical infrared microscope assembly. Infrared radiation from the spectrometer is focused onto a sample placed on a standard microscope x-y stage. After passing through the sample, the infrared beam is collected by a Cassegrain objective which produces an image of the sample within the barrel of the microscope. A variable aperture is placed in this image plane. The radiation is then focused on to a small-area mercury cadmium telluride (MCT) detector by another Cassegrain condenser. The microscope also contains glass objectives to allow visual inspection of the sample. In addition, by switching mirrors in the optical train, the microscope can be converted from transmission mode to reflectance mode.

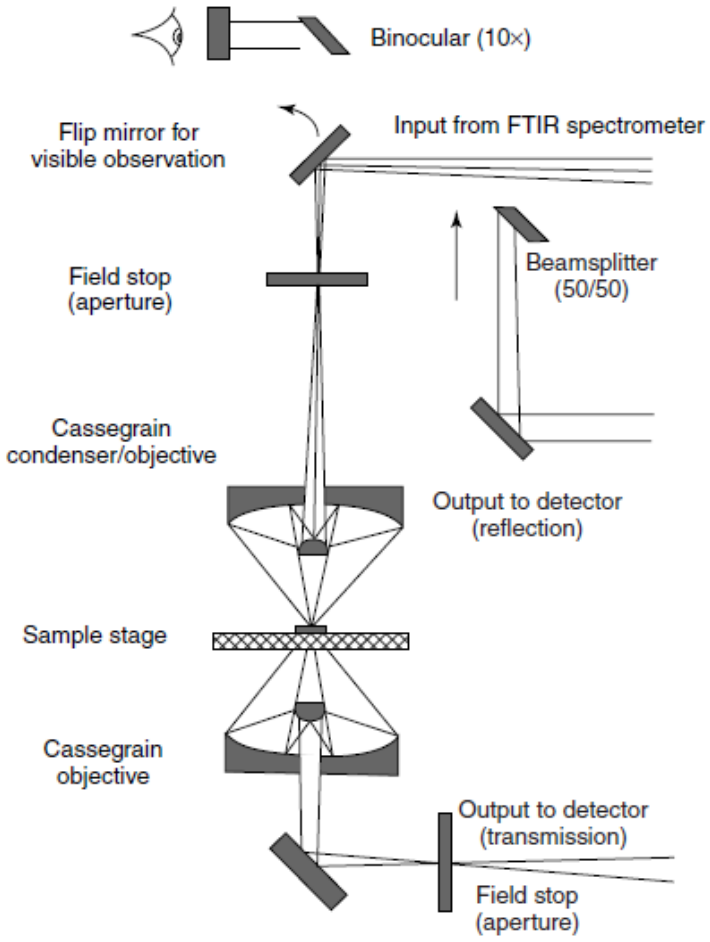

Figure 2.5 Layout of a typical FTIR microspectrometer (from Katon et al. 1989)

In the case of the equipment used in this study, a Perkin Elmer Spotlight 400, the sample stage is integrated to the microscopy devise. Two scan modes can be distinguished in the mid-IR region: the point- and imaging-scan mode. For the point-scan mode, the area of interest is first selected successively from a visible image (Fig. 2.6a) displayed by a CCD camera and then point scanned with mid-IR radiation. Spectra are then collected continuously from the area selected in the sample (Fig. 2.6b). The centre of each measurement area is recorded as the position of each spectrum and one average spectrum is collected from each measuring area.

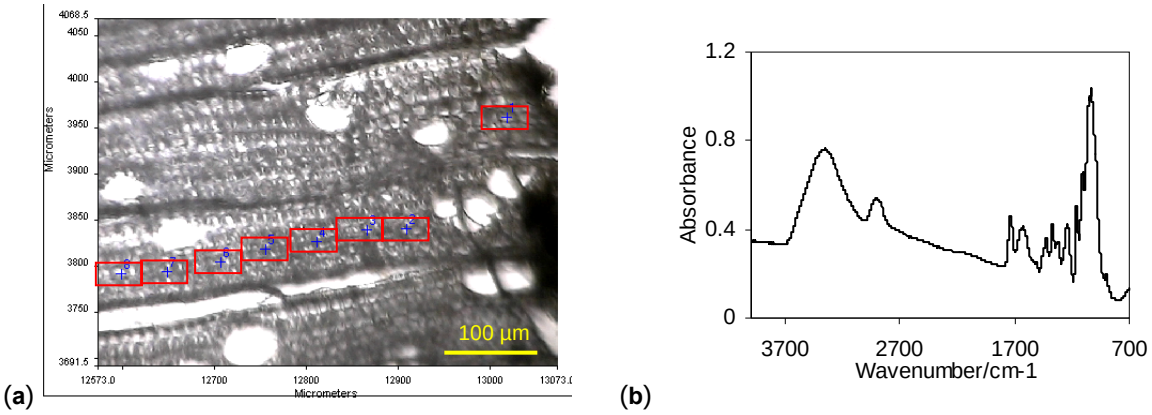

Figure 2.6 (a) Visible image of transverse section of poplar tension wood showing the measuring area (rectangle: 50×25 µm, R×T) and (b) An example showing one average spectrum collected form one measuring area

For imaging mode, scanning is performed by an array detector, i.e. a linear array 6.25 µm mercury cadmium telluride (MCT) detector (cooled in liquid nitrogen). The detector moves step by step across the preset area (red rectangle in Fig. 2.7a) until an IR full-spectral image including the spectral information (Fig. 2.7b) has been collected. This means that the sample is analyzed locally, at a micrometer scale with a pixel resolution of 6.25 µm, where one pixel has a size of 6.25 µm × 6.25 µm from which one infrared spectrum is collected. Thus for the given measuring area 25 µm×100 µm, 64 different spectra can be recorded with a pixel resolution of 6.25 µm × 6.25 µm. In the case of our experiment, imaging mode is used and expected to locate the spectrum at each pixel (or spatial location). Whereas the high noise to signal ratio in a single spectrum make it difficult to recognize the structure, finally the mean spectrum of the whole image is used for further data processing.

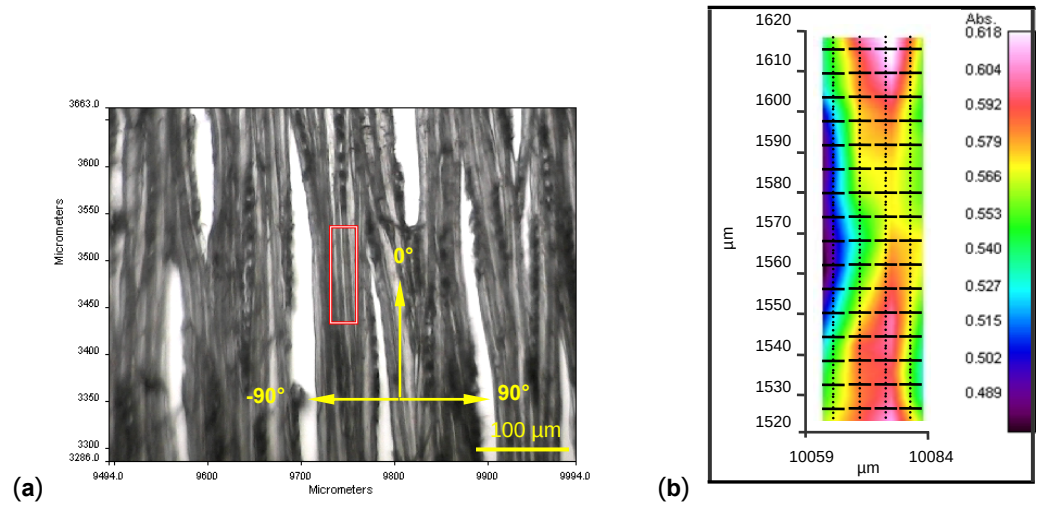

Figure 2.7 Visible images of (a) tangential section of poplar tension wood showing the measuring area (25×100 µm, T×L) and the polarization directions of the measurement, (b) IR full-spectral image of the measuring area, also showing 64 pixels selected from which 64 spectra can be analyzed

It is also possible to perform IR scanning with a polarisation, where the IR radiation is polarised by a gold wire grid polariser, in our case, from -90˚ to 90° polarisation in relation to the fibre axis with an interval of 10˚. In this way, information on the orientation of specific groups and of the polymer chains containing these groups in the wood structure can be obtained at a µm scales (Olsson et al. 2011). For the precise determination of the orientation of different polymers, the following equation can be used:

$$ROA=I_p/I_{max} \qquad (2.1)$$

where ROA is the relative orientation absorbance, Ip is the intensity of the absorbed IR radiation at a given polarisation angle for a specific wavenumber and Imax is the maximum intensity in the polarisation interval (-90° to 90°) for the specific wavenumber.

In the case of wood sample, the IR absorbance of functional groups with vibrations orientated parallel to the fibre axis will have the highest absorbance at low polarisation angles, whereas functional groups oriented perpendicular to the fibre axis will have the highest absorbance at high polarisation angles. Figures 2.8a and 2.8b shows an example of the relative orientation

absorbance distribution for the typical bands assigned to cellulose depend on the polarisation angle according to Eq. (2.1).

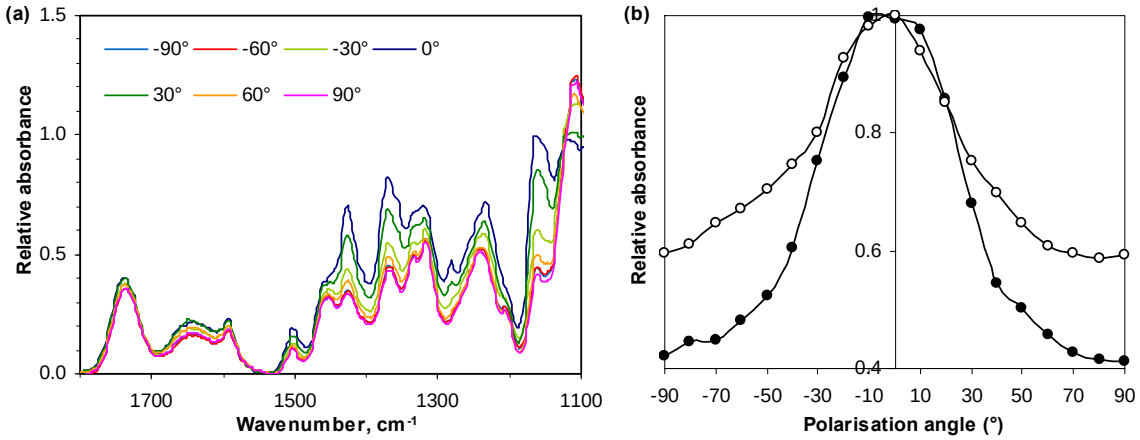

Figure 2.8 (a) Polarised FTIR spectra after normalization from 1,800 to 1,100 cm^{-1} in sample I and (b) the relative orientation distribution of specific absorption peak at 1160 cm^{-1} of 2 samples (according to equation (2.1)). Curve with solid symbols is drawn from the polarized FTIR spectra presented in (a) and curve with open symbols from another sample (polarized FTIR spectra data not shown)

From Fig. 2.8b, it is obvious that the cellulose signals in both samples show the highest intensity at the low polarisation angle around 0^{o}, indicating that cellulose in both samples are oriented more or less parallel to the fibre axis. However, relative absorbance allows to identify the degree of order. In sample I, most cellulose chain is organised parallel, whereas the other sample show a much larger distribution in angle even if they are centre around 0°. Therefore polarized FTIR spectroscopy allows investigating, for example, the orientation change of different wood polymers and thus obtaining a clearer picture of cell wall development, which is one of the objectives of this study.

2.2. Nitrogen sorption method

2.2.1. Phenomenon of adsorption

When a gas or vapour is brought into contact with a solid, the molecules either enter the inside of the solid, or remain on the outside adsorbed on the surface. The former phenomenon is termed *absorption* and the latter *adsorption*. The solid that takes up the gas is called the *adsorbent*, and the gas or vapour taken up on the surface is called the *adsorbate*. Molecules and atoms can attach themselves onto surfaces in two ways, namely, physical adsorption (physisorption) and chemical adsorption (chemisorption). During the process of physisorption, there is a weak van der Waals attraction of the adsorbate to the surface and the chemical identity of the adsorbate remains intact, i.e. no breakage of the covalent structure of the adsorbate takes place. In chemisorption, the adsorbate sticks to the solid by the formation of a chemical bond with the surface and the interaction is much stronger than physisorption. The chemisorption, which involves an exchange of electrons between the solid surface and the adsorbate molecules, modifies the properties of solid and therefore can not be used to characterize the texture of materials. This is why we discuss here only the physical adsorption

which does not involve the forces responsible for the interactions between the adsorbate molecules and the solid surface and does not change the properties of the material studied.

In practice, physisorption measurements are widely used for the determination of the structure of porous materials. Of all the many gases and vapours, which are readily available and could be use as adsorbate, nitrogen has remained universally. Measurement of the amount of adsorption/condensation as a function of pressure can give information on the pore structure. The amount of gas adsorbed at equilibrium depends upon pressure, temperature and the chemical nature of the solid surface. However, if temperature and pressure are kept constant, the amount adsorbed will depend on the nature of the solid surfaces, for example, surface area, porosity and the chemical nature of solid surface.

2.2.2. Classification of pores

The porosity of a solid refers to the volume that is not occupied by solid matter (Sing et al. 1985) and is usually classified according to the pore size. The pores are classified according to their effective width (IUPAC classification), the pores width which are less than 2 nm are called micropores; the pores width which are greater than 50 nm are called macropores; the pores of intermediated width which are between 2 nm and 50 nm are called mesopores. The size of adsorbed molecule and nature of adsorbate-adsorbate interactions are critical in determining the adsorption characteristics. In micropores the walls are very close so that interaction is very high leading to enhanced adsorption at a given relative pressure. In mesopores, adsorption is by capillary condensation showing a hysteresis loop (the adsorption and desorption curves follow different paths).

Pores can have a regular or, more commonly, an irregular shape, either an ink-bottle shape (pore body larger than pore mouth) or a funnel shape (the opposite). Pores can be closed (not accessible from the outside), blind (open only at one end), or through (open at both ends). Each pore can be isolated or, more frequently, connected to other pores to form a porous network (Rouquerol et al. 1999) (Fig. 2.9). The surface and structural properties of pores are the means by which the material physically interacts with gases, fluids and other solids. Hence, information on the textural features such as the surface area and porosity (pore size and pore volume) appears to be especially useful information.

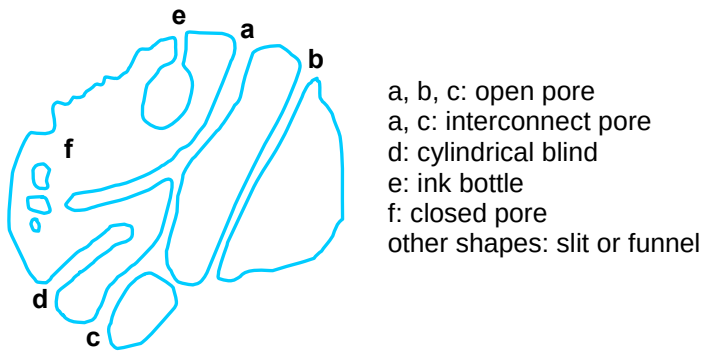

Figure 2.9 Physical picture of porous solid (from Rouquerol et al. 1999)

2.2.3. Classification of adsorption-desorption isotherms

The relationship between the amount of gas adsorbed at any given relative pressure and at constant temperature can be represented graphically by means of an adsorption isotherm. The determination is usually carried out at the temperature of liquid nitrogen. The amount of gas adsorbed can be measured by the volumetric method (Gregg and Sing 1982). Successive amounts of gas are introduced to a confined volume. At each defined pressure, the system is allowed sufficient time to equilibrium, which corresponds to a series of single points on the adsorption isotherm. Conversely, the desorption isotherms are achieved by measuring gas removed as relative pressure is reduced. Fig. 2.10 presents the different stages during the relative pressure increasing.

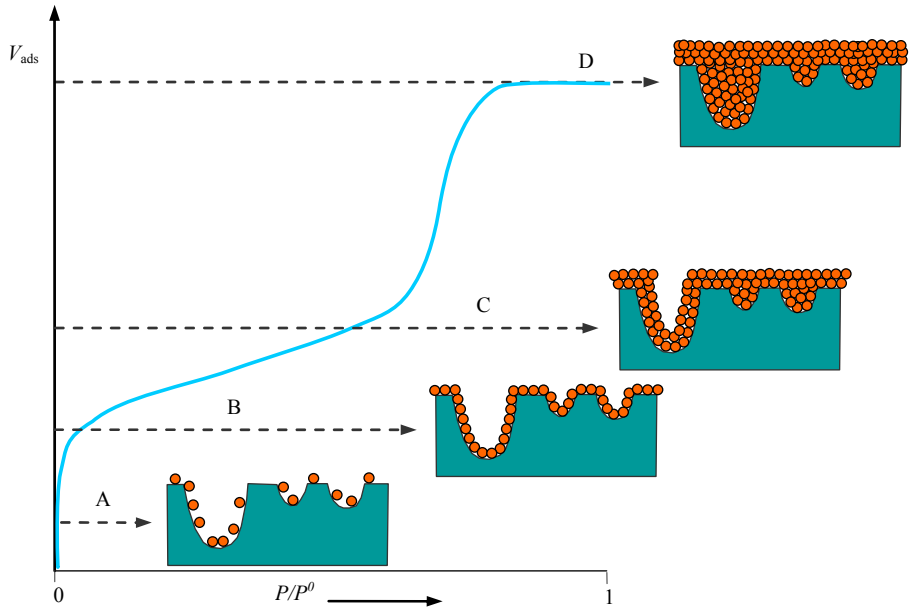

Figure 2.10 Physical adsorption procedures

At lower relative pressure, the isolated sites on the adsorbent surface begin to adsorb gas molecules (A). As relative pressure increases, coverage of gas molecules increases to form a monolayer (one molecular thick) (B). Further increase relative pressure will cause the beginning of multilayer coverage. After reaching a critical film thickness (C), capillary condensation occurs essentially in the core of the pore (from C to D). Still further increase in the relative pressure will cause complete coverage of the adsorbent and fill all the pores (D).

Isotherm shape depends on the porous texture of the materials. According to IUPAC classification six types of isotherms can be distinguished (Sing et al. 1985), but only three are usually found in the adsorption on polar materials (type I, type II and type IV in Fig. 2.11).

Type I is obtained with microporous (pore size < 2 nm) solids. The adsorption takes place at very low relative pressure region (the ratio between pressure and saturation pressure p/p° < 0.3) because of multidirectional interactions between pore walls and adsorbate.

Reversible type II isotherm is characteristic of non-porous or macroporous (pore size > 50 nm) solids. If the knee of the isotherm is sharp, the uptake at point B – the beginning of the middle

linear section – provides a measure of the monolayer capacity, from which the surface area of the adsorbent can be calculated.

Reversible type III isotherm is convex to the relative pressure axis over its entire range and therefore does not exhibit a point B. Isotherms of this type are not common and can be found in the adsorption of water vapour by a hydrophobic surface. In such cases, the adsorbent-adsorbate interaction is weak as compared with the adsorbate-adsorbate interactions.

Characteristic features of type IV isotherm are its hysteresis loop, which is associated with capillary condensation taking place in mesopores and the limited uptake at $p/p^o < 1$. The initial part of the isotherm is attributed to monolayer-multilayer adsorption since it follows the same path as the corresponding part of the type II isotherm. Type IV isotherms are characteristic of many mesoporous industrial adsorbents.

The isotherm of type V is much rare. It is related to the type II isotherm in that the adsorbent-adsorbate interaction is weak, but is obtained with certain porous adsorbents.

Type VI isotherm occurs as a results of stepwise multilayer adsorption on uniform non-porous surfaces. The adsorption of each layer takes place within a limited range of p/p^o and lateral interactions between the adsorbed molecules contribute to the layer-by-layer process.

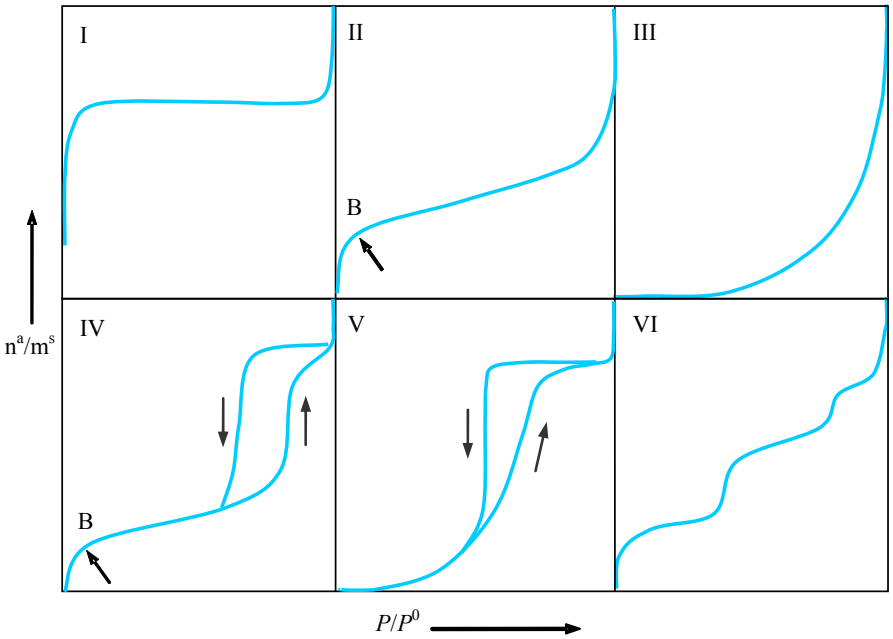

Figure 2.11 Classification of physical adsorption isotherms given by IUPAC (from Sing et al. 1985). P/P^0: relative pressure; n^a/m^s: quantities adsorbed per gram sample expressed as mmol g^{-1}

The adsorbate desorption, after saturation is reached, is the opposite of the adsorption, but evaporation from mesopores usually takes place at a pressure lower than that of capillary condensation giving a hysteresis loop (the desorption and adsorption curves follow different paths). The reason for the hysteresis is that the formation of the meniscus in capillary condensation is an activated phenomenon, while the retreat of meniscus in evaporation is usually an equilibrium phenomenon. Pore shape affects the mechanisms of condensation and evaporation and four types of hysteresis have been recognized according to IUPAC classification (Sing et al. 1985) (Fig. 2.12).

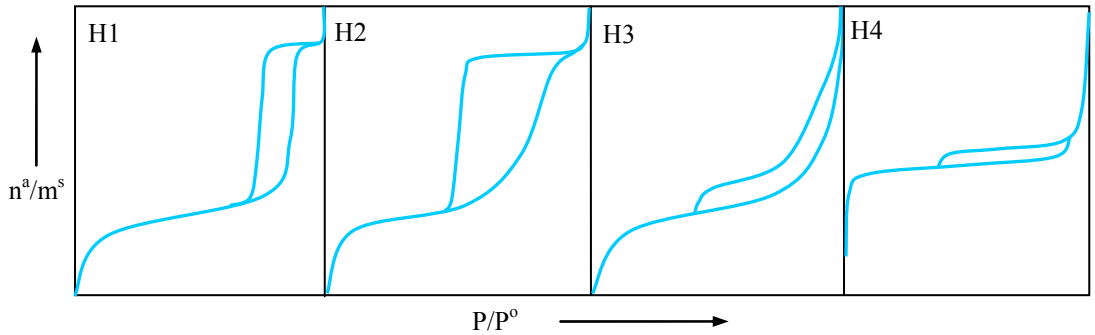

Figure 2.12 The four hysteresis loops of adsorption isotherms by IUPAC classification (from Sing et al. 1985). P/P^o: relative pressure; n^a/m^s: quantities adsorbed per gram sample expressed as mmol g^{-1}.

The shape of hysteresis loops have often been identified with specific pore structures. Type H1 loop exhibits parallel and nearly vertical branches at the capillary condensation region, which is often observed in the case of adsorbents having a high degree of pore-size uniformity. Type H2 hysteresis loop has a triangular shape and a steep desorption branch, while the adsorption branch gently increases at the capillary condensation region. It is often considered to be a result of the presence of mesopores with narrow mouth and wide body (ink-bottle pores), but it is recognised that this provides an over-simplified picture (Sing et al. 1985). Recent research results suggest that regarding a relatively uniform cylinder-like pores system, if the desorption branch happens at the proximity of a low-pressure limit of adsorption-desorption hysteresis, H2 hysteresis loops can also be observed (Zhao et al. 2012). Isotherms with type H3 loop that do not reach saturation at high relative pressure are often reported for materials in which aggregates of plate-like particles slit-like mesopres with wide distribution of pore size. Type H4 loops feature parallel and nearly horizontal branches over a wide range of p/p^o and their occurrence is attributed to adsorbents with microporous sheets having narrow slit-like pores. Mesoporous materials with lots of structural defects can also lead to the type H4 loop (Zhao et al. 2012).

2.2.4. Determination of surface area (BET method)

This theory was formulated in 1938 by Brunauer, Emmett and Teller to formalize the multilayer adsorption phenomena on the surface (Brunauer et al. 1938). The BET theory was an extension of the Langmuir theory, which relates the monolayer adsorption of gas molecules (Fig. 2.13a). The BET theory extends the Langmuir theory to multilayer adsorption (Fig. 2.13b) and describes the surface as a whole adsorption sites having the same adsorption energy. Each adsorbed molecule acts as a new location from the adsorption layer. Adsorption is therefore described as a different filling layers adsorption sites having two energy levels of adsorption: E1 for adsorption sites on the surface (corresponding to the first layer) and for the sites of EL for all of the following layers.

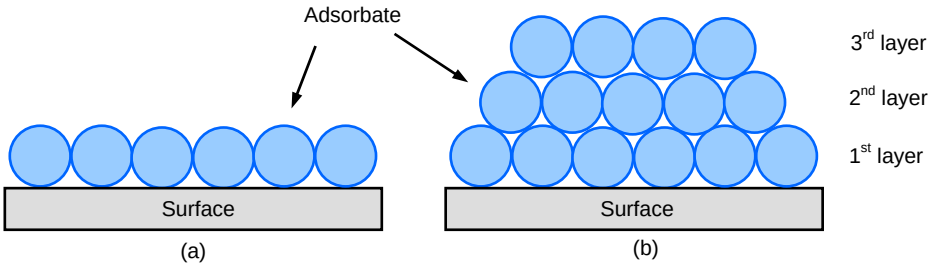

Figure 2.13 Schematic representation of the adsorption of gas molecules onto the surface of a sample showing (a) the monolayer adsorption model assumed by the Langmuir theory and (b) the multilayer adsorption model assumed by BET theory

This theory then leads to the equation, called BET:

$$\frac{\frac{P}{P_0}}{V_{ads}(1-\frac{P}{P_0})} = \frac{1}{V_m C} + \frac{C-1}{V_m C} \times \frac{P}{P_0} \qquad (2.2)$$

where V_{ads} is volume adsorbed ($cm^3.g^{-1}$), V_m the monolayer capacity ($cm^3.g^{-1}$), P/P^0 the relative pressure (P and P^0 are the equilibrium and the saturation pressure of adsorbates at the temperature of adsorption) and C is a constant related to the enthalpy of adsorption (BET constant).

Equation (2.2) is an adsorption isotherm and can be plotted as a straight line with $1/\{V_{ads}[(P^0/P)-1]\}$ on the y-axis and P/P^0 on the x-axis according to experimental results. This plot is called a *BET plot*. The linear relationship of this equation is maintained only in the P/P^0 range of 0.05 to 0.3. The value of the slope and the y-intercept of the line are used to calculate the monolayer adsorbed gas quantity V_{ads} and the BET constant C.

The widely application of the BET method is the calculation of the surface area (often termed *BET area*). When the area of the solid is completely covered with a layer of adsorbed molecules, the value of the specific surface area S_{BET} can be easily calculated by:

$$S_{BET} = \frac{V_m \cdot n_a \cdot a_m}{m \cdot V_L}$$

where V_m is the monolayer adsorbed gas quantity, n_a is Avogadro constant (6.02×10^{23}), a_m is the equivalent maximum cross sectional area of nitrogen molecules (the value generally accepted is 0.162 nm^2), m is the mass of adsorbent and V_L is the molar volume of nitrogen gas (22414 cm^3).

Substituting into the above data, the specific surface area S_{BET} (m^2/g) by nitrogen adsorption method is given by:

$$S_{BET} = 4.36 \cdot V_m / m$$

2.2.5. Assessment of mesoporosity

Many methods are now available to estimate the pore sizes and their distribution. BJH (Barrett-Joyner-Halenda) and BdB (Broekhoff-de Boer) are classical mesopore size distribution calculation methods, which are based on pore filling (Lowell et al. 2003). DR (Dubinin-Radushkevic), HK (Horvath-Kawazoe), and SF (Saito-Foley) are the models based on micropore filling in different types of materials, and can be used for micropore size distribution calculation. The emerging method of NLDFT (non-local density functional theory) is explored based on the normal DFT (density functional theory) method, and can measure both micropores and mesopres (Zhao et al. 2012).

The BJH and BdB methods are built on the Kelvin equation (Formula 2.3), in which the Kelvin radius r_k is a function of relative pressure P/P^0.

$$r_k = \frac{-2rV_L \cos\theta}{RT \ln(P/P_0)} \tag{2.3}$$

where r is a constant related to surface tension of liquid adsorbate; V_L is the molar volume of adsorbate; θ is the contact angle between adsorbate and interior surface of cylinder pores; and T is adsorption temperature.

Adsorbed layers of molecules form on the pore walls before condensation fills the pores. Therefore if the pore radius of a cylindrical pore is r_p and the actual pore diameters are corrected by adding the multilayer thickness t of the adsorbed gas layer to r_k (Fig. 2.14).

$$r_p = r_k + t \tag{2.4}$$

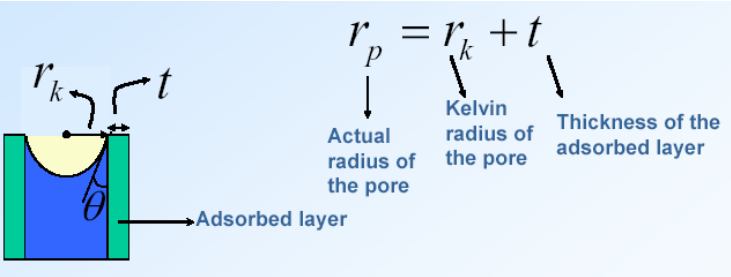

Figure 2.14 Schematic diagram of the multilayer thickness as well as the radius of curvature for a meniscus

Correspondingly, for a parallel-shaped slit, the slit width, d_p, is given by

$$d_p = r_k + 2t \tag{2.5}$$

Values of the multilayer thickness t, required for in Equations (2.4) and (2.5) are either interpolated from experimental t-curves or calculated using Halsey equation (Halsey 1948), which for nitrogen takes the form (2.6),

$$t = 0.354 \times \frac{5}{\ln\left(p/p_0\right)}^{0,333} \tag{2.6}$$

The pore size distribution is usually presented in the graphical form, $\Delta V_p/\Delta r_p$ vs. r_p. If r_1, r_2, $r_3 \ldots r_{i-1}$, r_i are the pore sizes at different relative pressure, $V(r)$ is the distribution function of pore volume, then the pore volume at r_i region can be expressed as

$$\Delta V_i = \int_{rpi}^{rpi-1} V(r)dr$$

and $\Delta V_i/(r_{pi}-r_{pi-1})$ as the differential pore size distribution. Generally, the adsorption branch of isotherm is preferred for pore size calculation, on the ground that it is more likely to represent the real sizes of the pores (Zhao et al. 2012). In particular, it is found that the pore size distribution curves obtained from desorption branch always show a false peak at 4 nm, which is thought to be made by the pore connectivity and is almost independent of the nature of the porous adsorbent (Sing et al. 1985).

In the BJH model, it is hypothesized that materials have cylinder-like pores in which multilayer adsorption could result in capillary condensation and the pressure at which capillary condensation occurs is determined by the pore sizes. This assumption reflects the real adsorption-desorption process in most mesoporous materials, thus the BJH model is always adopted for characterization of mesoporous materials. However, the sizes estimated from BJH normally have a relatively large difference with the real cases, in particular, when pore sizes are smaller than 5 nm, or the mesoporous materials owing relative large pore sizes (Zhao et al. 2012). The BdB model is just an improvement of the BJH model, which additionally considers the different adsorption thickness in the size-different pores. When pore sizes are larger than 5 nm, the BdB model is more accurate in calculating the pore sizes (Lukens et al. 1999). In this study, BdB model was adopted for pore size distributions calculation, which has been proved more accurate than the commonly used BJH method (Barrett et al. 1951; Galarneau et al. 1999).

Based on the general principles of nitrogen adsorption method, it is possible to apply this technique to measure the mesoporosity of tension wood and obtain the texture information during maturation, which is also one of the objectives of this study. In actual practice, the implement of nitrogen adsorption method on wood is relative new comparing to chemical materials. The difference in material properties determines the difference in actual operation. Thus, the developed methodologies for wood are explained in the following chapter.

3. Developed methodologies for wood

3.1. Optimization of experimental parameters for mesoporosity measurement in wood

Nitrogen adsorption method, typically used for the characterization of adsorbents or inorganic catalysts, has been recently applied to the texture study of biological materials such as tension wood (Clair et al. 2008; Chang et al. 2009b). As a porous material, wood has wide range pores from nanometer size to millimeter size which are occupied, *in vivo*, by water molecules. Prior to nitrogen adsorption measurements, the occupied pore space should be emptied by using various drying pre-treatment. Thus the choice of drying method directly affects the final results of mesoporosity measurement. Herein, the optimized experimental parameters for drying methods and dehydration solutions, as well as the tips and experience during experiment are discussed.

3.1.1. The selection of drying method

Usually the direct evaporative drying is avoided because the direct liquid-gas transition (green arrow in Fig. 3.1) inevitably results in the collapse of the network structure and completely loses the mesoporosity inside the wood samples (Clair et al. 2008). Instead of direct drying, freeze drying and CO_2 supercritical drying were often adopted. Freeze-drying works by freezing the material and then reducing the surrounding pressure to allow the frozen water in the material to sublimate directly from the solid phase to the gas phase (blue arrow in Fig. 3.1). Supercritical drying, on the other hand, goes around the high temperature, high-pressure side (red arrow in Fig. 3.1) and passes through the supercritical region where the shrinkage due to capillary pressure is prevented and the aerogel formed is expected to reproduce the original texture of hydrogel in the dry state (Pierre and Pajonk 2002; Cansell et al. 2003).

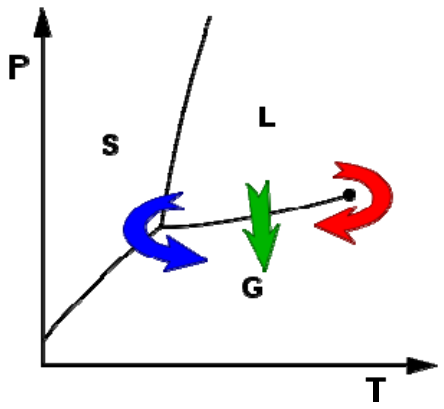

Figure 3.1 Typical phase diagram (from Wikipedia). Green arrow: ordinary drying with the direct liquid-gas transition; blue arrow: freeze drying brings the system around the triple point, where the three states of gas (G), liquid (L), and solid (S) coexist; red arrow: supercritical drying goes beyond the critical point of the working fluid avoiding the direct liquid-gas transition. P: pressure; T: temperature

Here, freeze drying and CO_2 supercritical drying were examined to search for the suitable one for wood samples, at the same time, ordinary drying (evaporation) was also tested for comparison. Experiments were performed on poplar tension and opposite woods. The macroscopic shrinkage due to each drying process was measured along longitudinal (L-) and tangential (T-) directions of the samples. Then the dried samples were tested on a micromeritics ASAP 2020 volumetric apparatus (Fig. 3.2) at 77K for nitrogen sorption measurements.

Figure 3.2 Equipment of ASAP 2020 physisorption analyzer

Figure 3.3 shows the macroscopic shrinkage of tension and opposite wood samples in L- and T- directions. The shrinkage values from CO_2 supercritical drying comprised the strains from ethanol solution dehydration and drying process itself. As expected, ordinary drying caused the largest deformation in both directions for both tension and opposite woods. Compared with CO_2 supercritical drying, freeze drying did not show obvious advantage, with large shrinkage close to ordinary drying. Nevertheless, the measured shrinkage from CO_2 supercritical drying was low and confirmed the effectiveness of supercritical drying to prevent most of the deformation of the wood samples.

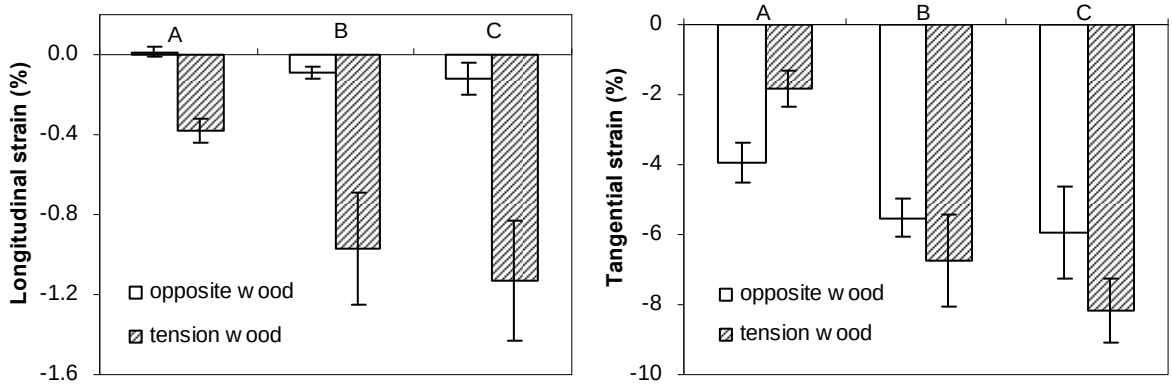

Figure 3.3 Longitudinal and tangential shrinkage of poplar tension wood and opposite wood upon different drying pretreatments. A: CO_2 supercritical drying; B: freeze drying; C: ordinal drying. Error bars show 95% confidence intervals

When these dried samples were subjected to mesoporosity measurements, the difference between the different drying methods was more significant at micro-level. Here, only tension wood samples were analysed due to the very low porosity in opposite wood (Clair et al. 2008; Chang et al. 2009b). It is evident from Figure 3.4 that only supercritical dried tension wood presents an isotherm of type IV with a typical hysteresis loop and adsorbs a much larger amount of nitrogen than the other two dried samples. Supercritical dried tension wood presents a high surface area (15 m^2/g) which is completely lost when the twin wood sample is freeze dried (0.97 m^2/g) and evaporatively dried (0.22 m^2/g).

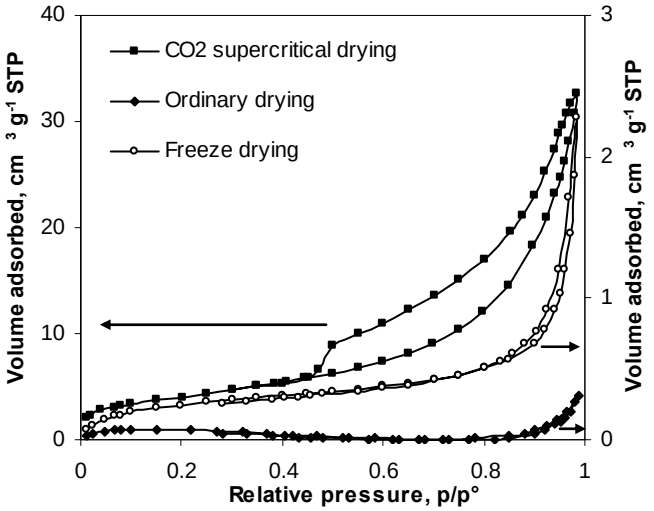

Figure 3.4 Nitrogen adsorption-desorption isotherms of poplar tension wood with different drying methods (left axis: CO_2 supercritical drying, right axis: ordinary drying and freeze drying)

From macro- and micro- results above, CO_2 supercritical drying is the primary drying pretreatment, providing a gentle process that can prevent most of the deformation and keep the micro-structure.

3.1.2. The selection of solvent for CO_2 supercritical drying

During CO_2 supercritical drying, the temperature raised the critical temperature, the liquid CO_2 changes to supercritical phase and is therefore extracted without surface tension effects able to distort morphology and ultra-structure. Because no interface is formed, this drying method provides a gentle process to produce aerogels (highly dispersed gels in gas environment) from hydrogels (gels formed in water). Since liquid CO_2 is not sufficiently miscible with water, it is necessary to use an intermediate fluid which is miscible with both water and liquid CO_2. In practice, intermediate fluids commonly used are methanol, ethanol, acetone, etc. However, the dehydration with solvent was suspected to modify the structure. In a previous study (Chang et al. 2009a, 2012), made before my PhD, we tested the effect of the solvents on a set of twin samples by measuring both the macroscopic strain and the resulting microstructure.

Dehydrations were performed in four serial solutions (ethanol, acetone, acetonitrile, and isopropanol) of increasing solvent concentration (10, 30, 50, 70, 90%, and anhydrous). Dehydration by a direct exchange in anhydrous ethanol repeated several times was also tested

to check the effect of serial dehydration on final dimensions. The dehydrated samples were then dried in the supercritical conditions to form aerogels and submitted to nitrogen adsorption-desorption measurements to evaluate the effect of solvent dehydration on gelatinous layer texture. A significant non-linear swelling was observed in tangential direction with the maximum swelling at intermediate solvent concentration. Figure 3.5 shows the maximum and the final strains during solvents substitutions in L- and T- direction. Along the longitudinal direction, tension wood shrunk proportionally to the increase of solution concentration, the maximum and final strains were therefore the same in this direction.

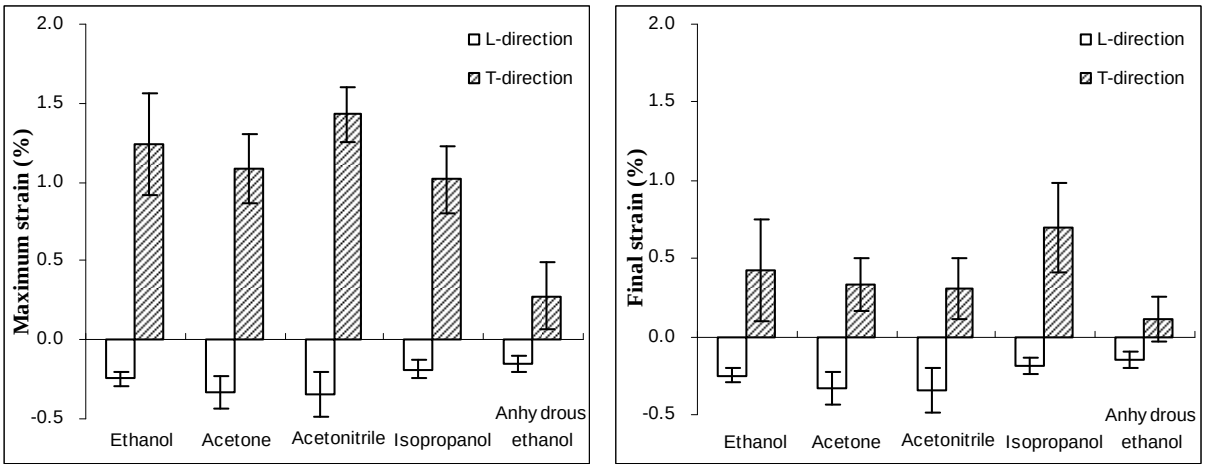

Figure 3.5 The maximum and final strains during solvents substitution along longitudinal and tangential directions in poplar tension wood. "Ethanol" referes to ethanol series of graduated increasing concentration, whereas "anhydrous ethanol" referes to direct transfere from pure water to pure ethanol. *Error bars* show 95% confidence intervals

From Figure 3.5 it can be seen that in L-direction, the more polar solvents (ethanol and isopropanol) bring the lowest effect both in the maximum and final dimensional deformations. In T-direction, the wood expressed less strain when under pure solvents (the final state) than when subject to mixed organic-water solvents (the maximum strain). When samples were dehydrated in anhydrous ethanol directly, the deformation value was slightly lower to the series ethanol in L-direction and much lower in T-direction. This shows that dehydration with solvents produces a certain degree of deformations during exchange, which is expectable to modify microstructure.

Nitrogen adsorption-desorption isotherms and pore size distribution determined from the nitrogen adsorption data by the method of Broekhoff and de Boer (1967) are given in Fig. 3.6. Concerning the shape of the isotherms, the hysteresis loop and pore size distribution, there is difference between samples exchanged with the different solvents but the defence is small enough to be attributed to the natural variability of tension wood with different amount of gelatinous layer from sample to sample. This can be seen more clearly from the pore size range distribution.

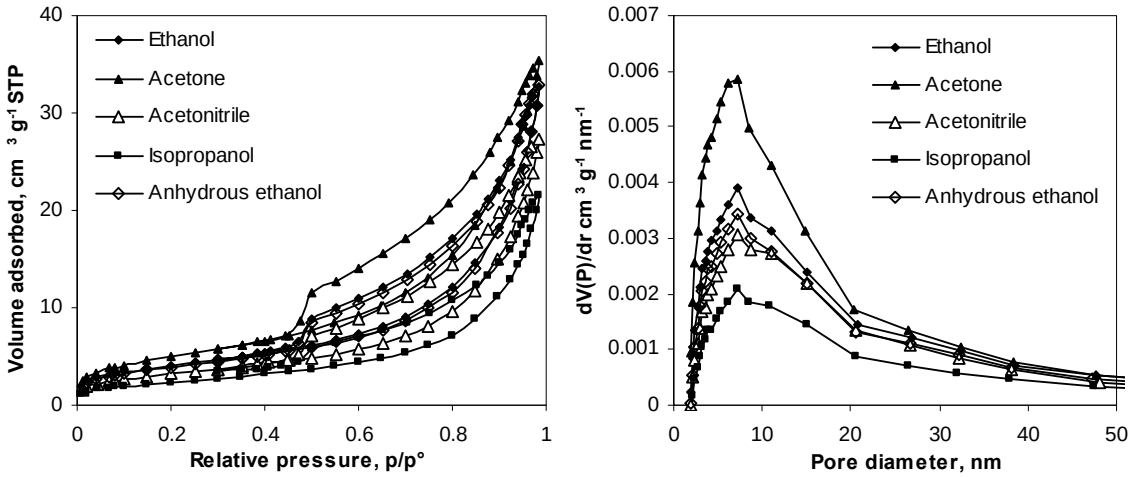

Figure 3.6 Nitrogen adsorption-desorption isotherms and pore size distribution of solvent-substituted poplar tension wood

In this study, in addition to pore size distribution determined by BdB method, the pore size range was calculated from adsorption pore size distribution diagrams (Fig. 3.7) after integration of the area under the curve of pore size distribution. Corresponding pore size at 50% of the volume and the range between 25% and 75% of the volume were plotted as the median pore size, and pore size range distribution, respectively.

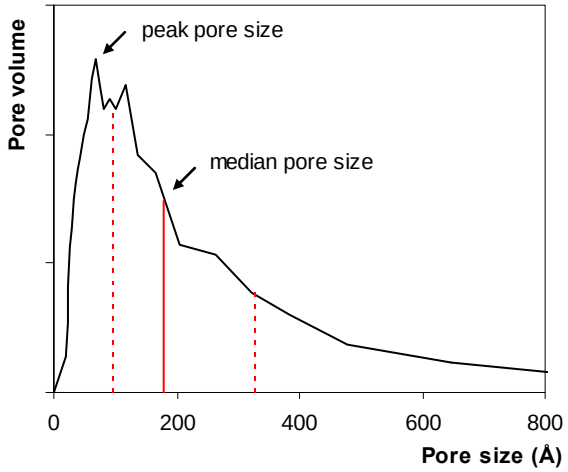

Figure 3.7 Representation of the median pore size and pore size range distribution calculated from the adsorption pore size distribution (Broekhoff and de Boer method). 50% of the pore volume has pore size in between the two vertical dotted lines (25% and 75%). Plane vertical line represents the median pore size (50%).

The peak pore size was identical for all treatments. According to calculation of Figure 3.7, the pore size range distribution as well as the mesopore volume is shown in Fig. 3.8. The pore size range distribution was similar for different solvent-substituted samples with median pore size 17 nm from range 10 to 32 nm. Only acetone treatment shows a significant lower median pore size compare to other treatments. This could be suspected as a modification link to the process or could be considered as the variability between samples.

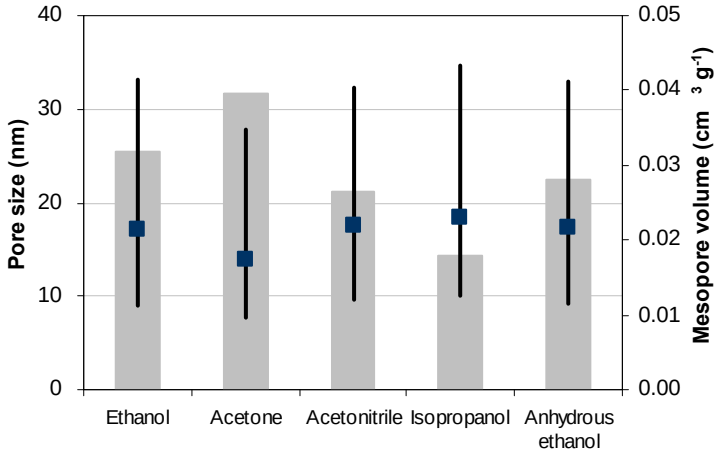

Figure 3.8 Median pore size (filled square), pore size range distribution (straight lines), and mesopore volume (histogram) of solvent-dehydrated poplar tension wood

The way of analysis (macroscopic deformation and mesoporosity measurement) did not allow us to see a significant difference between different solvent-substituted samples, but these results undoubtedly improve our understanding on the interactions between wood and organic solvents.

As isopropanol shows the high T- strain and acetonitrile shows the higher L- strains, because ethanol is much easier to use, we choose to use ethanol. Comparing the dehydration with ethanol series, direct dehydration in pure ethanol exchange shows some advantage especially the less strain in T-direction. However, this experiment was performed on mature wood, which was supposed to be less fragile than maturation wood and isolated G-layer. Considering the comparability of our results with other literatures, series ethanol dehydration was kept as the primary solvent for sample preparation including massive wood, differentiating wood and fragile isolated G-layers.

3.1.3. Experiment tips and experiences

As one of the most basic characterization method, nitrogen sorption method is widely used for catalyst study and material research, but only recently applied to the texture study of tension wood (Clair et al. 2008; Chang et al. 2009b). The significant difference between chemical materials and wood materials directly determines the operational difference during sample preparation. Herein, some tips and experiences concerning nitrogen adsorption experiment are summarised for further promotion.

- **The size of wood sample**

Theoretically, the sample size has no influence on the results. But considering the narrow neck and limited space (1.27 cm outside diameter) of sample tube (Fig. 3.9), sample with smaller sizes are recommended in order to more easily slide into and out of the sample tube.

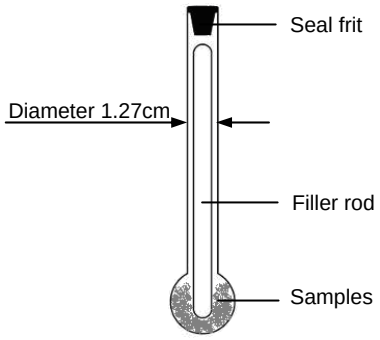

Figure 3.9 Sample tube used for nitrogen adsorption measurement

Due to the relatively low specific surface area of wood materials compared with chemical materials, more amount of sample are needed for analysis depending on the type of wood materials (e.g., tension wood with thick G-layer, wood near cambium zone, normal wood, etc.). Table 3.1 shows the approximate relationship between the specific surface area of sample and the sample dry mass needed. In practical operation, excessive samples are to be avoided. This may cause the less-tightened contact of seal frit to sample tube, and may eventually cause the analysis disruption of the instrument.

Table 3.1 Sample mass needed for nitrogen adsorption measurement

Specific surface area (m^2/g)	<1	1-3	3-10	10-30	30-100	100-800	>800
Sample dry mass for analysis (g)	>5	5-3	3-2	2-1	1-0.3	0.3-0.15	<0.15

Smaller sizes of samples are favourable for sample preparation, but it also increases the risk of air drying. It is recommended that, whenever possible, specimens are kept under water condition during the whole preparation.

- **CO_2 supercritical drying**

The supercritical drying is the key step to perform the nitrogen adsorption analysis successfully. In this study, the dehydrated samples were introduced in a Polaron 3100 apparatus (Fig. 3.10) which was then filled with liquid CO_2.

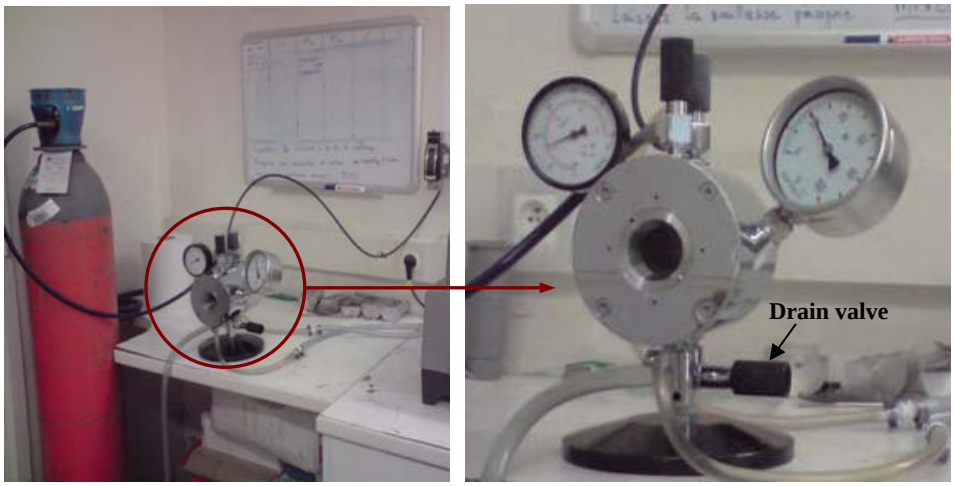

Figure 3.10 CO_2 supercritical drying device

Samples immersed in liquid CO_2 for 2 to 3 hours. The time mentioned refers to specimens less than 1mm in thickness. For larger or dense pieces a longer time was necessary. During the substitution process, it is necessary to open the drain valve (Fig. 3.10) to remove the substitution liquid and fill with liquid CO_2 to maintain the liquid level. This action should be continued every 10-15 min interval until flushing all of the substitution liquid. It is strongly recommend that the substitution step should be carried out thoroughly, because the more care taken with this the better the result. Figure 3.11 gives an example of twin specimens with two extreme immersion times: one hour and one night. The conditions of exchange (different immersion time) appears to be as important as the nature of the solvent.

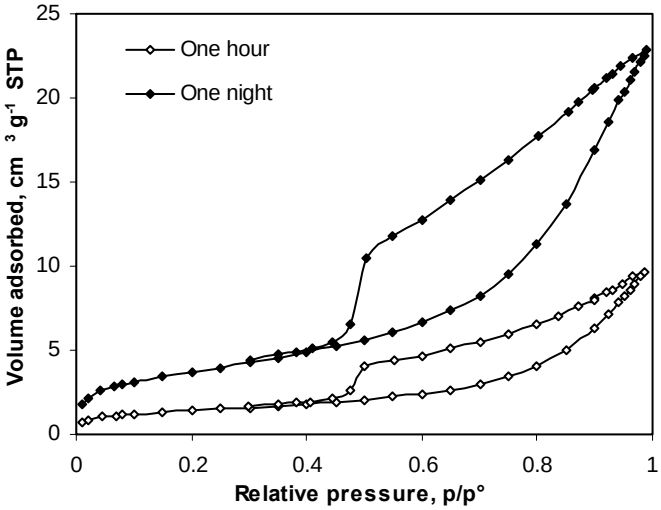

Figure 3.11 The effect of immersion time in liquid CO_2 on the nitrogen isotherms of chestnut tension wood

Another challenge of supercritical drying for wood is the specimen holder, the standard specimen holders are not suitable for wood specimens with smaller size, especially not available for isolated G-layer which has average dimension in 20-40 μm. In this case, dialysis membrane is used for molecules exchange and longer time (6-7 h) is needed for substitution.

- **Specify the step of relative pressure for adsoption-desorption procedure**

Compared with the multi steps for sample preparation, the nitrogen adsorption analysis performs much more procedure and automatic with less operator error. For the selection of analysis conditions, usually different types of files containing complete pressure tables are included in the ASAP 2020 software. In practice, we created an analysis conditions especially for wood materials by specifying the pressure points in the pressure table. In our case, the number of step between relative pressure p/p° 0.7-0.9 was increased in order to increase the resolution and distinguish more than one peak around the peak pore size (between 6 and 12 nm).

3.2. Optimisation of the experimental procedure for G-layer isolation

The occurrence of the G-layer is the most typical feature of the tension wood, and many studies mainly focus on producing G-layer species. As much research has been devoted to

understand the chemistry and ultrastructure of the G-layer, the identification or the separation of G-layer becomes more and more common for the preliminary sample preparation. Here, we explore the optimized methodologies concerning G-layer studies from the aspects of identification, measurement and isolation, aiming to make the sample preparation easier and faster.

3.2.1. Identification of G-layer

In our study and more generally in the micro-structural studies of G-layer, identifying the occurrence of G-layer is a common step to verify the severity of tension wood. In view of the peculiar composition of G-layer, which is cellulose rich and devoid of lignin, the use of stains makes it possible to prove the presence or absence of G-layer in wood tissues. There are several staining techniques that can be used to differentiate lignified and unlignified tissues, including Maüle reaction, zinc-chloro-iodide, and safranin O counterstained with fast green or astra blue or alcian blue (Gram and Jorgensen 1951; Rawlins and Takahashi 1952; Vazquez-Cooz and Meyer 2002; De Micco and Aronne 2007). Here, 20 µm microtome sections of poplar tension wood (with G-layer) were examined by light microscopy after treatment with four dyes: safranin O, which stains cellulose and lignin; fast green, as well as astra blue and alcian blue, which stain cellulose green or blue only in the absence of lignin. Eight staining protocols (Table 3.2) were investigated to search for the simple and reliable one for G-layer identification. The precise procedures for each protocol are described in the ***Annex I***.

Table 3.2 Eight staining protocols for G-layer identificaiton

Protocol	Staining technique
A	Safranin O (with bleach water)
B	Astra blue in alcoholic solution (with bleach water)
C	Alcian blue 8GX in alcoholic solution (with bleach water)
D	Safranin O and astra blue in alcoholic solution (with bleach water)
E	Safranin O and alcian blue 8GX in alcoholic solution (with bleach water)
F	Safranin O and alcian blue 8GX in acidified solution (with bleach water)
G	Safranin O and fast green (without bleach water)
H	Safranin O and fast green (with bleach water)

3.2.1.1. Single-staining and comparison of astra blue and alcian blue

The single-staining of safranin O shows that safranin O has strong affinity with cellulose (A in Fig. 3.12). All the tissues in the sections stained red with a darker red in cell corner. No difference was observed between the alcoholic solutions of alcian blue and astra blue (B and C in Fig. 3.12), both dyes show clear colour contrast with darker blue in un-lignified G-layers, and light blue in lignified cell walls. Compared to the single-staining of safranin O, the single-alcoholic solution stain of astra blue or alcian blue can be used as the rapid method for G-layer identification.

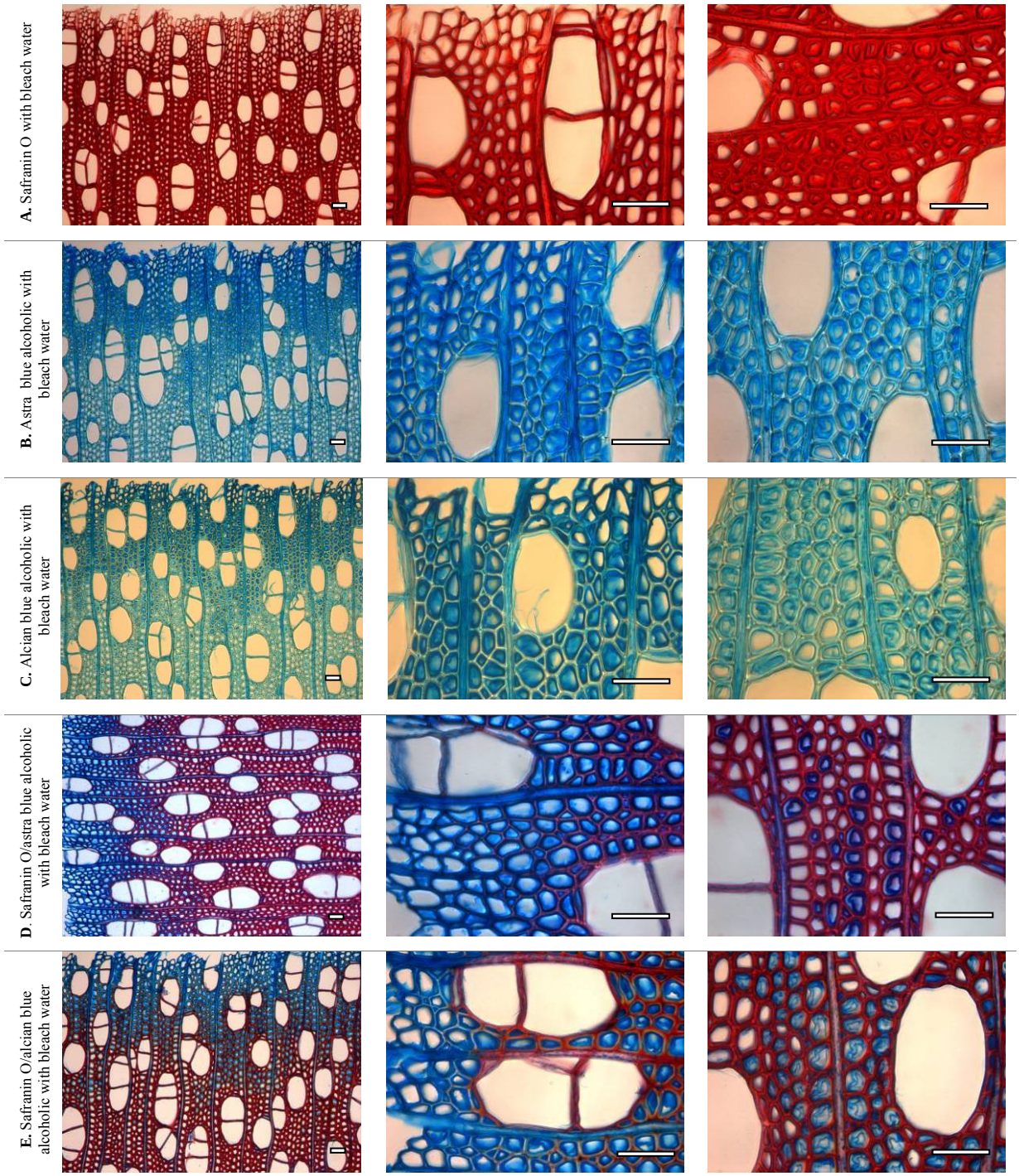

Figure 3.12 Cross sections of poplar tension wood stained with different protocols (A, B, C, D, and E are different protocols as shown in Table 3.2). Three microscopic images are displayed for each protocol showing different regions: maturating xylem, near cambium zone, and mature xylem respectively. Scale bar: 50 µm

3.2.1.2. Double-staining with or without bleach water

Usually, astra blue or alcian blue was used in association with safranin as combining staining for strong contrast, as protocols D and E in Fig. 3.12. Excellent colour contrast was observed with lignified cell wall layers stained in dark red, while not-fully mature cell wall and un-lignified G-layers stained in blue. However, when alcian blue dissolved in acidified solution, strong colour contrast can only be observed in phloem not in xylem (F in Fig. 3.13) where lignified cell walls stained in deep red and G-layer stained in very light blue or colourless.

This combining stain method is more effective for the identification of gelatinous fibres in phloem.

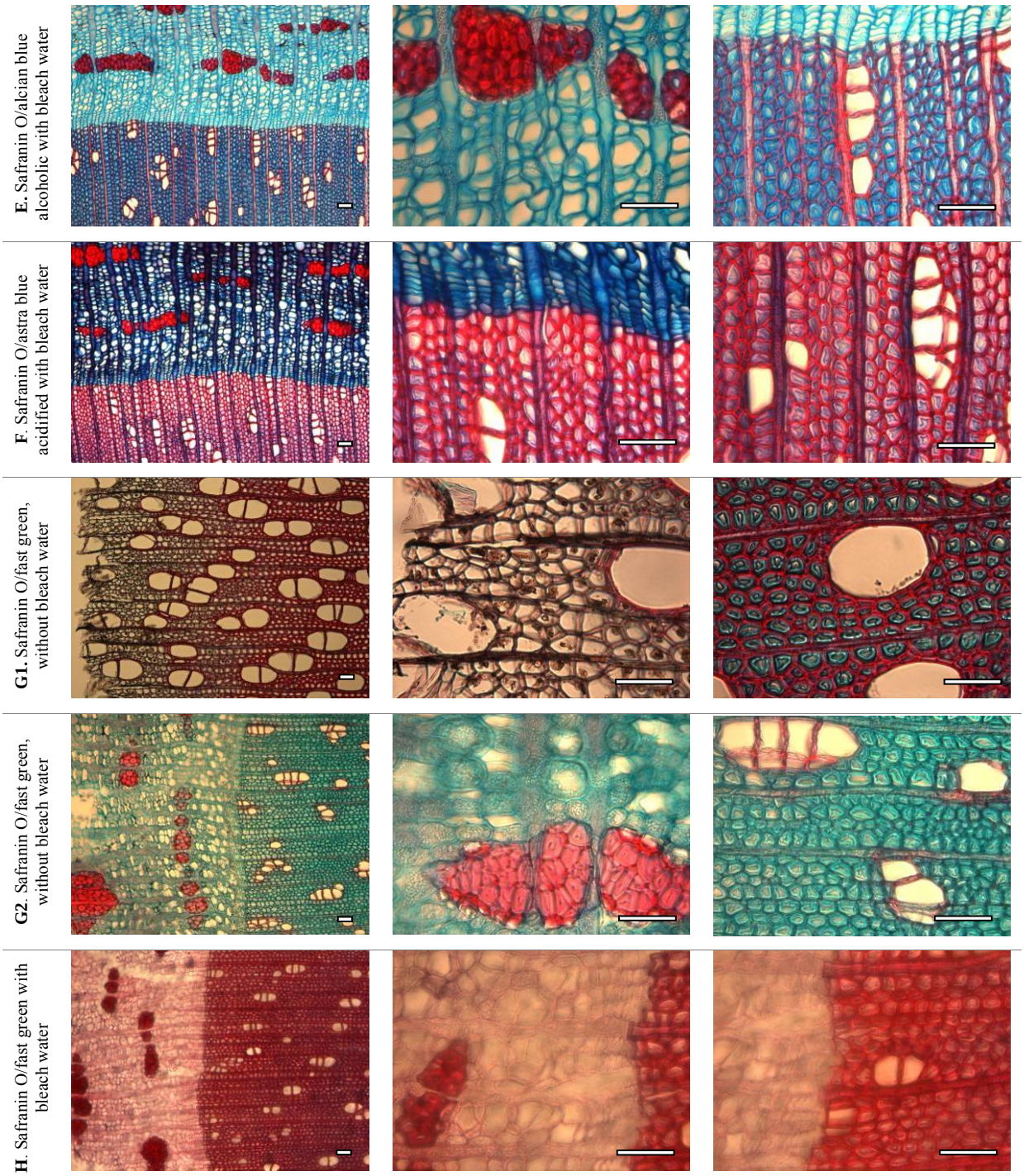

Figure 3.13 Cross sections of poplar tension wood stained with different protocols (E, F, G, and H are different protocols as shown in Table 3.2). Three microscopic images are displayed for each protocol showing different regions: phloem and xylem, phloem or near cambium part, and xylem part respectively. Scale bar: 50 µm

Similarly, the strong colour contrast also can be observed in the combination of safranin O and fast green (G1 in Fig. 3.13). The lignified cell wall stained in red and less lignified cell layers stained in green. But the colour contrast obtained by this double staining was largely affected by various experimental factors, such as sections thickness, bleach water wash, or rinsing time by 50% ethanol, etc. We found, however, that sections 20 µm thick gave better

results than thinner sections (e.g., 10-12 μm) because the colour reaction is more active in thicker sections. The rinsing time in 50% ethanol is more experience-dependent. Excessive or insufficient rinsing directly influenced the second stain reaction, resulting both the lignified and un-lignified xylem cell walls either total green (G2 in Fig. 3.13) or total red, or colour fade of cambium cells (H in Fig. 3.13). Moreover, the sections which were washed by bleach water before staining procedure greatly increase the transparency of the sections, especially eliminating the intracellular substances (e.g., cytoplasm) near the cambium region (G1 in Fig. 3.13).

The present results indicate that the single-staining of astra blue (or alcian blue 8GX) in alcoholic solution is a simple and rapid stain for G-layer identification, but association of safranin O and astra blue (or alcian blue 8GX) in alcoholic solution provides consistent colour and excellent contrast between G-layers and other layers. This staining is therefore kept for further studies on sliding microtome sections.

3.2.2. Measurement of G-layer thickness

Among the ways to trace the wood formation process; one of the simplest ways is to follow the variation of cell wall thickness. The measurement of cell wall thickness has many subjective factors and largely depends on the quality of slices and images, and the way to measure. In this study, some attempts concerning the sample preparation have been done in order to improve the accuracy for further measurement.

As a normal sectioning method with a sliding microtome results in an uncontrolled swelling and detachment of G-layer (Clair et al. 2005a, b), embedded ultrathin (1 μm thickness) sections were used. For each sample more than 100 sections were made to ensure that measured sections were far enough away from the sample border and avoid the border artefact (Clair et al. 2005a). Sections were mounted on glass slides and were observed under optical microscope. Figure 3.14 shows an example of a section stained with methylene blue/AzurII observed in two conditions: (a) bright field and (b) phase contrast mode. It can be seen that the image observed in phase contrast mode (b in Fig. 3.14) gives clearer outline of G-layer than in bright field (a in Fig. 3.14) where G-layer is distinguishable but not obvious. Under phase contrast mode, even without any staining, it is still easily to distinguish G-layer from other layers (b in Fig. 3.15), which largely saves the time for sample staining. With embedded section, the probability of G-layer detachment from the adjacent layer reduces greatly, which improve the quality of image. On the other hand, it is also possible to follow the cell wall maturation from cambium zone (Fig. 3.15a) to mature wood (Fig. 3.15b) and to record the G-layer thickness in an un-swollen state.

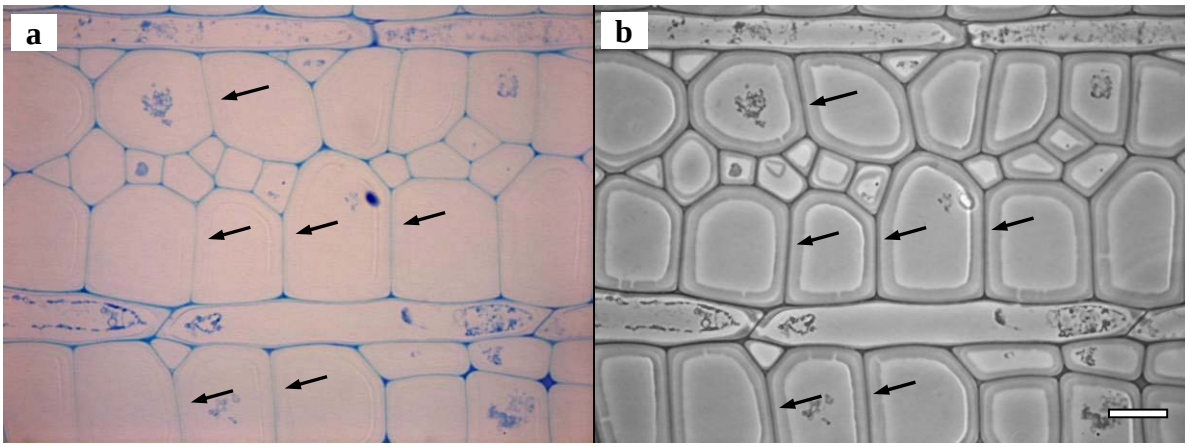

Figure 3.14 Transverse ultrathin (1 µm thickness) section stained with methylene blue/AzurII mix observed in (a) bright field and in (b) phase contrast mode, respectively. Arrows indicate the G-layers in the tension wood fibre. Scale bar: 10 µm (Images provided by B. Clair, section prepared by F. Laurans (AGPF, INRA Orléans))

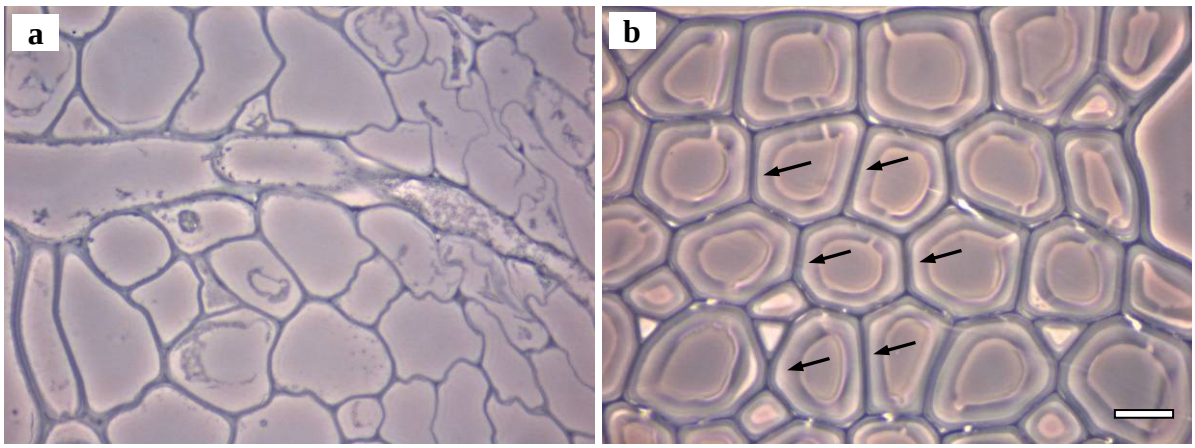

Figure 3.15 Transverse ultrathin (1 µm thickness) section without staining observed in phase contrast mode (a: near cambium; b: mature tension wood). Arrows indicate the G-layers in tension wood fibre. Scale bar: 10 µm

The traditional way to measure the cell wall thickness is by measuring the radial double wall thickness. By image analysis software Image J (National Institutes of Health, Bethesda, MD, USA), it is easy to obtain the thickness of different layers (Fang et al. 2008). However, due to the non-uniformity of the walls thickness around the fibres, the wall thickness measured by this way may be not representative of the mean thickness. The problem when following the thickening of the G-layer is that the thickness is also depended on the cell diameter (Okumura et al. 1977; Fang et al. 2008): cell tips having smaller G-layer thickness than the core of the fibre. To increase the accuracy of the measurement, Yoshinaga et al. (1977, 2012) considered the cell as a polygon and calculated the average G-layer thickness by measuring the area (Agl) and the inside (Pl) and outside (Pg) perimeters of the G-layer using image analysis. Mean G-layer thickness (GT) is therefore obtained by the following formula: $GT = Agl/[0.5 (Pg + Pl)]$

However, for irregular shape of cell, e.g., convex shapes which is often the case of G-layer on normal section, this method should be taken with caution since it may give the un-corrected results. Even some limitation exists in this method, but it still shows some superiority especially in obtaining the parameter of fibre diameter during the measurement, a requisite for quantitative calculation of cell wall thickness change. Unfortunately, the time needed for one

measurement is much longer, so finally we choose not to use it in this study and used the common method by measuring the radial double wall thickness.

3.2.3. Isolation of G-layer

As the study aims to understand the modification occurring during G-layer formation, it was important to analyse G-layer itself, isolated from its cellular context. This is especially interesting in the framework of studies made using nitrogen adsorption volumetry. Indeed, using this technique, volume or surface area is given related to the mass of the sample. It is therefore impossible to have a correct estimate of the G-layer itself as the surrounding wall layers increase the sample mass in a difficult to estimate amount. We therefore try to optimize the procedure for G-layer isolation and estimate the modifications that could occur during the process.

The isolation of G-layer is based on a purely physical method of ultrasonication derived from Norberg and Meyer (1966). This method takes advantage of the swollen morphology of G-layer and its detachment from secondary layer on sliding microtome sections. Since different conditions of ultrasonication can bring different effect on G-layer isolation, different parameters (shown in Tables 3.3 and 3.4) were investigated to optimise this technique. The selection of different frequencies, power and time were based on the common range in the literature (Norberg and Meier 1966; Nishikubo et al. 2007; Kaku et al. 2009; Olsson et al. 2011), and the choice of solvents was dictated by their miscibility with both water and the liquid CO_2 used for the following supercritical drying step.

3.2.3.1. The selection of solutions for G-layer isolation

Different aqueous organic solutions were tested (Table 3.3). Higher concentration (96%) is more effective than lower one (10%) to obtain the integral G-layers, a1-a2 and b1-b2 in Fig. 3.16. Acetone has no effect on G-layer isolation, e1-e2 in Fig. 3.16. Less amount of G-layers were obtained by using isopropanol and acetonitrile solutions (c1-c2 and d1-d2 in Fig. 3.16). In distilled water, G-layer can also be separated from sections but with the risk of splitting sections into pieces, f2 in Fig. 3.16. Ethanol is still the primary solvent to isolate G-layer by ultrasonic treatment.

Table 3.3 Different solutions used for ultrasonic treatment

Frequency kHz	Power (W)	Time (min)	Aqueous organic- solutions					
35	100	30	10% ethanol	96% ethanol	96% isopropanol	96% acetonitrile	96% acetone	Distilled water

Nevertheless, if the isolated G-layer is used for chemical analysis, distilled water may be the primary solvent, due to possible leaching of important components from G-layers by washing with organic solvent. However, the comparison of isolations made in water and in ethanol can be interesting as some sugars are more soluble in water than in ethanol.

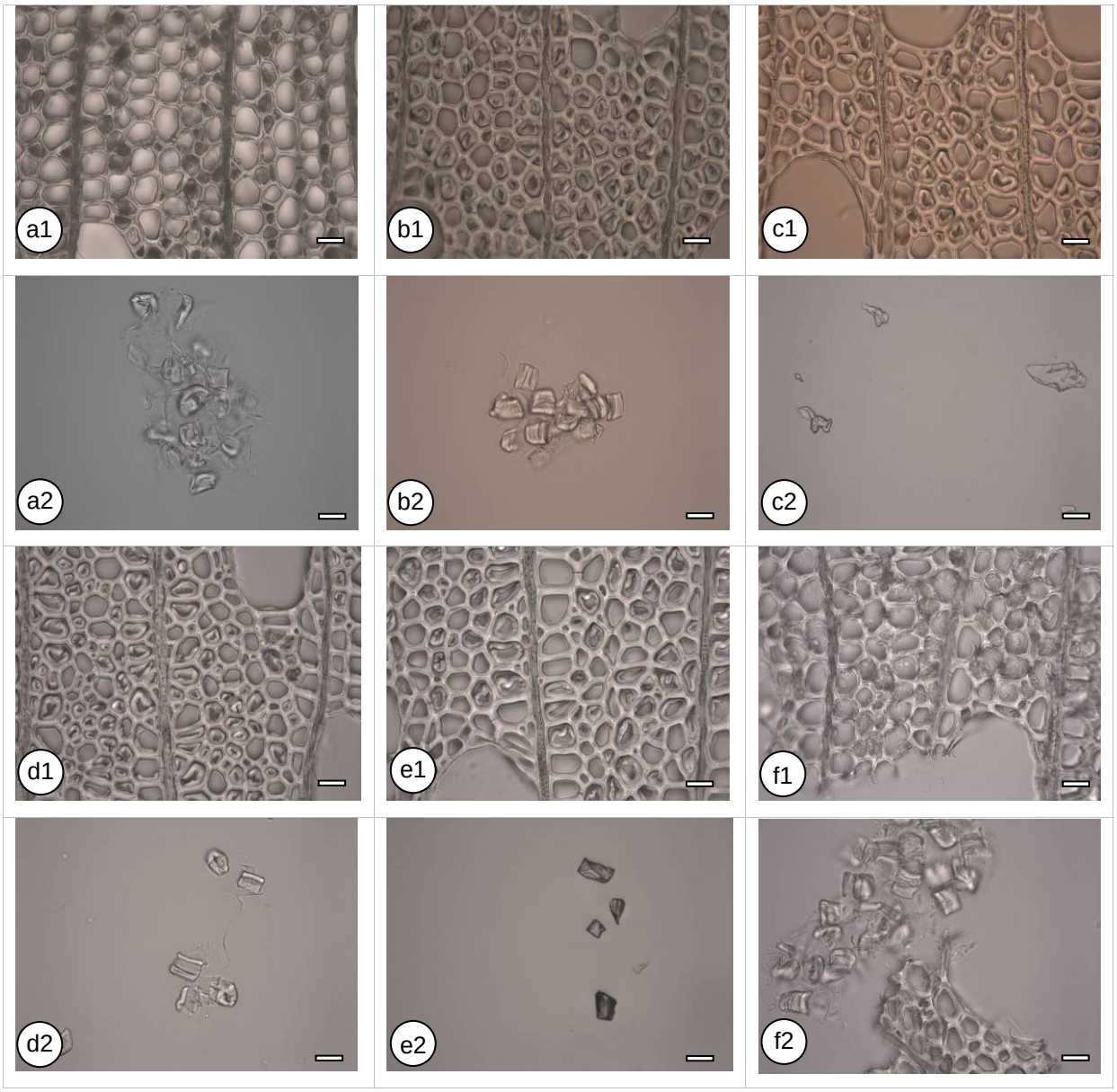

Figure 3.16 Cross sections and isolated G-layers of poplar tension wood after ultrasonic treatment by different solutions. 1, cross section; 2, isolated G-layers; a, 10% ethanol; b, 96% ethanol; c, 96% isopropanol; d, 96% acetonitrile; e, 96% acetone; f, distilled water. Scale bar: 20 µm

3.2.3.2. The selection of power, frequency and time

According to the common range used in the literature (Norberg and Meier 1966; Nishikubo et al. 2007; Kaku et al. 2009; Olsson et al. 2011), two different powers, two frequencies and two different sonication times were tested for the improvement of the methodology. These tested parameters are presented in Table 3.4.

Table 3.4 Different protocols for ultrasonic treatment

Protocols	Frequency kHz	Power (W)	Time (min)	solution
A	45	50	10	96% ethanol
B	45	100	10	96% ethanol
C	25	100	10	96% ethanol
D	25	100	30	96% ethanol

The ultrasonic power is related to the liquid cavitation intensity. In our case, half power (50W) is not enough for G-layer isolation, and full power (100W) is appropriate, A1-A2 and B1-B2 in Fig. 3.17. Increasing the frequency (from 25 to 45 kHz) cannot improve the efficiency of G-layer isolation, B1-B2 and C1-C2 in Fig. 3.17. It is because cavitation intensity is directly correlated with the frequency: the higher the frequency, the smaller the cavitation bubbles, and the weaker the cavitation intensity. 10 min ultrasonic treatment is enough to obtain pure G-layers. Increasing sonication time may increase the amount of G-layers, but also increases the risk to damage G-layers and other cell wall layers.

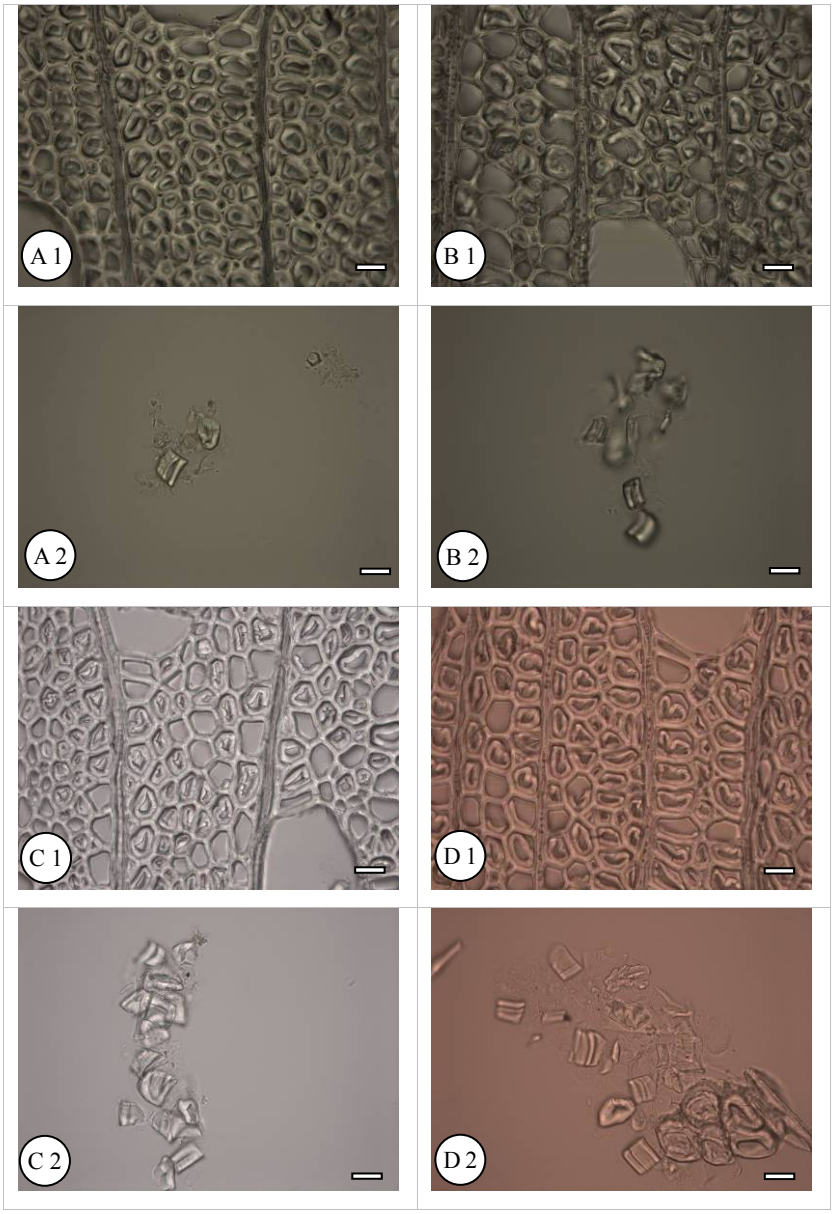

Figure 3.17 Cross sections and isolated G-layers of poplar tension wood after sonication under different protocols. 1, cross section; 2, isolated G-layers; A, B, C, and D are different protocols as shown in Table 3.4. Scale bar: 20 μm

The present results indicate that the 96% ethanol is still the primary solvent for G-layer isolation, if G-layers are not used for chemical analysis. Under the condition of full power (100W) and low frequency (25 kHz), 10 min is enough to obtain pure G-layers.

3.2.4. Ultrasonic treatment effect on the structural properties of isolated G-layer

The separation of G-layer by ultrasonication is more and more used to obtain the isolated G-layers for different studies. However, the effect of ultrasound on the morphology and structure of G-layer is not well described. However, Tischer et al. (2010) reported that ultrasonic treatment degrades the nanostructure of bacterial cellulose. Therefore, a dedicated study is here proposed to analyse changes in structural properties of G-layers with different sonication time by scanning electron microscopy, nitrogen sorption isotherm, and X-ray diffraction.

The results, as reported in the following manuscript (to be submitted) show that the mesoporosity, crystallite parameters as well as the microfibrils aggregates arrangements change with increasing sonication time. As ultrasonic treatment has some influence on the ultrastructure of isolated G-layers, special caution will be taken when analysing the morphology of G-layers extracted from tension wood sections as it should not be representative of its native state.

Article to be submitted[1]

Ultrasonic treatment effect on the structural properties of isolated gelatinous layer from poplar tension wood

CHANG Shan-Shan[1], QUIGNARD Françoise[2], CLAIR Bruno[1, 3]

[1]: Laboratoire de Mécanique et Génie Civil (LMGC), CNRS, Université Montpellier 2, cc 048, Place E. Bataillon, 34095 Montpellier, France

[2]: Institut Charles Gerhardt Montpellier, UMR 5253 CNRS-UM2-ENSCM-UM1, 8 rue de l'Ecole Normale, 34296 Montpellier cedex 5, France

[3]: CNRS, UMR Ecologie des Forêts de Guyane (EcoFoG), Campus Agronomique, BP 701, 97387 Kourou, French Guiana

Abstract: The increasing interest on the understanding of tensional stress generation in tension wood with the gelatinous layer (G-layer) has attracted more attention on the specific role of G-layer. To distinguish the contribution from other layers, the separation of G-layer by ultrasonication is more and more used to obtain the isolated G-layers for different studies. The aim of this study is to identify the effect of duration of ultrasonic treatment on the structural properties of isolated G-layer. The results confirmed that the high mesoporosity previously reported in mature tension wood comes from the G-layer itself. The morphological analysis, scanning electron microscopy revealed that this treatment cause the disarray in the microfibrils aggregates arrangements, at least at the surface layer of the isolated G-layer. Nitrogen adsorption-desorption analysis showed a significant reduction in pore surface area and mesopore volume. Increasing the time of ultrasonic treatment reduces even further the porosity of G-layers, and the peak pore size shifted to larger mesopores domain accompanied with a broader size distribution. X-ray diffraction demonstrated that the ultrasonication increases the degree of crystallinity and the average crystallite dimension. The changes of the structural characteristics of the G-layers may be explained by the ultrasonic cavitation effects.

Keywords: *Tension wood; Gelatinous layer; Morphology; Mesoporosity; Ultrasonic treatment*

Introduction

Plants control their orientation by bending their stems or branches to respond to environmental variation (Timell 1986). This bending is performed by the asymmetrical production of stress in the newly formed secondary xylem around the stem. The reaction wood in angiosperm woody species is called tension wood. It is formed on the upper side of the leaning stem (Fisher and Stevenson 1981) and produces a bending moment allowing stem reorientation. In many commonly studied species such as poplar, oak or chestnut, tension wood is characterised by the occurrence of fibres with a particular morphology and chemical composition due to the development of the so-called gelatinous layer (G-layer). This layer is composed of highly crystalline cellulose with microfibrils oriented nearly parallel to the fibre axis (Norberg and Meier 1966), and embedded in an amorphous matrix of hydrated

[1] Following discussions during and after the defence of the PhD, this manuscript will be partially modified before submission.

polysaccharide (Nishikubo et al. 2007; Mellerowicz et al. 2008; Bowling and Vaughn 2008). Like gels, the structure of G-layer is characterised by a large amount of water-filled meso- or macropores, with most pores centred on 7 nm in chestnut (*Castanea sativa* Mill.) (Clair et al. 2008) and 6-12 nm in several tropical species (Chang et al. 2009). It has been shown that in normal wood, without G-layer, the mesoporosity is much lower (but non nil), suggesting that the high mesoporosity of tension wood can be attributed to the G-layer itself. However, due to the difficulty in sample preparation at the cellular level, up to now, the measurement of porosity of G-layer was always performed on wood samples, and is then contaminated by eventual porosity of primary and other secondary layers. For example, small amount of mesopores in normal wood was attributed to pit membrane. Indeed, it is known that the pit membranes of angiosperm vessels are made of similar microfibril-reinforced hydrogels, with pores size calculated from a modified capillary equation varying between 5 and 20 nm (Choat et al. 2003, 2004). To get direct information about porosity of G-layer itself, quantitative measurements on isolated G-layers are needed to separate the pore contribution from other layers.

In view of the particular morphology, on sliding microtome sections, G-layers are easy to identify by its swollen appearance and the detachment from the adjacent layer. This artefact (Clair et al. 2005a, b) once hampered the understanding of the active role of the G-layer in tension wood properties, but it provides an opportunity for G-layer isolation. A purely physical method of ultrasonication has been proposed for the isolation of G-layer (Norberg and Meier 1966) and followed by several authors (Nishikubo et al. 2007; Kaku et al. 2009; Olsson et al. 2011). The energy of ultrasound is transferred to the polymer chains through a process called cavitation, which include the formation, the growth and the implosive collapse of bubbles in a liquid (Suslick 1990). Within the cavitation bubbles and the immediate surrounding area, violent shock waves are produced, which can be used to the fibrils isolation (Wang and Cheng 2009). Although it is effective to separate G-layer, the effect of ultrasound on the morphology and structure of G-layer is not described. However, recent study showed that when bacterial cellulose subjected to ultrasonic processing for different time intervals, the ultrasonic treatment degraded the polysaccharide linkage leading to nanostructural change of bacterial cellulose (Tischer et al. 2010). This led us to revisit the impact of ultrasonic treatment on G-layer isolation.

The aim of this study is first, to investigate the structure of G-layer in an independent state, and second, to analyze the effect of different sonication times on the structure of G-layer matrix and its cellulose network.

Materials and Methods

Materials

A natural tilted poplar (*Populus deltoides* × *P. nigra*) stem (diameter at breast height, 24 cm) grown in Grabels (Domaine Maspiquet, Lycee Agropolis Montpellier) in south of France was

used throughout the investigation. Poplar is known to produce tension wood with a typical G-layer (Fang et al. 2008). After tree falling, wood pieces were maintain in wet condition until been conserved as centimeter wood block in 70% ethanol until sectioning.

Ultrasonic process

Separation of G-layer was performed as described by Norberg and Meier (1966). About 20 μm thick transverse sections were prepared from the tension wood area with a sliding microtome. The sections were stored in 96% ethanol for a few hours, as proposed by Norberg and Meier, to loosen the G-layer from the adjacent secondary cell wall. The sections were then treated in 96% ethanol with ultrasonic waves (Fisher Scientific ultrasonic cleaner, Transsonic TI-H-10, 25 kHz) at 100W and 25 kHz. Sonication time was optimised to 15 min as shorter sonication time makes the lower efficiency of G-layer isolation, whereas longer one increases the risk of other layer separation. After 15 min, approximately 50% G-layers were shaken out from wood section (Fig. 1).

The ultrasonic treatment was carried out in a cold bath (cooled with ice water), and the cold water was maintained throughout the entire treatment. After this process, parts of the G-layers were shaken out of the sections. The sections were firstly removed by filtration through a filter with mesh around 1 mm, and then the G-layers were filtered by 40 μm nylon filters (Millipore, France). The purity of the G-layer fraction was confirmed by microscopic observation. The G-layer obtained from the sections by 15 min sonication time was marked as G15. In order to test the effect of longer sonication time but avoiding contamination by other layer residues, part of G15 samples were continued for 5, 15, 30, and 45 min sonication and the obtained samples were labelled as G20, G30, G45 and G60 respectively.

The G-layers samples were dehydrated in anhydrous ethanol and dried under supercritical CO_2 conditions in a Polaron 3100 apparatus like previously done on tension wood studies (Chang et al. 2009). As a reference, tension wood sections sampled at the vicinity were dehydrated and supercritical dried without sonication treatement.

Section staining

Sections before and after sonication were observed with an optical microscope at ×400 magnification after double staining with safranin O/alcian blue 8GX to demonstrate the presence of the G-layer. Lignified tissues were red mixed with varying degrees of blue while essentially cellulosic cell wall layers, like the G-layers, were blue.

Nitrogen adsorption-desorption measurement

The supercritically dried samples (around 0.07-0.1g) were out gassed at 323 K under vacuum until a stable 3×10^{-5} Torr pressure was reached without pumping. This is done to remove physically adsorbed gases from the sample surface, in particular, water or ethanol vapour. Nitrogen adsorption-desorption isotherms were recorded at 77 K on a micromeritics ASAP 2020 volumetric apparatus. This experimental technique allows the specific surface area

(Brunauer et al. 1938), pore volume (Gregg and Sing 1982) and the pore size distribution (Broekhoff and de Boer 1967) of the samples to be evaluated.

Scanning electron microscopy analysis

Scanning electron microscopy (SEM) was conducted to observe the microscopic morphology of supercritical dried G-layers with different sonication time. Samples were sputter coated with platinum and examined using a Hitachi S-4800 with the accelerating voltage between 5 or 20 kV.

X-ray diffraction

The supercritical dried G-layers were subjected to X-ray diffraction measurement. XRD identification was carried out with a Bruker D80 X-ray diffractometer in a scanning range of 4 ~ 50° (2θ) at a rate of 4° (2θ) /min with Cu-Kα radiation, 40 kV/35 mA. The crystalline index (*CI*) of the G-layers was calculated from the X-ray diffraction patterns according to Segal et al. (1959) empirical method as follows:

$$CI = \frac{I_{200} - I_{am}}{I_{200}} \times 100\% \quad (1)$$

where I_{200} is the peak intensity from the (200) lattice plane (2θ angle between 22˚ and 23˚), which represents both crystalline and amorphous phases. And I_{am} is the minimum intensity representing the amorphous phases (2θ angle between 18˚ and 19˚). It should be noted that although the Segal method generally underestimate and is not as reliable as the Rietveld method for sample crystallinity (Thygesen et al. 2005), however, our main concern here is the comparation of crystallinity change rather than the absolute value of crystallinity of crystalline regions.

Apparent crystallite dimension was estimated according to Scherrer equation (Scherrer 1918; Cao and Tan 2005) as follows:

$$T = \frac{0.9\lambda}{\beta \cos\theta_{200}} \quad (2)$$

where T is the thickness of the crystal, λ is the X-ray wavelength (0.154 nm), β is the half-width of the (200) diffraction peak, θ_{200} the peak position from the (200) plane.

As for crystalline index, Scherrer equation has to be interpreted with caution and is here used just for comparison of different stage of a same product and do not plan to absolute value of crystal thickness.

The value of lattice distance d_{200} was determined based on Bragg's equation:

$$d_{200} = \frac{\lambda}{2\sin\theta_{200}}(nm) \quad (3)$$

Results

Isolated G-layer

Figures 1a and 1b show light micrographs of twin transverse sections of tension wood before and after ultrasonic treatment (15 min). It appears that G-layers are still present in part of the cells. Full detachment occurred in only 15% of the cells whereas a partial detachment occurred in nearly 40% of the cells. In others cells, G-layer remains attached after sonication.

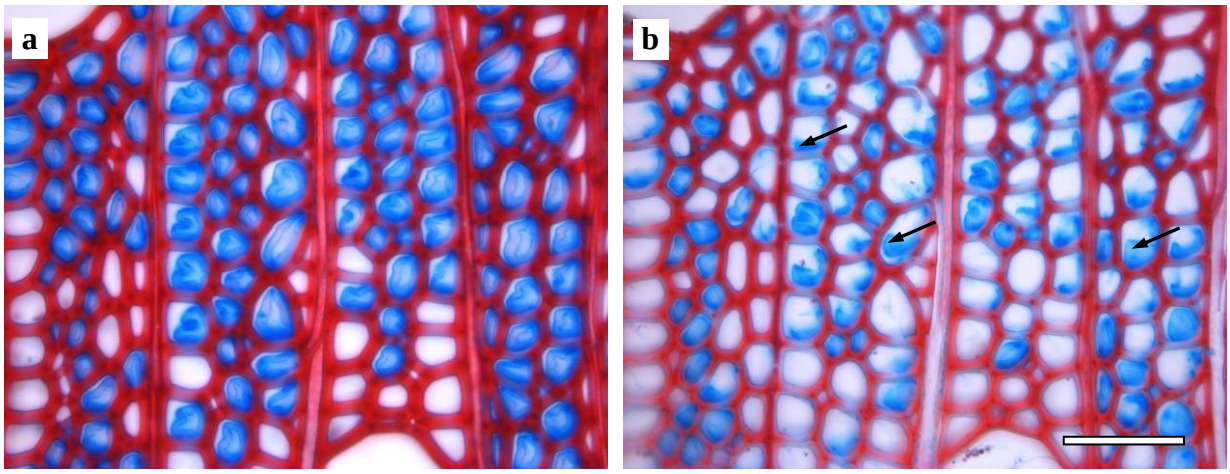

Figure 1 Transverse sections of tension wood before (a) and after (b) ultrasonication for 15 min. After ultrasonic treatment G-layers are still present in part of the cells (in arrow), for others it has been shaken out. Sections are stained with Safranine O and Alcian blue 8GX. Scale bar: 50 µm

Figure 2a shows the hydrated G-layers loosened from the sliced transverse sections using sonication. The purity of the isolated G-layer fraction was examined by microscopic observation. Observation showed nearly 100% of G-layers but few contaminations from other cell wall layers were detectable. To preserve the original volume and the microscopical texture of the hydrogel G-layer, aerogel G-layers were obtained by CO_2 supercritical drying (Fig. 2b). The G-layer particles are agglomerated in a very low density material. In this way, the shrinkage due to capillary pressure was prevented and the aerogel formed is expected to reproduce in the dry state the texture of the original hydrogel (Pierre and Pajonk 2002; Cansell et al. 2003).

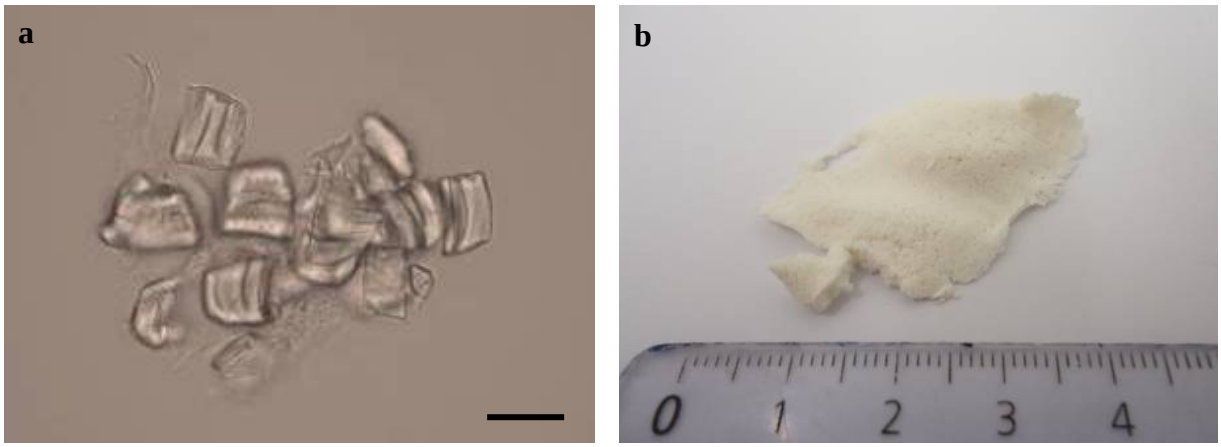

Figure 2 (a) G-layer fraction in water as extracted from transverse sections of tension wood with 15 min ultrasonic treatment and (b) the G-layers after CO_2 supercritical drying, Scale bar: 20 µm

The source of the high porosity in tension wood

Figure 3 shows the isotherms and pore size distributions for poplar tension wood and G-layers extracted from the same tension wood sections. The isolated G-layers exhibited the similar isotherm type and pore shape as the tension wood sample, i.e. an isotherm of type IV, presenting a typical hysteresis loop H3 with slit-like pores. Both samples exhibited broad pore size distributions ranging from 2 to 50 nm, with the most probable values between 2 and 20 nm with two peaks pore size at 6 and 12 nm. However, compared to isolated G-layers, tension wood sample shows wider pore size distribution with the peak pore with higher proportion of pores at 12 nm. When the pure G-layers were measured directly, the total volume of nitrogen adsorbed increased greatly and exhibited a specific pore surface area 3.5 times higher than that in tension wood (66 m^2/g and 19 m^2/g for isolated G-layers and tension wood sample respectively).

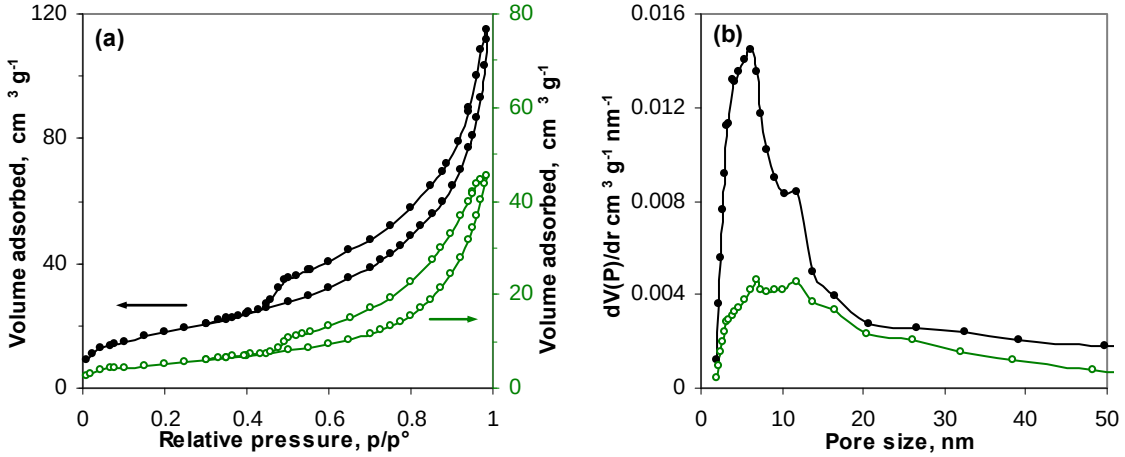

Figure 3 (a) N_2 adsorption-desorption isotherms at 77 K and (b) pore size distributions for poplar tension wood (green curves with open symbols), G-layers extracted from the same tension wood sample with 15min sonication (G15, black curves with solid symbols)

Mesoporosity change with sonication time

Figure 4 present the nitrogen adsorption-desorption isotherms of isolated G-layer after different duration of sonication. The shape of the nitrogen adsorption-desorption isotherms informs on the shape of the pores in the samples. According to IUPAC classification (Sing et al. 1985), the sample G15 exhibited typical type IV with a H3 type hysteresis loop, indicating the aggregates of plate-like particles slit-like mesopores with wide distribution of pore size. As the sonication time increased, samples G20 and G30 followed the similar isotherm type as G15, whereas the nitrogen adsorbed decreased significantly (data not shown, but can be reflected from the following surface area S_{BET} and pore volume). At longer treatment time, however, the types of isotherms for G45 and G60 were intermediated between type IV and type II, indicating the characteristic of non-porous or large mesopores with a broad size distribution that continues into the macropore (pore size >50 nm) domain. From sample G45, especially for sample G60, the hysteresis loop became narrow and less steep at the relative pressure 0.4-0.5. The adsorption and desorption branches being more vertical and do not

reach saturation at high relative pressure, confirming that the material contains pores at the upper limit of mesoporosity and in the macropores domain.

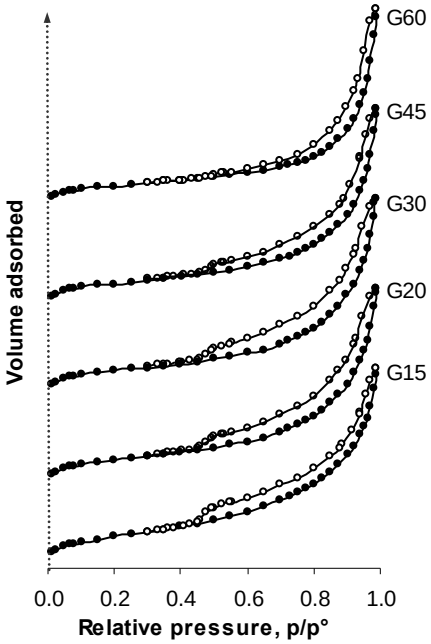

Figure 4 Normalised N_2 adsorption-desorption isotherms at 77 K of the G-layers extracted from tension wood sections with 15min (G15), 20 min (G20), 30min (G30), 45min (G45) and 60min (G60) of sonication. (Filled symbol: adsorption; void symbol: desorption)

The amount of nitrogen needed to form a monolayer of adsorbed molecules provides a good estimate of the surface area of the samples. The pore surface areas as measured by the B.E.T. method were 66, 36, 33, 33, and 25 m^2/g for samples G15, G20, G30, G45, and G60, respectively. The surface area data were strongly correlated with the mesopore volume. The volume of pores smaller than 50 nm was 77, 43, 39, 38, and 18 mm^3/g for samples G15, G20, G30, G45, and G60, respectively. The high surface area is accompanied by a significant porosity. It is clear that the G-layers have a large amount of mesopores, however, the rich porosity greatly reduced when G-layers were longer submitted to the ultrasonic treatment. Increasing the sonication time reduces the porosity of G-layers even further, and the peak pore size shifted to larger mesopores. This feature is evidenced by the pore size distributions presented in Fig. 5.

The pore size distribution determined from the nitrogen adsorption data by Broekhoff and de Boer (1967) method are plotted in Fig. 5. All the samples exhibited broad pore size distributions ranging from 2 to 50 nm, with the most probable values around 2-20 nm. Compared to other samples, sample G15 shows sharp pore size distribution with the peak pore diameter at 6 nm and 12 nm. Increasing the sonication time on G-layer directly, the total volume of nitrogen adsorbed reduced greatly and the distribution curve was shifted slightly. Especially, the proportion of the two peak pore sizes at 6 and 12 nm gradually changed and the peak pore size was evolved from 6 nm to be dominated by 12 nm.

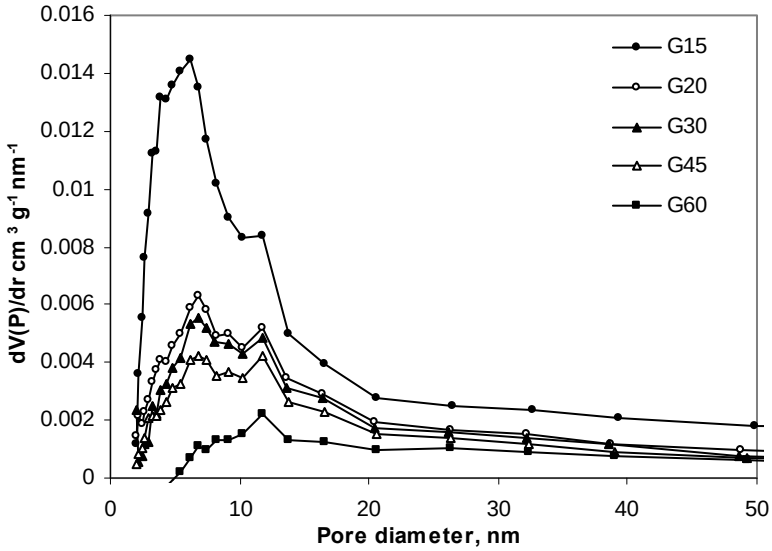

Figure 5 Pore size distribution for the G-layer extracted from tension wood sections with 15min (G15), 20 min (G20), 30min (G30), 45min (G45) and 60min (G60) of sonication

Morphological observation

Figure 6 shows the SEM images of the surface of isolated G-layers after different sonication time. After 15 mn sonication (Fig. 6a), the aggregates of cellulose microfibrils are nearly aligned along the G-layer. With longer sonication, surface of the G-layers appears disorganized (Fig. 6b-d). Apparently, ultrasonic treatment causes the morphology change and the surface becomes more compact (b to d in Fig. 6).

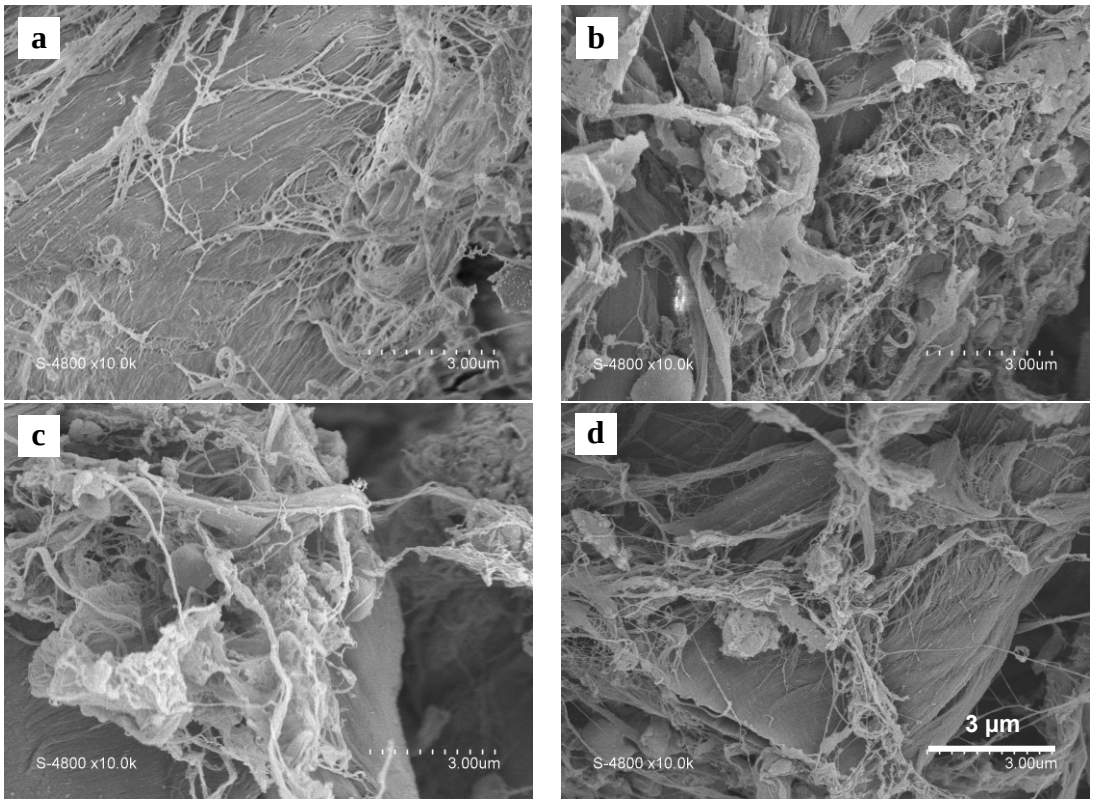

Figure 6 Scanning electron micrographs of G-layer extracted from tension wood sections with 15min (G15, a), 20min (G20, b), 30min (G30, c) and 60min (G60, d) of sonication

X-ray diffraction properties in isolated G-layers with different sonication time

Figure 7 shows the X-ray diffraction patterns of supercritical-dried G-layers with different sonication time in the 2θ angular range from 10° to 40°. Four main peaks could be recognized at 14.8˚, 16.4˚, 22.8˚, and 34.7˚ corresponding to the (1-10), (110), (200), and (004) lattice planes, respectively. The diffraction curves for all the samples analyzed fit well the typical crystalline forms of cellulose I (Parikh et al. 2007), which confirms that the G-layer contains large amounts of native cellulose crystallites.

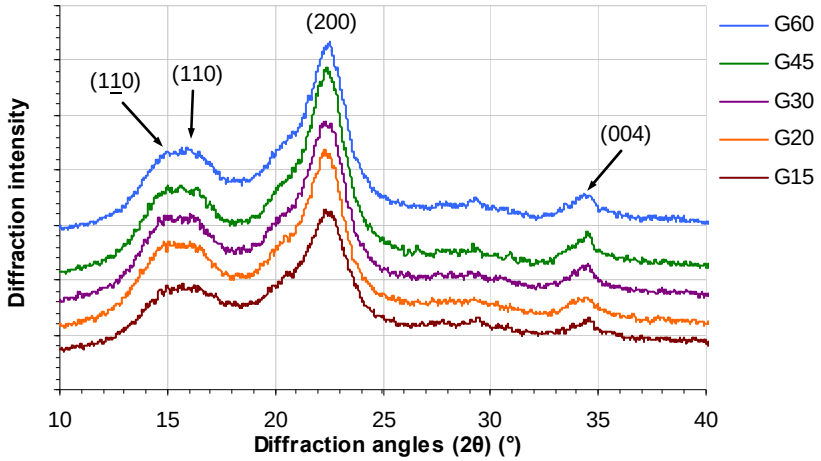

Figure 7 X-ray diffractograms of G-layers extracted from tension wood sections with 15min (G15), 20 min (G20), 30min (G30), 45min (G45) and 60min (G60) of sonication. The samples were analysed in supercritical dried condition

Figure 8a shows the crystallinity index (*CI*) of G-layers with different sonication time. The value of *CI* increased gradually from 76% to 82% with increased sonication time, corresponding to an increase ratio (calculated on the basis of G15) of almost 8%. Figure 8b shows the crystallite thickness, calculated from Eq. 2, in G-layers under different sonication time. No trend was observed in the change of crystallite thickness with increasing sonication time.

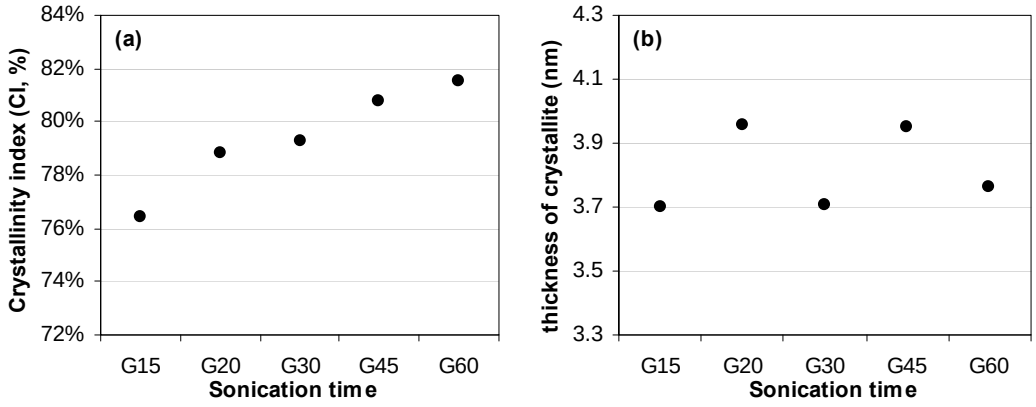

Figure 8 (a) The crystallinity index and (b) thickness of the crystallite in the direction perpendicular to the (200) plane in G-layers extracted from tension wood sections with 15min (G15), 20 min (G20), 30min (G30), 45min (G45) and 60min (G60) of sonication; One measurement for each sonication time.

Figure 9a shows the lattice distance in the (200) plane (d_{200}) in G-layers with different sonication time. The values of d_{200} decreased as increasing the sonication time, with the ratio of decrease being 0.23% from sample G15 to G60.

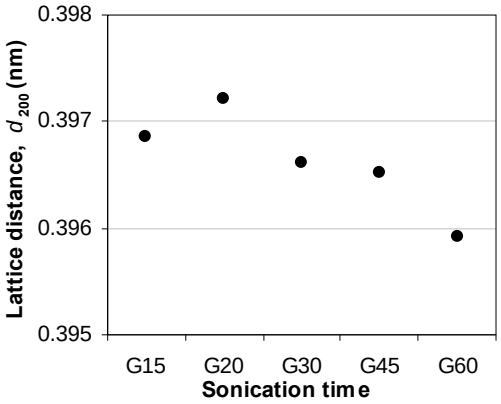

Figure 9 Lattice distance in the (200) plane (d_{200}); G15 are G-layers extracted from tension wood sections with 15min sonicaton; G20, G30, G45, and G60 are G-layers sonicated with additional 5, 15, 30 and 45min on the basis of sample G15; One measurement for each sonication time.

Discussions

Nanostructural characteristics (mesoporosity, crystallinity and crystallite dimension) of G-layers prepared with ultrasound-assisted extraction for different times have been characterized. After 15 min ultrasonic vibration, nearly half of the G-layers were isolated from the transverse wood sections, but others were still on the wood sections. The G-layers extracted directly from wood sections shows an extremely high mesoporosity. Pore volume per gram and surface area are much higher in isolated G-layer. This is easily explained by the absence of lignified wall. Indeed, lignified wall increase mass without increasing much the mesopore volume.

General trend of pore size distribution is similar to what was previously reported for poplar tension wood (Chang et al. 2012) and tension wood from other species (Clair et al. 2008; Chang et al. 2009). Obviously, most of the large amount of mesopores previously reported in tension wood compare to normal wood comes from the G-layer itself. However, it should be noted that pore size distribution is slightly moved compare to what is generally observed in massive tension wood with higher contribution of pores centred at 6 nm compare to pores at 12 nm. The difference of pore size range distribution may be due to the effect of ultrasonic treatment[2], which is discussed in the following part.

When the extracted G-layers were submitted to ultrasonic treatment directly, the structural characteristics of the G-layers changed. The scanning electron microscopy revealed that this treatment changed the microfibrillar arrangement leading to a more disarray arrangement of microfibrillar aggregates at the surface. Nitrogen adsorption-desorption analysis showed a significant reduction in pore surface area and pore volume for the ultrasonicated samples.

[2] Another explanation, lately imagined, based on the contribution of other layers could be proposed, as suggested in Chapter 5.3.

Increasing the sonication time reduces the porosity of G-layers even further, and the peak pore size shifted to larger mesopores domain showing a broad size distribution. The mean crystallite size measured by X-ray diffraction was 3.8 nm which is a bit larger than 3.31 nm in tropical tension wood (Ruelle et al. 2007) and 3.6 nm in Eucalyptus tension wood (Washusen and Evans 2001). Prolonged the treatment of sonication increases the degree of crystallinity and reduces the lattice distance in the (200) plane to value of 0.395 nm which is still larger than the value of G-layer obtained under various moisture conditions (Yamamoto et al. 2010).

According to the above mentioned results, it is clear that the structure and characteristics of G-layers depends on the time of ultrasonic treatment. It may be explained by the ultrasonic cavitation effects (Li et al. 2003). As treatment time increased, the cavitation increased the kinetic energy of the molecules around the micro-bubbles, which is within the hydrogen bond energy scale (Li et al. 2003). The heat emission produced by the cavitation effect can make the degradation of some polysaccharide linkages (Vodenicarova et al. 2006; Tischer et al. 2010) and lead to the bond breakages. Thus, the ultrasonic impact will gradually change the morphology of microfibrils and reduce the organisation of microfibrils aggregates. The ultrasonic process is also quite likely to destroy the smaller pores thus enlarging the exposed pores to some extent. In addition, the prolonged ultrasonication time also likely increases the possibility of the amorphous regions of microfibrils contacting with the micro bubbles generated by the ultrasonication process because these are the regions where water can more effectively penetrate. The ultrasound energy is transferred through the shearing and cavitation to the glucan chains promoting the conversion of amorphous material into crystalline material (Tischer et al. 2010). Therefore, the crystallinity increased. The change in crystallinity is compatible with the decrease in porosity obtained from the nitrogen adsorption analysis.

Conclusions

In the present study, the fact that high porosity of tension wood comes from the G-layer itself has been confirmed experimentally. Although the G-layers can be prepared by the method of ultrasonication, the microfibrillar structure of the G-layer was affected by the ultrasonic treatment to some extent. The ultrasonic treatment reduced the organisation of microfibrillar arrangement thus leading to a more disorganised surface. As treatment time increased, the degree of crystallinity increased. Increasing the sonication time reduces the porosity of G-layers even further, and the peak pore size shifted to larger mesopores domain showing a broad size distribution.

Thus for study on G-layers isolated with ultrasonic, interpretation on the structure should be taken with care, as it may be already in a non-native state. Minimizing the time of sonication is to be advised to reduce its impact on the structure of isolated G-layer.

Acknowledgements Shan Shan Chang was supported by a fellowship from the Scientific Council of Montpellier University. The authors wish to thank T. Cacciaguerra (ICG Montpellier, France) for SEM observation and Mao Chen for helping the isolation of G-layer. Part of this work was performed in the framework of the project “StressInTrees” funded by the French National Research Agency (ANR-12-BS09-0004).

References

Bowling AJ, Vaughn KC (2008) Immunocytochemical characterization of tension wood: gelatinous fibers contain more than just cellulose. American Journal of Botany 95: 655-663

Broekhoff JCP, de Boer JH (1967) Studies on pore systems in catalysts: IX. Calculation of pore distributions from the adsorption branch of nitrogen sorption isotherms in the case of open cylindrical pores A. Fundamental equations. Journal of Catalysis 9: 8-14

Brunauer S, Emmett PH, Teller E (1938) Adsorption of gases in multimolecular layers. Journal of the American Chemical Society 60: 309-319

Cansell F, Aymonier C, Loppinet-Serani A (2003) Review on materials science and supercritical fluids. Current Opinion in Solid State and Materials Science 7: 331-340

Cao Y, Tan H (2005) Study on crystal structures of enzyme-hydrolyzed cellulosic materials by X-ray diffraction. Enzyme and Microbial Technology 36: 314-317

Chang SS, Clair B, Ruelle J, Beauchêne J, Di Renzo F, Quignard F, Zhao GJ, Yamamoto H, Gril J (2009) Mesoporosity as a new parameter in understanding of tension stress generation in trees. Journal of Experimental Botany 60: 3023-3030

Chang SS, Quignard F, Di Renzo F, Clair B (2012) Solvent Polarity and internal stresses control the swelling behaviour of green wood during dehydration in organic solution. Bioresources 7: 2418-2430

Choat B, Ball M, Luly J, Holtum J (2003) Pit membrane porosity and water stress-induced cavitation in four co-existing dry rainforest tree species. Plant Physiology 131: 41-48

Choat B, Jansen S, Zwieniecki MA, Smets E, Holbrook NM (2004) Changes in pit membrane porosity due to deflection and stretching: the role of vestured pits. Journal of Experimental Botany 55: 1569-1575

Clair B, Gril J, Di Renzo F, Yamamoto H, Quignard F (2008) Characterization of a gel in the cell wall to elucidate the paradoxical shrinkage of tension wood. Biomacromolecules 9: 494-498

Clair B, Gril J, Baba K, Thibaut B, Sugiyama J (2005a) Precautions for the structural analysis of the gelatinous layer in tension wood. IAWA Journal 26:189-195

Clair B, Thibaut B, Sugiyama H (2005b) On the detachment of the gelatinous layer in tension wood fiber. Journal of Wood Science 51: 218-221

Fang CH, Guibal D, Clair B, Gril J, Liu YM, Liu SQ (2008) Relationships between growth stress and wood properties in poplar I-69 (*Populus deltoides Bartr*. cv. "Lux" ex I-69/55). Annals of Forest Science 65: 307-315

Fisher JB, Stevenson JW (1981) Occurrence of reaction wood in branches of dicotyledons and its role in tree architecture. Botanical Gazette 142: 82-95

Gregg SJ, Sing KSW (1982) Adsorption, surface area and porosity. London: Academic Press, 218-228

Kaku T, Serada S, Baba K, Tanaka F, Hayashi T (2009) Proteomic analysis of the G-layer in poplar tension wood. Journal of Wood Science 55:250-257

Li SY, Liu XF, Zhuang XP, Guan YL, Cheng GX (2003) Ultrasonic treatment of cotton pulp cellulose. Chinese Journal of Applied Chemistry 20: 1030-1034

Mellerowicz EJ, Immerzeel P, Hayashi T (2008) Xyloglucan: the molecular muscle of trees. Annals of Botany 102: 659-665

Nishikubo N, Awano T, Banasiak A, Bourquin V, Ibatullin F, Funada R, Brumer H, Teeri TT, Hayashi T, Sundberg B, Mellerowicz EJ (2007) Xyloglucan *endo*-transglycosylase (XET) functions in gelatinous layers of tension wood fibers in poplar: a glimpse into the mechanism of the balancing act of trees. Plant and Cell Physiology 48: 843-855

Norberg PH, Meier H (1966) Physical and chemical properties of the gelatinous layer in tension wood fibre of aspen (*Populus tremula* L.). Holzforschung 20: 174-178

Olsson AM, Bjurhager I, Gerber L, Sundberg B, Salmén L (2011) Ultra-structural organization of cell wall polymers in normal and tension wood of aspen revealed by polarization FTIR microspectroscopy. Planta 233:1277-1286

Parikh DV, Thibodeaux DP, Condon B (2007) X-ray crystallinity of bleached and crosslinked cottons. Textile Research Journal 77: 612-616

Pierre AC, Pajonk GM (2002) Chemistry of aerogels and their applications. Chemical Reviews 102: 4243-4266

Ruelle J, Yamamoto H, Thibaut B (2007) Growth stresses and cellulose structural parameters in tension and normal wood from three tropical rainforest angiosperms species. BioResources 2: 235-251

Scherrer P (1918) Bestimmung der Grosse und der inneren Struktur von Kolloidteilchen mittels Röntgenstrahlen. Nachr. Ges. Wiss. Göttingen 26: 98-100

Segal L, Creely JJ, Martin AE, Conrad CM (1959) An empirical method for estimating the degree of crystallinity of native cellulose using the X-ray diffractometer. Textile Research Journal 29: 786-794

Sing KSW, Everett DH, Haul RAW, Moscou L, Pierotti RA, Rouquerol J, Siemienewska T (1985) Reporting physisorption data for gas-solid systems. Pure and Applied Chemistry 57: 603-619

Suslick KS (1990) Sonochemistry. Science 247: 1439-1445
Timell TE (1986) Compression wood in Gymnosperms. Springer, Berlin, Heidelberg, New York, Vol.1-3
Tischer PCSF, Sierakowski MR, Westfahl H Jr, Tischer CA (2010) Nanostructural reorganization of bacterial cellulose by ultrasonic treatment. Biomacromolecules 11: 1217-1224
Thygesen A, Oddershede J, Lilholt H, Thomsen AB, Stahl K (2005) On the determination of crystallinity and cellulose content in plant fibres. Cellulose 12: 563-576
Vodenicarova M, Drimalova G, Hromadkova Z, Malovikova A, Ebringerova A (2006) Xyloglucan degradation using different radiation sources: a comparative study. Ultrason Sonochem 13: 157-164
Wang S, Cheng Q (2009) A novel process to isolate fibrils from cellulose fibers by high-intensity ultrasonication, part 1: process optimization. Journal of Applied Polymer Science 113: 1270-1275
Washusen R, Evans R (2001) The association between cellulose crystallite width and tension wood occurrence in *Eucalyptus globulus*. IAWA Journal 22: 235-243
Yamamoto H, Ruelle J, Arakawa Y, Yoshida M, Clair B, Gril J (2010) Origin of the characteristic hygro-mechanical properties of the gelatinous layer in tension wood from Kunugi oak (*Quercus acutissima*). Wood Science and Technology 44: 149-163

4. Macromolecular and structural modifications during the maturation of tension wood cell wall

In this chapter, the following 3 main subjects will be studied.

- The composition and organisation of polymers within the secondary cell wall, as well as its orientation during the maturation of poplar tension wood cell wall.

- The mesoporosity and its evolution during the maturation of tension wood cell wall in G-layer species (Poplar).

- The mesoporosity and its evolution during the maturation of tension wood cell wall in non-G-layer species (Simarouba).

The results are reported in the form of publication as following. The first has been accepted for publiocation in *Planta,* the other two will be submitted. These results will be latter crossed for a discussion following the cell wall maturation process (cambium zone, during maturation, and mature tension wood), as reported in Chapter 5.

4.1 Macromolecular modification during maturation of tension wood cell wall

This article has been published in ***Planta*** *(2014) 239:243–254 (DOI 10.1007/s00425-013-1980-3)*

Deposition and organization of cell wall polymers during maturation of poplar tension wood by FTIR microspectroscopy

Shan-Shan Chang[1*], Lennart Salmén[2], Anne-Mari Olsson[2], Bruno Clair[1]

[1]Laboratoire de Mécanique et Génie Civil (LMGC), Université Montpellier 2, CNRS, Pl. E. Bataillon, cc 048, 34095 Montpellier Cedex 5, France,

[2]Innventia AB, Drottning Kristinas väg 61, Box 5604, SE-114 28 Stockholm, Sweden

* corresponding author: shanshan.chang@univ-montp2.fr, changelxy@hotmail.com

Abstract: To advance our understanding of the formation of tension wood, we investigated the macromolecular arrangement in cell walls by Fourier transform infrared microspectroscopy (FTIR) during maturation of tension wood in poplar (*Populus tremula* x *P. alba*, clone INRA 717-1B4). The relation between changes in composition and the deposition of the G-layer in tension wood was analysed. Polarised FTIR measurements indicated that in tension wood, already before G-layer formation, a more ordered structure of carbohydrates at an angle more parallel to the fibre axis exists. This was clearly different from the behaviour of opposite wood. With the formation of the S_2 layer in opposite wood and the G-layer in tension wood, the orientation signals from the amorphous carbohydrates like hemicelluloses and pectins were different between opposite wood and tension wood. For tension wood, the orientation for these bands remains the same all along the cell wall maturation process, probably reflecting a continued deposition of xyloglucan or xylan, with an orientation different to that in the S_2 wall, throughout the whole process. In tension wood, the lignin was more highly oriented in the S_2 layer than in opposite wood.

Keywords: *FTIR microscopy, Maturation, Orientation, Polarization, Polymers, Populus tremula x P. alba, Tension wood*

Abbreviations:

CCD	Charge-coupled device
FTIR	Fourier transform infrared
G-layer	Gelatinous layer
I	Intensity absorbance
L	Longitudinal
MCT	Mercury cadmium telluride
OW	Opposite wood
R	Radial
RA	Relative absorbance
ROA	Relative orientation absorbance
S_1	Secondary cell wall layer, first layer
S_2	Secondary cell wall layer, middle layer
S_3	Secondary cell wall layer, third layer
T	Tangential
TW	Tension wood
XET	Xyloglucan-endotransglycosylase

Introduction

In response to changes in environmental factors like slope, winds, snow, or light, trees maintain or reorient their stems and branches by developing reaction wood on one side of the axis (Timell 1986). In angiosperm woody species, this wood, called tension wood, is generally formed on the upper side of the leaning stem and associated with the development of large tensile stresses within the structure (Wardrop 1964; Fisher and Stevenson 1981). In many species, tension wood is characterised by the peculiar longer fibres, called G-fibres, with an inner gelatinous layer, the G-layer. Before fibres reach maturity, the newly divided cells in the vascular cambium pass through four major developmental stages: (i) an increase in cell size (cell elongation and radial enlargement), (ii) secondary cell wall deposition, (iii) lignification and (iv) cell death. At the beginning of differentiation, the young xylem cells become both longer and wider. At this stage, they only have an ultra-thin primary wall, which comprises cellulose, pectic polysaccharides, xyloglucans and lesser amounts of arabinoxylans and proteins (Cosgrove and Jarvis 2012). Once cell expansion is completed, the secondary cell wall gradually thickens inwards to form a multilayer (S_1, S_2 and S_3) structure comprising cellulose microfibril bundles embedded in an amorphous matrix of hemicelluloses (mainly xylans and glucomannans) and lignin. Cell wall characteristics can be modified during cell maturation by external mechanical stresses, e.g. wind or stem lean, which is the case of G-fibre formation in tension wood in angiosperms. In the G-fibres of tension wood, a thick G-layer may replace the S_3 layer and part of or the whole S_2 layer (Wardrop and Dadswell 1955). This layer is almost free of lignin and consists mainly of highly crystalline cellulose with microfibrils oriented nearly parallel to the fibre axis (Norberg and Meier 1966). Recent analyses indicate that the G-layers in *Populus* also contain some non-cellulosic polysaccharides like xyloglucans and pectin, the two which differ strongly from those in the adjacent secondary (S) layers that mainly contain xylans and glucomannans (Nishikubo et al. 2007; Bowling and Vaughn 2008; Mellerowicz et al. 2008). More recently, Kim and Daniel (2012) also found xylan in the G-layer itself.

The properties of the fibres are mainly determined by the arrangement of the polymers cellulose, hemicelluloses (xylans and glucomannans) and lignin within the cell wall, as well as by interactions among them (Salmén and Burgert 2009). Fourier transform infrared (FTIR) microscopy makes it possible to monitor the development and compositional changes in the cell walls and thus obtain a clearer picture of cell wall development. By using polarised radiation, information on the orientation of specific groups and of the polymer chains containing these groups in the wood structure can be obtained at a µm scale (Olsson et al. 2011). The aim of this study was to better understand how the deposition and organisation of the cell wall polymers relates to tension wood formation by comparing their behaviour to that of opposite wood during wood maturation. FTIR (Fourier transform infrared) microscopy was applied to a sequence of cell differentiation during the formation of the cell wall in poplar tension wood.

Materials and methods

Materials

In *vitro* shoots of poplar (*Populus tremula* x *P. alba,* clone INRA 717-1B4) were produced at INRA Orleans, France and acclimatised in a greenhouse on the 10th of February 2009. On the 13th of May 2009, the trees were moved outside and artificially tilted at an angle of 35° to the natural curvature to trigger the formation of tension wood, as shown in Fig. 1. Figure 1 also clearly shows that even before tilting, these trees formed tension wood to keep themselves upright. The trees were regularly watered until sampling. About one month later (15th of June 2009), the trees were sampled and the samples were frozen and stored until required.

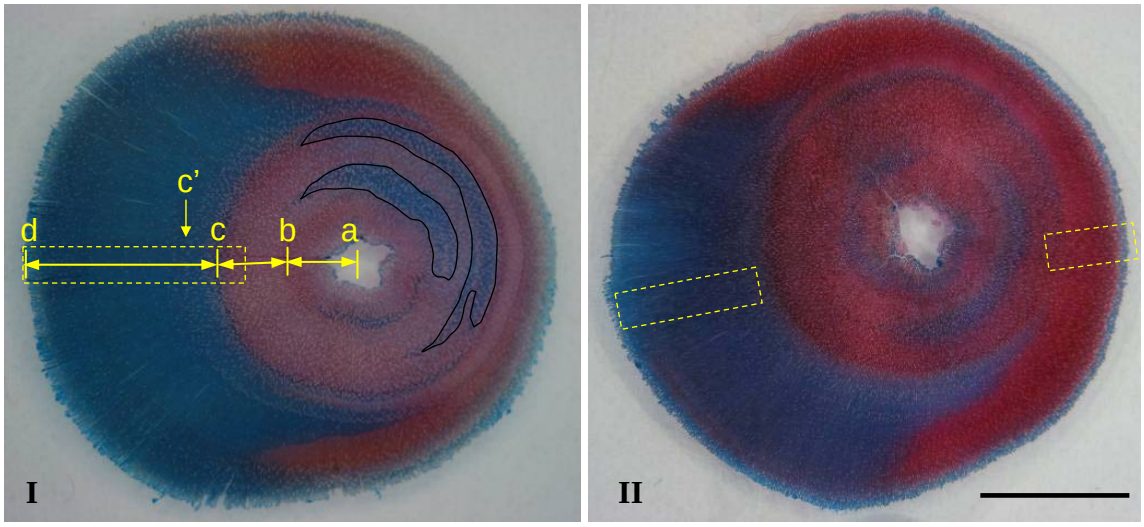

Figure 1 Light micrograph of transverse section from 1-year-old poplar wood stems stained with safranin/astra blue indicating high concentrations of CH structures, i.e. places where carbohydrate content is high and lignin content is consequently low. Both trees I and II were used for the study of tension wood, only tree II was used for the study of opposite wood. **a-d** Different growth conditions in tree I: *in vitro* (**a-b**), grown in the greenhouse (**b-c**), grown outdoors (**c-d**). **a-c** Growth before artificial tilting (unintended tension wood produced on the opposite side; curve regions). **c-d** Growth after tilting at an angle of 35°. **c** Boundary between normal wood and tension wood on the tension wood side. **c'** End of the transition zone. The dotted rectangle indicates the area where FTIR measurements were made. *Scale bar* 5 mm (Images provided by F. Laurans, INRA Orléans, France)

Figure 1 presents transverse sections of stems stained with safranin/astra blue showing the formation of tension wood after tilting of the stem, represented by the blue-stained G-layers. In the periphery of the stems near the cambium, the newly dividing cells were also stained blue like the G-layer because these cells were not yet lignified and consequently contained relatively more carbohydrate components (cellulose, hemicelluloses and pectin). Sample blocks with a diameter of 20 mm (including differentiating cells) from the upper side of tilted stems from trees marked I and II in the growth season were used. For the sake of comparison, observations were also made on an opposite wood block, but a sample was only taken from the tree marked II because the same section of tree I was too narrow.

Microscopic observations and measurement of cell wall thickness

The wood blocks were dehydrated with ethanol and embedded in LR White resin (two changes of resin/ethanol mixture for 1 h, followed by two exchanges in pure resin for 1 h and kept overnight at room temperature, then polymerised at 65 °C overnight). Transverse sections (1 µm thick) were cut with a diamond knife and observed with an optical microscope (Leica Microsystems) in phase contrast mode. The thickness of the radial cell walls (with and without the G-layer) was measured manually from the raw images using the image analysis software ImageJ (National Institutes of Health, Bethesda, MD, USA).

FTIR measurement

FTIR spectra were recorded in transmission mode on a Spectrum 100 FTIR Spectrometer equipped with a microscope, Spectrum Spotlight 400 FTIR Imaging System (Perkin Elmer). Transverse sections 20-µm thick and successive 20-µm-thick tangential sections (for handling purposes, the tangential sections near the cambium were 30-µm thick to compensate for their low density) from the cambium to full maturation were cut with a vibratome (Leica Microsystems) from both tension and opposite wood blocks. The distance from the cambial zone was recorded for each tangential section. Air-dried samples were mounted on the autosampler stage which was incorporated in the microscope. The area of interest was first selected from a visible image displayed by a CCD camera and then irradiated with mid-IR light. The transverse microtome sections were then point scanned. Spectra were collected continuously from fibres in small areas of 50×25 μm^2 (radial×tangential, R×T) along the radial direction (Fig. 2a). The centre of each measurement area was recorded as the position of each spectrum. One average spectrum was collected from each measuring area.

In each tangential section, a 25×100 μm^2 (tangential×longitudinal, T×L) area of fibres (Fig. 2b) was subjected to polarised light by a wire grid polariser from -90˚ to 90° polarisation in relation to the fibre axis with an interval of 10˚. Scanning was performed in imaging mode by an array detector. The detector moved step by step across the preset area until all the spectra had been collected. For each polariser angle of a given measurement area, 64 different spectra were recorded with a pixel resolution of 6.25 µm × 6.25 µm. The number of spectra collected corresponded to the number of pixels and the preset measuring area. In this way, an IR full-spectral image including spectral information was obtained for each polariser angle of each measuring area. The mean spectrum of the whole image at each polariser angle was used for further data processing. All the spectra discussed above were the average of 16 scans recorded at a resolution of 4 cm^{-1} in the range from 4,000 to 700 cm^{-1} with an MCT detector (cooled in liquid nitrogen).

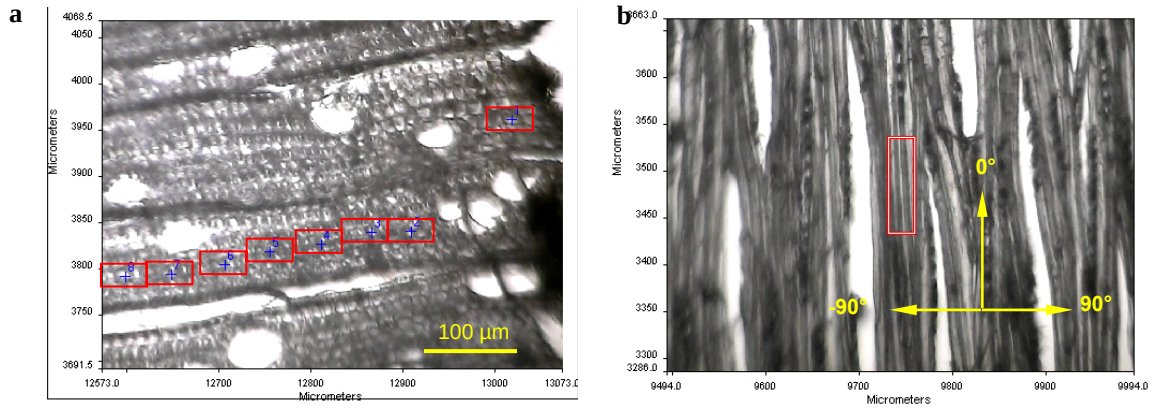

Figure 2 Visible images of transverse (**a**) and tangential (**b**) sections of poplar tension wood showing the measuring area (a: 50×25 µm, R×T; b: 25×100 µm, T×L) and the polarization directions of the measurement

Data processing

The FTIR spectra were processed using the software Spotlight 1.5.1, HyperView 3.2 and Spectrum 6.2.0 (Perkin Elmer Inc., Shelton, CT, USA). The spectra were corrected by applying an atmospheric correction function to minimise the effects of CO_2 and H_2O. The spectra were baseline corrected at 1,850, 1,540, 1,488, 1,188 and 800 cm^{-1}.

For the spectra acquired with un-polarised light (point mode), the differences in total absorbance due to variations in the thickness of the cell walls of the measured samples were compensated for by normalising the spectra with the total absorbance in the wavenumber range of 1,800-1,140 cm^{-1} (avoiding noise between 1,140 to 800 cm^{-1} due to too high absorbance). The relative absorbance, *RA*, was calculated as:

$$RA=I_a/I_t \qquad (1)$$

where I_a is the absorbance at a given wavenumber and I_t is the total absorbance in the wavenumber range of 1,800 to 1,140 cm^{-1}.

To compare orientation spectra, the relative orientation absorbance, *ROA*, was calculated for each specific absorbance peak as:

$$ROA=I_p/I_{max} \qquad (2)$$

where I_p is the intensity of the absorbed IR radiation at a given polarisation angle for a specific wavenumber and I_{max} is the maximum intensity in the polarisation interval (-90° to 90°) for the specific wavenumber. A few aberrant points caused by measurement disturbances (e.g., a less flat sample or a sample that became loose during the experiment) were not used in subsequent analyses. As IR absorbance peaks always have some influence from neighbouring peaks, as well as the fact that for small peaks the signal to noise ratio is decreased in these calculations, differences smaller than 0.1 units in peak height in the orientation spectra should be taken with precaution.

IR absorbance of functional groups with vibrations orientated parallel to the fibre axis will have the highest absorbance at low polarisation angles, whereas functional groups oriented perpendicular to the fibre axis will have the highest absorbance at high polarisation angles.

Because the IR transmission light will pass through at least two cell walls of adjacent cells (with the middle lamella in between) with opposite fibrillar angles, the oriented molecules will display an average absorption for the two angles, with a peak either at 0^o or at 90^o. The position depends on whether the main orientation of the molecules is at a lower or higher angle than 45^o. The extent of the molecular orientation will instead be noted by the magnitude of the differences in absorbance between polarization angles. This also implies that molecular groups oriented other than 0 or 90^o to the backbone may be difficult to use for orientation assessments.

Results

Change in cell wall thickness

Figures 3a and 4a show variations in the thickness of cell wall layers during maturation of tension wood from tree I and tree II, respectively. The thickness is plotted against the distance from the cambial zone. Figures 3d and 4d are light micrographs of corresponding transverse sections showing cell differentiation from the cambial zone to full maturation.

The gradual thickening of the fibre in the secondary wall layer in tension wood of tree I was clearly visible up to 350 µm from the cambial zone (Fig. 3a; d1-d3 in Fig. 3d). After 350 µm, G-layers started becoming visible (d4 in Fig. 3d) along with an almost linear increase in the thickness of the G-layer. The thickening of the G-layer was complete in fibres located 900 µm after the cambial zone, after which the cell wall thickness remained constant. The tension wood of tree II showed a similar tendency. The thickness of the G-layer increased linearly from 400 µm until ~900 µm from the cambial zone (Fig. 4a). The sharp increase in the thickness of the G-layer is in agreement with changes in G-layer thickness during fibre differentiation reported by Yoshinaga (Yoshinaga et al. 2012).

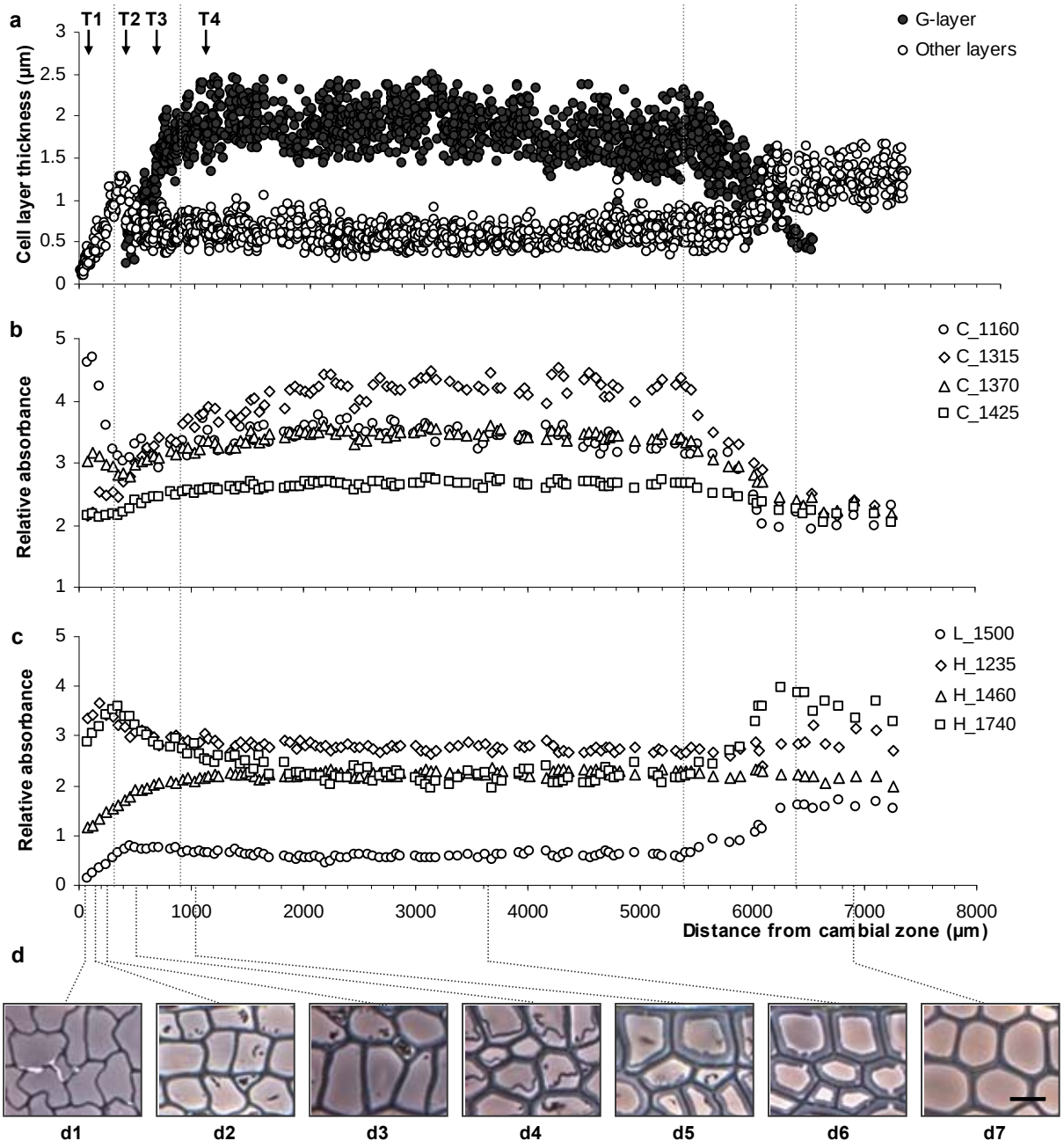

Figure 3 Changes in cell layer thickness (a) and relative intensity of absorbance bands for cellulose and other carbohydrates (b), hemicellulose and lignin (c) and morphological details of fibre (d) during cell wall maturation as well as the annual ring and the normal wood region in poplar tension wood from tree I. Vertical dotted lines indicate the different stages of maturation in tension wood, T1, T2, T3 and T4 indicate the four stages of G-layer formation. The light micrographs (d1-d7) were collected with an optical microscope in phase contrast mode. At 5,400 µm, the transition from the previously formed normal wood layer is visible. Other layers: sum of all other layers in the cell wall except the G-layer. *Scale bar* (shown in d7) = 10 µm

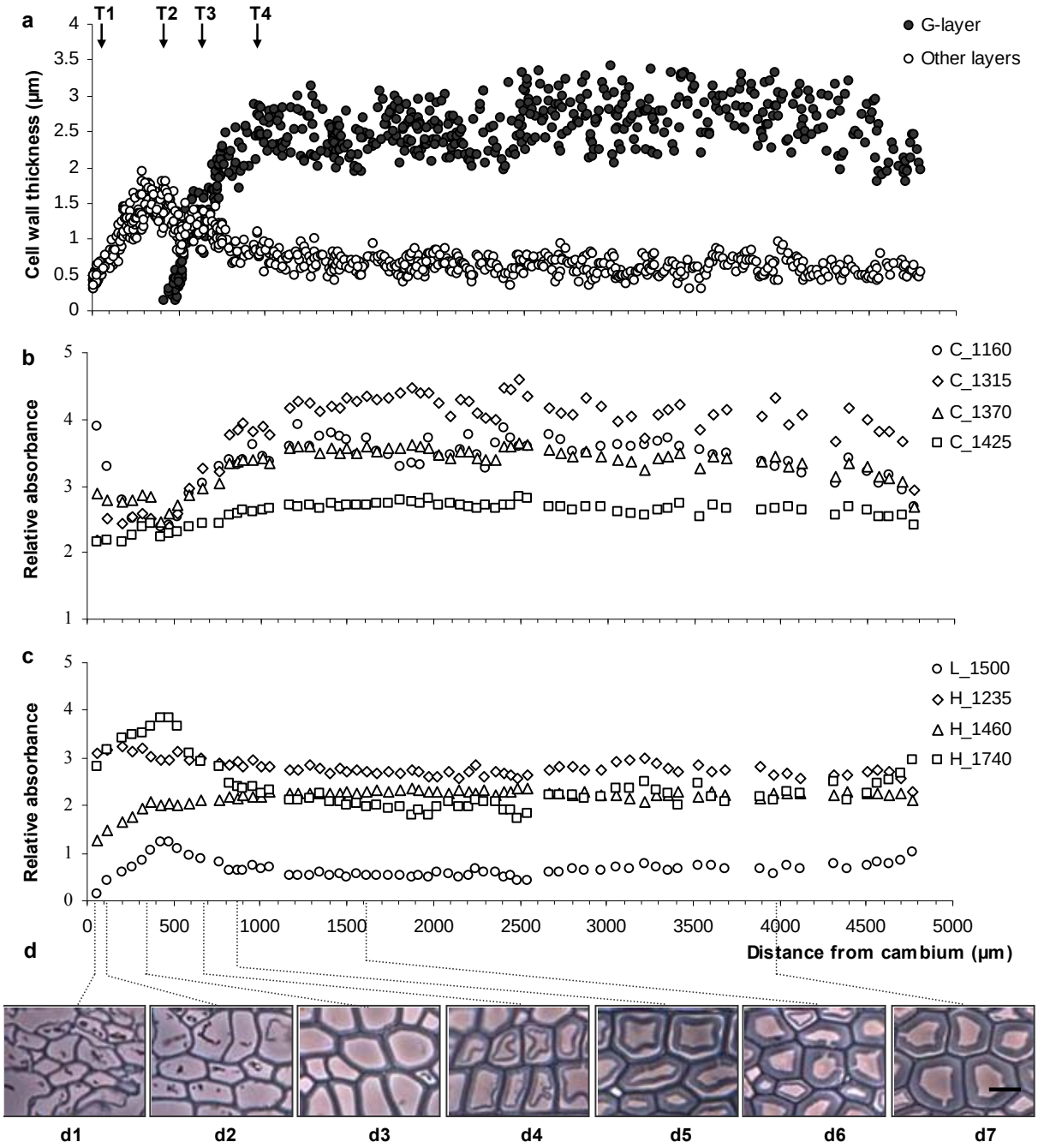

Figure 4 Changes in cell layer thickness (a) and relative intensity of absorbance bands for cellulose and other carbohydrates (b), hemicellulose and lignin (c) and morphological details of fibre (d) during cell wall maturation in poplar tension wood from tree II. T1, T2, T3 and T4 indicate the four stages of G-layer formation. The light micrographs (d1-d7) were collected with an optical microscope in phase contrast mode. Other layers: sum of all other layers in cell wall except G-layer. *Scale bar* (shown in d7) = 10 µm

Changes in FT-IR spectra

Figure 5 shows a comparison of FTIR spectra at different stages of cell maturation in tension wood of tree I. The selection of the different stages was based on the G-layer formation (Figs. 3a and 4a): before G-layer formation (stage 1, T1), early stage of G-layer formation (stage 2, T2), later stage of G-layer formation (stage 3, T3) and completion of the thickening of the G-layer (stage 4, T4). The main differences in the absorption spectra were visible at wavenumbers 1,160, 1,235, 1,315, 1,370, 1,425, 1,460, 1,500 and 1,740 cm^{-1}.

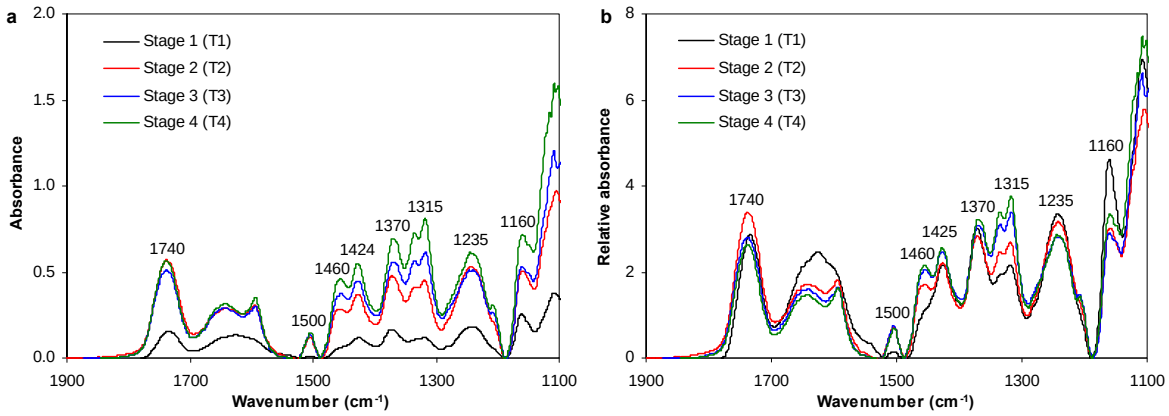

Figure 5 Non-polarised FTIR spectra in the region from 1,800 to 1,100 cm^{-1} at four stages (T1, T2, T3, T4) of cell wall differentiation in poplar tension wood from tree I. a Non-normalized spectra; b Normalized spectra. The peak numbers refer to the assignments in Table 1

Chemical composition

Table 1 lists the typical bands assigned to cellulose, lignin, and xylan (the dominating hemicellulose in hardwood) as well as to pectins and xyloglucans, in the wavenumber interval 1,800-1,100 cm^{-1}. For each assignment of an IR band to a functional group, an interval is given reflecting the range of the maxima reported in the literature.

Table 1 Assignment of IR bands in the range of 1,800-1,100 cm^{-1} to functional groups of wood polymers

Wavenumber (cm^{-1}) range of maxima	Assignment	Orientation of polarisation to main axis of polymer	Components
1158-1162	C-O-C asymmetric stretch	0°	Dominated by cellulose (Liang and Marchessault 1959; Liang et al 1960; Marchessault 1962), but present in all carbohydrates
1232-1239	C-O stretching in O=C-C group	90°	Xylan, lignin-carbohydrate complex (Marchessault 1962)
1312-1316	CH_2 wagging	90°	Cellulose (Liang and Marchessault 1959)
1365-1372	C-H bending	0°	Cellulose (crystalline) (Liang and Marchessault 1959; Marchessault 1962)
1421-1430	C-OH bending of the CH_2-OH group	0°	Cellulose (Marchessault 1962)
1452-1462	CH_2 symmetric bending on xylose ring	90° (0° to glucan chain in xyloglucan)	Xylan (Marchessault 1962), Xyloglucan (Vodenicarova et al. 2006)
	CH deformation in CH_3 and CH_2	-	Lignin (Faix 1991)
1500-1510	C=C aromatic symmetrical stretching	0°	Lignin (Marchessault 1962; Faix 1991)
1730-1742	C=O stretching in glucuronic acid	54°	Xylan (Marchessault 1962; Marchessault and Liang 1962)
	C=O stretching in galacturonic acid/acetyl esters	?	Pectins (Synytsya et al. 2003; Fellah et al. 2009)

The relative absorbance of characteristic FTIR absorbance bands is plotted as a function of the stage of maturation of the cell walls in the tension wood of tree I in Figs. 3b, c, and for tree II in Figs. 4b, c. In the tension wood of tree I, early in the cell wall development within the first 350 µm, the absorbance peak of the carbohydrate C-O-C vibration at 1,160 cm^{-1} dominated the spectra. At this stage, the signal can be specifically assigned to cellulose, as indicated by the 1,370 cm^{-1} absorbance peak, and to pectins, as indicated by the large relative sorption peak at 1,740 cm^{-1}, assigned to C=O stretching in the galacturonic acid of pectic substances. At this stage, the discrepancy between the absorbance level of the 1,160 peak and that at 1,315, 1,370 and 1,425 may be due to the high pectin content compared with that of cellulose. Changes in the 1.740 cm^{-1} peak were at this stage also influenced by the deposition of xylan. With lignification, absorbance increased at 1,500 cm^{-1} and the relative absorbance peaks associated with carbohydrates generally diminished except for the 1,460 cm^{-1} band related to xylan deposition which occurred at the same time. This band shows also contribution from lignin vibrations, but is more strongly influenced by molecular vibrations of the xylose unit (Stevanic and Salmén 2009). The decrease was especially apparent in the 1,740 cm^{-1} band and could be associated with a drop in relative pectin content. With the formation of the G-layer, identified by the change in cell wall thickness (Fig. 3a) and by microscope observations (d4-d5 in Fig. 3d), relative cellulose content increased (the relative increase in the absorbance peaks at 1,315, 1,370 and 1,425 cm^{-1}). At the same time, a further increase in the relative absorbance peak of the 1,460 cm^{-1} band was visible. This was probably due to the deposition of xyloglucans. After completion of G-layer formation in the interval from 900 to 5,400 µm from the cambial zone, the relative intensity of each band remained constant until the transition, between 5,400 µm and 6,400 µm (c'-c in Fig. 1) to normal wood (c-b in Fig. 1). The light micrographs of the transverse sections (Fig. 1) did not show the presence of a G-layer in this region, which was created before the tilting of the stem and consequently contained relatively less cellulose and more lignin and hemicellulose than tension wood. The tension wood of tree II revealed similar changes in band intensities during maturation of the cell wall (Fig. 4b, c). However, measurements were not made right up to the stage of the normal wood before tilting.

Concerning opposite wood, it was not possible to monitor the early part of the cell wall formation with FTIR measurements. After formation of the final secondary cell wall, the relative intensities of the IR absorbance bands were constant, as observed in the normal wood region in the tension wood side (data not shown).

Molecular orientation

Figures 6, 7 and 8 compare the molecular orientation assigned to cellulose, lignin, and hemicelluloses and pectins at four stages during cell differentiation of tension and opposite wood from tree I and tree II, respectively. For tension wood, the selection of the four stages was the same as for FTIR spectra comparison (Fig. 5). For opposite wood, the stages were

defined as: O1, early stage of cell wall thickening; O2, later stage of cell wall thickening; O3, completion of cell wall thickening and O4, the mature cell wall.

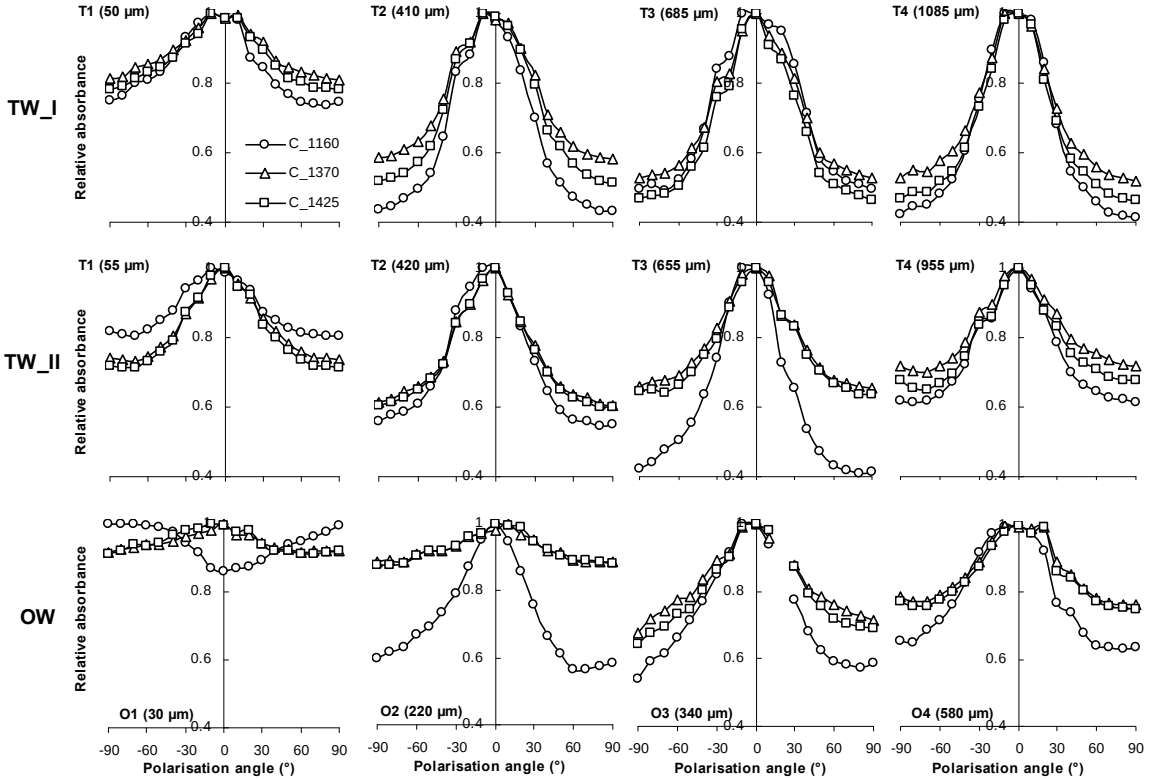

Figure 6 Orientation distribution of typical bands assigned to cellulose for spectra taken from four stages (T1/O1, T2/O2, T3/O3, T4/O4) during cell differentiation of poplar tension (TW) and opposite wood (OW) (TW_I and TW_II denotes tension wood taken from tree I and tree II respectively; the distance from the cambium zone is given in brackets; a few aberrant points due to measurement disturbances were removed from the figure)

Figure 6 presents diagrams of the orientation of the absorbance peaks assigned primarily to cellulose. For tension wood, no apparent changes were observed as a function of the stages of cell maturation and the fibrillar orientation was in all cases parallel to the fibrillar axis; i.e. to the fibre axis considering that the microfibril angle is generally low for these fibres. As G-layer formation proceeded, the amount of highly orientated cellulose increased, following the completion of thickening of the G-layer, as indicated by the increased difference in absorbance between polarisation angles. For the opposite wood, at the early stage of cell wall thickening, indications of orientation are rather small, if any; a small orientation of the 1,160 cm^{-1} band perpendicular (90°) to the fibre axis was noted (absorbance differences between 1.0 and 0.9 may be too low to indicate orientation). At this stage, microscope observation only indicated the presence of the primary wall and/or S_1 layer, while the S_2 layer was subsequently formed and thickened when the distance from the cambial zone was greater than 60 µm. At this stage the C-O-C orientation probably may reflect a perpendicular orientation of cellulose in the primary wall, S_1 layer. However it should be noted that the C-O-C absorption peak at 1,160 cm^{-1} also have contributions from all carbohydrates present and the discrepancy in the orientation of the peaks at 1,370 and 1,425 cm^{-1} may point to orientation contribution in these layers, the primary and S_1 layer, from other carbohydrates. At

later stages of cell wall formation, when the S_2 layer was laid down, the difference in absorbance between polarisation angles indicated a smaller proportion of cellulose oriented at an angle of 0^o than that observed in tension wood. Compared with tension wood, the orientation distributions for bands assigned to cellulose in opposite wood generally had wider peaks, especially the bands at 1,370 and 1,425 cm^{-1}. This probably reflects the fact that, unlike in tension wood, in opposite wood, absorbance was not dominated by the thick G-layer but showed a mix of contributions from the orientations of microfibrils in the S_1, S_2 and S_3 layer.

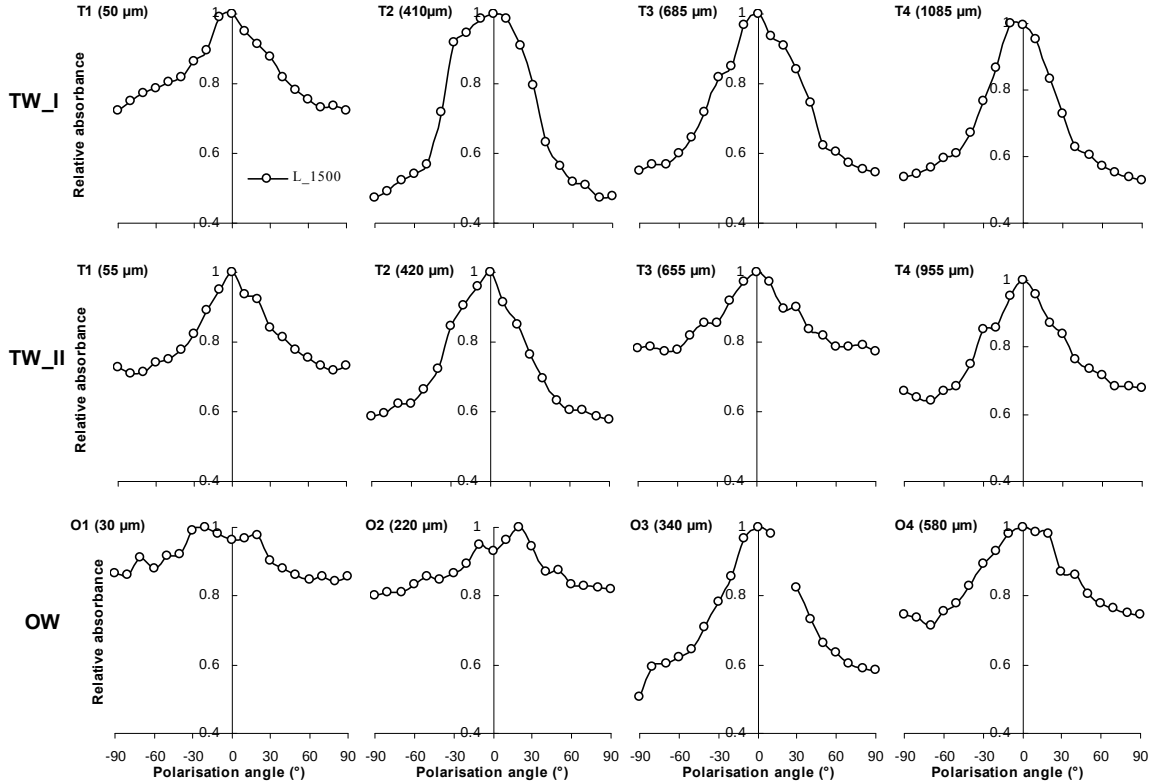

Figure 7 Orientation distribution of the absorption band assigned to lignin for spectra taken from four stages (T1/O1, T2/O2, T3/O3, T4/O4) of cell differentiation of poplar tension (TW) and opposite wood (OW) (TW_I and TW_II denotes tension wood taken from tree I and tree II respectively; the distance from the cambium zone is given in brackets; a few aberrant points due to measurement disturbances were removed from the figure)

The absorbance peak at 1,500 cm^{-1}, assigned to lignin (Fig. 7), showed a surprisingly high degree of orientation compared to that observed for cellulose (only slightly lower in magnitude between the differences in absorbance between polarisation angles; Fig. 6) both for tension wood and opposite wood. This orientation of lignin has also previously been demonstrated by Raman spectroscopy (Agarwal and Atalla 1986) in the transverse plane and by FTIR in the longitudinal direction (Salmén et al. 2012). In all cases, the peak was clearly centred around 0^o, indicating that lignin was oriented more or less parallel to the fibre axis except during the early stages of cell maturation in opposite wood. In tension wood, oriented lignin was observed early in the cell wall development at low lignin content and before G-layer deposition. As the formation of the G-layer advanced, the degree of orientation increased and became more distinct at the later stage of G-layer formation. Opposite wood generally showed a higher relative absorbance for the lignin peak at 1,500 cm^{-1}, reflecting the higher overall lignin content compared to tension wood. The lignin present in tension wood is

mostly associated with the S_2 wall and the lignin content in the G-layer is low or even nil (Pilate et al. 2004). In the present study, the difference in absorbance between polarisation angles was however generally found to be lower in opposite wood than in tension wood (Fig. 7).

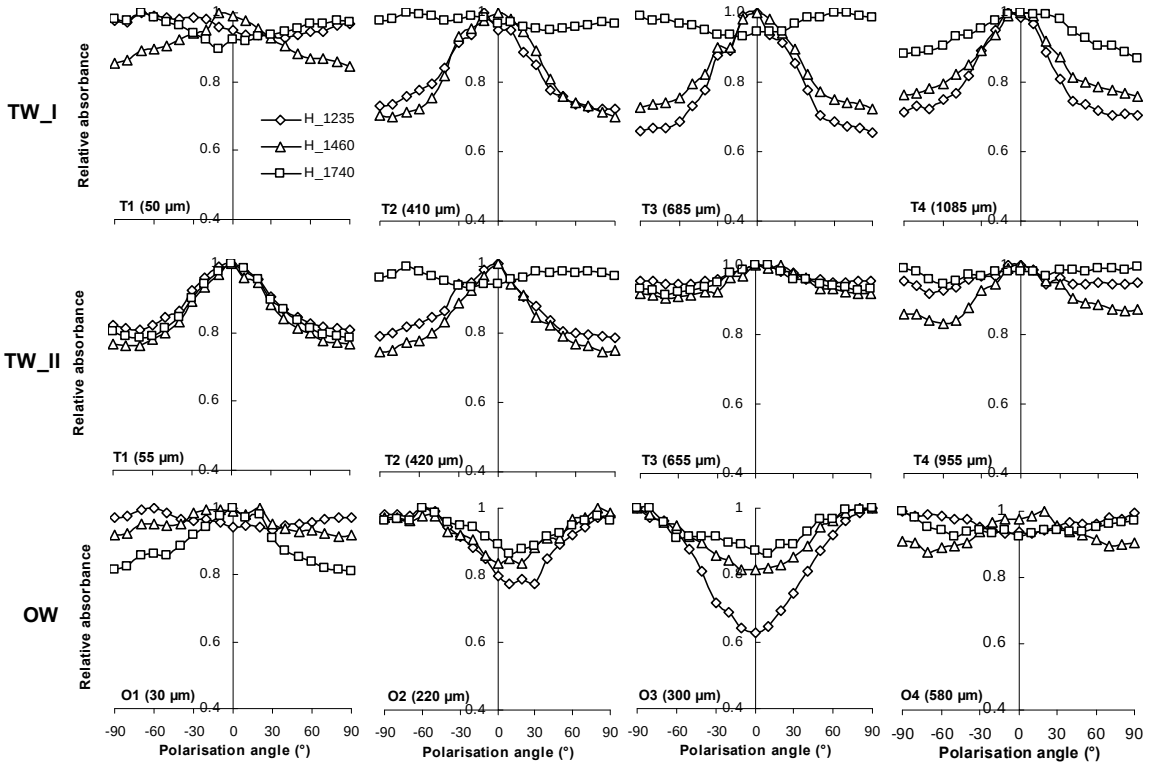

Figure 8 Orientation distribution of typical bands assigned to carbohydrates like hemicelluloses and pectins for spectra taken from four stages (T1/O1, T2/O2, T3/O3, T4/O4) during cell differentiation in poplar tension (TW) and opposite wood (OW) (TW_I and TW_II denotes tension wood taken from tree I and tree II respectively; the distance from the cambium zone is shown in brackets)

Figure 8 shows the orientation dependence of peaks assigned to hemicelluloses and pectin. At 1,235 and 1,460 cm^{-1}, vibrations are traditionally thought to be dominated by the C-O stretching in the O=C-O group of xylans and the CH_2 asymmetric bending of the xylose ring, respectively. Both are assigned as being perpendicular to the main chain axis (Marchessault 1962). During the formation of the G-layer in tension wood, these two absorbance signals showed clear orientation dependence, with higher absorbance at lower polarisation angels; i.e. at an angle of 0^o. This implies an orientation of the structure of xylose units of the carbohydrates at an angle of 90^o to that of the cellulose, a fact that has also previously been observed and related to the presence of xyloglucans oriented parallel to the cellulose in the same direction as the fibre axis (Olsson et al. 2011) (the xylose units of xyloglucan being oriented perpendicular to the glucan backbone). It should here be noted that a difference in absorbance between 1.0 and 0.9 with polarization angle may not be taken as an indication of orientation due to the normal variation in this type of measurements. Also in the early stage, T1, of cell differentiation in tension wood, the orientation of the CH_2 1,460 cm^{-1} peak was similar to that in the later stage.

In the early stage of cell differentiation, the vibration at 1,740 cm^{-1} was assigned to C=O stretching in galacturonic acid of pectic substances. In the later stage of secondary cell wall thickening, the band at 1,740 cm^{-1} was assigned to C=O stretching in glucuronic acid of xylan. This vibration is predominately oriented at an angle of 54° to the xylose unit of the xylan backbone in hardwood (Marchessault and Liang 1962) which is why little information may be gained regarding orientation from this absorbance peak, as discussed earlier. In opposite wood, at a later stage of cell wall thickening (stage 2, O2) and the stage of completion of cell wall thickening (stage 3, O3), the peaks at 1,235, 1,460 and 1,740 cm^{-1} in general had a maximum relative absorbance at high angles. This is in agreement with earlier findings, suggesting the orientation of xylan parallel to that of the cellulose microfibrils (Marchessault and Liang 1962; Olsson et al. 2011).

Before the deposition of the G-layer in tension wood, the hemicellulose signals at 1,235, 1,460 and 1,740 cm^{-1} showed similar orientations both in tension and opposite wood. In the following stages of G-layer formation, the orientation of the signals in tension wood remained the same, while in opposite wood the orientation of the signals at the stage of secondary cell wall thickening changed and was opposite to those in tension wood.

Discussion

In cells at the early stage of cell wall thickening (Stage 1, O1) in opposite wood, which only contained primary wall/S_1 wall, a perpendicular (90°) orientation of the cellulose 1,160 cm^{-1} peak was observed. In the following cell wall thickening stages when the S_2 wall dominated, the cellulose showed a more parallel (0°) orientation. This is in agreement with general microscope observations of cellulose microfibril orientation and with results of studies of changes in cellulose structure during maturation by Kataoka and Kondo (1998). The orientation of the primary wall cellulose is directly related to the enlarging cells, resulting in a less orientated distribution than that in the mature wood cell wall. However, in tension wood, an orientation parallel to the fibre axis was already visible at the early stage of cell wall development. This orientation was less clear than that of cells with full S_2 wall formation, but nevertheless distinct. This is surprising considering the rather low cellulose content compared to other carbohydrates. The more distinct orientation of the lignin at this stage also indicates a more ordered cell wall formation and a difference in the structure of tension wood to that of opposite wood already at this stage of cell wall maturation.

Although small amounts of lignin-like compounds have been detected in the G-layer of some tension wood fibres (Joseleau et al. 2004; Gierlinger and Schwanninger 2006), we conclude that most of the lignin signal originates from the lignified S_2 layer and very little from the G-layer (given the marked difference in lignin content between the G-layer and the adjacent S_2 layer and also the fact the G-layer is thicker). The orientation distribution of lignin was more or less parallel to the fibre axis, which was in line with earlier observations in hybrid aspen (Olsson et al. 2011). However, it should be noted that, compared to opposite wood, the higher degree of orientation of the lignin found in tension wood probably implies a higher degree of

ordering and orientation of the secondary wall in tension wood fibres than in the corresponding S_2 wall of opposite wood.

In the case of hemicelluloses and pectins, different orientations were observed between tension and opposite wood during formation of the G-layer. Although the mechanism behind the generation of stress in tension wood remains unknown, the matrix polysaccharides in the G-layer probably undergo mechanical stress due to chemical reactions and interaction with the cellulose microfibrils (Mellerowicz et al. 2008) which could result in increased orientation of the polymers. It is also possible that at this stage of development, other polysaccharides like xyloglucan or pectins in the G-layer (Nishikubo et al. 2007; Bowling and Vaughn 2008; Mellerowicz et al. 2008; Kaku et al. 2009; Mellerowicz and Gorshkova 2012) may dominate the signals, as has been suggested in aspen tension wood (Olsson et al. 2011). The tensional stress in the G-layer can only be transmitted to adjacent layers when these are connected by xyloglucan cross-links or long-lived xyloglucan-endo-transglycosylase (XET) activity (Mellerowicz et al. 2008). However some of the signals may also be related to xylan as it was recently reported that the G-layer may also contain xylan (Kim and Daniel 2012). The question remains, however, why, if so, this xylan is organised perpendicular to the orientation seen in opposite wood.

Conclusion

Polarised FTIR measurements revealed that in tension wood, at the early stage of cell wall development already before the formation of the G-layer, the C-O-C adsorption peak from carbohydrates showed an orientation more parallel to the fibre axis. This behaviour clearly differed from that in opposite wood. In the later stages of G-layer formation, a higher degree of orientation of cellulose was observed in tension wood than in opposite wood. In all cases, the orientation of lignin was parallel to that of cellulose microfibrils, with a higher degree of orientation in tension wood than in opposite wood. This is attributed to a more ordered S_2 wall in tension wood than in opposite wood. During the formation of the G-layer in tension wood, signals attributed to amorphous carbohydrates (hemicelluloses and pectins) were oriented at an angle of 90^o to that measured in opposite wood. These signals may originate from the generation of xyloglucan regulating stress in *Populus* tension wood (Baba et al. 2009), but could also be attributed to xylan (Kim and Daniel 2012). In tension wood, the orientation of the bands assigned to amorphous carbohydrates remained the same throughout the cell wall maturation process, probably reflecting continued deposition of xyloglucan or of xylan with a different orientation from that in the S_2 wall of opposite wood.

Acknowledgements This work was supported by COST Action FP0802 through the Short Term Scientific Mission (STSM) funding for Shan Shan Chang. Shan Shan Chang benefits a fellowship from the Scientific Council of Montpellier University. Lennart Salmén received support from the Wallenberg Wood Science Center (WWSC). The authors wish to thank Gilles Pilate and Françoise Laurans (AGPF, Genobois technical platform, INRA Orleans, France) for providing the wood samples and for making the stained sections presented in Fig. 1, Jasna Stevanic Srndovic and Joanna Hornatowska (Innventia Stockholm, Sweden) for their assistance during FTIR experiment. Thanks are also extended to Cécile Barron (INRA Montpellier, France) and Antonio Pizzi (ENSTIB-LERMAB

Epinal, France) for critical discussions. Part of this work was performed in the framework of the project “StressInTrees” funded by the French National Research Agency (ANR-12-BS09-0004).

References

Agarwal UP, Atalla RH (1986) In-situ Raman microprobe studies of plant cell walls: macromolecular organization and compositional variability in the secondary wall of *Picea mariana* (Mill.) B.S.P. Planta 169: 325-332

Baba K, Park YW, Kaku T, Kaida R, Takeuchi M, Yoshida M, Hosoo Y, Ojio Y, Okuyama T, Taniguchi T, Ohmiya Y, Kondo T, Shani Z, Shoseyov O, Awano T, Serada S, Norioka N, Norioka S, Hayashi T (2009) Xyloglucan for generating tensile stress to bend tree stem. Mol Plant 2: 893-903

Bowling AJ, Vaughn KC (2008) Immunocytochemical characterization of tension wood: gelatinous fibers contain more than just cellulose. Am J Bot 95:655-663

Cosgrove DJ, Jarvis MC (2012) Comparative structure and biomechanics of plant primary and secondary cell walls. Front Plant Sci 3:204. doi: 10.3389/fpls.2012.00204

Faix O (1991) Classification of lignins from different botanical origins by FTIR spectroscopy. Holzforschung 45:21-27

Fellah A, Anjukandi P, Waterland MR, Williams M AK (2009) Determining the degree of methylesterification of pectin by ATR/FT-IR: Methodology optimisation and comparison with theoretical calculations. Carbohyd Polym 78:847-853

Fisher JB, Stevenson JW (1981) Occurence of reaction wood in branches of dicotyledons and its role in tree architecture. Bot Gaz 142:82-95

Gierlinger N, Schwanninger M (2006) Chemical imaging of poplar wood cell walls by confocal Raman microscopy. Plant Physiol 140:1246-1254

Joseleau JP, Imai T, Kuroda K, Ruel K (2004) Detection in situ and characterization of lignin in the G-layer of tension wood fibres of *Populus deltoids*. Planta 219:338-345

Kaku T, Serada S, Baba K, Tanaka F, Hayashi T (2009) Proteomic analysis of the G-layer in poplar tension wood. J Wood Sci 55:250-257

Kataoka Y, Kondo T (1998) FT-IR microscopic analysis of changing cellulose crystalline structure during wood cell wall formation. Macromolecules 31:760-764

Kim JS, Daniel G (2012) Distribution of glucomannans and xylans in poplar xylem and their changes under tension stress. Planta 236:35-50

Liang CY, Bassett KH, McGinnes EA, Marchessault RH (1960) Infrared spectra of crystalline polysaccharides. Tappi J 43:1017-1024

Liang CY, Marchessault RH (1959) Infrared spectra of crystalline polysaccharides. II. native celluloses in the region from 640–1,700 cm^{-1}. J Polym Sci 39:269-278

Marchessault RH (1962) Application of infra-red spectroscopy to cellulose and wood polysaccharides. Pure Appl Chem 5:107-129

Marchessault RH, Liang CY (1962) The infrared spectra of crystalline polysaccharides. VIII. xylans. J Polym Sci Pol Chem 59:357-378

Mellerowicz EJ, Gorshkova TA (2012) Tensional stress generation in gelatinous fibres: a review and possible mechanism based on cell-wall structure and composition. J Exp Bot 63:551-565

Mellerowicz EJ, Immerzeel P, Hayashi T (2008) Xyloglucan: the molecular muscle of trees. Ann Bot-London 102:659-665

Nishikubo N, Awano T, Banasiak A, Bourquin V, Ibatullin F, Funada R, Brumer H, Teeri T, Hayashi T, Sundberg B, Mellerowicz EJ (2007) Xyloglucan endotransglycosylase (XET) functions in gelatinous layers of tension wood fibers in poplar - a glimpse into the mechanism of the balancing act of trees. Plant Cell Physiol 48:843-855

Norberg PH, Meier H (1966) Physical and chemical properties of gelatinous layer in tension wood fibers of aspen (*Populus tremula* L.). Holzforschung 20:174-178

Olsson AM, Bjurhager I, Gerber L, Sundberg B, Salmén L (2011) Ultra-structural organization of cell wall polymers in normal and tension wood of aspen revealed by polarization FTIR microspectroscopy. Planta 233:1277-1286

Pilate G, Chabbert B, Cathala B, Yoshinaga A, Leplé JC, Laurans F, Lapierre C, Ruel K (2004) Lignification and tension wood. C R Biol 327:889-901

Salmén L, Burgert I (2009) Cell wall features with regard to mechanical performance COST Action E35: Wood machining – micromechanics and fracture. Holzforschung 63:121-129

Salmén L, Olsson A-M, Stevanic J, Simonović J, Radotić K (2012) Structural organisation of the wood polymers in the wood fibre structure. BioResources 7:521-532

Stevanic J, Salmén L (2009) Orientation of the wood polymers in the cell wall of spruce wood fibres. Holzforschung 63: 497-503
Synytsya A, Copikova J, Matejka P, Machovic V (2003) Fourier transform Raman and infrared spectroscopy of pectins. Carbohyd Polym 54:97-106
Timell TE (1986) Compression wood in gymnosperms. Springer-Verlag, Heidelberg
Vodenicarova M, Drimalova G; Hromadkova Z, Malovikova A, Ebringerova A (2006) Xyloglucan degradation using different radiation sources: A comparative study. Ultrasonics Sonochem 13: 157-164
Wardrop AB (1964) The reaction anatomy of arborescent angiosperms. In: Zimmermann MH (ed) The formation of wood in forest tree, Academic Press, New York, pp 405-456
Wardrop AB, Dadswell HE (1955) The nature of reaction wood IV. variations in cell wall organization of tension wood fibres. Aust J Bot 3:177-189
Yoshinaga A, Kusumoto H, Laurans F, Pilate G, Takabe K (2012) Lignification in poplar tension wood lignified cell wall layers. Tree Physiol 32: 1129-1136

4.2 Mesoporosity changes during the cell wall maturation of tension wood in a G-layer specie

Article to be submitted[3]

Changes in mesoporosity in wood cell walls during tension wood formation in regard to maturation stress generation in poplar trees

CHANG Shan-Shan[1], QUIGNARD Françoise[2], CLAIR Bruno[1, 3]

[1]: Laboratoire de Mécanique et Génie Civil (LMGC), CNRS, Université Montpellier 2, cc 048, Place E. Bataillon, 34095 Montpellier, France

[2]: Institut Charles Gerhardt Montpellier, UMR 5253 CNRS-UM2-ENSCM-UM1, 8 rue de l'Ecole Normale, 34296 Montpellier cedex 5, France

[3]: CNRS, UMR Ecologie des Forêts de Guyane (EcoFoG), Campus Agronomique, BP 701, 97387 Kourou, French Guiana

Abstract: To progress in the understanding of stress generation in tension wood, the mesoporosity of the cell wall and its evolution during maturation of tension wood and opposite wood were measured by nitrogen adsorption-desorption. Variations in the thickness of the gelatinous layer (G-layer) were also measured to clarify whether the mesoporosity change simultaneously with the deposition of the G-layer in tension wood. Results shows that mesoporous structure of tension and opposite wood were very similar in early development stages before the deposition of G-layers. With the formation of the S_2 layer in opposite wood and the G-layer in tension wood, the mesopore volume decreased steeply due to lignification. However, in tension wood only, the decrease in mesopore volume occurred together with the pore shape change and a progressive increase in pore size range. The different patterns observed in tension and opposite wood revealed new information about the particular ultrastructure of G-layer. Pores from G-layers appear with a different shape and size compared to the mesoporosity of the middle lamella and primary wall. However, it appears difficult to record a change during maturation that could be attributed to the mechanism of tensile stress.

Keywords: *Mesoporosity; tension wood; cell wall maturation; growth stress*

Introduction

Trees have a remarkable ability to modulate their secondary growth to adapt their material to environmental stresses (slope, winds, snow or light). More than just modifying the wood amount around the circumference, trees adapt the mechanical state of the wood produced. All around the circumference of the trunk, newly formed wood layer are produced under tensile stress. When modulating the level of stress, tree can develop a dissymmetry of the stresses around the tree generating a bending moment allowing the trunk to recover verticality or maintain a branch at a defined angle. In angiosperm trees, asymmetry is produced by developing a wood with high tensile stress, called tension wood, on the upper side of the

[3] Following discussions during and after the defence of the PhD, this manuscript will be largely modified before submission, changing discussion and conclusion.

leaning stem (Wardrop 1964; Fisher and Stevenson 1981). In tension wood, tensile tress is around 5 to 10 times higher than in opposite wood (Archer 1986; Fournier et al. 1994; Clair et al. 2013). The generation of this stress occurs during the maturation of the cell wall, and is then called maturation stress. This process may start after differentiation and elongation as during these early phases the cell membrane is too soft to support the stress. Then, stress generation is suspected to finish when cell wall is stiff enough, possibly (but not surely) with the cell dead.

In most of the temperate species, such as poplar, tension wood is characterized by the presence of gelatinous (G-) fibres which contain a peculiar cell-wall layer, called G-layer (Onaka 1949; Dadswell and Wardrop 1955) replacing S_3 and part or whole of the S_2. The G-layer is highly cellulosic with highly crystalline cellulose and microfibrils oriented nearly parallel to the fibre axis (Fujita et al. 1974; Daniel et al. 2006). Cellulose microfibrils are embedded within a matrix of polysaccharides, including pectin (Bowling and Vaughn 2008), hemicelluloses (xyloglucan (Nishikubo et al. 2007), glucomannan and xylan (Kim and Daniel 2012), AGP (arabino-galactan proteins) (Andersson-Gunneras et al. 2006; Lafarguette et al. 2004; Bowling and Vaughn 2008). A strong activity of a xyloglucan transglucosylase /hydrolase (XTH)) was also detected in the G-layer (Nishikubo et al. 2007; Mellerowicz et al. 2008; Hayashi and Kaida 2010) but recent observations by Guedes et al. (2013, in press) tend to infirm this result. Contrary to any other secondary wall, G-layer is almost devoid of lignin (Pilate et al. 2004; Yoshinaga et al. 2012).

Although there is some controversy regarding the origin of the tensile maturation stresses, when it is present, the G-layer is recognised as playing the essential role in the mechanism of stress generation in tension wood. First evidence come from the relationship between amount of G-layer and the stress level; the higher the amount of G-layers, the higher the tensile stress (Yamamoto et al. 2005; Clair et al. 2003; Fang et al. 2008). Second evidence, at the cell wall level, is the high contracting strain of G-layer when creating a free surface in a tension wood sample (Clair et al. 2005), proving that G layer is not only the driver (as proposed by Münch 1938 and Goswami et al. 2008) but is also the support of the tensile stress. Finally, the observation of the cellulose lattice spacing changes in the fibre direction using synchrotron X-ray diffraction during stress release (Clair et al. 2006) and following maturation process (Clair et al. 2011) revealed that tensile stress is directly supported by cellulose microfibrils and that the stress is generated synchronously with the synthesis of the G-layer in poplar tension wood.

However, still remain to address the mechanism of maturation stress: what generate this tension inside G-layer microfibrils? Different hypotheses have been proposed and discussed to explain this mechanism towards elucidating G-layer functions: due to the structure modification of the cellulose (Bamber 2001; Mellerowicz et al. 2008), the contraction of amorphous zones within the cellulose microfibrils (Okuyama et al. 1994; Yamamoto 2004), or the biochemical activity of hemicellulose in the G-layer matrix during the formation of microfibril aggregates (Nishikubo et al. 2007; Mellerowicz et al. 2008; Bowling and Vaughn 2008). Alméras et al. (2012) proposed several mechanisms where the stress would be

transferred to the cellulose microfibrils by the swelling or shrinkage of the matrix in an interconnected network of cellulose microfibrils. These mechanisms are based on the hydrophilic properties of gels. Indeed, G-layer has a structure similar to gels with a large amount of water-filled mesopores (Clair et al. 2008; Chang et al. 2009). Gels are known to be able to exhibit high shrinkage or swelling in response to physicochemical changes, like ion concentration change. In angiosperm, similar cellulose-based hydrogels have been shown the pit membranes of vessels and it has been proposed that the microstructure change depend on the change of cation concentration (van Ieperen 2007). Therefore, physicochemical changes by pectin-like substances in the G-layer matrix could make swell or shrink the G-layer matrix and then be the driving force of the growth stress generation in tension wood. These strains are expected to induce textural modification of the gel of the G-layer. The aim of this study is to follow these changes during the maturation process of poplar tension wood.

Nitrogen adsorption method allows estimating the pore size and surface area of materials with cavities from 2 to 50 nm (Gregg and Sing 1982; Rouquerol et al. 1999). This technique applied to the study of the texture of tension wood allowed to identify the hydrogel structure of the G-layer characterized by a large amount of water-filled mesopores, with peak-pore size ranging from 6 to 12 nm in chestnut (*Castanea sativa* Mill.) tension wood (Clair et al. 2008), poplar tension wood (Chang et al. 2011, 2012) and in several tropical species (Chang et al. 2009).

In this study, wood tissues were sampled at different deepness from the cambium to mature wood on the upper side (tension wood) and the lower side (opposite wood) of a naturally tilted poplar tree. Mesopore texture of the sample were analysed thanks to nitrogen isotherm technique in order to record the shape and size of mesopores during wood formation and check the assumption of G-layer matrix swelling or shrinkage during maturation stress generation.

Materials and Methods

Sampling

A naturally tilted poplar (*Populus deltoides* × *P. nigra*) tree (diameter at breast height, 24 cm) grown in Grabels (Domaine Maspiquet, Lycee Agropolis Montpellier) in south of France was sampled on 7 June 2012 during a fast growing period. Tree was fall down at 11:00 AM and sampling was performed early afternoon at the laboratory. The sampling was made on both upper side (tension wood) and lower side (opposite wood) of the leaning stem according to the procedure described below. The bark and phloem were carefully removed to open a "window" (Fig. 1A). For the bark side, the inner surface of the phloem was peeled with knife blade and the peeled sample was marked as T0 and O0 respectively for tension side and opposite side. For the xylem side, the back of scalpel blade was used to peel the entire surface gently, and the first peeled sample was marked as T1 and O1. For the second and third peeled samples (numbered #2 and #3), the front of scalpel blade and a knife blade were used

respectively with increasing the peeling force but carefully avoiding sectioning. After three peeled samples, it becomes impossible to obtain the samples by peeling due to the increase of cell wall stiffness. Then wood blocks (20×10×10 mm, L×T×R) were extracted from the peeled area with care to avoid compression tangential side and maintain samples in wet condition during the time of sampling. Then 300µm (3×100µm/section) thick tangential sections were further cut successively from the wood blocks with a sliding microtome until cross the previous growth ring. Finally 12 sectioned samples for tension wood side, numbered T4 to T15 and 9 sectioned samples for opposite wood side, numbered O4 to O12 were obtained respectively. Immediately after peeling and sectioning, samples were kept in 30% ethanol and dehydrated in a graded series of ethanol solutions (30%, 50%, 70%, 85%, 96% and 100%). The distance from the cambial zone was recorded for each peeled sample and tangential section. The dehydrated samples were exchanged with liquid CO_2 and supercritically dried before nitrogen adsorption measurements to keep intact the mesoporosity avoiding the collapse of the gel (Clair et al. 2008).

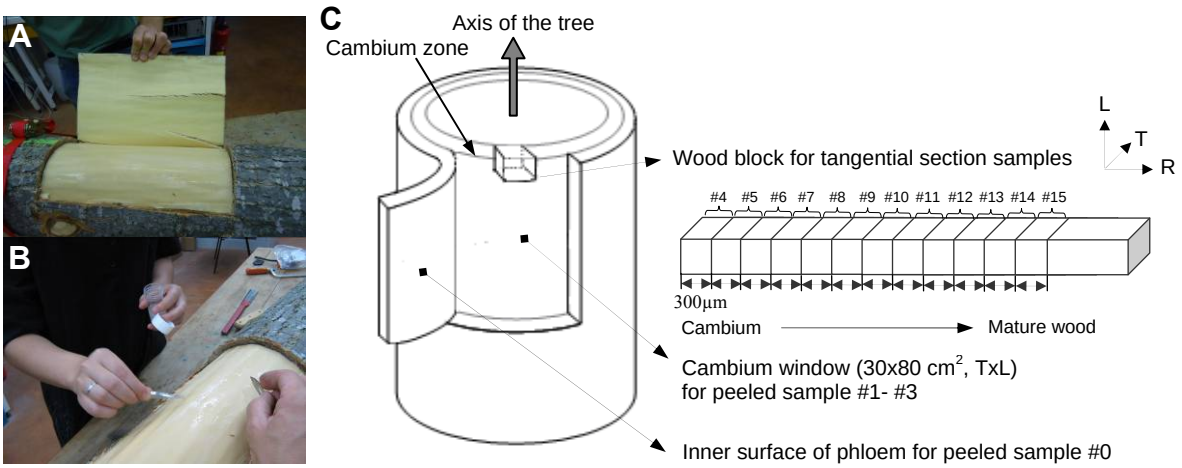

Figure 1 Picture of the peeling experiment. A, debarking; B, peeling T1; C, schematic diagram showing sample preparation for N_2 adsorption-desorption measurement to examine the mesoporosity from each developmental stage of poplar tension wood cell wall formation (tension wood side taken as example)

Microscopic observations and cell wall thickness measurement

A wood block extracted from un-peeled sample block at the vicinity of the peeled part were dehydrated with ethanol and embedded in LR White resin (two exchanges of resin/ethanol mixture for 1 hour, followed by two exchanges in pure resin for 1 hour and kept overnight at room temperature, then polymerised at 65°C overnight). Transverse sections of 1 µm thickness were cut with a diamond knife and observed with an optical microscope (Leica Microsystems) in phase contrast mode. The radial cell wall thicknesses (with and without G-layer) were manually measured from the images using the image analysis software ImageJ (National Institutes of Health, Bethesda, MD, USA). Measurement of cell wall thicknesses without G-layer allows calculation of non-G-layer cell wall (called other layers: OL), and measurement of thicknesses with G-layer allows calculation of G-layer thickness (GL) by subtracting OL.

N_2 adsorption–desorption measurement

The supercritically dried samples (around 0.4-0.7g) were outgassed at 323 K under vacuum until a stable 3×10^{-5} Torr pressure was reached without pumping. This is done to remove physically adsorbed gases from the sample surface, in particular, water vapour. Nitrogen adsorption-desorption isotherms were recorded at 77 K on a micromeritics ASAP 2020 volumetric apparatus.

This experimental technique allows evaluating the specific surface area (S_{BET}, Brunauer et al. 1938) which is directly correlated to the pore volume (Gregg and Sing 1982) and the pore size distribution (Broekhoff and de Boer 1967) of the samples. In order to characterise the change in the whole distribution of pore sizes, pore size is not only characterised by its peak pore size (size of the pores the more represented) but by its range of distribution. The pore size range was calculated from adsorption pore size distribution diagrams (Fig. 2) after integration of the area under the curve of pore size distribution. Corresponding pore size at 25%, 50% (median) and 75% of the volume were then plotted for each peeling or section sample (Figs. 3c, 4c).

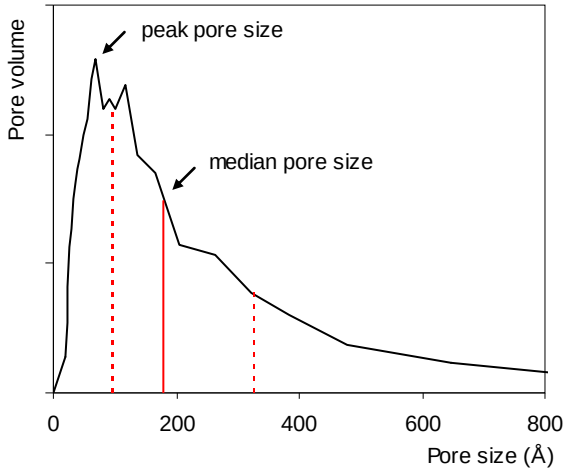

Figure 2 Representation of the median pore size and pore size range distribution calculated from the adsorption pore size distribution (Broekhoff and de Boer method). 50% of the pore volume has pore size in between the two vertical dotted lines (25% and 75%). Plane vertical line represents the median pore size (50%).

Other poplar trees where sampled, some in cambial zone (unpublished data) and, some in mature wood (Chang et al. 2011, 2012) and results were in good agreement with presented data. In order to validate the repeatability of our measurements, part of the samples were also duplicated and here again, results were in perfect accordance.

Results

Cell wall thickness

Figures 3b and 4b show variations in the average thickness of cell wall layers during maturation of opposite wood and tension wood respectively. The thicknesses are plotted versus the distance of the measured fibres from the cambial zone. In figures 3a and 4a light micrographs of the transverse sections of opposite wood and tension wood respectively are shown, displaying the cell differentiation at different distance from the cambium. These

photographs demonstrated that the optical microscopy in phase contrast mode allows one to easily trace G-layer formation from un-stained transverse sections.

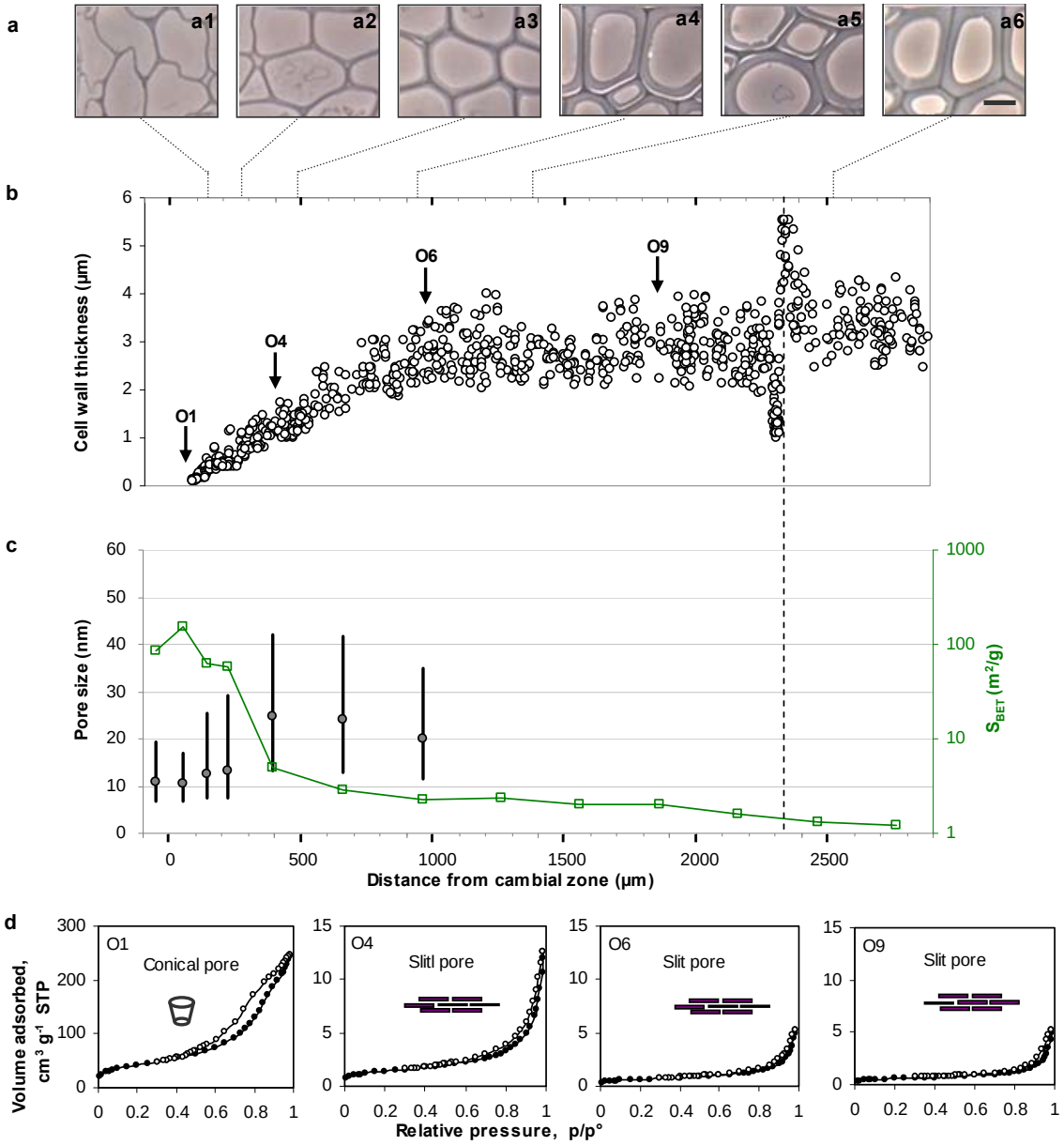

Figure 3 Characterization parameters of poplar opposite wood during cell wall maturation. (a) morphological fibre details according to the distance from the cambial zone in poplar opposite wood, (b) cell layer thickness, (c) median pore size (filled circle), pore size range distribution (straight lines), and specific surface area (open squares with green line) and (d) nitrogen isotherms at four stages (filled symbols, adsorption; open symbols, desorption; the corresponding pore shape presented in each figure). The specific surface area was shown in logarithmic scale. O1, O4, O6 and O9 indicate the four stages of cell wall maturation. The light micrographs (a1-a6) were acquired with an optical microscope in phase contrast mode. Scale bar (shown in a6) =10 µm

In the first 500 µm after the cambium, the gradual thickening of the fibre secondary wall layer is clearly visible both in opposite wood and tension wood (a1-a3 in Fig. 3 and a1-a2 in Fig. 4). No difference in cell morphology between opposite wood and tension wood could be observed in this area. In opposite wood, the thickening of the cell walls is completed at 1100 µm after the cambium where the cell wall thickness remains constant (a5-a6 in Fig. 3). No G-layer was observed in the opposite wood sample (Fig. 3a). In tension wood, after 500 µm, G-

layers start to become visible (a3 in Fig. 4), however, the sudden decrease of OL at the same position, let think that a very thin G-layer could be already produced at around 400µm (doted line in fig. 4b is an interpolation from zero of the G-layer thickening) but is not detectable (Fig.4 a2) before 500µm. Then, the thickness increased almost linearly until ~1600 µm (Fig. 4b, a3 to a5).

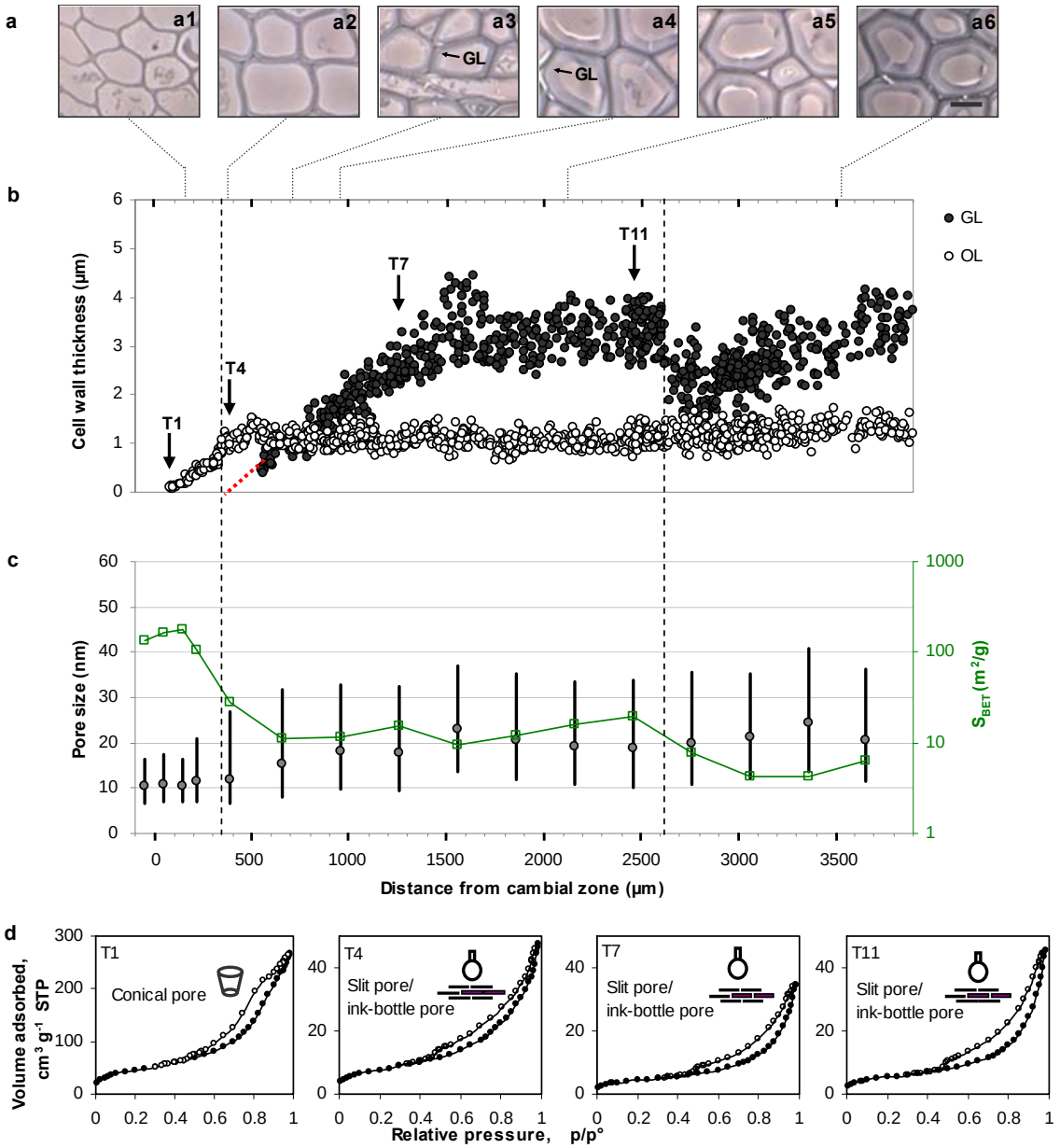

Figure 4 Characterization parameters of poplar tension wood during cell wall maturation. (a) morphological fibre details according to the distance from the cambial zone, (b) cell layer thickness, (c) median pore size (filled circle), pore size range distribution (straight lines), and specific surface area (open squares with green line) and (d) nitrogen isotherms at four stages (filled symbols, adsorption; open symbols, desorption; the corresponding pore shape presented in each figure). Vertical dotted lines at distance 350 µm were supposed to appear G-layer; vertical dotted line around distance 2600 µm was the previous growth ring. T1, T4, T7 and T11 indicate the four stages of G-layer formation during tension wood maturation. The specific surface area was shown in logarithmic scale. The light micrographs (a1-a6) were acquired with an optical microscope in phase contrast mode. GL: G-layer; OL: sum of all other layers in cell wall except G-layer. Scale bar (shown in a6) =10 µm

Since the G-layer thickness was positively correlated with fibre diameter (Fang et al. 2008), the G-layer thickness change abruptly at growth ring region around 2600-2800 µm (Fig. 4b).

The similar phenomenon also occurred in opposite wood, which showed sharp change of the cell wall thickness at growth ring region around 2300-2400 μm (Fig. 3b).

Pore shape

The shape of the nitrogen adsorption-desorption isotherms combined with the difference in pore shape distribution obtained from adsorption and desorption inform on the shape of the pores in the samples (Groen and Pérez-Ramirez 2004). Isotherms are compared at all stages during cell differentiation of tension wood and opposite wood; only four stages are presented in Fig. 3d and Fig. 4d (full set of data is presented in supplementary material, Figs. 8 and 9). For opposite wood, the selection of the four stages were defined as follow: O1, early stage of cell wall thickening; O4, later stage of cell wall thickening; O6, the completion of cell wall thickening and O9, the mature cell wall. For tension wood, the selection of the four stages was based on the G-layer formation: before G-layer deposition (T1), early stage of G-layer formation (T4), later stage of G-layer formation (T7) and completion of the thickening of the G-layer (T11). Measurements at other locations showed similar isotherms for each differentiation stages.

The amount of nitrogen needed to form a monolayer of adsorbed molecules provides a good estimate of the surface area of the samples. The high surface area is accompanied by a significant porosity. According to the IUPAC classification (Sing et al. 1985), the isotherms of tension wood are types IV with a H3 type hysteresis loop, indicating the presence of mesopores with a non-uniform size. For opposite wood, the isotherm of the first stage (O1) is similar with tension wood. For the next three stages of opposite wood, the isotherms are intermediated between type IV and type II, indicating the presence of large mesopores with a broad size distribution that continues into the macropore domain. The hysteresis loop is very narrow, the adsorption and desorption branches being almost vertical and nearly parallel above 0.9 relative pressure.

Peak pore size determined from the adsorption branch of the isotherm corresponds to the cavity size, while that of the desorption branch corresponds to the throat size of a pore (Groen and Pérez-Ramirez 2004). Thus, comparing the adsorption and desorption pore size distribution leads to information about the pore shapes. At stage 1, for both tension wood and opposite wood, the peak pore size measured from the adsorption branch (7 nm) is smaller than the peak pore size measured from the desorption branch (8 nm). And both isotherms show a wide hysteresis loop between the adsorption and desorption branches with the gradually desorption near $p/p°=0.48$. This behaviour has been observed in adsorbents with highly connected three-dimensional pore systems (Fan et al. 2001) and can be attributed to cone-shape pores with a wide opening, which decreases the activation energy of condensation.

Different from stage 1, with the G-layer formation (stages 2 to 4) in tension wood, a sudden desorption appears near $p/p°=0.48$ in all the isotherms, presenting the pore opening is somewhat narrower than the pore body. The peak pore size calculated from desorption branches are still 8 nm, whereas more than one peak appears on the adsorption pore size

distribution, with mean size of 7 and 12 nm. To produce such a similar distribution, some of the pores have an ink-bottle shape with pore cavities that are less than twice the diameter of the throats, while others could have a slit-shape character with nearly constant cavity and throat sizes. Even the hysteresis loop type at these stages are not similar as type H2 which often presents the mesopores with ink-bottle shape, the comparison of peak pore size from adsorption and desorption branches shows the possibility of pore with ink-bottle shape. This typical mesopore shape is characteristic of G-layer as previously described in mature poplar (Chang et al. 2011) and chestnut tension wood (Clair et al. 2008). The transition from conical pores to ink-bottle shape pores appears clearly between samples T3 and T4, indicating that a mesoporosity typical from G-layer is already observed before the G-layer is visible in phase contrast microscopy.

For opposite wood at stages 2 to 4, the hysteresis loops are very narrow, and the adsorption data shows similar pore size to that of the desorption data (mean peak size of 8 nm). It indicates the presence of mesopores between the cellulose microfibrils or in the matrix forming slit-shaped pores. However, it should be noted that due to the low mesopore volume and low surface area in opposite wood, the pore shape and pore size distributions have to be interpreted with caution.

Specific surface area S_{BET} and pore size distribution

The changes in the specific surface area S_{BET} of opposite wood and tension wood are shown in Figures 3c and 4c, respectively. The value of S_{BET} increases near the cambium zone, corresponding to the thickening of the meristematic cell walls, which consists mainly of an unorganised cellulose network embedded in the hydrogel made of hemicelluloses and pectic components. In this stage, similar values are observed in both tension wood and opposite wood, where the former shows wider range of increase, probably due to the higher growth rate of tension wood side. After this stage, as expected, the specific surface area (expressed as $m^2.g^{-1}$) decrease with the lignin impregnation, filling the pores and increasing mass. The specific surface area of opposite wood decreases greatly until close to disappear (1.2-1.5 m^2/g), parallel to the linear increase of the cell wall thickness. In tension wood, the steep decrease of specific surface area starts from sample T3 at 105 m^2/g to sample T5 at 11 m^2/g and then maintain constant, thanks to the appearance of G-layer from T4.

Pore size ranges are shown in Figures 3c and 4c and a detail on some of the pore size distribution (determine from absorption isotherm) is given in Fig. 5. Opposite wood and tension wood have very similar patterns near the cambium zone (at the first +300 µm after cambium) with median pore size around 10 nm and peak pore size at around 7 nm. Cell walls at this stage are mainly composed of the middle lamella and primary walls. After this stage, a new contribution of pores with peak pore size of 11.5 nm is observed in both opposite wood and tension wood (Fig. 5). The contribution of this peak increases during maturation to become higher than the peak at 7 nm at the end of the maturation process, both in opposite and tension wood (Fig. 5). This stage of cell maturation is also accompanied by an increasing

median pore size and a wider pore range (Fig. 3c and 4c). In tension wood, the pore size range progressively increases with wider pore size range centred around 20 nm, nearly 2 times higher than in the cambial zone, synchronously with the deposition of the G-layer. This range remains nearly constant after tension wood cell wall reaches its final thickness. In opposite wood, median pore size increase much faster to reach around 25 nm in sample O4 and sample O5. After 1000 µm, it becomes impossible to follow the pore size change in opposite wood due to the low volume of nitrogen adsorbed closes to the instrumental limitation.

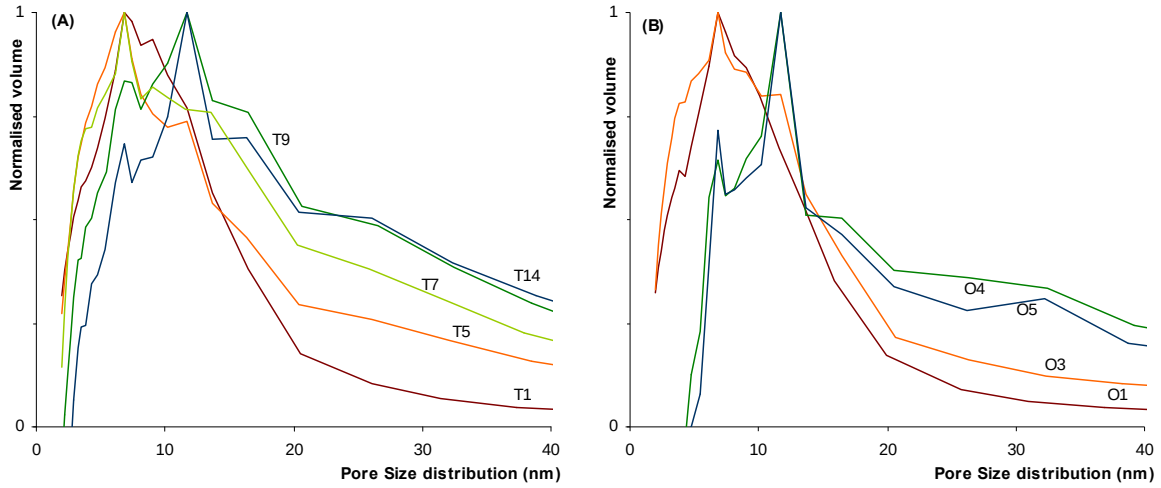

Figure 5 Pore size distributions determined from absorption branch of the isotherms of 5 of the samples from tension wood (A) and 4 of the samples from opposite wood (B). Pore volume is normalised by the maximum value in volume (at peak pore size) in order to emphasis the shift in pore size with increasing contribution of pores around 11.5 nm

Discussion

The nitrogen adsorption-desorption isotherm method allowed to explore the mesoporosity changes during cell wall maturation in tension wood and opposite wood. The development of the primary wall started with the deposition of material with porous matrix with high mesopore volume for both tension and opposite wood. The similar hysteresis loop indicates both tension wood and opposite wood have a network of large-mouth conical pores in this developmental stage. With the cell wall thickening, the high porosity in the primary wall of opposite wood decreases abruptly and is nearly lost. This can be explained by the lignification process that fills the pores and increase the weight of the wall, hiding the remaining mesoporosity as the mesopore volume is given by its ratio to sample mass. However, in tension wood the decreases linked to the lignification of the developing wall is compensated by a new mesoporosity, with ink-bottle shape pores, maintaining the mesopore amount. This new mesoporosity, characterized by a pore shape typical of what was observed in G-layer (Clair et al. 2008; Chang et al. 2009, 2011, 2012), is observable shortly before G-layer was distinguished in phase contrast optical microscopy and remains all along the G-layer development up to mature wood. This ink-bottle pore shape is never observed in opposite wood, even during the maturation process. However, peak pore size is shifted from 7 to 11 nm in the early stage of maturation of opposite wood like in tension wood indicating that the mesoporous texture of secondary wall in opposite wood do not differ by the shape of

pores but differ in pore size compare to middle lamella and primary wall. In mature opposite wood, very low but not-nil mesopore volume was detected. This mesoporosity was proposed to be affected to the pit membranes of the vessels (Clair et al. 2008; Chang et al. 2009), which are known to be composed of unlignified primary wall with pectin gel as the G-layer (Van Ieperen 2007). Interestingly, this mesoporosity is characterized by a pore size range wider than G-layer and nearly three times wider than in primary wall of the same specimen. This would suggest that, if well attributed to the pits, primary wall at the pit position would be modified during the maturation by enlarging the pores in order to achieve its conductive functions.

Main interest for the understanding of maturation stress generation is the specific behaviour of mesoporosity during maturation of G-layer. It appears that pore size range increase progressively from a median value at 12 nm where first ink-bottle pore are visible (T4, around 400 µm from the cambium) to around 20 nm at 1600 µm far from the cambium when G-layer thickness remain stable and G-layer can be considered as mature. However, because the method does not allow localisation of the mesoporosity, two hypotheses (Fig. 6) can be formulated on this increasing pore range and need to be analysed before any conclusion.

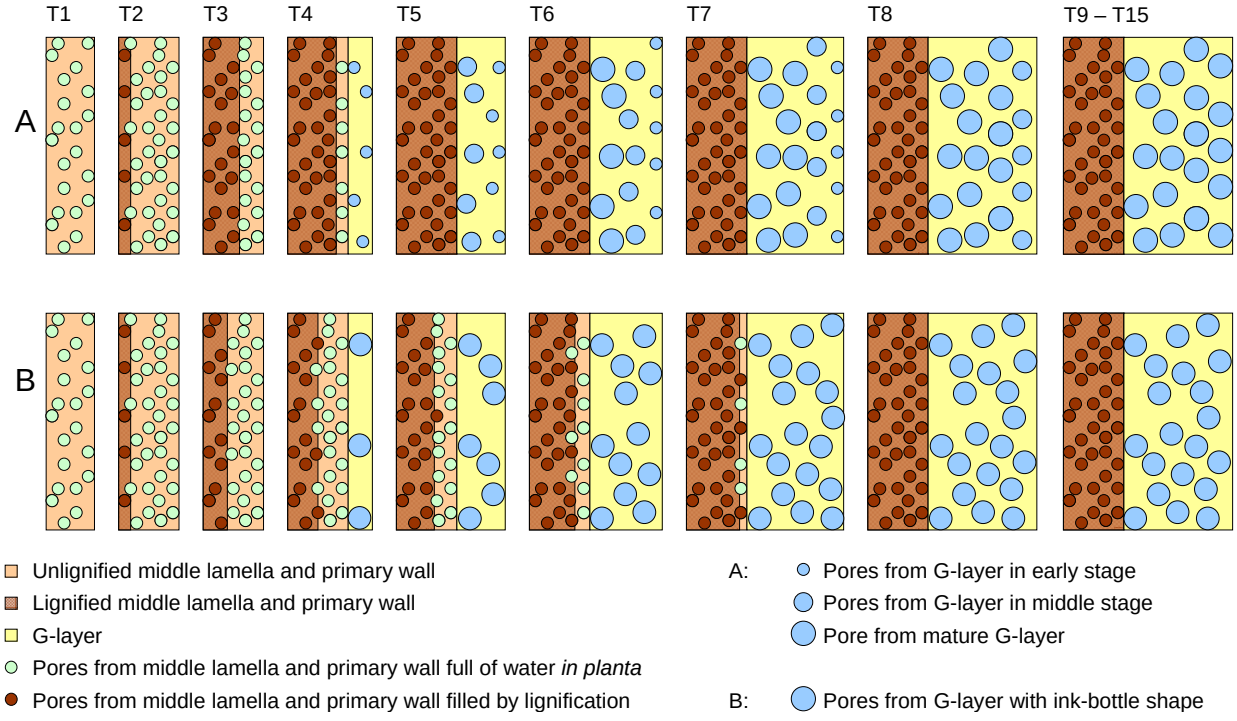

Figure 6 Schematics drawing of the change in mesoporosity during maturation of the tension wood cell wall. Circles represent a mean pore size whereas it as been shown that a wide distribution of pore sizes are present. A: hypothesis of pore swelling, B: hypothesis of pore mixture without swelling.

In a first hypothesis (Fig. 6A), the mesopores measured from T4 are assumed to relate to G-layer only. Then, increasing pore size range can be attributed to the swelling of the pores during the maturation process. In a second hypothesis (Fig. 6B), part of the pores from layers deposited before the G-layer (OL) are still present when start the deposition of the G-layer and are filled during the thickening of G-layer. Then, apparent increase in pore size would

results from the mixture of these two kinds of pores with different sizes; smaller pores in OL and wider pores in G-layer, with a decreasing amount of small pores (filled during maturation) and an increasing amount of bigger pores with the thickening of G-layer.

In order to test these hypothesis, a mixture law model have been built to reconstruct each isotherm curve by a combination of isotherms T1 (considered as typical of OL) and T15 (considered as typical of mature tension wood) and proportion of each were adjusted thanks to least-squares minimisation method. Results (Fig. 7) show that the level of resemblance to mature TW is already more than 50% in sample T3, before G-layer was observed and isotherms present hysteresis typical of ink-bottle pores. However, considering the much higher level of mesoporosity in OL compare to mature TW, after correction by pore volume of respective samples T1 and T15 it appear a much more progressive increase of the T15 pore contribution from only 5.5% in T3 to reach 100% in sample T8 (Fig. 7 left). The good agreement in the comparison of the median pore size calculated from the results of the mixture model and the measured values (Fig. 7 right) validates the use of the mixture law to evaluate the amount of both contributions.

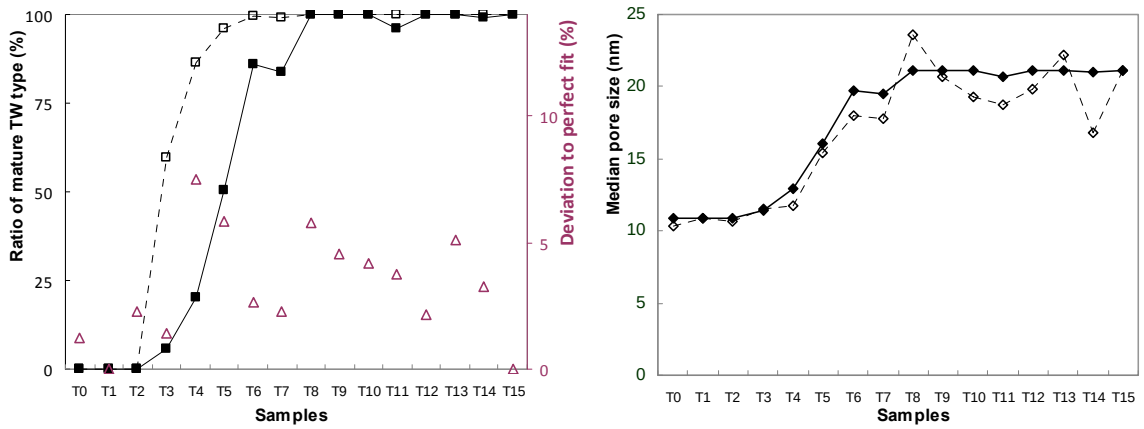

Figure 7 Left: Results of the mixture law between sample T1 (considered as representative of OL mesoporosity) and T15 (considered as representative of mature tension wood mesoporosity). Empty square: relative amount of T15 sample (tissue level), full square: relative amount of T15 mesopores. Triangles represent the deviation to perfect fit resulting from mixture law calculation. Right: Mediane pore size measured (empty diamond) and modelized median pore size thanks to ratio determined by the mixture law model (full diamond).

This model allows to confirm that the mixture hypothesis (B) cannot be rejected. This hypothesis is also supported by the work from Yoshinaga et al. (2012) evidencing that lignification process of OL is not finished when G-layer appears and continue during the thickening of the G-layer. This would explain that some pores from OL remains accessible even after the start of deposition of the G-layer and are progressively filled synchronously with the apparition of G-layer. Following this hypothesis, our results would show that pores from G-layer could be formed with a typical size, around two times bigger than pores from OL and would not swell during maturation.

The swelling hypothesis (A) could not rather been rejected as identical mixture law would be possible considering that new formed pores in the G-layer have similar shape and size than pores present in OL. However the clear change in isotherm shape between T3 and T4 (see

supplementary material, Figs. 8 and 9) demonstrate that even in the early stage of G-layer deposition, pores from G-layer have already a shape similar to mature G-layer and not to OL pores.

An alternative hypothesis still remains if we reconsider the kinetic of the maturation process. This experiment was setup to observe a change occurring all along the thickening of the wall. However, it can be supposed that the swelling process, if any, occurs in a very short time with a fast swelling of pores just after their deposition. In these condition the ratio of smaller pore in the sample compare to already swelled pores would be very low and not distinguishable. This hypothesis is supported by the higher deviation to perfect fit observed for T4 in the mixture model (Fig. 7a). This deviation indicate that fitting was more difficult in this sample, letting think that a different pore type may have contribute to the T4 isotherm. The section of 300µm on which this measurement was done would have been interestingly divided in thinner ones to allow detection of intermediary step during this stage, before the G-layer was too thick. This hypothesis cannot be excluded but remain speculative and our data do not allow to be conclusive on the eventual swelling of pores from G-layer.

Conclusion

The study shows that middle lamella and primary wall have a highly mesoporous texture, identical in tension wood and opposite wood, composed of conical pores with peak pore size centred at 7 nm. In this area, 50% of the mesoporous volume is comprised in a narrow range of pore size between 7 and 16 nm. In secondary wall, peak pore is centred on 11 nm both in tension wood and opposite wood but pore shape differs. Whereas pores of the secondary wall in opposite wood show only slit-shaped pores, in G-layer slit-shaped pores are mixed with ink-bottle pores. Pore size range is much wider in secondary wall than in middle lamella and primary wall with median pore size comprise between 10 and12 nm whereas median pore size is around 18-23 nm for mature tension wood and 20 to 25 nm with wider range in early opposite wood.

This new step in the understanding of cell wall maturation process and especially in tension wood let several questions open. Next step could be to isolate G-layer from these different stages of maturating G-layer in order to avoid the contamination in the signal due to other layers. The method of sonication proposed by Norberg and Meier (1966) have been largely reproduced these last years and would allow to remove the undesired noise produced by the presence of the maturation other layers. However, first will be needed to evaluate the damages produced by sonication on the texture of G-layer as it as been already observed in bacterial cellulose (Tischer et al. 2010).

Acknowledgements Shan Shan Chang was supported by a fellowship from the Scientific Council of Montpellier University. The authors wish to thank P. Brunier from Domaine Maspiquet in Grabels (Lycee Agropolis Montpellier) for the poplar tree used for this study. Thanks also go to T. Alméras (LMGC Montpellier, France) for his help in data processing and critical reading of the manuscript. Part of this work was performed in the framework of the project “StressInTrees” funded by the French National Research Agency (ANR-12-BS09-0004).

References

Alméras T, Gril J, Clair B (2012) The origin of maturation stress in tension wood: using a wide range of observations and mechanical considerations to discriminate between hypothetic mechanisms. 7th plant biomechanics international conference, Clermont-Ferrand, France.

Andersson-Gunneras S, Mellerowicz EJ, Love J, Segerman B, Ohmiya Y, Coutinho PM, Nilsson P, Henrissat B, Moritz T, Sundberg B (2006) Biosynthesis of cellulose-enriched tension wood in Populus: global analysis of transcripts and metabolites identifies biochemical and developmental regulators in secondary wall biosynthesis. The Plant Journal 45: 144-165

Archer RR (1986) Growth Stresses and Strains in Trees. Springer Verlag, Berlin

Bamber RK (2001) A general theory for the origin of growth stresses in reaction wood: how trees stay upright. IAWA Journal 22: 205-212

Bowling AJ, Vaughn KC (2008) Immunocytochemical characterization of tension wood: gelatinous fibers contain more than just cellulose. American Journal of Botany 95: 655-663

Broekhoff JCP, de Boer JH (1967) Studies on pore systems in catalysts: IX. Calculation of pore distributions from the adsorption branch of nitrogen sorption isotherms in the case of open cylindrical pores A. Fundamental equations. Journal of Catalysis 9: 8-14

Brunauer S, Emmett PH, Teller E (1938) Adsorption of gases in multimolecular layers. Journal of the American Chemical Society 60: 309-319

Chang SS, Clair B, Ruelle J, Beauchêne J, Di Renzo F, Quignard F, Zhao GJ, Yamamoto H, Gril J (2009) Mesoporosity as a new parameter in understanding of tension stress generation in trees, Journal of Experimental Botany 60: 3023-3030

Chang SS, Hu JB, Clair B, Quignard F (2011) Pore structure characterization of poplar tension wood by nitrogen adsorption-desorption method (*in chinese*). Scientia Silvae Sinicae 47: 134-140

Chang SS, Quignard F, Di Renzo F, Clair B (2012) Solvent polarity and internal stresses control the swelling behavior of green wood during dehydration in organic solution. BioResources 7: 2418-2430

Clair B, Alméras T, Pilate G, Jullien D, Sugiyama J, Riekel C (2011) Maturation stress generation in poplar tension wood studied by synchrotron radiation micro-diffraction. Plant Physiology 155: 562-570

Clair B, Alméras T, Yamamoto H, Okuyama T, Sugiyama J (2006) Mechanical state of native cellulose microfibrils in tension wood. Biophysical Journal 91: 1128-1135

Clair B, Alteyrac J, Gronvold A, Espejo J, Chanson B, Alméras T (2013) Patterns of longitudinal and tangential maturation stresses in *Eucalyptus nitens* plantation trees. Annals of Forest Science 70: 801-811

Clair B, Gril J, Baba K, Thibaut B, Sugiyama J (2005) Precautions for the structural analysis of the gelatinous layer in tension wood. IAWA Journal 26: 189-195

Clair B, Gril J, Di Renzo F, Yamamoto H, Quignard F (2008) Characterization of a gel in the cell wall to elucidate the paradoxical shrinkage of tension wood. Biomacromolecules 9: 494-498

Clair B, Ruelle J, Thibaut B (2003) Relationship between growth stress, mechanical-physical properties and proportion of fibre with gelatinous layer in chestnut (*Castanea sativa* Mill.). Holzforschung 57: 189-195

Dadswell HE, Wardrop AB (1955) The structure and properties of tension wood. Holzforschung 9: 97-104

Daniel G, Filonova L, Kallas AM, Teeri T (2006) Morphological and chemical characterisation of the G-layer in tension wood fibres of *Populus tremula* and *Betula verrucosa*: Labelling with cellulose-binding module CBM1(HjCel7A) and fluorescence and FE-SEM microscopy. Holzforshchung 60: 618-624

Fan J, Yu CZ, Wang LM, Tu B, Zhao DY, Sakamoto Y, Terasaki O (2001) Mesotunnels on the silica wall of ordered SBA-15 to generate three-dimensional large-pore mesoporous networks. Journal of the American Chemical Society 123: 12113-12114

Fang CH, Clair B, Gril J, Liu SQ (2008) Growth stresses are highly controlled by the amount of G-layer in poplar tension wood. IAWA Journal 29: 237-246

Fisher JB, Stevenson JW (1981) Occurrence of reaction wood in branches of dicotyledons and its role in tree architecture. Botanical Gazette 142: 82-95

Fournier M, Chanson B, Thibaut B, Guitard D (1994) Measurement of residual growth strains at the stem surface. Observations of different species (*in French*). Annals of Forest Science 51: 249-266

Fujita M, Saiki H, Harada H (1974) Electron microscopy of microtubules and cellulose microfibrils in secondary wall formation of poplar tension wood fibers. Mokuzai Gakkaishi 20: 147-156

Goswami L, Dunlop JWC, Jungnikl K, Eder M, Gierlinger N, Coutand C, Jeronimidis G, Fratzl P, Burgert I (2008) Stress generation in the tension wood of poplar is based on the lateral swelling power of the G-layer. Plant Journal 56: 531-538

Gregg SJ, Sing KSW (1982) Adsorption, surface area and porosity. London: Academic Press, 218-228

Groen JC, Pérez-Ramirez J (2004) Critical appraisal of mesopore determination by adsorption analysis. Applied Catalysis A: General 268: 121-125

Hayashi T, Kaida R (2010) Functions of Xyloglucan in Plant Cells. Molecular Plant 4: 17-24

Kim JS, Daniel G (2012) Distribution of glucomannans and xylans in poplar xylem and their changes under tension stress. Planta 236: 35-50

Lafarguette F, Leplé JC, Déjardin A, Laurans F, Costa G, Lesage-Descauses M-C (2004) Poplar genes encoding fasciclin-like arabinogalactan proteins are highly expressed in tension wood. New phytologist 164: 107-121

Mellerowicz EJ, Immerzeel P, Hayashi T (2008) Xyloglucan: the molecular muscle of trees. Ann Botany 102:659-665

Münch E (1938) Statik und Dynamik des Schraubigen Baus der Zwellwand, besonders der Druck- and Zugholzes. Flora 32: 357-424

Nishikubo N, Awano T, Banasiak A, Bourquin V, Ibatullin F, Funada R, Brumer H, Teeri T, Hayashi T, Sundberg B, Mellerowicz EJ (2007) Xyloglucan endotransglycosylase (XET) functions in gelatinous layers of tension wood fibers in poplar - A glimpse into the mechanism of the balancing act of trees. Plant Cell Physiology 48: 843-855

Norberg PH, Meier H (1966) Physical and chemical properties of the gelatinous layer in tension wood fibre of aspen (*Populus tremula* L.). Holzforschung 20: 174-178

Okuyama T, Yamamoto H, Yoshida M, Hattori Y, Archer RR (1994) Growth stresses in tension wood: role of microfibrils and lignification. Annals of Forest Science 51: 291-300

Onaka F (1949) Studies on compression and tension wood (translation). Wood research 1: 1-88

Pilate G, Chabbert B, Cathala B, Yoshinaga A, Leplé JC, Laurans F, Lapierre C, Ruel K (2004) Lignification and tension wood. Comptes Rendus Biologies 327: 889-901

Rouquerol F, Rouquerol J, Sing K (1999) Adsorption by powders and porous solids: principles, methodology and applications. San Diego: Academic Press, 439-467

Sing KSW, Everett DH, Haul RAW, Moscou L, Pierotti RA, Rouquerol J, Siemienewska T (1985) Reporting physisorption data for gas-solid systems. Pure and Applied Chemistry 57: 603-619

Tischer PCSF, Sierakowski MR, Westfahl H Jr, Tischer CA (2010) Nanostructural reorganization of bacterial cellulose by ultrasonic treatment. Biomacromolecules 11: 1217-1224

van Ieperen W (2007) Ion-mediated changes in xylem hydraulic resistance in planta: fact or fiction? Trends in Plant Science 12:137-142

Wardrop AB (1964) The reaction anatomy of arborescent angiosperms. In: Zimmermann, M. H. (ed.), The Formation of Wood in Forest Tree, Academic Press, New York, 405-456

Yamamoto H (2004) Role of the gelatinous layer on the origin of the physical properties of the tension wood. Wood Science and Technology 50: 197-208

Yamamoto H, Abe K, Arakama Y, Okuyama T, Gril J (2005) Role of the gelatinous layer on the origin of the physical properties of the tension wood of *Acer sieboldianum*. Wood Science and Technology 51: 222-233

Yoshinaga A, Kusumoto H, Laurans F, Pilate Gilles, Takabe K (2012) Lignification in poplar tension wood lignified cell wall layers. Tree Physiology 32: 1129-1136

Supplementary material: N_2 adsorption-desorption isotherms of poplar tension and opposite wood during the cell wall maturation

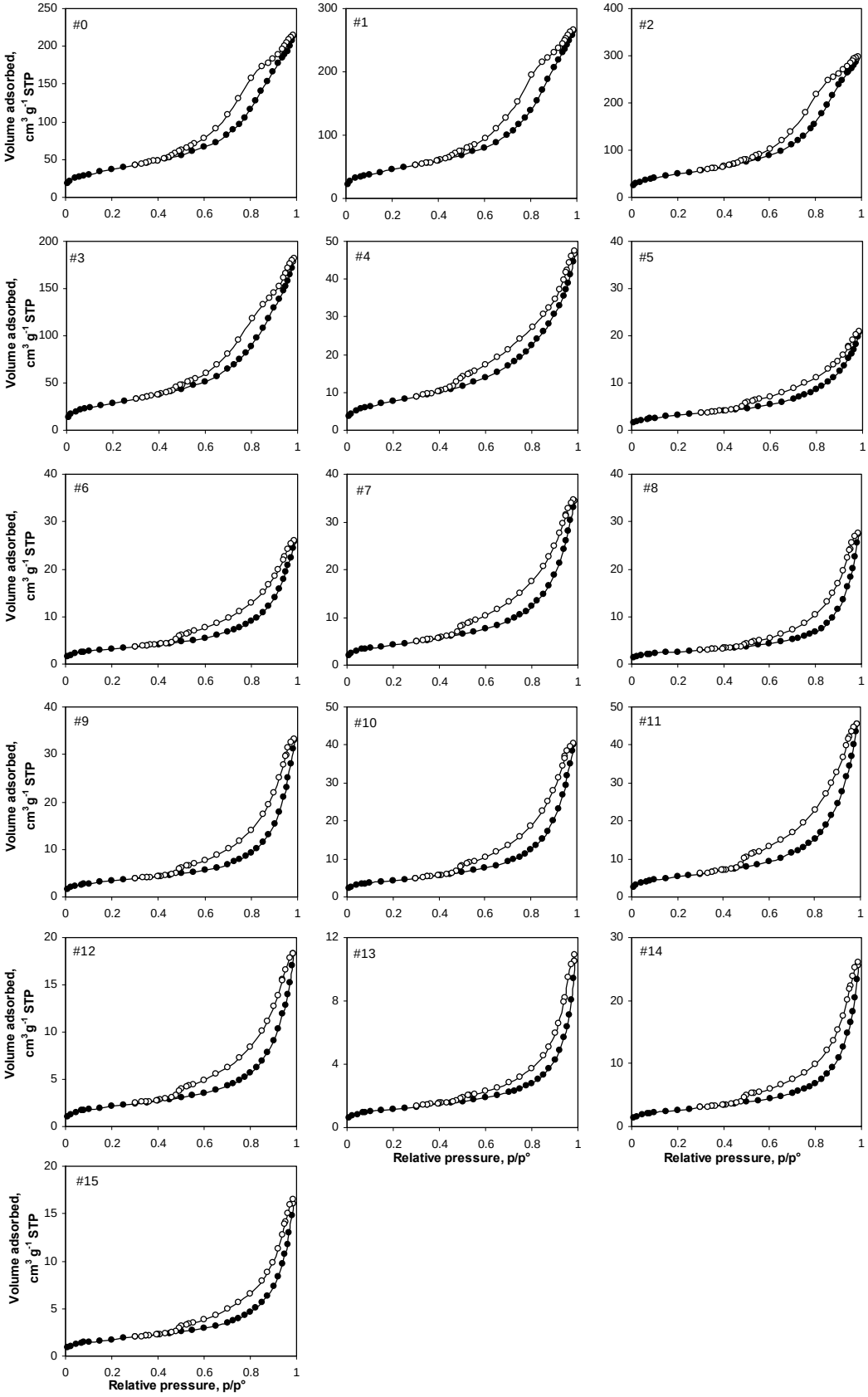

Figure 8 N_2 adsorption-desorption isotherms of poplar (II) tension wood at each location of cell wall maturation (filled symbols, adsorption; open symbols, desorption)

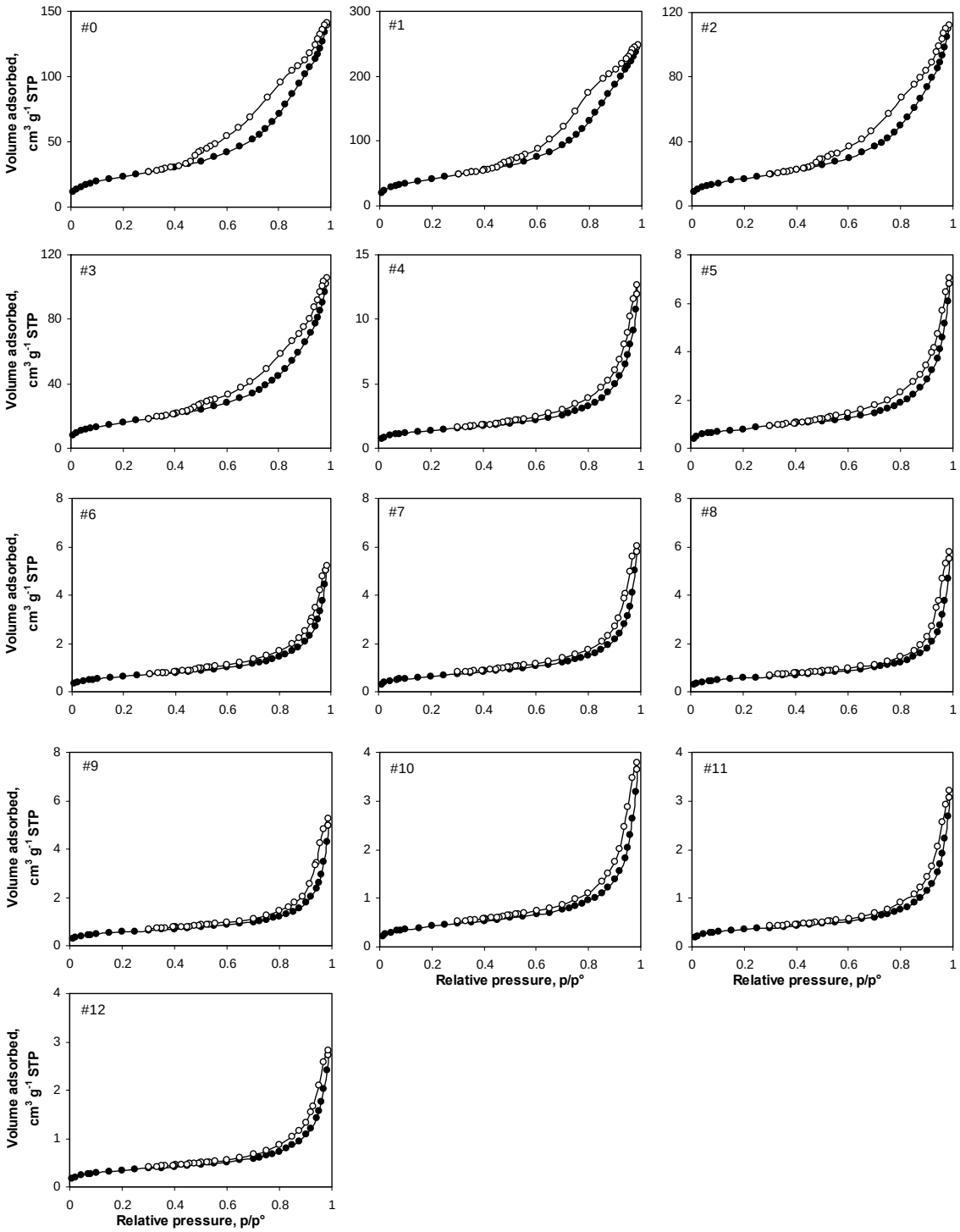

Figure 9 N_2 adsorption-desorption isotherms of poplar (II) opposite wood at each location of cell wall maturation (filled symbols, adsorption; open symbols, desorption)

4.3 Mesoporosity changes during the cell wall maturation of tension wood in a non-G-layer specie

Article to be submitted [4]

Mesoporosity change in developing tension wood and opposite wood cell walls of a non-G-layer species: *Simarouba amara* Aubl.

CHANG Shan-Shan[1], QUIGNARD Françoise [2], CHEN Mao[3], CLAIR Bruno [1, 4]

[1]: Laboratoire de Mécanique et Génie Civil (LMGC), CNRS, Université Montpellier 2, cc 048, Place E. Bataillon, 34095 Montpellier, France

[2]: Institut Charles Gerhardt Montpellier, UMR 5253 CNRS-UM2-ENSCM-UM1, 8 rue de l'Ecole Normale, 34296 Montpellier cedex 5, France

[3]: College of Material Science and Engineering, Central South University of Forestry and Technology, 410004, Changsha, Hunan, P.R.China;

[4]: CNRS, UMR Ecologie des Forêts de Guyane (EcoFoG), Campus Agronomique, BP 701, 97387 Kourou, French Guiana French Guyana

Abstract: Tension wood generates a large tensile mechanical stress to perform essential biomechanical functions such as optimizing the orientation of the stem, but the mechanism of tensile stress generation is still not fully understood. Most studies aiming to understand the tensile stress generation in tension wood mainly focuses on producing gelatinous layer (G-layer) species, while most tropical species keep the same efficiency to produce tensile stress without presenting the G-layer. In order to progress the understanding of active stress generation in non-G-layer species, this study investigated the mesoporosity change in developing cell walls in tension and opposite wood of simarouba (*Simarouba amara* Aubl.). Results shows that mesoporous structure of tension and opposite wood were very similar during the cell wall maturation. With the cell wall thickening, the total mesopore volume decreased significantly due to lignification in both tension and opposite wood. However, in tension wood, before to disappear, pores appears very similar to what is commonly observed in mature G-layer. This finding may let think a common mechanism in G-layer and non-G-layer species, and the trace of this mechanism being later hidden by lignification.

Keywords: *Cell wall maturation; growth stress; mesoporosity; non-G-layer species; tension wood*

Introduction

Tropical rain forest offers a diversity of tree species with strategies of growth that can largely differ from temperate species. This diversity can be observed in most of wood properties, providing both the lighter and the denser wood, a large range of wood colour due to numerous heart-wood production strategies with a large panel of secondary components and a huge diversity of anatomical organisation of cell types in wood. From a mechanical point of view,

[4] Following discussions during and after the defence of the PhD, this manuscript will be partially modified before submission.

tress seems also to offer a large range of strategies when regarding at the cellular level. Indeed, whereas most temperate species produce a typical un-lignified gelatinous layer in their tension wood, tropical species shows a wider range of anatomical patterns, from the typical G-layer its total absence with even no evidence of fibre cell wall thickening (Onaka 1949; Fisher and Stevenson 1981; Clair et al. 2006; Sultana et al. 2010). However, even without G-layer, these species are able to produce tension wood with strong tensile stress higher on the lower side of the stem (Clair 2006, Yoshida et al. 2002), allowing to maintain tree verticality or actively modify there angle. Among these species, the angiosperm specie *Simarouba amara* (Aubl.) have been largely studied by Ruelle et al. (2007a, b), ensuring its ability to produce tensile stress without the production of the typical G-layer. Ruelle et al, however, found some common features as the G-layer, such as a low microfibril angle, a higher crystal size and lower lignin content. Therefore, it has been speculated that the structure and chemical modifications throughout the secondary cell walls are responsible to the generation of high tensile growth stresses in non-G-layer species (Yoshida et al. 2002; Qiu et al. 2008). Since most studies aiming to understand tension stress generation in tension wood enriched G-layers, no literature is available for non-G-layer species. The question is to determine if the mechanism during maturation process is similar with G-layer species or if there is another way for non-G-layer species to produce the high tensile stress.

The G-layer in tension wood actually has a structure similar to that of gels: a large amount of water-filled mesopores (Clair et al. 2008; Chang et al. 2009) and disappear after it dries (Clair et al. 2008). Gels are known to be able to have high shrinkage or swelling behaviour in response to physicochemical changes, like water content or ion concentration change. The physicochemical changes by pectin-like substances in the G-layer matrix could be the driving force of the growth stress generation in G-layer tension wood species (Alméras et al. 2012; Chang et al. to be submitted 2013). Thus, for non-G-layer tension wood species, we may hypothesise that there is a similar gel-like structure involved in the tensile stress generation, and later the gel structure is filled by lignin during the maturation. Thus, all the angiosperm would share a common mechanism of tensile stress generation, regardless of the presence or absence of G-layer. Or, non-G-layer tension wood may show another maturation process possibly same as normal wood, and then the angiosperm would have two different ways to reach the same goal of maturation stress generation.

Nitrogen adsorption method allows estimating the pore size and surface area of materials with cavities from 2 to 50 nm (Gregg and Sing 1982; Rouquerol et al. 1999). Recently this technique has been applied to the study of the texture of biological material such as tension wood. Considering the relative lower surface area in wood samples compare to mesoporous materials such as catalytic material, more amount of material (dry mass 0.4-0.7g) is needed for nitrogen adsorption-desorption analysis on wood, which causes the difficulties for sampling especially in cambium zone. In this study, following a dedicated method set-up for a similar study on poplar (Chang et al. to be submitted 2013), peeled samples and tangential sections were used for porosity measurement. On the upper (tension wood side) and lower

side (normal wood side) surface of the leaning stem, the soft part near the cambium, was peeled and harder wood was prepared with serial tangential sections. The aim of this study is to record the surface area of mesopores and pore shape along the maturation sequence in a non-G-layer tension wood species by monitoring the porosity structural modifications of cell wall from cambium zone to mature tension wood by nitrogen sorption isotherms to better understand the tensile stress generation in tension wood without G-layer.

Materials and Methods

Materials

Simarouba (*Simarouba amara* Aubl.) was chosen as the model to represent the non-G-layer species. The biomechanical properties of simarouba have been well described by Ruelle et al. (2007a, b). This species does not develop G-fibers even when growth stress measurements indicate the tension wood production. A natural tilted simarouba tree (Fig. 1A) (diameter at breast height: 30 cm; tilting angle: 27°) was selected near the Paracou experimental field in French Guiana, near Kourou. Large crown and large amount of seeds at the bottom indicated the tree was in good growth conditions.

Field sampling

Sampling was performed on the living tree on 9th January 2013, one month after the beginning of the rain season. The peeling was made on both upper side (tension wood) and lower side (opposite wood) of the leaning stem according to the procedure described below. The bark and phloem were carefully removed to open a "window" (Fig. 1A). On the upper face, the bark can easily be detached and newly formed cells were juicy and easy to peel. On the opposite side, the bark was much more difficult to be removed and very few liquid accompanied the peeling announcing a lower cambial activity than on the upper side. For the bark side, the inner surface of the phloem was peeled with knife blade and the peeled sample was marked as #0 (T0 and O0 respectively for tension side and opposite side). For the xylem side, the back of scalpel blade was used to peel the entire surface gently (Fig. 1B), and the first peeled sample was marked as T1 and O1. For the second and third peeled samples (#2 and #3), the front of scalpel blade and a knife blade were used respectively with increasing force but carefully avoiding any sectioning by using the blade perpendicular to the surface. All peeled samples were directly kept in 70% ethanol and did not stay in air more than few second in order to avoid any drying. After the three peeling, it becomes difficult to obtain the samples by peeling due to the increase of cell wall rigidification. Then wood blocks (20×10×10 mm, L×T×R) were extracted from the peeled area with care to avoid compression tangential side and kept in a fridge with 70% ethanol to be sectioned with a microtome at the laboratory.

Laboratory sample preparation

In laboratory, with a sliding microtome, 300 µm (3×100 µm/section) thick tangential sections were further cut successively from the wood blocks until cross the previous growth ring (Fig. 1C). Finally 12 sectioned samples for tension wood side, namely T4 to T15 were obtained. For opposite wood side, tangential sections 200-µm thick (2×100 µm/section) were cut due to the slow growth rate. Finally 9 sectioned samples for opposite wood side, namely O4 to O12 were obtained. Immediately after sectioning, samples were kept in 70% ethanol and dehydrated in a graded series (70%, 85%, 96% and 100%) of ethanol solutions. The distance from the cambial zone (without peeling position) was recorded for each peeling and sectioning sample.

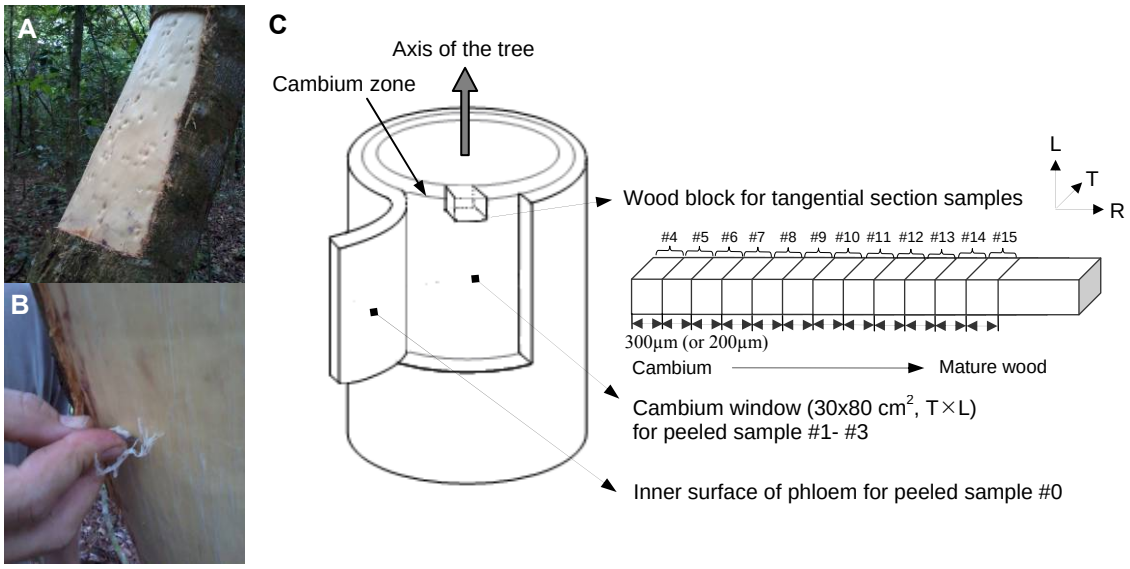

Figure 1 Schematic diagram showing sample preparation for N_2 adsorption-desorption measurement to examine the mesoporosity from each developmental stage of wood cell wall formation in simarouba (tension wood side taken as example) A, leaning stem debarking; B, peeling T3 on xylem side; C, sectioning sample preparation.

Microscopic observations and cell wall thickness measurement

A wood block extracted after peeling was sectioned with a sliding microtome (15 µm thickness) and stained with Safranin/Alcian-blue. This stain is commonly use in study concerning tension wood with G-layer as it stains lignified wall in red and the un-lignified G-layer in blue.

Another wood core extracted before peeling at the vicinity of the peeled part was dehydrated with ethanol and embedded in LR White resin (two exchanges of resin/ethanol mixture for 1 hour, followed by two exchanges in pure resin for 1 hour and kept overnight at room temperature, then polymerised at 65°C overnight). Transverse sections of 1 µm thickness were cut with a diamond knife and observed with an optical microscope (Leica Microsystems) in phase contrast mode. The cell wall thicknesses were measured manually from the calibrated images using the image analysis software ImageJ (National Institutes of Health, Bethesda, MD, USA).

N_2 adsorption–desorption measurement

The dehydrated samples were exchanged with liquid CO_2 and supercritically dried before nitrogen adsorption measurements to keep intact the mesoporosity avoiding the collapse of the gel (Clair et al. 2008). The supercritically dried samples (around 0.4-0.7g) were outgassed at 323 K under vacuum until a stable 3×10^{-5} Torr pressure was reached without pumping. This was done to remove physically adsorbed gases from the sample surface, in particular, water/ethanol vapour. Nitrogen adsorption-desorption isotherms were recorded at 77 K on a micromeritics ASAP 2020 volumetric apparatus.

This experimental technique allows the specific surface area (S_{BET}, Brunauer et al. 1938) and the pore size distribution (Broekhoff and de Boer 1967) of the samples to be evaluated. The pore size range was calculated from adsorption pore size distribution diagrams following same procedure as explain in Chang et al. (submitted 2013). Median pore size and range comprising from 25 to 75% of the pore volume were then plotted for each peeling or section sample (Figs. 2c, 3c).

Results

Cell wall thickness

Figures 2b and 3b show variations in the average radial thickness of cell wall layers during maturation of simarouba tension wood and opposite wood respectively. The thickness is plotted versus the distance of the analysed fibres from the cambial zone. Figures 2d and 3d are light micrographs of corresponding transverse sections showing cell differentiation from the cambial zone to full maturation.

In simarouba tension wood, the thickness of the fibre secondary wall layer increases almost linearly until ~1100 μm after the cambium and then remains constant (Fig. 2b). The gradual thickening of cell morphology is also clearly visible (#1-#6 in Fig. 2d) and no difference can be observed after the cell wall lignified. However, opposite wood shows a sharp increase in the cell wall thickness, and reaches constant at 320 μm from the cambial zone (Fig. 3b). No G-layer was observed in simarouba sample (Fig. 2d, 3d).

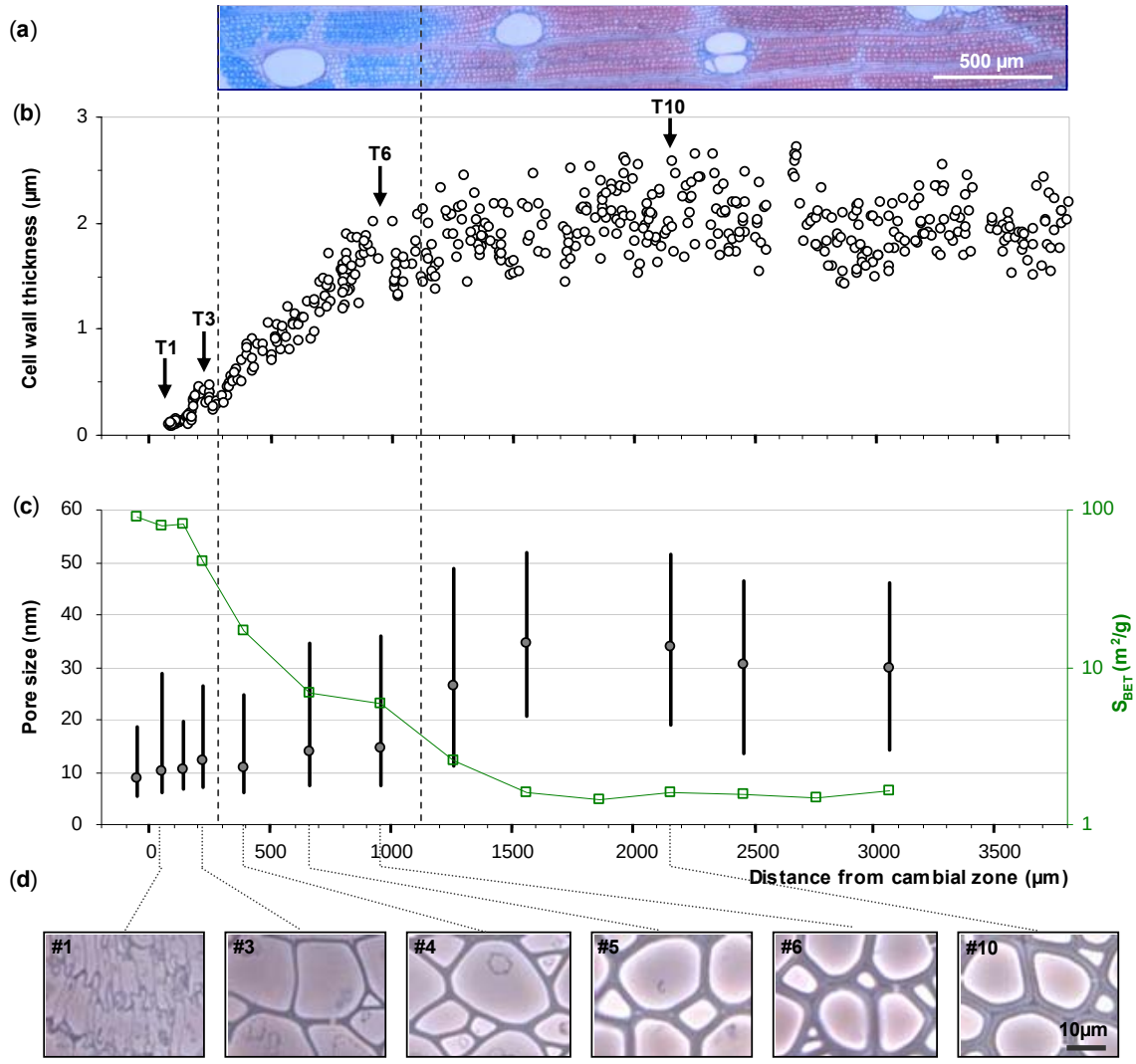

Figure 2 Characterization parameters of simarouba tension wood during cell wall maturation. (a) section stained with safranin-alcian Blue, (b) evolution of fiber cell layer thickness (excluding parenchyma cells), (c) median pore size (filled circle), pore range size range (straight lines) distribution and specific surface area (open squares with green line), (d) morphological fibre details (images done on 1 µm section after embedding and observed in phase contrast) according to the distance from the cambial zone in simarouba tension wood. The two vertical dotted lines indicate the blue region after peeling T3 where carbohydrate content is high and lignin content is consequently low after staining with safranin O/alcian-blue. T1, T3, T6 and T10 indicate the four stages of cell wall maturation. The specific surface area S_{BET} is plotted in logarithmic scale. The light micrographs in (d) were acquired with an optical microscope in phase contrast mode.

Fig. 2a and 3a show the transverse sections after peeling #3 stained with safranin-alcian-blue. The dividing cells near cambium were also stained blue like the G-layer indicating that these cells are not yet fully lignified and thus contain relatively more carbohydrate components (cellulose, hemicelluloses and pectin). As expected, tension wood growth was more active than opposite wood as attested from the stained sections where the blue region is much larger in tension wood than that in opposite wood.

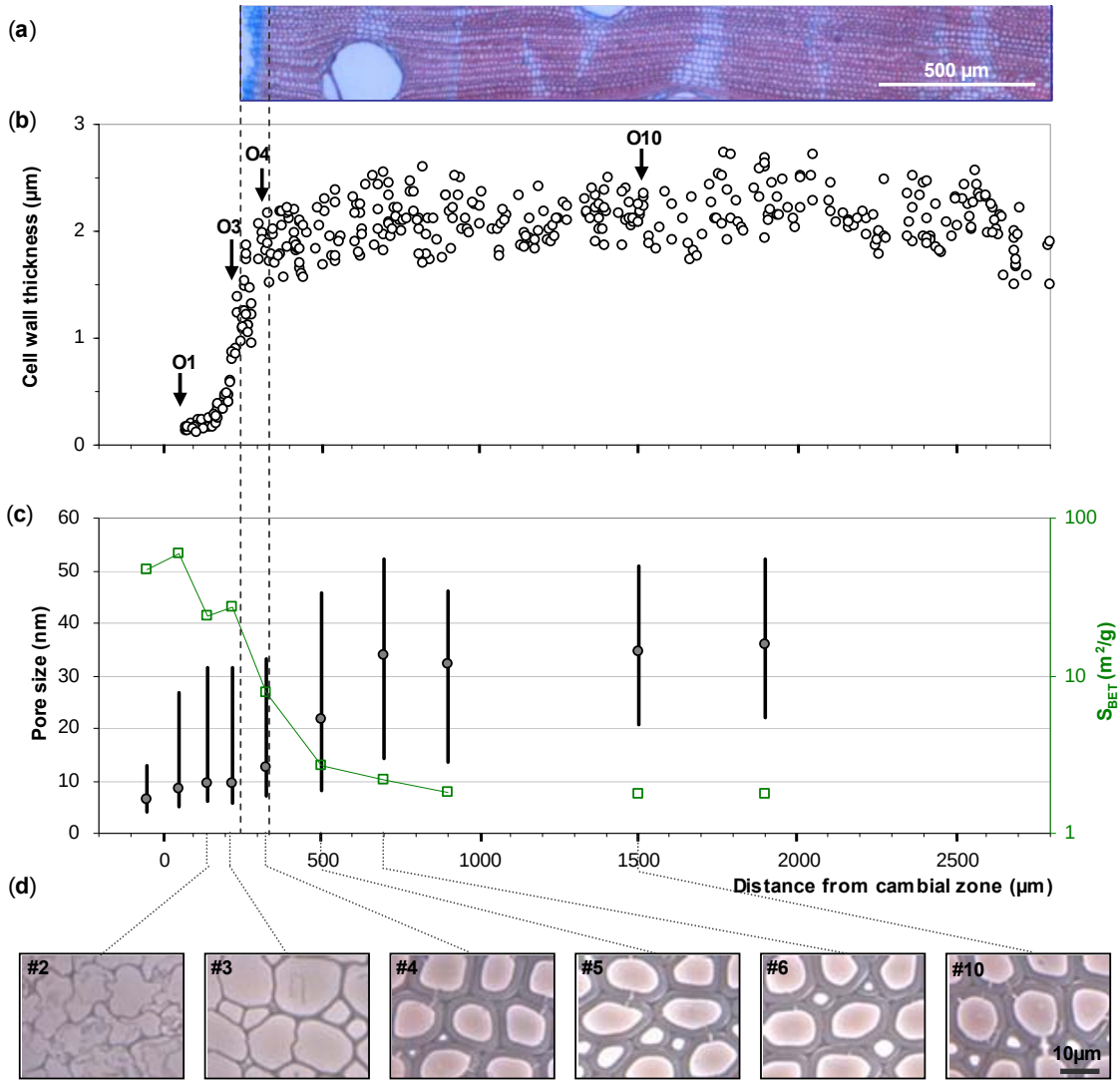

Figure 3 Characterization parameters of simarouba opposite wood during cell wall maturation. (a) section stained with safranin-alcian blue, (b) evolution of cell layer thickness, (c) median pore size (filled circle), pore size range (straight lines) distribution, and specific surface area S_{BET} (open squares with green line), (d) morphological fibre details according to the distance from the cambial zone. The two vertical dotted lines indicate the blue region after peeling O3 where carbohydrate content is high and lignin content is consequently low after staining with safranin/alcian-blue. O1, O3, O4 and O10 indicate the four stages of cell wall maturation. The specific surface area SBET was shown in logarithmic scale. The light micrographs (d) were acquired with an optical microscope in phase contrast mode.

Pore shape

Isotherms are compared at all stages during cell differentiation of simarouba tension wood and opposite wood; only four stages are presented in Fig. 4 (full set of data is presented in supplementary material, Figs. 5 and 6). The four stages were selected during cell wall maturation: early stage of cell wall thickening (Stage 1), later stage of cell wall thickening (stage 2), the completion of cell wall thickening (stage 3) and the mature cell wall (stage 4). For tension and opposite wood, T1, T3, T6, T10 and O1, O3, O4, O10 were selected as the four stages, respectively. Measurements at other locations showed similar isotherms for each differentiation stages.

According to the IUPAC classification (Sing et al. 1985), the isotherms of tension wood in the first three stages are types IV with a H3 type hysteresis loop, indicating the presence of mesopores with a non-uniform size. For the fourth stage of tension wood, the isotherm is intermediated between type IV and type II, indicating the presence of large mesopores with a broad size distribution that continues into the macropore domain. The hysteresis loop is very narrow, the adsorption and desorption branches being almost vertical and nearly parallel above 0.9 relative pressure, confirming the presence of a significant outer surface. For opposite wood, samples at each stage exhibit the similar isotherm type as tension wood.

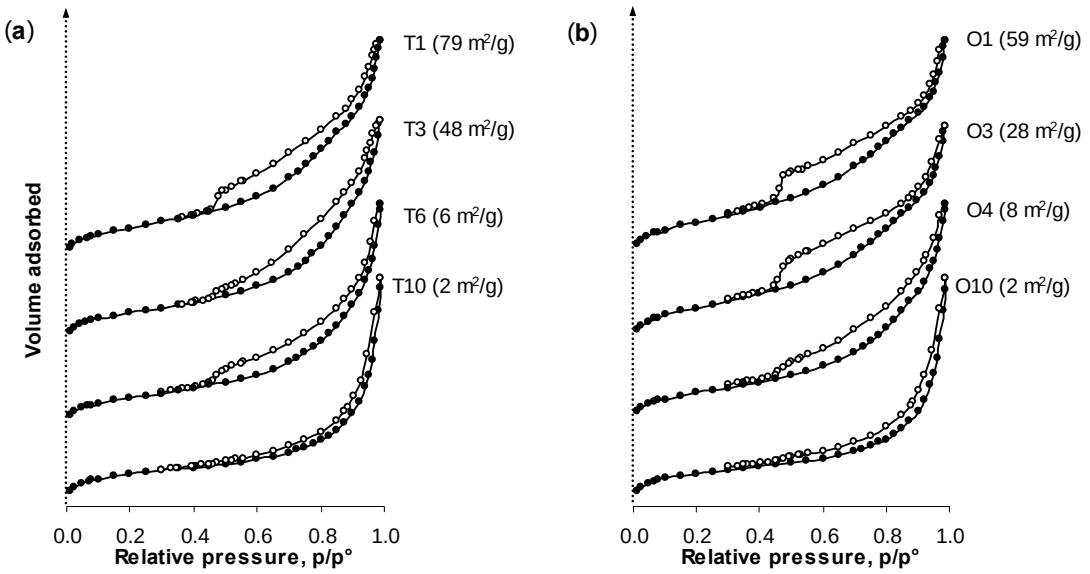

Figure 4 Normalised N_2 isotherms at four stages (tension wood: T1, T3, T6 and T10; opposite wood: O1, O3, O4, and O10) during cell differentiation of simarouba (a) tension wood and (b) opposite wood. Filled symbols, adsorption; open symbols, desorption; the corresponding specific surface area is displayed in the brackets. For clarity, the curves are arbitrary shifted up.

The shape of the nitrogen adsorption-desorption isotherms (Fig. 4) combined with the difference in pore shape distribution obtained from adsorption and desorption inform on the shape of the pores in the samples (Groen and Pérez-Ramirez 2004). Before the completion of cell wall thickening, isotherms for both tension (T1 to T6) and opposite wood (O1 to O4) show a wide hysteresis loop between the adsorption and desorption branches with a sudden desorption near p/p°=0.48. The sudden desorption near p/p° =0.48 is a cavitation phenomenon and indicates that the opening of a fraction of the mesopores is smaller than about 4 nm (Ravikovitch and Neimark 2002).

The pore shape can also be reflected from the pore size distributions. Peak pore size determined from the adsorption branch of the isotherm corresponds to the cavity size, while that of the desorption branch corresponds to the throat size of a pore (Groen and Pérez-Ramirez 2004). From stage 1 to stage 3, for both tension wood and opposite wood, the peak pore size calculated from desorption branches was 6 nm, whereas more than one peak appears on the adsorption pore size distribution, with peak size of 7 and 12 nm. Thus, some of the pores could be ink-bottle shape with pore cavities that are less than twice the diameter of the throats, while others could have a slit-shape character with nearly constant cavity and throat

sizes. Even the type of hysteresis loop at these stages are not the same as type H2 (according to the IUPAC classification, Sing et al. 1985) which often presents the mesopores with ink-bottle shape, the comparison of peak pore size from adsorption and desorption branches shows the presence of pore with ink-bottle shape.

In the last stage, both in tension wood and opposite wood, the narrow hysteresis could correspond to a network of cellulose microfibrils forming slit-shape pores character with the similar cavity and throat sizes (peak pore size at 7 nm). However, it should be noted that due to the low mesopore volume and low surface area in this stage, the pore shape and pore size distributions have to be interpreted with caution.

Specific surface area S_{BET}

Fig. 4 shows that at the earliest stage of cell wall thickening (T1/O1), both tension wood and opposite wood presents a much larger surface area than the other stages. With the deposition of lignin, surface area sharply decreases in both tension wood and opposite wood (Fig. 4). The surface area is directly linked to the pore volume. In the early stage of cell wall thickening, both tension wood and opposite wood have a large amount of mesopores, however, the rich porosity greatly reduced with the gradual deposition lignin in the cell wall. This phenomenon was also observed in poplar (Chang et al. to be submitted 2013),

Figures 2c and 3c show the changes in the specific surface area S_{BET} of simarouba tension wood and opposite wood during cell wall maturation. For both tension wood and opposite wood, the surface area is much higher near the cambium zone, which consists mainly of an unorganised cellulose network embedded in the hydrogel made of hemicelluloses and pectic components. With the cell wall thickening, as expected, the specific surface area (expressed as $m^2.g^{-1}$) decrease with the progressed lignification, filling the pores and increasing the mass. This is true for both tension and opposite wood, whereas the former shows slow decline, probably due to the more active growth in tension wood side. When the cell wall thickness reach to constant, the specific surface area in both tension and opposite wood decreases until close to disappear (1.4-1.6 m^2/g).

Pore size distribution

In Figures 2c and 3c, the pore size range distributions are plotted after integration of the area under the curve of pore size distribution. In tension wood (Fig. 2c), the median pore size progressively increases with increase pore size range till the completion of cell wall thickening. The increase in this stage clearly corresponds to the development of the cell wall, starting from 8 nm near cambial zone to nearly 2 times larger (14 nm) when cell wall are not fully lignified corresponding to the blue zone in Fig. 2a. For opposite wood side, the amount of maturating cells is relatively narrow, whereas the pore size change before the cell wall fully lignified still can be detected by nitrogen adsorption-desorption isotherm. As shown in Fig. 3c, opposite wood shows similar pattern as tension wood with median pore size centered around 6 nm near cambial zone increasing to 12 nm (2 times) when cell wall thickness begins to constant. However, after ~1100 μm from the cambium in tension wood and ~320 μm in

opposite wood, the cell wall thickness becomes constant, and it becomes difficult to follow the pore size change in some of the sample due to the low volume of nitrogen adsorbed closes to the instrumental limitation. More generally, due to the low ratio mesopore per mass, pore size distribution have to be taken with caution.

Discussion

This study characterizes the mesoporosity change during cell wall maturation in non-G-layer species. Consistent with the previous results on poplar wood (Chang et al. to be submitted 2013), the high mesoporosity is recorded near cambium zone, which contains mainly primary wall with high mesopore volume for both tension and opposite wood. In present study, during the stage of cell wall thickening, the similar hysteresis loop indicates both simarouba tension and opposite wood have a slit-shaped pores mixed with ink-bottle pores However, the high specific surface area decreases gradually corresponding to the increasing of cell wall thickness in both tension wood and opposite wood. It is clear that the decline of porosity is due to the lignificaton activity during cell wall maturation, which fills the pore and increases the mass of the cell wall as the specific surface area is given by its ratio to sample mass. When the cell wall thickness remains constant, the specific surface area declines greatly to low in both tension wood and opposite wood. At this stage, the nitrogen adsorption isotherms with narrow hysteresis loop shows that the lignified layers have a network of cellulose microfibrils forming slit-shape pores which is different with the early developmental stage. This low but non-zero surface area coincides with the previous results of non-G-layer species and was attributed to pit membrane (Clair et al. 2008; Chang et al. 2009).

The cell wall maturation process is not only associated with the change of total surface area, also accompanied by the changes of median pore size as a new population of bigger pores appears. Both tension and opposite wood increase the median pore size to nearly 2 times larger than in primary wall when cell wall thickness begins to stabilize. However, very limit maturation process can be monitored in opposite wood side due to its slow growth rate compared to tension wood side. The mesoporosity measured may belong to the cavities between microfibrils within the hemicellulosic hydrogel matrix. These observations suggest that, like in poplar, pores from secondary wall have bigger pores and a wider range of pore size than middle lamella and primary wall. Interestingly, pores in maturating secondary wall have pores shape typical of what was observed in mature G-layer. This ink-bottle pore shape was also found in normal wood contrary to opposite wood in poplar which never shows this pore shape. However, this is observed in only on one section (O4) due to the slow growth rate in opposite wood compare to tension wood where this typical pore shape was observed in 3 sections (T4 to T6). If, as suspected for G-layer tension wood, this mesoporosity play a major role in maturation stress generation, our results support the idea of a common mechanism between G-layer and non-G-layer species. Even more, as opposite wood exhibits a similar pore shape, this mechanism could be also used to generate the low tensile stress observed in normal wood.

This study only opens the question on the tensile stress generation in non-G-layer species. Obviously, there is still a lot to do in order to better understand how the matrix swells during cell wall maturation in both simarouba tension and opposite wood. This could be concerned with the comparative investigation of polysaccharide composition between the G-layer and non-G-layer cell wall, especially along its differentiation.

Conclusion

This study shows that the mesoporosity change in non-G-layer species during the cell wall maturation can be monitored by nitrogen adsorption-desorption isotherm method. High mesoporosity can always be detected near cambium zone, which contains mainly primary wall with high surface area for both tension and opposite wood. The modification of pore shape during secondary wall thickening towards pores typical from G-layer let think that this porosity may play a major role for the maturation stress generation. However, in order to confirm a common mechanism in G-layer and non-G-layer species, it will be interesting to investigate the distribution in specific polysaccharides involved during the maturation process of G-layer as observed in poplar (Guedes et al. 2013, submitted) to compare with the ones produced in simarouba tension wood.

Acknowledgements Shan Shan Chang was supported by a fellowship from the Scientific Council of Montpellier University. Thanks go to Onoefe N'Gwuete (Cirad, Kourou), Julie Bossu (EcoFoG, Kourou) and François Clair for their help the field sampling. Part of this work was performed in the framework of the project "StressInTrees" funded by the French National Research Agency (ANR-12-BS09-0004).

References

Alméras T, Gril J, Clair B (2012) The origin of maturation stress in tension wood: using a wide range of observations and mechanical considerations to discriminate between hypothetic mechanisms. 7th plant biomechanics international conference, Clermont-Ferrand, France.

Arche, RR (1986) Growth stresses and strains in trees. Springer Series in Wood Science. Springer-Verlag, Berlin, Heidelberg, New-York.

Broekhoff JCP, de Boer JH (1967) Studies on pore systems in catalysts: IX. Calculation of pore distributions from the adsorption branch of nitrogen sorption isotherms in the case of open cylindrical pores A. Fundamental equations. Journal of Catalysis 9: 8-14

Brunauer S, Emmett PH, Teller E (1938) Adsorption of gases in multimolecular layers. Journal of the American Chemical Society 60: 309-319

Chang SS, Clair B, Ruelle J, Beauchêne J, Di Renzo F, Quignard F, Zhao GJ, Yamamoto H, Gril J (2009) Mesoporosity as a new parameter in understanding of tension stress generation in trees, Journal of Experimental Botany 60: 3023-3030

Clair B, Alméras T, Pilate G, Jullien D, Sugiyama J, Riekel C (2011) Maturation stress generation in poplar tension wood studied by synchrotron radiation micro-diffraction. Plant Physiology 155: 562-570

Clair B, Gril J, Di Renzo F, Yamamoto H, Quignard F (2008) Characterization of a gel in the cell wall to elucidate the paradoxical shrinkage of tension wood. Biomacromolecules 9: 494-498

Clair B, Ruelle J, Beauchene J, Prevost MF, Fournier M (2006) Tension wood and opposite wood in 21 tropical rain forest species 1. occurrence and efficiency of the G-layer. IAWA Journal 27: 329-338

Dadswell HE, Wardrop AB (1955) The structure and properties of tension wood. Holzforschung 9: 97-104

Daniel G, Filonova L, Kallas AM, Teeri T (2006) Morphological and chemical characterisation of the G-layer in tension wood fibres of *Populus tremula* and *Betula verrucosa*: Labelling with cellulose-binding module CBM1(HjCel7A) and fluorescence and FE-SEM microscopy. Holzforshchung 60: 618-624

Fang CH, Clair B, Gril J, Liu SQ (2008) Growth stresses are highly controlled by the amount of G-layer in poplar tension wood. IAWA Journal 29: 237-246

Fisher JB, Stevenson JW (1981) Occurrence of reaction wood in branches of dicotyledons and its role in tree architecture. Botanical Gazette 142: 82–95
Fournier M, Baillères H, Chanson B (1994) Tree biomechanics: growth, cumulative prestresses and reorientations. Biomimetics 2: 229–252
Fujita M, Saiki H, Harada H (1974) Electron microscopy of microtubules and cellulose microfibrils in secondary wall formation of poplar tension wood fibers. Mokuzai Gakkaishi 20: 147-156
Gregg SJ, Sing KSW (1982) Adsorption, surface area and porosity. London: Academic Press, 218-228
Groen JC, Pérez-Ramirez J (2004) Critical appraisal of mesopore determination by adsorption analysis. Applied Catalysis A: General 268: 121-125
Onaka F (1949) Studies on compression and tension wood. Wood research. Bulletin of the Wood Research Institute, Kyoto University, Japan, 24: 1-88
Pilate G, Chabbert B, Cathala B, Yoshinaga A, Leplé JC, Laurans F, Lapierre C, Ruel K (2004) Lignification and tension wood. Comptes Rendus Biologies 327: 889-901
Qiu D, Wilson IW, Gan S, Washusen R, Moran GF, Southerton S G (2008) Gene expression in Eucalyptus branch wood with marked variation in cellulose microfibril orientation and lacking G-layers. New Phytologist 179: 94-103
Ravikovitch PI, Neimark AV (2002) Experimental confirmation of different mechanisms of evaporation from ink-bottle type pores: equilibrium, pore blocking, and cavitation. Langmuir 18: 9830-9837
Rouquerol F, Rouquerol J, Sing K (1999) Adsorption by powders and porous solids: principles, methodology and applications. San Diego: Academic Press, 439-467
Ruelle J, Beauchene J, Thibaut A, Thibaut B (2007a) Comparison of physical and mechanical properties of tension and opposite wood from ten tropical rainforest trees from different species. Annals of Forest Science 64: 503-510
Ruelle J, Yamamoto H, Thibaut B (2007b) Growth stresses and cellulose structural parameters in tension and normal wood from three tropical rainforest angiosperms species. BioResources 2: 235-251
Sing KSW, Everett DH, Haul RAW, Moscou L, Pierotti RA, Rouquerol J, Siemienewska T (1985) Reporting physisorption data for gas-solid systems. Pure and Applied Chemistry 57: 603-619
Sultana RS, Ishiguri F, Yokota S, Iizuka K, Hiraiwa T, Yoshizawa N (2010) Wood anatomy of nine Japanese hardwood species forming reaction wood without gelatinous fibers. IAWA Journal 31: 191-202
Wardrop AB (1964) The reaction anatomy of arborescent angiosperms. In: Zimmermann, M. H. (ed.), The Formation of Wood in Forest Tree, Academic Press, New York, 405-456
Yamamoto H, Abe K, Arakama Y, Okuyama T, Gril J (2005) Role of the gelatinous layer on the origin of the physical properties of the tension wood of *Acer sieboldianum*. Wood Science and Technology 51: 222-233
Yoshida M, Ohta H, Yamamoto H, Okuyama T (2002) Tensile growth stress and lignin distribution in the cell walls of yellow poplar, *Liriodendron tulipifera* Linn. Trees 16: 457-464
Yoshinaga A, Kusumoto H, Laurans F, Pilate Gilles, Takabe K (2012) Lignification in poplar tension wood lignified cell wall layers. Tree Physiology 32: 1129-1136

Supplementary material: N_2 adsorption-desorption isotherms of tension wood and opposite wood during the cell wall maturation

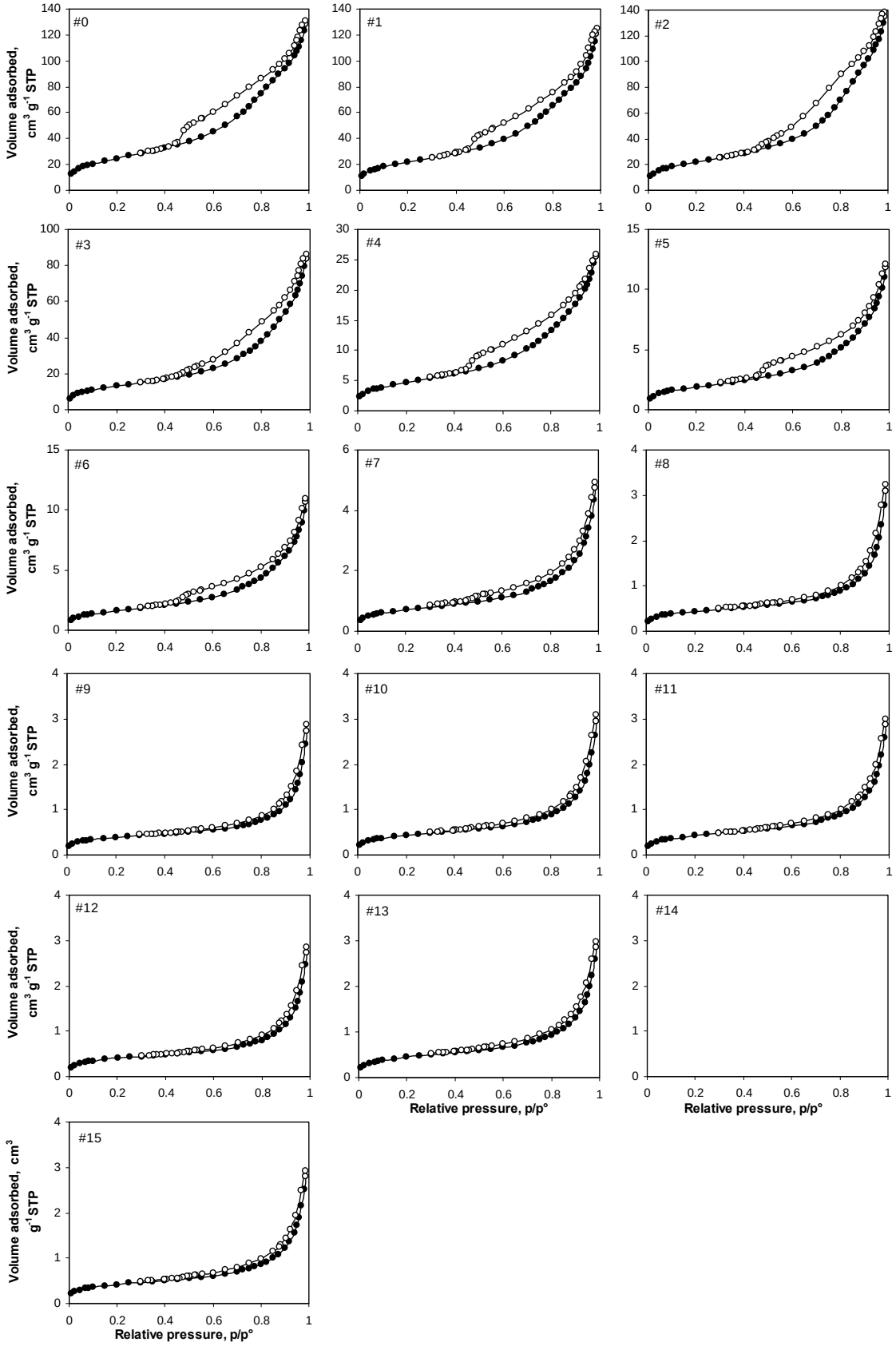

Figure 5 N_2 adsorption isotherms of simarouba tension wood at each location of cell wall maturation (filled symbols, adsorption; open symbols, desorption; untested samples were in blank)

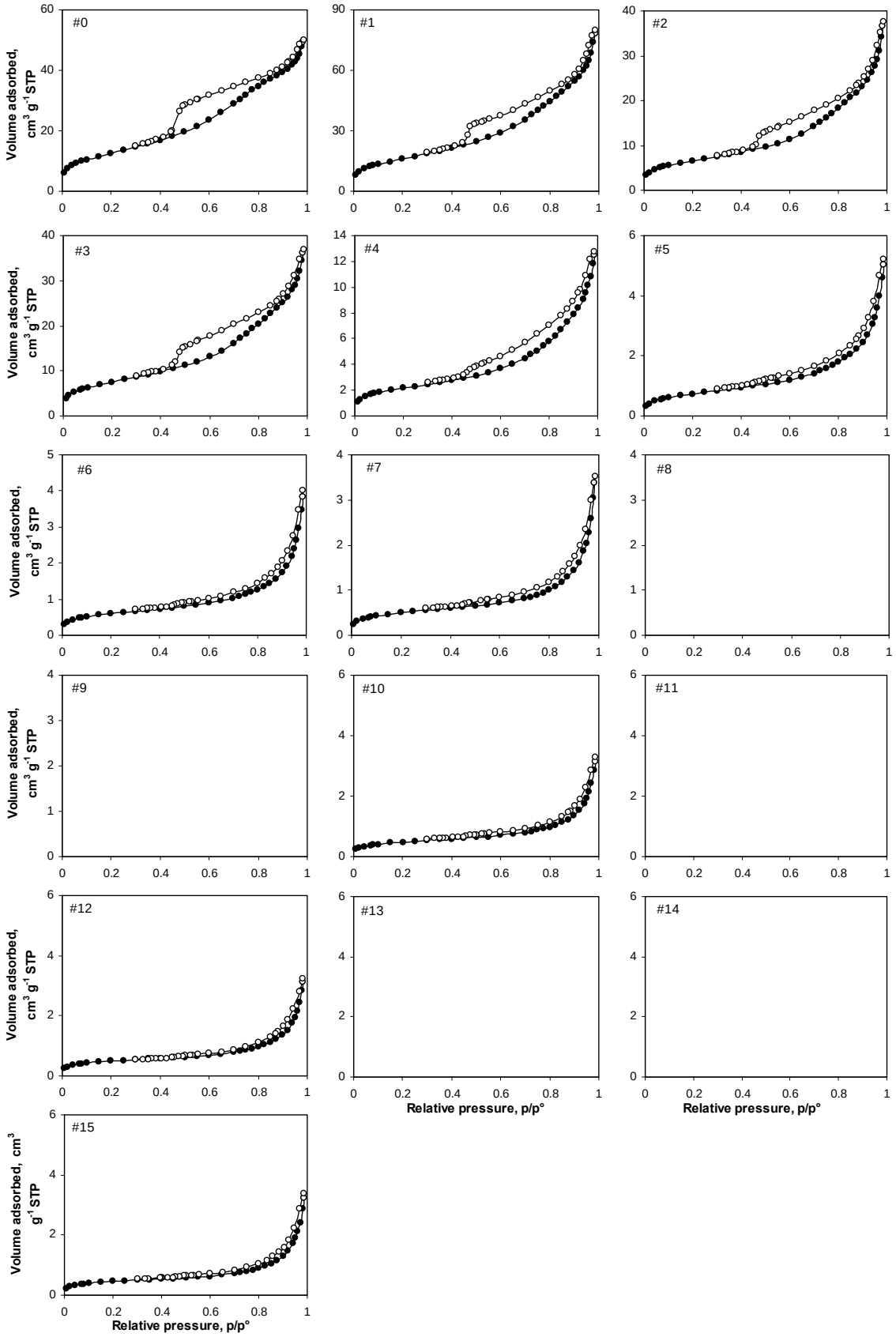

Figure 6 N_2 adsorption isotherms of simarouba opposite wood at each location of cell wall maturation (filled symbols, adsorption; open symbols, desorption; untested samples were in blank)

5. General discussion

FTIR and nitrogen adsorption-desorption isotherms allowed the exploration of changes in macromolecular arrangement and mesoporosity along sequences of cell wall development in tension and opposite wood. Variations in intensity of absorbance bands and the volume of adsorbed nitrogen were consistent with the development of chemical composition and pore volume during the progressive thickening of the cell walls. However, the different patterns observed in tension and opposite wood revealed new information about the particular ultrastructure of tension wood secondary walls and their modifications during fibre development.

5.1. Cambial zone

In the periphery of the stems near the cambium zone, which only contained, middle lamella then primary wall then S_1 layer, the newly dividing cells are not yet lignified and thus contain relatively more carbohydrate components (cellulose, hemicelluloses and pectin). This is evidenced from the high absorbance peak signal in non-polarised IR spectra in both tension and opposite wood (Figs. 3 and 4 in Chapter 4.1 for tension wood, data of opposite wood are not shown). Interestingly, the former shows a higher content of cellulose than the latter one. Letting suppose that even of the early stage of cell development, cell is already programmed to achieve a different function in tension wood compare to opposite wood. Early in the cell wall development, the cellular enlarging growth is directly related to the orientation change of the cellulose in the primary wall, resulting in a perpendicular (90°) orientation of the cellulose. Our observation in opposite wood is consistent with results by Kataoka and Kondo (1998), in normal wood. However, for tension wood, already at the early stage of cell wall development an orientation more parallel to the fibre axis was noticeable. Even if we were not able to explain this observation, it is interesting to notice the early change of the cellulose organisation associated to tension wood production compare to opposite wood.

The variations in the composition content and the orientation may come from the activity in different cambium region, as cell production is more active in tension wood side than that in opposite side. This may also directly relate to the difference in mechanism of maturation stress generation. Concerning the low lignin content, it is similar for both types of wood as cambial cells are not yet lignified.

In the discussion concerning the mesoporosity, new results, not presented in the paper are presented. These results come from a previous experiment on another tree (called poplar I in the following). This tree was unfortunately not presenting developing G-fibre near the cambial zone. This absence of reaction was *a posteriori* explained by a preliminary test performed on this tree several weeks before that clearly affected the tree growth. However, even if G-layer was absent in the differentiating zone, mature G-layer (formed before the

disturbance) and cambial zone are presented here as repetition conforming the data presented in the paper.

Near the cambium zone[5], even before the presence of G-layer, all the samples in both tension and opposite wood adsorbed a large amount of nitrogen (Figs. 5.1 and 5.2), which is much larger than that of mature wood, as previously described in mature poplar (Chang et al. 2011, 2012) and chestnut tension wood (Clair et al. 2008). However, the fact that G-layer species always show higher amount of nitrogen adsorbed than that the non-G-layer one, as well as tension wood always higher than that the corresponding opposite wood, was not totally elucidated but may be influenced by the different cambium activities which are largely dependent on the surrounding growth environment, such as temperature/ or photoperiod (Uggla et al. 2001).

Even though the variation exists among different types of wood, they have similar isotherm type IV with H3 type hysteresis loop according to the IUPAC classification (Sing et al. 1985). This kind of isotherm indicates the presence of slit-like mesopores with wide pore size distribution in a non-uniform size. These common characterizes for all samples also can be reflected from the comparison of specific surface area and pore range size distribution (calculated according to Fig. 3.7) in Fig. 5.3.

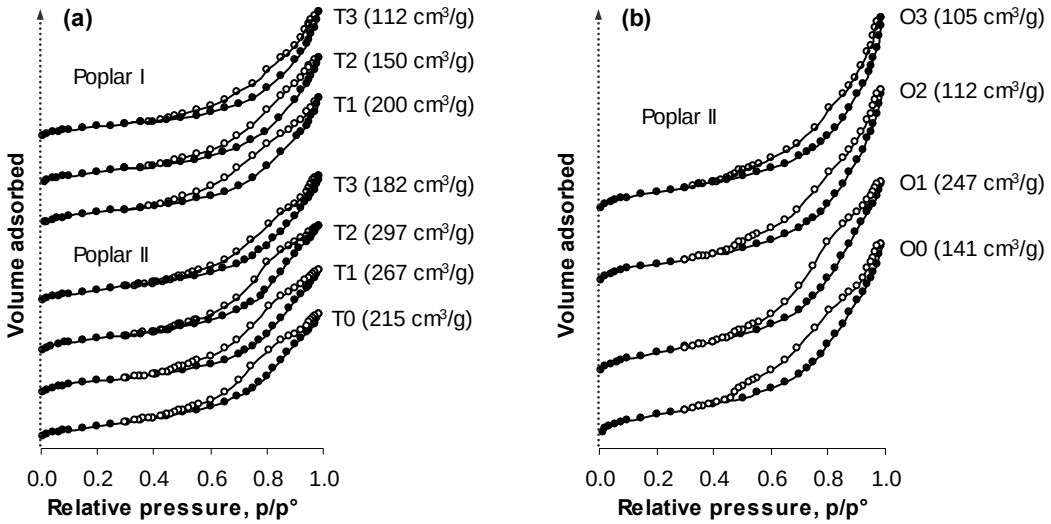

Figure 5.1 N_2 adsorption-desorption isotherms of (a) poplar tension wood and (b) opposite wood near cambium zone (filled symbols, adsorption; open symbols, desorption; the maximum volume of adsorbed nitrogen is displayed in the brackets. Two poplar trees (poplar I and poplar II) were used for tension wood analysis)

[5] The cambium zone is classified according to their easy peeling on the tree and confirmed with microscope observation. Two poplar trees (poplar I and poplar II) and one simarouba tree were used for the analysis near cambium. Poplar I: tension wood sample #1 to #3; Poplar II: samples #0 to #3 for both tension and opposite wood; Simarouba: samples #0 to #3 for both tension and opposite wood; the isotherms were shown in Annex II (Fig. 6.1), in Chapter 4.2 (Figs. 8 and 9) and in Chapter 4.3 (Figs. 5 and 6).

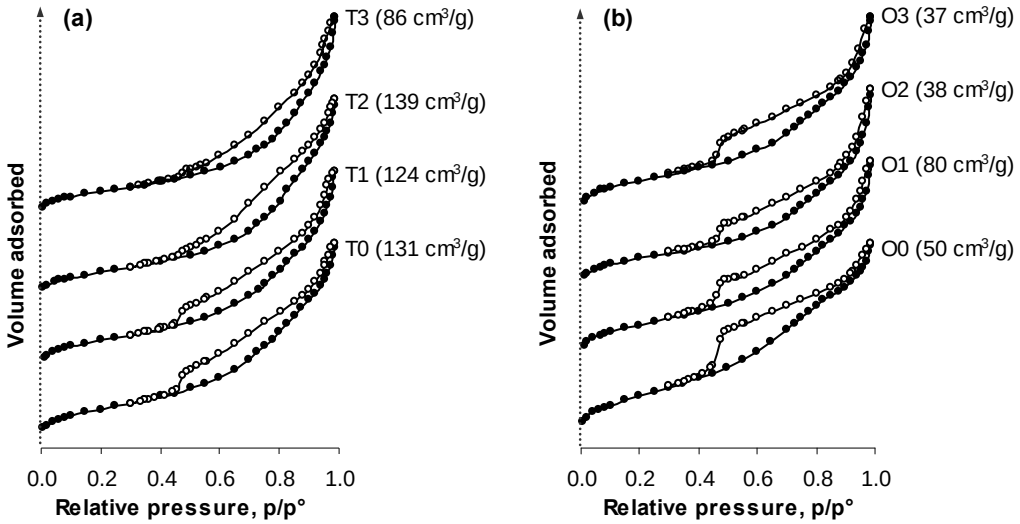

Figure 5.2 N_2 adsorption-desorption isotherms of simarouba tension wood (a) and opposite wood (b) near cambium zone (filled symbols, adsorption; open symbols, desorption; the maximum volume of adsorbed nitrogen is displayed in the brackets)

The median pore size in both tension and opposite wood samples was centred between 10-12 nm regardless of the absence of G-layer, whereas a slight increase trend observed when the sample distance gradually away from cambium zone. Samples from two poplar tension woods were tested, and very similar median pore size was obtained.

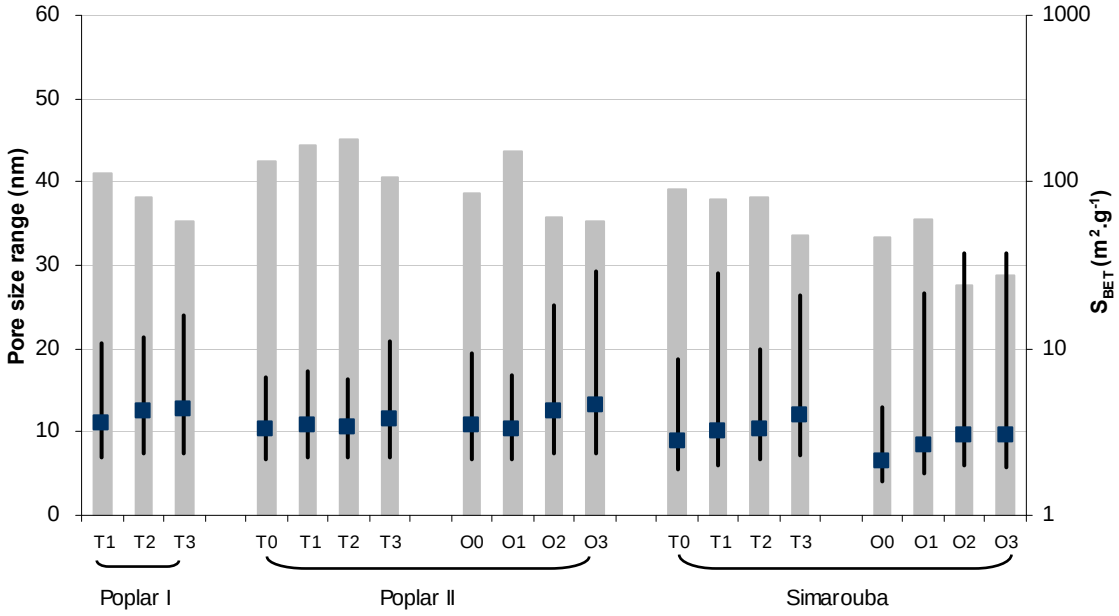

Figure 5.3 The median pore size (filled square), pore size range distribution (straight lines) and specific surface area, S_{BET} (grey histogram) of poplar and simarouba near cambium zone. (Poplar I and poplar II denote sample taken from tree I and II. The S_{BET} is shown in logarithmic scale. T0-T3: tension wood samples; O1-O3: opposite wood samples.)

The high value of specific surface area (S_{BET}) measured in all samples confirms the porous structure near cambium zone. In the early stage of cell wall formation, the primary wall consists mainly of a cellulose network embedded in the hydrogel made of hemicelluloses and pectic components. Since there is no deposition of lignin, all the samples show the common

characteristics with high surface area and similar median pore size, but slight variation exists among different wood types.

5.2. During maturation

When the cells reach their final diameter, a thick multilayered secondary cell wall will be deposited and lignified. Lignin deposition starts before the entire layers of secondary cell wall are deposited (Donaldson 2001 in normal wood, Yoshinaga et al. 2012 in tension wood), accompanying with filling the pores and increasing the mass to form a hydrophobic environment. Non-polarised FTIR spectra well monitored the development and compositional changes in cell walls. As expected, the relative absorption peaks associated to lignin increased greatly, whereas carbohydrates generally diminished especially apparent for the relative content of pectins (Figs. 3 and 4 in Chapter 4.1). With the G-layer formation in tension wood, the signal related to xylose units increased simultaneously, but it was not possible to follow this signal in opposite wood due to the narrow growth. The results obtained from polarised spectra make the difference between tension and opposite wood more clear. Lignin has a parallel orientation with regard to the orientation of cellulose in the secondary wall in both tension and opposite wood, but is more highly oriented in the former than in the latter (Fig. 7 in Chapter 4.1). However, the opposite orientation of carbohydrates (hemicelluloses and pectins) signals along the G-layer maturation in tension wood (Fig. 8 in Chapter 4.1) could reflect a continued deposition of xyloglucan or xylan, with an orientation different to that in the S_2 wall of opposite wood throughout the whole process.

The orientation difference in the matrix polysaccharides probably directly related to the generation of stress in tension wood, which may also influence the ultrastructure change in the matrix of microfibrils. During the cell wall maturation[6], the surface area (expressed as $m^2.g^{-1}$, Fig. 5.4) decreases abruptly (compared to Fig. 5.3) with the deposition of lignin that fills the pores and increases mass. This is particularly evident in the cells without G-layer (simarouba), but not the case for cells with G-layers (poplar II). The hidden porosity is compensated by a new mesoporosity, which corresponds to the development of the G-layer. It should be noted that due to the tree growth has been disturbed by a preliminary test performed several weeks before, tension wood in poplar I stopped to produce G-layer during the cell wall maturation. So the low specific surface area and large median pore size observed in poplar I (Fig. 5.4) were more close to normal wood. Compared to the samples from cambium zone, the isotherms of poplar tension wood show clear steep at the relative pressure 0.4-0.5 during its maturation (Fig. 6.1 in Annex II, Fig. 8 in Chapter 4.2). However, the corresponding opposite wood changes the isotherms to the intermediated type II and IV (Fig. 9 in Chapter 4.2), indicating the presence of large mesopores continues into the

[6] The maturation process is classified according to the variation of cell wall thickness and the isotherms of all the samples were displayed in Annex II (Fig. 6.1), in Chapter 4.2 (Figs. 8 and 9) and in Chapter 4.3 (Figs. 5 and 6); two poplar trees (poplar I and poplar II) and one simarouba tree were used for the analysis of maturation process. Poplar I: samples #4 to #7 for tension wood; Poplar II: samples #4 to #8 for tension wood and samples #4 to #6 for opposite wood; Simarouba: samples #4 to #6 for tension wood and only samples #4 for opposite wood.

macropore domain. However, even without G-layer, simarouba also shows the similar isotherm shape (Fig. 5 in Chapter 4.3) like G-layer species but with relatively lower surface area except sample #4 which is more close to cambium zone (Fig. 5.4). Supposing the S_2 layer of fibres in simarouba tension wood may play the similar role as G-layers, since the similar features as the G-layers has been reported (Yoshizawa et al. 2000; Yoshida et al. 2002b; Ruelle et al. 2006, 2007). In particular, similar isotherm type was also observed in opposite wood of simarouba, but only in one sample (O4). This limited sample probably relate to the slow growth speed in opposite wood compare to tension wood where this typical isotherm was observed in 3 samples (T4 to T6).

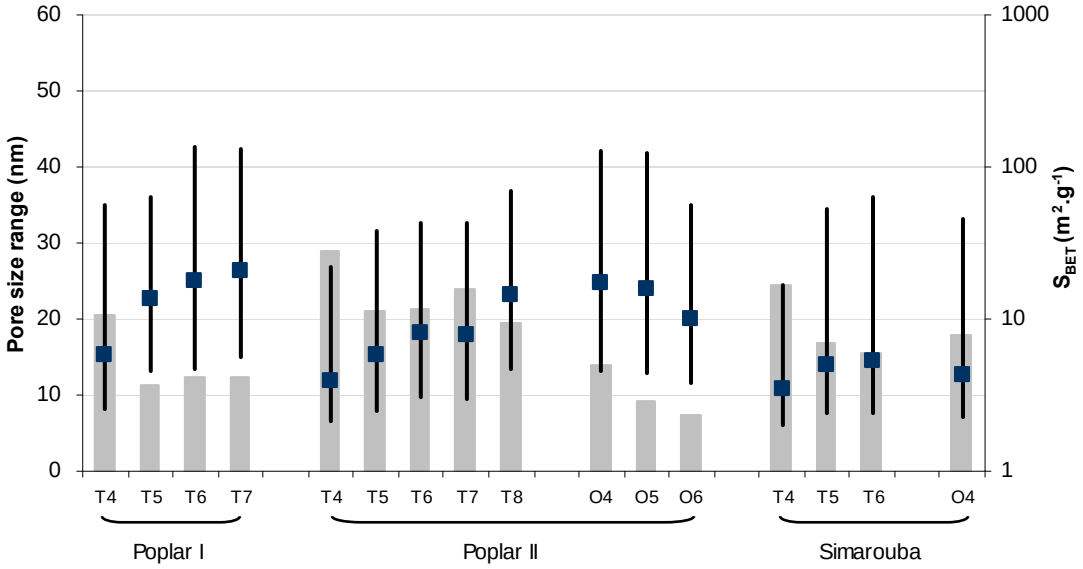

Figure 5.4 The median pore size (filled square), pore size range distribution (straight lines) and specific surface area, S_{BET} (grey histogram) of poplar and simarouba during cell wall maturation. (Poplar I and poplar II denote sample taken from tree I and II. The S_{BET} were shown in logarithmic scale. T4-T8: tension wood samples; O4-O6: opposite wood samples)

More similarity between the two kinds of tension wood can be seen from the pore size range distribution in Fig. 5.4. Interestingly, regardless of the presence of G-layer, the median pore size from tension wood samples increase gradually from 12 nm near cambium to 23 nm in poplar II and 14 nm in simarouba. This suggests that pores from secondary wall have bigger pores and a wider range of pore size than middle lamella and primary wall. In opposite wood, if well attributed the pore change to the pits, primary wall at the pit position would be modified during the maturation by enlarging the pores in order to achieve its conductive functions. In tension wood, the increase in pore size range could correspond to the maturation of G-layer or more probably to changing ratio of MLP and G contributing to the signal.

5.3. Mature tension wood

When the cell wall reach a constant thickness, the cells have well-developed structural patterns and relatively stable behaviour. The wood is thus called mature wood. Herein, the samples which have the stable cell wall thickness are considered as mature wood. In mature wood region, non-polarised spectra show that the relative intensity of the IR absorbance bands

were constant in both tension and opposite wood, indicating that no more components are added or modified after the end of the thickening. However, regarding the overall composition of tension wood compare to opposite wood, the general knowledge can be confirmed: a higher content of cellulose and a lower content of lignin. Each typical band assigned to polymers follow the same orientation as observed in maturation. Whereas, compared to maturation stage, the degree of orientation increased and became more distinct at the mature stage. Thus the apparent difference during the maturation process would be a transition state that was later hidden in mature stage. This can also be reflected from the ultrastructure features in the matrix of the cell wall.

In the mature stage[7], G-layer species follows the respective isotherm type as observed in maturation process for both tension and opposite wood. However, non-G-layer species changes the isotherms to the intermediated type II and IV with lower surface area (Fig. 5.5), as observed in opposite wood of G-layer species. It is clear that the decreased mesoporosity is due to the lignificaton activity which is not compensated as G-layer tension wood. When the cell wall thickness becomes constant, it becomes difficult to follow the pore size change in non-G-layer sample due to the low volume of nitrogen adsorbed closes to the instrumental limitation.

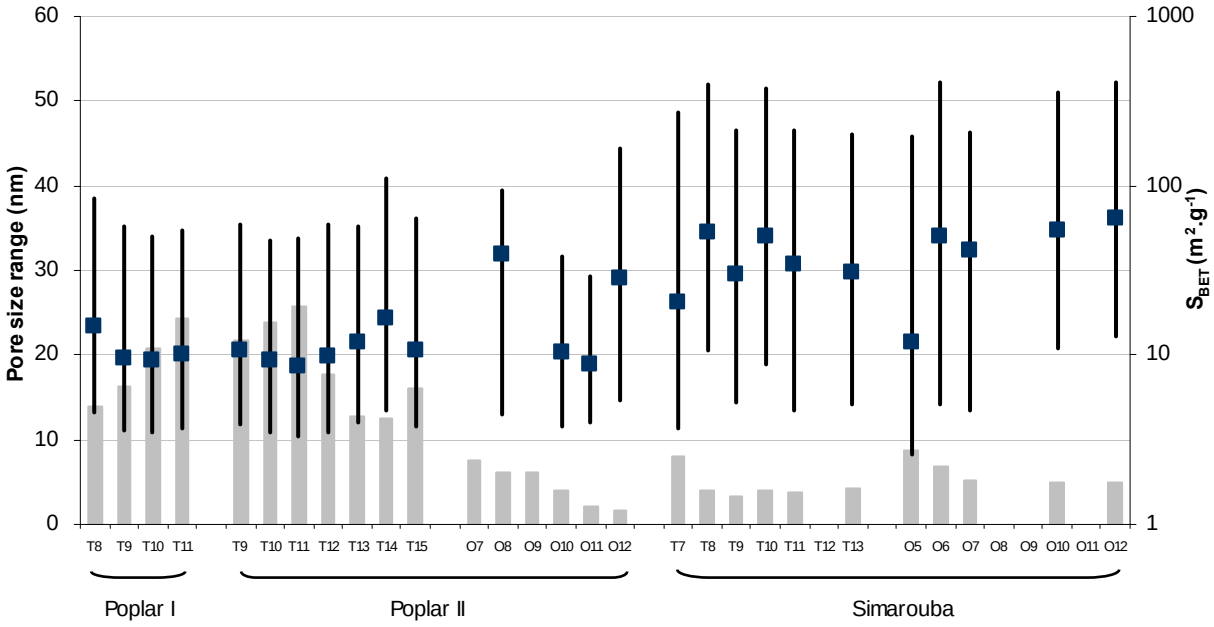

Figure 5.5 The median pore size (filled square), pore size range distribution (straight lines) and specific surface area, S_{BET} (grey histogram) of poplar and simarouba after cell wall thickness constant. (Poplar I and poplar II denote sample taken from tree I and II. The S_{BET} was shown in logarithmic scale. T7-T15: tension wood samples; O5-O12: opposite wood samples)

[7] The selection of mature stage is according to the stable cell wall thickness, and two poplar trees (poplar I and poplar II) and one simarouba tree were used for the analysis of mature wood. Poplar I: samples #8 to #11 for tension wood; Poplar II: samples #9 to #15 for tension wood and samples #7 to #12 for opposite wood; Simarouba: samples #7 to #13 for tension wood and samples #5 to #12 for opposite wood. The isotherms of all the samples were displayed in Annex II (Fig. 6.1), in Chapter 4.2 (Figs. 8 and 9) and in Chapter 4.3 (Figs. 5 and 6).

In Fig. 5.5, the very low but not-nil surface areas and an estimated pore size centered around 30 nm are proposed to be assigned to the pit membrane of the vessels (Clair et al. 2008; Chang et al. 2009b), which is known to be composed of unlignified primary wall with pectin gel as the G-layer (Van Ieperen 2007). This pore size is in the range of what was measured on pit membrane by using diffusion of colloidal gold particles method (Choat et al. 2003, 2004).

Our results also show that the high mesoporosity of mature tension wood can be detected only when G-layer is present. This result was compared with previous reports about the mesoporosity in several kinds of mature tension woods. Nine tension woods (7 tropical species and 2 temperate species in Table 5.1) with different fibre patterns from thick G-layer to G-layer absent were compared.

Table 5.1 Characteristics of 9 tension wood species studied

Family	Species	Abbreviation	Tree diam. (cm)	Fiber pattern*	S_{BET} (m^2/g)	V_{MP} (cm^3/g)
Fagaceae	*Chestnut* (*Castanea sativa* Mill.)*	Cs	12	G_{thick}	13.6	0.025
Lauraceae	*Sextonia rubra***	Sr	25	G_{thick}	64.6	0.133
Salicaceae	*Poplar (Populus deltoides × P. nigra)****	Pop	24	G_{thin}	14.8	0.028
Fabaceae	*Inga alba***	Ia	29	G_{thin}	9.0	0.014
Lauraceae	*Ocotea guyanensis***	Og	19	G_{thin}	2.8	0.003
Fabaceae	*Tachigali melinonii***	Tm	18	G_{thin}	4.8	0.004
Myristicaceae	*Virola michelii***	Vm	36	no G	2.6	0.002
Myristicaceae	*Iryanthera sagotiana***	Is	26	no G	4.7	0.005
Simaroubaceae	*Simarouba amara* Aubl.****	Sa	30	no G	1.6	0.0004

V_{MP}: mesopore volume evaluated by the α_S method (Gregg and Sing 1982); S_{BET}: specific surface area; *Three types of wood fiber were classified according to the G-layer patterns: G_{thin}, with thin G-layer; G_{thick}, with thick G-layer; no G, G-layer absent. Data come from *: Clair et al. 2008, **: Chang et al. 2009b, *** : present study.

Anatomical sections of tension wood in nine species are illustrated in Figure 5.6. G-layers are easy to be identified after staining; however there are notable differences in morphology, thickness, and distribution. In tension wood fibres of chestnut and *S. rubra*, thick G-layers almost fills up the entire lumen, whereas in *O. guyanensis*, poplar, *I. alba*, or *T. melinonii* tension wood, the G-layer is thinner, sometimes delaminated from the adjacent S_2 and folded into the lumen towards the same direction. This detachment phenomenon results from sample preparation with classical sectioning (Clair et al. 2005a). In *T. melinonii*, the thin G-layer was only observed in a limited number of fibres whereas, in the other five species, most fibres contained G-layers. For the other three species (*V. michelii*, *I. sagotiana,* and simarouba), no G-layers were detected in fibres.

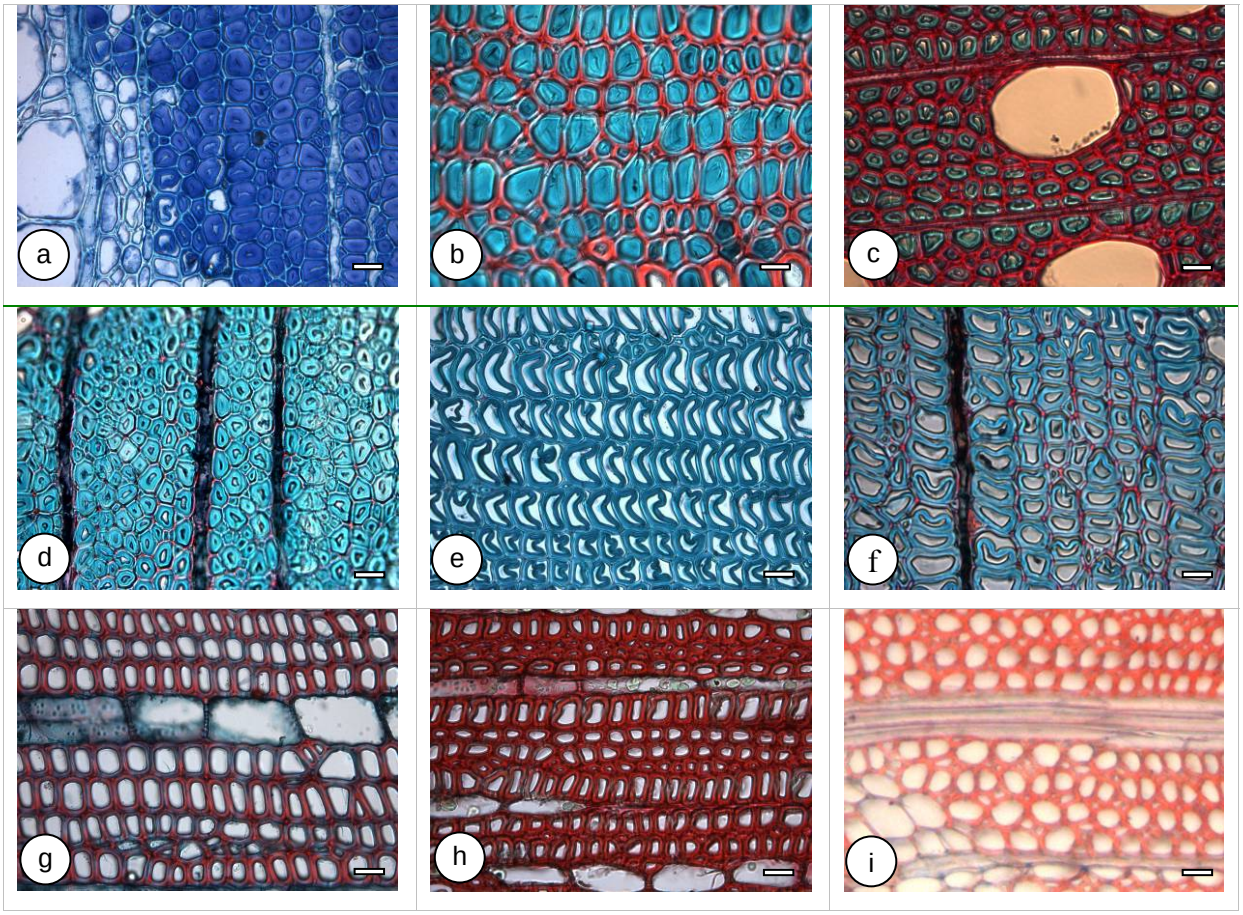

Figure 5.6 Cross sections of tension wood in 9 species. a: Chestnut (*Castanea sativa* Mill.), b: *Sextonia rubra*, c: Poplar (*Populus deltoides* × *P. nigra*), d: *Inga alba*, e: *Ocotea guyanensis*, f: *Tachigali melinonii*, g: *Virola micheli*, h: *Iryanthera sagotiana*, i: Simarouba (*Simarouba amara* Aubl.), Scale bar=20 µm. The G-layers are detected in images (a), (b), (c), (d), (e) and (f) from its swollen aspect and its detachment from the S_2 layer. (a, b) tension wood with thick G-layers; (c, d, e, f) tension wood with thin G-layers; (g, h, i) tension wood without G-layers. In (f), a thin G-layer was observed but it was sparse on the wood sample. Image (a) was stained with O-Toluidine blue, others were stained with stained with safranin/fast green. Image (a) cited from Clair et al. 2008 and images (b, d, e, f, g and h) cited from Chang et al. (2009b)

Figure 5.7 shows the nitrogen adsorption-desorption isotherms (77K) of tension wood in nine species. It clearly shows that the typical isotherm for G-layer with high surface area can always be detected in tension wood with thick G-layers (Fig. 5.8), indicating a type IV with a H3 type hysteresis loop according to the IUPAC classification (Sing et al. 1985). When tension wood with a thin G-layer (*b* in Fig. 5.7), the mesoporosity can be detected only in the case of poplar and *I. alba* which have thin G-layers nearly filled with fibers. Other tension woods with a thin G-layer, like *O. guyanensis* (Og) and *T. melinonii* (Tm), present an extremely narrow hysteresis loops with low surface area S_{BET} (Fig. 5.8), as observed in tension wood without G-layer (*c* in Fig. 5.7). We can assume that in *T. melinonii* the amount of fibers with G-layer was not sufficient to give clear hysteresis loop or some species (*O. guyanensis* and *T. melinonii*) could have a partial lignification filling most of the mesopores. Another explanation would be that not all G-layers present a porosity which can be easily stabilized by supercritical drying. In species without G-layer recognized from the staining, the whole mesoporosity has been filled by lignin and remaining pores correspond to what was observed in normal wood.

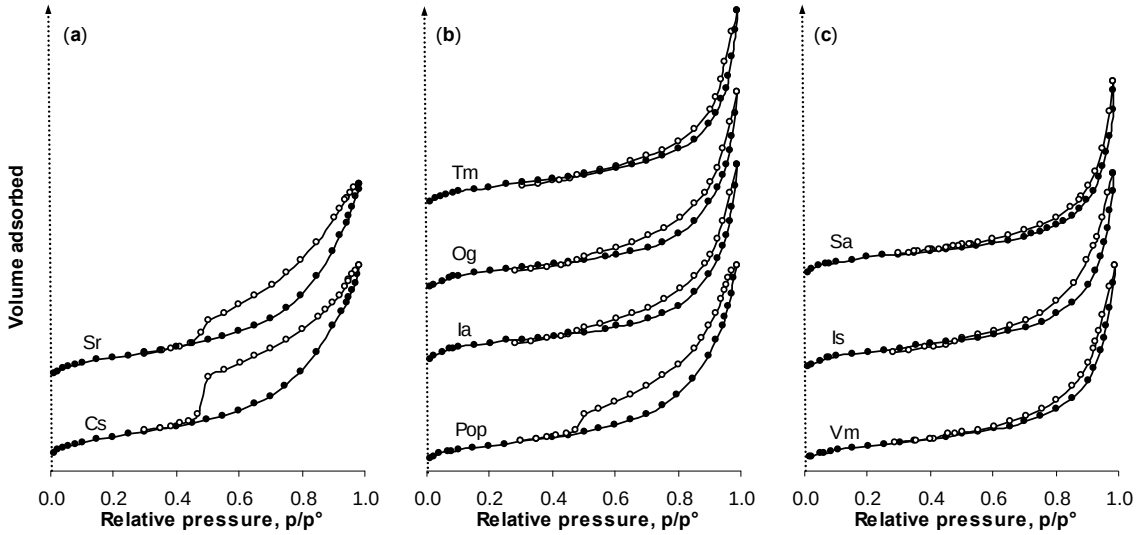

Figure 5.7 Normalised N_2 adsorption-desorption isotherms of 9 tension wood species. (a): tension wood with thick G-layer, (b): tension wood with thin G-layer, (c): tension wood without G-layer (filled symbols, adsorption; open symbols, desorption)

When comparing the pore size range distribution between different type of tension wood, the results clearly show that the estimated median pore size for typical G-layer are centered around 15 nm for tension wood with G-layer full or nearly full of the fibers, however, others show large pore size (30 nm) like normal wood which are supposed to originate from the pit membrane of the vessels. It should be noted that poplar presented here has lower median pore size when compared with results from the same species in Fig. 5.5. The poplar presented here was artificial bended young tree with diameter 8 cm, whereas natural titled poplar tree with diameter 24 cm was used in Fig. 5.5. This suggests that even if the same species used, it seems the median pore size largely depend on the specific tree tested.

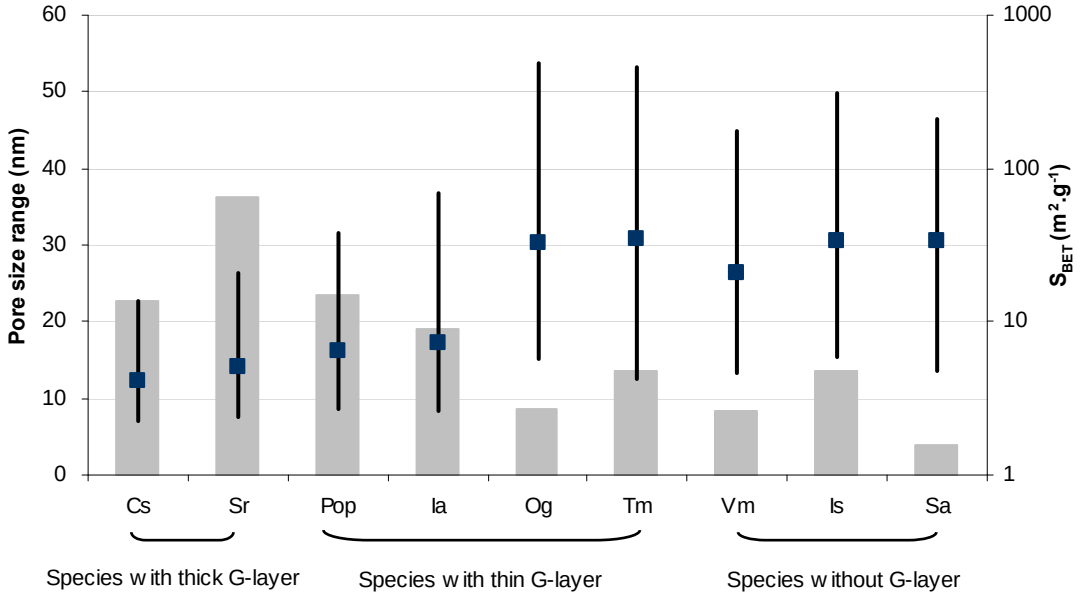

Figure 5.8 The median pore size (filled square), pore size range distribution (straight lines) and specific surface area, S_{BET} (grey histogram) of 9 tension woods with different fiber patterns. (The S_{BET} was shown in logarithmic scale. The full name of each species are shown in Table 5.1)

It is especially significant that the tension wood without G-layer samples present very little surface area and wide pore size range with large median pore size. Tension wood with thick G-layer presents high porosity and narrow pore size range with small median pore size. However, for tension wood with thin G-layer or G-layer less filled with fibers, the porosity was in intermediate and seems to depend on the proportion between G-layer and normal wood cell wall. This result led us to revisit the porosity measured in tension wood and to explore the possible contribution of porosity hidden in the cell wall.

From the staining transverse light micrographs of poplar tension wood (one micrograph is shown in Fig. 1a in Chapter 3.2.4), the area ratio between G-layers and other layers was measured around 45% (1: 2.22), this value is known to be over-estimated considering the swelling occurring with this kind of preparation (Clair et al. 2005a; Fang et al. 2008). The uncontrolled transverse swelling in G-layer during the normal sectioning has been measured around 25-50% depend on the residual growth strain of the sample (Fang et al. 2008). If one considers that 30% swelling happened in our case, the area ratio between G-layers and other layers was corrected as 31.5%. Considering the disappearance of pores during drying (as proved by the evaporative dried tension wood isotherm in Fig. 3.4), the oven dry state allows measurement of the amount of dense microfibrils. At cell wall level, the transverse shrinkage in G-layer and other layer during drying was around 20% and 15% respectively (Fang et al. 2007). Considering this shrinkage, then the mass fraction of G-layer in the tension wood sample has been evaluated to about 23%. As a consequence, in tension wood sample, including G-layer and other layer, only 23% of the mass contribute to mesopore volume. Following this calculation, one can estimate the isotherm or pore size distribution of G-layer from tension wood sample as approximately 4 times the volume of nitrogen per mass unit of the tension wood sample.

Based on the assumption above, the isotherm and pore size distribution of "native" G-layer deduced from the mature tension wood in the same tree (T11 of poplar II was used) are shown in Fig. 5.9 and compared to experimental results on isolated G-layer (sonication 15 min: G15).

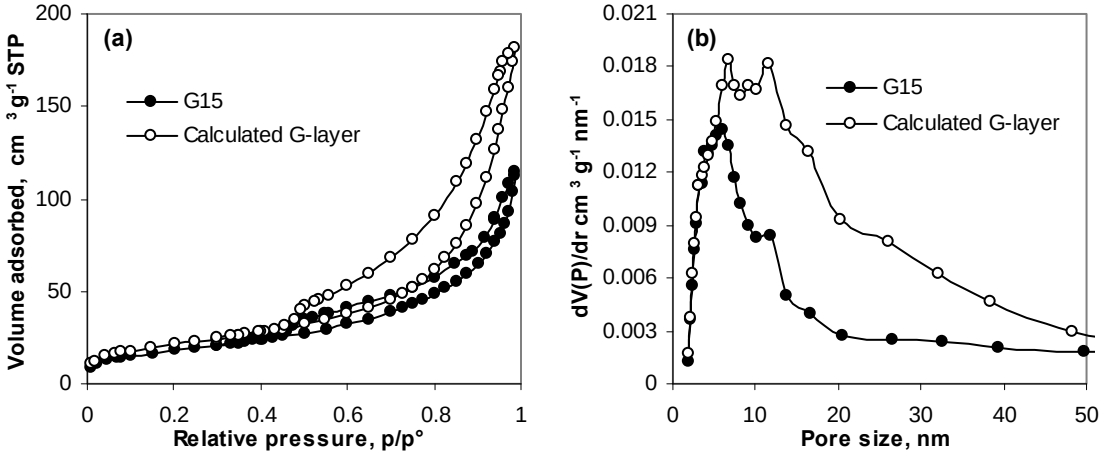

Figure 5.9 (a) N_2 adsorption-desorption isotherms and (b) pore size distributions for G-layer extracted by 15 min sonication (G15, curve with solid symbols) and calculated G-layer (curve with open symbols) based on mature tension wood (sample T11 of poplar II) from the same tree

The calculated volume of nitrogen adsorbed (182 cm^3/g) is higher than the value obtained from G15 (115 cm^3/g), but the isotherm shape from calculated G-layer well fit the one obtained from experiment. However, the former shows relatively wider pore size distribution than the latter one. The difference between the pore size distributions is less likely to be influenced by sonication, since this treatment more likely to affect the smaller pores than the bigger ones as shown in *Chapter 3.2.4*. It is very probable that this difference may come from the contribution of other layers, as tension woods without G-layer as well as normal wood present non-negligible low porosity and large median pore size. This non-nil porosity in other layers is proposed from pits membrane, and is supposed as the main contribution of the porosity when G-layer absent. In this way, it could explain the instability of porosity in tension wood with thin G-layer, which may depend on the proportion of G-layer and other layers.

5.4. Interpretation in relation to maturation stress generation

Based on the results from FTIR and N_2 adsorption-desorption measurements in two kinds of tension wood and the corresponding opposite wood, it appears that the difference between tension and opposite wood mainly occurs during maturation just when G-layer deposition take place. The opposite orientations of molecular groups assigned to amorphous carbohydrates like hemicelluloses and pectins are observed in tension wood during G-layer formation. Although the mechanism of tension stress generation in tension wood remains unknown, the matrix polysaccharides in the G-layer probably are subjected to mechanical stress due to chemical reactions and interaction with the cellulose microfibrils (Mellerowicz et al. 2008) which could result in an increased orientation. The tensional stress in the matrix can be transferred to the cellulose microfibrils by the swelling of the matrix in an interconnected network of cellulose microfibrils. Regardless of the presence of G-layer, the increase of pore size can always be detected during maturation. The measured mesoporosity may result from the cavities between microfibrils within the hemicellulosic hydrogel matrix. These observations suggest that pores from secondary walls have bigger size and a wider range of pore size than middle lamella and primary walls. However, the typical isotherm shape and an increase of pore size were also observed in the opposite wood of non-G-layer species, but very limit maturation process (only sample #4) can be monitored due to its slow growth rate compared to tension wood side. If the mesoporosity plays a major role in maturation stress generation, our results support the idea of a common mechanism between G-layer and non-G-layer species. Even more, this mechanism could be also used to generate the low tensile stress, as observed in opposite wood.

However, the origin of the pores is still not unambiguous, since the increased size of pores may come not from the change of size of given pores but could reflect a change in the relative proportion of pores from different cell layers.

Results however allow to conclude on the kinetic of the process. If swelling occurs during maturation, this swelling takes place in a very short time, shortly after the deposition of G-

layer, that we were not able to record. Or the swelling could be too small to be recordable with our technique. Whereas, it is also possible that the mechanisms may not be directly linked to mesoporosity, an alternative hypothesis may be proposed to explain the generation of high tensile stress for tension wood. This study opens the question on the mechanism of tensile stress generation in non-G-layer species. Obviously, there is still a lot to do in order to better understand why the mesoporosity changes during cell wall maturation in both tension and opposite wood. This could be concerned with the comparative investigation of polysaccharide composition between the G-layer and non-G-layer cell wall, especially along its differentiation.

Conclusions and future prospects

The macromolecular and structural modifications during the building and maturation of tension wood cell wall were here demonstrated.

(a) From the study using FTIR microscopy on the developing poplar tension and opposite wood cell walls, it could be concluded that:

- At the early stage of cell wall development already before the formation of the G-layer, the C-O-C adsorption peak from carbohydrates showed an orientation more parallel to the fibre axis, which was clearly different from that in opposite wood. In the later stages of G-layer formation, a higher degree of orientation of cellulose was observed in tension wood than in opposite wood.
- In all cases, the orientation of lignin was parallel to that of cellulose microfibrils, with a higher degree of orientation in tension wood than in opposite wood. This was attributed to a more ordered S_2 wall in tension wood than in opposite wood.
- During the formation of the G-layer in tension wood, signals attributed to amorphous carbohydrates (hemicelluloses and pectins) were oriented at an angle of 90^o to that measured in opposite wood. These signals were suspected to originate from the generation of xyloglucan regulating stress in *Populus* tension wood (Baba et al. 2009) but recent results from Guedes et al. (2014, submitted) argue for the absence of Xyloglucan, so the second hypothesis attributing these signals to xylan (Kim and Daniel 2012) is more likely. In tension wood, the orientation of the bands assigned to amorphous carbohydrates remained the same throughout the cell wall maturation process, probably reflecting continued deposition of xylan with a different orientation from that in the S_2 wall of opposite wood.

To improve the current knowledge on the change in composition and orientation of the polymers during building and maturation of tension wood cell wall, the tension wood from other species could be investigated and compared.

(b) The studies using nitrogen adsorption method on the developing poplar (with typical G-layer) and simarouba (without G-layer) wood cell walls, demonstrated that:

- No matter the species with or without G-layer, mesoporosity can always be detected near cambium zone, which contains mainly primary wall with high mesopore volume for both tension and opposite wood. With the cell wall differentiation, the high porosity near the cambium zone decreases abruptly and is nearly lost due to the lignification, with an exception in tension wood with G-layer.

- Not depending on the presence of G-layer, the typical isotherm type and the increase of pore size are observed in both kinds of tension woods, but only tension wood with G-layer retains some mesoporosity all along the maturation process up to mature wood.
- Non-G-layer species may share the same mechanism of tensile stress generation as in tension wood with G-layer. However, the mechanisms could not directly link to mesoporosity, and alternative hypothesis cannot be excluded for the generation of high tensile stress for tension wood without G-layer.

To further understand the maturation stress generation in trees, we still need to identify the location of pore size increase. Obviously, there is still a lot to do to better understand the mechanisms associated to tension stress generation in species not producing a G-layer. The next step could be concerned with the comparative investigation of polysaccharide composition between the G-layer and non-G-layer cell wall, especially along its differentiation.

(c) From the results of the study on the ultrastructure of mature tension wood and isolated G-layers, it could be concluded that:

- The porosity parameters of isolated G-layers correspond to what was described for mature tension wood sample. Thus the large amount of mesopores previously reported in tension wood compare to normal wood comes from the G-layer itself.
- The typical isotherms and the median pore size characterized for G-layer can not be always detected in tension wood, only in tension wood filled with thin G-layer or thick G-layer.
- Ultrasonic treatment and an increased treatment time influence the ultrastructure of isolated G-layers. The G-layers extracted from tension wood sections after only 15 min (100 W and 25 kHz) sonication can better represent the properties of G-layer, but may already not perfectly reflect the native state, even if very high mesoporosity is obtained.

Taking the advantage of this treatment on G-layer isolation, it could be interesting to perform the measurement of swelling properties on pure G-layers, this would allows an easier interpretation of the nitrogen isotherms as they would not be contaminated by remaining porosity from other layers.

Annex I Staining protocols for G-layer identification

Solutions and reagents:

- Safranin O solution (2% wt/v in EtOH-H_2O solution (50-50 v/v) (referred as 2% in 50% ethanol)
- Fast green solution (0.5% wt/v in EtOH-H_2O solution (95-5 v/v) (referred as 0.5% in 95% ethanol)
- Astra blue alcoholic solution (1% wt/v in EtOH-H_2O solution (100-0 v/v) (referred as 1% in 100% ethanol)
- Alcian blue alcoholic solution (1% wt/v in EtOH-H_2O solution (100-0 v/v) (referred as 1% in 100% ethanol)
- Alcian blue acidified solution (1% wt/v in Glacial acetic acid-H_2O solution (3-97 v/v) (referred as 1% in 3% acetic acid)

Procedure:

A. Safranin O stain (with bleach water)

(1) Wash gently in bleach water, approximately 6 min

(2) Rinse in distilled water until odorless

(3) Rinse in 50% ethanol, 1 min

(4) Stain in 2% safranin O solution, 3 min30

(5) Rinse in 50% ethanol, 5 min

(6) Rinse in 70%, 85%, 95% ethanol, 5 min respectively

(7) Dehydrate with three changes of 100% ethanol, 5 min

(8) Mount section by resin, cover quick

B. Astra blue in alcoholic solution stain (with bleach water)

(1) Wash gently in bleach water, approximately 6 min

(2) Rinse in distilled water until odorless

(3) Rinse in 50%, 70%, 85%, 95%, 100% ethanol, 5 min respectively

(4) Stain in astra blue alcoholic solution, 6 min

(5) Dehydrate with three changes of 100% ethanol, 5 min

(6) Mount section by resin, cover quick

C. Alcian blue 8GX in alcoholic solution stain (with bleach water)

(1) Wash gently in bleach water, approximately 6 min

(2) Rinse in distilled water until odorless

(3) Rinse in 50%, 70%, 85%, 95%, 100% ethanol, 5 min respectively

(4) Stain in alcian blue 8GX alcoholic solution, 6 min

(5) Dehydrate with three changes of 100% ethanol, 5 min

(6) Mount section by resin, cover quick

D. Safranin O and astra blue in alcoholic solution stain (with bleach water)

(1) Wash gently in bleach water, approximately 6 min

(2) Rinse in distilled water until odorless

(3) Rinse in 50% ethanol, 1 min

(4) Stain in 2% safranin O solution, 3 min30

(5) Rinse in 50% ethanol, 5 min

(6) Rinse in 70%, 85%, 95%, 100% ethanol, 5 min respectively

(7) Stain in astra blue alcoholic solution, 6 min

(8) Dehydrate with three changes of 100% ethanol, 5 min

(9) Mount section by resin, cover quick

E. Safranin O and alcian blue 8GX in alcoholic solution stain (with bleach water)

(1) Wash gently in bleach water, approximately 6 min

(2) Rinse in distilled water until odorless

(3) Rinse in 50% ethanol, 1 min

(4) Stain in 2% safranin O solution, 3 min30

(5) Rinse in 50% ethanol, 5 min

(6) Rinse in 70%, 85%, 95%, 100% ethanol, 5 min respectively

(7) Stain in alcian blue 8GX alcoholic solution, 6 min

(8) Dehydrate with three changes of 100% ethanol, 5 min

(9) Mount section by resin, cover quick

F. Safranin O and alcian blue 8GX in acidified solution stain (with bleach water)

(1) Wash gently in bleach water, approximately 6 min

(2) Rinse in distilled water until odorless

(3) Pass through 3% acetic acid solution quickly

(4) Stain in alcian blue 8GX acidified solution, 5 min

(5) Rinse in distilled water

(6) Rinse in 30%, 50% ethanol, 1 min respectively

(7) Stain in 2% safranin O solution, 3 min30

(8) Rinse in 50% ethanol, 5 min

(9) Rinse in 70%, 85%, 95% ethanol, 5 min respectively

(10) Dehydrate with three changes of 100% ethanol, 5 min

(11) Mount section by resin, cover quick

G. Safranin O and fast green stain (without bleach water)

(1) Wash gently in distilled water, 3 min

(2) Rinse in 50% ethanol, 5 min

(3) Stain in 2% safranin O solution, 3 min30

(4) Rinse in 50% ethanol, 5 min or longer**

(5) Rinse in 70%, 85%, 95% ethanol, 5 mn respectively

(6) Stain in fast green solution, 5 min

(7) Rinse in 95% ethanol, 5 min

(8) Dehydrate with three changes of 100% ethanol, 5 min

(9) Mount section by resin, cover quick

H. Safranin O and fast green stain (with bleach water)

(1) Wash gently in bleach water, approximately 6 min

(2) Rinse in distilled water until odorless

(3) The same procedure as protocol G. (2)-(9)

** This step need the practice experience, which depends on samples, section thickness, softness, interact. If rinse is not enough in 50% ethanol, it will be difficult for the second stain (fast green); if too much, the tissue become colourless during the fist stain (safranin O), and the second stain will replace the first stain completely, then there is meaningless by using double colour staining method.

Annex II N_2 adsorption-desorption isotherms during wood formation

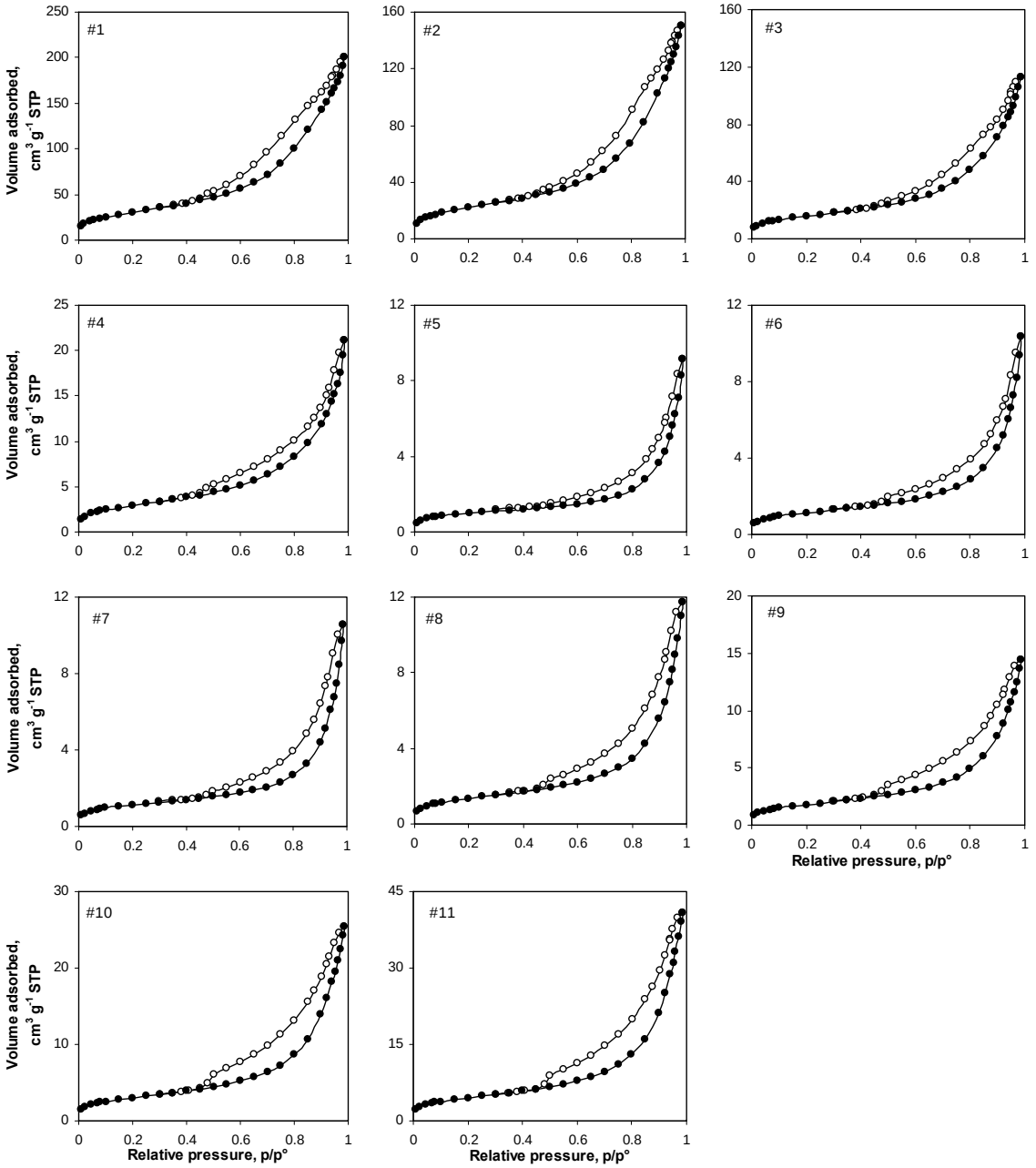

Figure 6.1 N_2 adsorption isotherms at each location of tension wood cell wall maturation from poplar I (filled symbols, adsorption; open symbols, desorption)

References

Alder E (1977) Lignin chemistry: Past, present and future. Wood Science and Technology 11:169-218

Alméras T, Fournier M (2009) Biomechanical design and long-term stability of trees: morphological and wood traits involved in the balance between weight increase and the gravitropic reaction. Journal of Theoretical Biology 256: 370-381

Alméras T, Gril J, Clair B (2012) The origin of maturation stress in tension wood: using a wide range of observations and mechanical considerations to discriminate between hypothetic mechanisms. 7th plant biomechanics international conference, Clermont-Ferrand, France.

Alméras T, Thibaut A, Gril J (2005) Effect of circumferential heterogeneity of wood maturation strain, modulus of elasticity and radial growth on the regulation of stem orientation in trees. Trees, Structure and Function 19: 457-467

Andersson-Gunneras S, Mellerowicz EJ, Love J, Segerman B, Ohmiya Y, Coutinho PM, Nilsson P, Henrissat B, Moritz T, Sundberg B (2006) Biosynthesis of cellulose-enriched tension wood in Populus: global analysis of transcripts and metabolites identifies biochemical and developmental regulators in secondary wall biosynthesis. The Plant Journal 45:144-165

Antonova GF, Stasova VV (1997) Effects of environmental factors on wood formation in larch (*Larix sibirica* Ldb.) stems. Trees 11: 462-468

Araki N, Fujita M, Saiki H, Harada H (1983) Transition of fibre wall structure from normal wood to tension wood in certain species having gelatinous fibres of S_1+G and S_1+S_2+S_3+G types. Mokuzai Gakkaishi 29: 267-273

Archer RR (1986) Growth stresses and strains in trees. In: T. E. Timell (Ed.): Springer Series in Wood Science. Berlin: Springer Verlag

Baba K, Park YW, Kaku T, Kaida R, Takeuchi M, Yoshida M, Hosoo Y, Ojio Y, Okuyama T, Taniguchi T, Ohmiya Y, Kondo T, Shani Z, Shoseyov O, Awano T, Serada S, Norioka N, Norioka S, Hayashi T (2009) Xyloglucan for generating tensile stress to bend tree stem. Molecular Plant 2: 893-903

Badia MA, Mothe F, Constant T, Nepveu G (2005) Assessment of tension wood detection based on shiny appearance for three poplar cultivars. Annals of Forest Science 62: 43-49

Bamber RK (1987) The origin of growth stresses: a rebuttal. IAWA Bulletin n.s 80-84

Bamber RK (2001) A general theory for the origin of growth stresses in reaction wood: how trees stay upright. IAWA Journal 22: 205-212

Barnett JR, Bonham VA (2004) Cellulose microfibril angle in the cell wall of wood fibres. Biological Reviews 79: 461-472

Barrett EP, Joyner LG, Halenda PH (1951) The determination of pore volume and area distributions in porous substances. Journal of the American Chemical Society 73: 373-380

Bowling AJ, Vaughn KC (2008) Immunocytochemical characterization of tension wood: gelatinous fibers contain more than just cellulose. American Journal of Botany 95: 655-663

Boyd JD (1950) Tree growth stresses: Part I - Growth stress evaluation. Australian Journal of Scientific Research, series B, Biological Sciences 3: 270-293

Boyd JD (1985) The key factor in growth stress generation in trees. Lignification or crystallisation. IAWA Bull. n. s. 6: 139-150

Broekhoff JCP, de Boer JH (1967) Studies on pore systems in catalysts: IX. Calculation of pore distributions from the adsorption branch of nitrogen sorption isotherms in the case of open cylindrical pores A. Fundamental equations. Journal of Catalysis 9: 8-14

Brunauer S, Emmett PH, Teller E (1938) Adsorption of gases in multimolecular layers. Journal of the American Chemical Society 60: 309-319

Burgert I (2006) Exploring the micromechanical design of plant cell walls. American Journal of Botany 93: 1391-1401

Cansell F, Aymonier C, Loppinet-Serani A (2003) Review on materials science and supercritical fluids. Current Opinion in Solid State and Materials Science 7: 331-340

Chaffey N (2000) Microfibril orientation in wood cells: new angles on an old topic. Trends in Plant Science 5: 360-362

Chaffey N, Barlow P, Sundberg B (2002) Understanding the role of the cytoskeleton in wood formation in angiosperm trees: Hybrid aspen (*Populus tremula* x *P. tremuloides*) as the model species. Tree Physiology 22: 239-249

Chang SS, Clair B, Gril J, Yamamoto H, Quignard F (2009a) Deformation induced by ethanol substitution in normal and tension wood of chestnut (*Castanea sativa* Mill.) and simarouba (*Simarouba amara* Aubl.). Wood Science and Technology 43: 703-712

Chang SS, Clair B, Ruelle J, Beauchêne J, Di Renzo F, Quignard F, Zhao GJ, Yamamoto H, Gril J (2009b) Mesoporosity as a new parameter for understanding tension stress generation in trees. Journal of Experimental Botany 60: 3023-3030

Chang SS, Hu JB, Clair B, Quignard F (2011) Pore structure characterization of poplar tension wood by nitrogen adsorption-desorption method (*in Chinese*). Scientia Silvae Sinicae 47:134-140

Chang SS, Quignard F, Di Renzo F, Clair B (2012) Solvent polarity and internal stresses control the swelling behavior of green wood during dehydration in organic solution. BioResources 7: 2418-2430

Choat B, Ball M, Luly J, Holtum J (2003) Pit membrane porosity and water stress-induced cavitation in four co-existing dry rainforest tree species. Plant Physiology 131: 41-48

Choat B, Jansen S, Zwieniecki MA, Smets E, Holbrook NM (2004) Changes in pit membrane porosity due to deflection and stretching: the role of vestured pits. Journal of Experimental Botany 55: 1569-1575

Clair B (2001) Etude des propriétés mécaniques et du retrait au séchage du bois à l'échelle de la paroi cellulaire: essai de compréhension du comportement macroscopique paradoxal du bois de tension à couche gélatineuse. PhD Thesis. Ecole Nationale du Génie Rural des Eaux et Forêts Montpellier.

Clair B, Almeras T, Pilate G, Jullien D, Sugiyama J, Riekel C (2011) Maturation stress generation in poplar tension wood studied by synchrotron radiation microdiffraction. Plant Physiology 155: 562-570

Clair B, Alméras T, Yamamoto H, Okuyama T, Sugiyama J (2006a) Mechanical behaviour of cellulose cellulose microfibrils in tension wood, in relation with maturation stress generaton. Biophysical Journal 91:1128-1135

Clair B, Gril J, Baba K, Thibaut B, Sugiyama J (2005a) Precautions for the structural analysis of the gelatinous layer in tension wood. IAWA Journal 26:189-195

Clair B, Gril J, Di Renzo F, Yamamoto H, Quignard F (2008) Characterization of a gel in the cell wall to elucidate the paradoxical shrinkage of tension wood. Biomacromolecules 9: 494-498

Clair B, Ruelle J, Beauchene J, Prevost MF, Fournier M (2006b) Tension wood and opposite wood in 21 tropical rain forest species 1. occurrence and efficiency of the G-layer. IAWA Journal 27:329-338

Clair B, Ruelle J, Thibaut B (2003) Relationship between growth stress, mechanical-physical properties and proportion of fibre with gelatinous layer in chestnut (*Castanea Sativa* Mill.). Holzforschung 57: 189-195

Clair B, Thibaut B (2001) Shrinkage of the gelatinous layer of poplar and beech tension wood. IAWA Journal 22: 121-131

Clair B, Thibaut B, Sugiyama H (2005b) On the detachment of the gelatinous layer in tension wood fiber. Journal of Wood Science 51: 218-221

Cosgrove DJ, Jarvis MC (2012) Comparative structure and biomechanics of plant primary and secondary cell walls. Frontiers in Plant Science 3: 204. doi: 10.3389/fpls.2012.00204

Coutand C, Loup C, Chanson B, Jeronimdis G (2004) Comparison of mechanical properties of tension and opposite wood in populus. Wood Science and Technology 38: 11-24

Dadswell HE, Wardrop AB (1949) What is reaction wood? Australian Forestry 13: 22-33

De Micco V, Aronne G (2007) Combined histochemistry and autofluorescence for identifying lignin distribution in cell walls. Biotechnic and Histochemistry 82: 209-216

Déjardin A, Laurans F, Arnaud D, Breton C, Pilate G, Leplé JC (2010) Wood formation in angiospermes. Comptes Rendus Biologies 333: 325-334

Donaldson LA (2001) Lignification and lignin topochemistry-an ultrastructural view. Phytochemistry 57: 859-873

Eriksson O, Goring DAI, Lindgren BO (1980) Structural studies on the chemical bonds between lignins and carbohydrates in spruce wood. Wood Science and Technology 14: 267-279

Fang CH (2007) Contribution of gelatinous layer to tension wood behaviour in poplar: growth stresses and wood material properties. PhD Thesis. University Montpellier II, Montpellier, France

Fang CH, Clair B, Gril J, Alméras T (2007) Transverse shrinkage in G-fibers as a function of cell wall layering and growth strain. Wood Science and Technology 41: 659-671

Fang CH, Clair B, Gril J, Liu SQ (2008) Growth stresses are highly controlled by the amount of G-layer in poplar tension wood. IAWA Journal 29: 237-246

Felten J, Sundberg B (2013) Biology, chemistry and structure of tension wood. In cellular aspects of wood formation. Plant Cell Monographs 20: 203-224

Fengel D, Wegener G (1984) Wood: chemistry, ultrastructure, reactions. Walter De Gruyter, Berlin, New York, ISBN 3-11-008481-3

Fisher JB, Stevenson JW (1981) Occurrence of reaction wood in branches of dicotyledons and its role in tree architecture. Botanical Gazette 142: 82-95

Formm J (2013) Xylem development in trees: from cambial divisions to mature wood cells. *In* cellular aspects of wood formation. Plant cell monographs. 20: 3-40

Fournier M, Baillères H, Chanson B (1994) Tree biomechanics: growth cumulative prestresses, and reorientations. Biomimetics 2: 229-251

Galarneau A, Desplantier D, Dutartre R, Di Renzo F (1999) Micelle-templated silicates as a test-bed for methods of pore size evaluation. Microporous and Mesoporous Materials 27: 297-308

Goring DAI, Timell TE (1962) Molecular weight of native cellulose. Tappi 45:454-460

Gorshkova TA, Gurjanov OP, Mikshina PV, et al. (2010) Specific type of secondary cell wall formed by plant fibers. Russian Journal of Plant Physiology 57: 328-341

Goswami L, Dunlop JWC, Jungnikl K, Eder M, Gierlinger N, Coutand C, Jeronimidis G, Fratzl P, Burgert I (2008) Stress generation in the tension wood of poplar is based on the lateral swelling power of the G-layer. The Plant Journal 56: 531-538

Gram K, Jorgensen F (1951) An easy, rapid and effieient method of counter-staining plant tissues and hyphae in wood sections by means of fast green or light green and safranin. Friesia 4: 262-266

Gregg SJ, Sing KSW (1982) Adsorption, surface area and porosity. London: Academic Press, 218-228

Grzeskowiak V, Sassus F, Fournier M (1996) Coloration macroscopique, retraits longitudinaux de maturation et de séchage du bois de tension du peuplier (*Populus* x *euramericana* cv I.214). Annals of Forest Science 53: 1083-1097

Guedes FTP, Laurans F, Quemener B, Assor C, Boizot N, Vigouroux J, Lesage-Descauses MC, Leplé JC, Déjardin A, Pilate G (submitted 2014). Evaluation of noncellulosic polysaccharide distribution in differentiating and mature poplar tension wood fibers: evidence for abondance of rhamnogalacturonan I and absence of xyloglucan in the G-layer.

Halsey G (1948) Physical adsorption on non-uniform surfaces. Journal of Chemical Physics 16:931-937

Joseleau JP, Imai T, Kuroda K, Ruel K (2004) Detection in situ and characterization of lignin in the G-layer of tension wood fibres of *Populus deltoides*. Planta 219: 338-345

Jourez B, Riboux A, Leclercq A (2001) Anatomical characteristics of tension wood and opposite wood in young inclined stems of poplar (*Populus euramericana* cv 'Ghoy'). IAWA Journal 22: 133-157

Kaku T, Serada S, Baba K, Tanaka F, Hayashi T (2009) Proteomic analysis of the G-layer in poplar tension wood. Journal of Wood Science 55: 250-257

Kataoka Y, Kondo T (1998) FT-IR microscopic analysis of changing cellulose crystalline structure during wood cell wall formation. Macromolecules 31: 760-764

Katon (1996) Infrared microspectroscopy: A review of fundamentals and applications. Micron 27: 303-314

Katon JE, Sommer AJ, Lang PL (1989-90) Infrared Microspectroscopy. Applied Spectroscopy Reviews 25: 173-211

Kim JS, Daniel G (2012) Distribution of glucomannans and xylans in poplar xylem and their changes under tension stress. Planta 236: 35-50

Klemn D, Heublein B, Fink HP, Bohn A (2005) Cellulose: Fascinating biopolymer and sustainable raw material. Angewandte Chemie International Edition 44: 3358-3393

Kubler H (1987) Growth stresses in trees and related wood properties. Forest Products Abstracts 10: 62-119

Lafarguette F, Leplé JC, Déjardin A, Laurans F, Costa G, Lesage-Descauses MC, Pilate G (2004) Poplar genes encoding fasciclin-like arabinogalactan proteins are highly expressed in tension wood. New Phytologist 164:107-121

Larson PR (1994) The vascular cambium: development and structure. Springer Verlag, Berlin

Lowell S, Shields JE, Thommes M (2003) Characterization of porous solids and powders: surface area, pore size and density. Dordrecht: Kluwer Academic Publishers.

Lukens WW, Schmidt-Winkel P, Zhao DY, Feng JL, Stucky GD (1999) Evaluating pore sizes in mesoporous materials: a simplified standard adsorption method and a simplified Broekhoff-de Boer method. Langmuir 15: 5403-5409

Mellerowicz EJ, Baucher M, Sundberg B, Boerjan W (2001) Unravelling cell wall formation in the woody dicot stem. Plant Molecular Biology 47: 239-274

Mellerowicz EJ, Gorshkova TA (2012) Tensional stress generation in gelatinous fibres: a review and possible mechanism based on cell-wall structure and composition. Journal of Experimental Botany 63: 551-565

Mellerowicz EJ, Immerzeel P, Hayashi T (2008) Xyloglucan: the molecular muscle of trees. Annals of Botany 102: 659–665

Moulia B and Fournier M (2009) The power and control of gravitropic movements in plants: a biomechanical and system biology view. Journal of Experimental Botany 60: 461-486

Muller M, Burghammer M, Sugiyama J (2006) Direct investigation of the structural properties of tension wood cellulose microfibrils using microbeam X-ray fibre diffraction. Holzforschung 60: 474-479

Navi P, Sandberg D (2012) Thermo-hydro-mechanical processing of wood. EPFL press, Lausanne p63

Nishikubo N, Awano T, Banasiak A, Bourquin V, Ibatullin F, Funada R, Brumer H, Teeri T, Hayashi T, Sundberg B, Mellerowicz EJ (2007) Xyloglucan endotransglycosylase (XET) functions in gelatinous layers of tension wood fibers in poplar - a glimpse into the mechanism of the balancing act of trees. Plant Cell Physiology 48: 843-855

Norberg PH, Meier H (1966) Physical and chemical properties of the gelatinous layer in tension wood fibre of aspen (*Populus tremula* L.). Holzforschung 20: 174-178

Obst JR (1982) Frequency and alkali resistance of lignin-carbohydrate bonds in wood. Tappi 65: 109-112

Ohsako Y (1978) A study on the material properties and the formation of wood. VII. Viscoelastic properties of newly formed xylem of Japanese black pine (*Pinus thunbergii* Parl.). (*In Japanese*) Journal of the Japan Wood Research Society 24: 852-856

Okumura S, Harada H, Saiki H (1977) Thickness variation of the G-layer along a mature and a differentiating tension wood fiber in *Populus euramericana*. Wood Science and Technology 11: 23-32

Okuyama T, Yamamoto H, Yoshida M, Hattori Y, Archer RR (1994) Growth stresses in tension wood: role of microfibrils and lignification. Annals of Forest Science 51: 291-300

Olsson AM, Bjurhager I, Gerber L, Sundberg B, Salmén L (2011) Ultra-structural organization of cell wall polymers in normal and tension wood of aspen revealed by polarization FTIR microspectroscopy. Planta 233: 1277-1286

Onaka F (1949) Studies on compression and tension wood. Wood research. Bulletin of the Wood Research Institute, Kyoto University, Japan 24: 1-88

Pallardy SG (2008) Physiology of woody plants, Academic Press, Burlington, San Diego, London pp454

Panshin AJ, de Zeeuw C (1980) Textbook of wood technology. 4th edition. McGraw-Hill Book Co., New York.

Panshin AJ, de Zeeuw C, Brown HP (1964) Textbook of wood technology. Volume I: structure, identification, uses, and properties of the commercial woods of the United States. (second edition) McGraw-Hill Book Company, New York, San Francisco.

Pierre AC, Pajonk GM (2002) Chemistry of aerogels and their applications. Chemical Reviews 102: 4243-4266

Pilate G, Chabbert B, Cathala B, Yoshinaga A, Leplé JC, Laurans F, Lapierre C, Ruel K (2004a) Lignification and tension wood. Comptes Rendus Biologies 327: 889-901

Pilate G, Déjardin A, Laurans F, Leplé JC (2004b) Tension wood as a model for functional genomics of wood formation. New Phytologist 164: 63-72

Plomion C, Leprovost G, Stokes A (2001) Wood formation in trees. Plant Physiology 127: 1513-1523

Post IL (1977) An incremental longitudinal growth stress distribution model. Holzforschung 33: 107-111

Prodhan AKMA, Ohtani J, Funada R, Abe H, Fukazawa K (1995) Ultrastructural investigation of tension wood fiber in *Fraxinus-Mandshurica* Rupr. Var. *japonica Maxim*. Annals of Botany 75: 311-317

Rawlins TE, Takahashi WN (1952) Technics of plant histochemistry and virology. National press, Millbrae, CA. pp. 26-40

Rouquerol F, Rouquerol J, Sing K (1999) Adsorption by powders and porous solids: principles, methodology and applications. San Diego: Academic Press, 439-467

Rowell RM, Pettersen R, Han JS, Rowell JS, Tshabalala MA (2005) Cell wall chemistry. In Handbook of wood chemistry and wood composites. RM Rowell (Ed.) CRC Press, 35-74

Ruelle J, Clair B, Beauchene J, Prévost MF, Fournier M (2006) Tension wood and opposite wood in 21 tropical rain forest species. 2. Comparison of some anatomical and ultrastructural criteria. IAWA Journal 27: 341-376

Ruelle J, Yamamoto H, Thibaut B (2007) Growth stresses and cellulose structural parameters in tension and normal wood from three tropical rainforest angiosperms species. BioResources 2: 235-251

Sassus F (1998) Déformations de maturation et propriétés du bois de tension chez le hêtre et le peuplier: Mesures et modèles. PhD Thesis. ENGREF, Montpellier.

Schrader J (2003) Developmental biology of wood formation-finding regulatory factors through functional genomics. PhD Thesis. Umea, Swedish University of Agricultural Sciences.

Settle FA (1997) Handbook of instrumental techniques for analytical chemistry. Prentice Hall PTR (ECS Professional)

Sing KSW, Everett DH, Haul RAW, Moscou L, Pierotti RA, Rouquérol J, Siemienewska T (1985) Reporting physisorption data for gas-solid systems with special reference to the determination of surface area and porosity. International Union of Pure and Applied Chemistry. Pure and Applied Chemistry 57: 603-619

Sjöström E (1981) Wood polysaccharides. In wood chemistry, fundamentals and applications. Academic Press, New York, pp. 51-67

Stuart B (2004) Infrared spectroscopy: Fundamentals and applications. John Wiley and Sons, Ltd.

Timel TE (1980) Organization and ultrastructure of the dormant cambial zone in compression wood of Picea abies.Wood Science and Technology 14: 161-179

Timell TE (1986) Compression wood in Gymnosperms. Springer, Berlin, Heidelberg, New York, Vol.1-3

Tischer PCSF, Sierakowski MR, Westfahl H Jr, Tischer CA (2010) Nanostructural reorganization of bacterial cellulose by ultrasonic treatment. Biomacromolecules 11: 1217-1224

Uggla C, Magel E, Moritz T, Sundberg B (2001) Function and dynamics of auxin and carhydrates during earlywood/latewood transition in Scots pine. Plant Physiology 125: 2029-2039

Van Ieperen W (2007) Ion-mediated changes in xylem hydraulic resistance in planta: fact or fiction? Trends in Plant Science 12: 137-142

Vazquez-Cooz I, Meyer RW (2002) A differential staining method to identify lignified and unlignified tissues. Biotechnic and Histochemistry 77: 277-282

Wardrop AB (1964) The reaction anatomy of arborescent angiosperms. In: Zimmermann, M. H. (ed.). The Formation of Wood in Forest Tree, Academic Press, New York, 405-456

Wardrop AB, Dadswell HE (1955) The nature of reaction wood. IV. Variations in cell wall organization in tension wood fibers. Australian Journal of Botany 3: 177-189

Wardrop AB, Dadswell HE (1957) Variations in the cell wall organization of tracheids and fibers. Holzforschung 11: 33

Washusen R, Evans R (2001) The association between cellulose crystallite width and tension wood occurrence in eucalyptus globulus. IAWA Journal 22: 235-243

Wilson BF, Wodzicki TJ, Zahner R (1966) Differentiation of cambial derivatives: proposed terminology. Forest Science 12: 438-440

Yamamoto H (1998) Generation mechanism of growth stresses in wood cell walls: roles of lignin deposition and cellulose microfibril during cell wall maturation. Wood Science and Technology 32: 171-182

Yamamoto H (2004) Role of the gelatinous layer on the origin of the physical properties of the tension wood. Wood Science and Technology 50: 197-208

Yamamoto H, Abe K, Arakawa Y, Okuyama T, Gril J (2005) Role of the gelatinous layer (G-layer) on the origin of the physical properties of the tension wood of *Acer sieboldianum*. Journal of Wood Science 51: 222-233

Yoshida M, Ohta H, Okuyama T (2002a) Tensile growth stress and lignin distribution in the cell walls of black locust (*Robinia pseudoacacia*). Journal of Wood Science 48: 99-105

Yoshida M, Ohta H, Yamamoto H, Okuyama T (2002b) Tensile growth stress and lignin distribution in the cell walls of yellow poplar, *Liriodendron tulipifera* Linn. Trees 16: 457-464

Yoshinaga A, Fujita M, Saiki H (1997) Secondary wall thickening and lignification of oak xylem components during latewood formation. Mokuzai Gakkaishi 43: 377-383

Yoshinaga A, Kusumoto H, Laurans F, Pilate G, Takabe K (2012) Lignification in poplar tension wood lignified cell wall layers. Tree Physiology 32: 1129-1136

Yoshizawa N, Inami A, Miyake S, Ishiguri F, Yokota S (2000) Anatomy and lignin distribution of reaction wood in two *Magnolia* species. Wood Science and Technology 34: 183-196

Zhao DY, Wan Y, Zhou WZ (2012) Ordered mesoporous materials. John Wiley abd Sons.

Zhou C, Wu Q (2012) Recent development in applications of cellulose nanocrystals for advanced polymer-based nanocomposites by novel fabrication strategies. *In* nanocrystals-synthesis, characterization and applications. Neralla S (Ed.), 103-120

Etude des modifications macromoléculaires et structurales ayant lieu pendant la construction de la paroi cellulaire du bois de tension: une contribution à la compréhension de l'origine des contraintes de maturation chez les arbres

Résumé: Les arbres sont capables de contrôler leur forme et réagir à des sollicitations par la fabrication d'un type de bois sous contrainte, nommé bois de tension. Cette contrainte apparait pendant la maturation de la paroi cellulaire, mais le mécanisme de mise en place reste inconnu. L'objectif est de mieux comprendre l'origine des contraintes de maturation par l'étude des modifications macromoléculaires et structurales ayant lieu pendant la construction de la paroi cellulaire du bois de tension. Une étude en spectroscopie FTIR a permis d'observer le dépôt des constituants et leur orientation pendant la maturation. Parallèlement, l'étude des isothermes d'adsorption-désorption d'azote, a permis de mettre en évidence l'évolution de la mesoporosité, à la fois pour les espèces avec et sans couche G. La forte évolution de la mesoporosité pendant la maturation laisse penser que celle-ci joue un rôle majeur dans la génération des contraintes de maturation.
Mots-clés: Bois de tension, Contrainte de maturation, Maturation cellulaire, Couche gélatineuse, Peuplier, Simarouba, Microscopie à transformée de Fourier infra-rouge (FTIR), Mésoporosité, Sonication

Study of macromolecular and structural modifications occurring during the building of the tension wood cell wall: a contribution to the understanding of the maturation stress generation in trees

Abstract: Trees are able to control their shape and to react to mechanical event by formation of a special wood type, named tension wood, under high tensile stress. This stress is generated during the cell maturation but the underlying mechanism is still unknown. This work aims at studying the macromolecular and structural modifications during the building of the tension wood cell wall. An FTIR spectroscopy study allowed monitoring the deposition of component and their orientation during wood cell wall maturation. In parallel, the technique of adsorption-desorption volumetry of nitrogen was improved for the study of wood. The measure of mesoporosity and its evolution during the maturation of tension wood cell wall indicated that both G-layer and non-G-layer species exhibit clear difference in pore volume and pore shape, from cambial zone to tension wood cell wall suggesting that porosity may play a major role in the maturation stress generation.
Key words: Tension wood, Maturation stress, Cell wall maturation, Gelatinous layer, Poplar, Simarouba, Fourier transform infrared (FTIR) microscopy, Mesoporosity, Sonication

Laboratoire de Mécanique et Génie Civil (LMGC), CNRS UMR 5508, Université Montpellier II, CC 048, Place Eugène Bataillon, 34095 Montpellier Cedex 5, France.